National Library of Canada
Bibliothèque nationale du Canada

Canadian Theses Service
Service des thèses canadiennes

Ottawa, Canada
K1A 0N4

NOTICE

The quality of this microform is heavily dependent upon the quality of the original thesis submitted for microfilming. Every effort has been made to ensure the highest quality of reproduction possible.

If pages are missing, contact the university which granted the degree.

Some pages may have indistinct print especially if the original pages were typed with a poor typewriter ribbon or if the university sent us an inferior photocopy.

Previously copyrighted materials (journal articles, published tests, etc.) are not filmed.

Reproduction in full or in part of this microform is governed by the Canadian Copyright Act, R.S.C. 1970, c. C-30.

AVIS

La qualité de cette microforme dépend grandement de la qualité de la thèse soumise au microfilmage. Nous avons tout fait pour assurer une qualité supérieure de reproduction.

S'il manque des pages, veuillez communiquer avec l'université qui a conféré le grade.

La qualité d'impression de certaines pages peut laisser à désirer, surtout si les pages originales ont été dactylographiées à l'aide d'un ruban usé ou si l'université nous a fait parvenir une photocopie de qualité inférieure.

Les documents qui font déjà l'objet d'un droit d'auteur (articles de revue, tests publiés, etc.) ne sont pas microfilmés.

La reproduction, même partielle, de cette microforme est soumise à la Loi canadienne sur le droit d'auteur, SRC 1970, c. C-30.

NL-339 (r. 88/04)

Canada

THE UNIVERSITY OF ALBERTA

GEOLOGY AND GEOCHEMISTRY OF GOLD-BEARING IRON FORMATION IN THE CONTWOYTO LAKE-POINT LAKE REGION, NORTHWEST TERRITORIES, CANADA.

by

Paul G. Lhotka

A THESIS

SUBMITTED TO THE FACULTY OF GRADUATE STUDIES AND RESEARCH
IN PARTIAL FULFILMENT OF THE REQUIREMENTS FOR THE DEGREE OF
Doctor of Philosophy

DEPARTMENT OF GEOLOGY

EDMONTON, ALBERTA

Fall, 1988

Permission has been granted to the National Library of Canada to microfilm this thesis and to lend or sell copies of the film.

The author (copyright owner) has reserved other publication rights, and neither the thesis nor extensive extracts from it may be printed or otherwise reproduced without his/her written permission.

L'autorisation a été accordée à la Bibliothèque nationale du Canada de microfilmer cette thèse et de prêter ou de vendre des exemplaires du film.

L'auteur (titulaire du droit d'auteur) se réserve les autres droits de publication; ni la thèse ni de longs extraits de celle-ci ne doivent être imprimés ou autrement reproduits sans son autorisation écrite.

ISBN 0-315-45483-0

THE UNIVERSITY OF ALBERTA

RELEASE FORM

NAME OF AUTHOR: Paul G. Lhotka

TITLE OF THESIS: GEOLOGY AND GEOCHEMISTRY OF GOLD-BEARING IRON FORMATION IN THE CONTWOYTO LAKE-POINT LAKE REGION, NORTHWEST TERRITORIES, CANADA.

DEGREE: Doctor of Philosophy

YEAR THIS DEGREE GRANTED: Fall, 1988

Permission is hereby granted to THE UNIVERSITY OF ALBERTA LIBRARY to reproduce single copies of this thesis and to lend or sell such copies for private, scholarly or scientific research purposes only.

The author reserves other publication rights, and neither the thesis nor extensive extracts from it may be printed or otherwise reproduced without the author's written permission.

Paul G. Lhotka

Paul G. Lhotka

PERMANENT ADDRESS:

11111-64 Avenue

Edmonton, Alberta

T6H 1T4

DATE: April 28 1988.

THE UNIVERSITY OF ALBERTA

FACULTY OF GRADUATE STUDIES AND RESEARCH

The undersigned certify that they have read, and recommend to the Faculty of Graduate Studies and Research, for acceptance, a thesis entitled GEOLOGY AND GEOCHEMISTRY OF GOLD-BEARING IRON FORMATION IN THE CONTWOYTO LAKE-POINT LAKE REGION, NORTHWEST TERRITORIES, CANADA submitted by Paul G. Lhotka in partial fulfilment for the requirements for the degree of Doctor of Philosophy.

Dr. B. E. Nesbitt - Supervisor

Dr. H. Baadsgaard

Dr. P. A. Cavell

Dr. P. Erdmer

Dr. J. M. Whiting

Dr. B. J. Fryer

Date: April 28, 1988

ABSTRACT

Numerous gold occurrences, including the Lupin mine, exist in Archean iron formation (IF) within the Slave Province. Early studies suggested that gold was a syngenetic component of the IF; however, the present study suggests that the gold and sulphides are epigenetic.

Gold is associated with quartz veins and concentrations of pyrrhotite or pyrite, and arsenides (arsenopyrite ± loellingite) in IF. The veins contain from 0.03 to 1.00 parts per million (ppm) Au and comprise sulphide-poor quartz. A zoned sequence of hydrothermal alteration is present adjacent to quartz veins. Immediately adjacent to the veins a calc-silicate lithology (0.03 to 1.00 ppm Au) is sometimes developed that comprises hedenbergite + quartz ± epidote ± scheelite ± grossular. Next is an arsenide-rich zone (5 to 30 ppm Au) comprising hornblende + quartz ± hedenbergite ± epidote ± actinolite. The next zone is an Fe-sulphide zone (5 to 30 ppm Au), lacking abundant arsenides, but containing pyrrhotite or pyrite and hornblende + quartz ± hedenbergite ± epidote ± actinolite. Further from the veins the IF is unmineralized (≤0.03 ppm Au), lacks sulphides, and comprises grunerite + quartz ± magnetite. In the transition zone hornblende replaces grunerite. The scale of the sequence of zones varies from millimetres to metres. Mineralization occurred after most of the Archean deformation coincident, or nearly coincident, with peak thermal conditions.

Hornblende and grunerite show trends of decreasing X_{Fe} (defined as Fe/[Fe+Mg]) towards quartz veins as the concentration of sulphides increases. These trends represent sulphidation reactions during which S combines with Fe from Fe-silicates to form Fe-sulphides. This forces the Fe-silicates to lower X_{Fe}

values. Deposition of S forces the precipitation of Au due to the breakdown of aqueous gold-sulphide complexes.

Whole rock analyses of the alteration zones are characterized by relative additions of greater than 100 percent of the following elements (listed from greatest to least): calc-silicate rocks W, Au, Sr, As, Ca, S, Al, Sc, Pb, La, P and Ce; arsenide-rich IF As, Au, S, Cu, Bi, Ni, W, P, Co, Ag and Sr; Fe-sulphide-rich IF Au, As, S, W, Cu, Bi, Sr, Ca and Pb; weakly mineralized IF Au, As, S, W, and Sr.

Lead isotopic analyses of whole rocks and minerals indicate that the gold-bearing-zones are more radiogenic (higher $^{207}Pb/^{204}Pb$) than the non-gold-bearing IF. Analyses of strontium isotopic ratios of whole rocks and minerals from Lupin indicate that the strontium added during alteration of IF was homogeneous and had an $^{87}Sr/^{86}Sr$ ratio of 0.70203 ± 0.0008 (1 sigma). The lead and strontium isotopic data are consistent with the addition of these elements from an external, older, crustal source.

Together the field, petrographic, geochemical and isotopic data strongly suggest that the gold mineralization in IF is epigenetic.

ACKNOWLEDGEMENTS

I gratefully acknowledge the guidance of my supervisor Dr. B. E. Nesbitt and my examining committee, Dr. H. Baadsgaard, Dr. P. A. Cavell, Dr. P. Erdmer, Dr. J. Whiting and Dr. B. J. Fryer.

Trigg, Woollett, Olson Consulting Ltd. and Echo Bay Mines Ltd. provided logistical support for the fieldwork and allowed access to unpublished data, exploration properties and the Lupin mine. The encouragement and support of C. M. Trigg, R. A. Olson and in particular G. N. Woollett, throughout the thesis project is sincerely appreciated.

Numerous geologists and explorationists either contributed valuable discussions in the course of the fieldwork or assisted in the execution of the fieldwork. They include D. Dudek, Z. Rebic, R. Bullis, M. Strachan, K. Scott, G. Linassi, R. Ogilvie, V. Pullar, T. Kinshella. Discussions with J. Kerswill and J. Gardiner also contributed to this work.

S. Launspach's efforts in assisting in the electron microprobe analyses at the University of Alberta are sincerely acknowledged. J. Machacek ably assisted in the electron microprobe analyses at the University of Calgary.

Gold fire-assays by J. German of Echo Bay Mines Ltd. Lupin Assay Laboratory were greatly appreciated.

J. Duke volunteered to do instrumental neutron activation analyses and his efforts, together with the accessibility of the Slowpoke Facility at the University of Alberta, are gratefully acknowledged.

Thanks are due to Dr. H. Baadsgaard, W. Day, P. Wagner, D. Kristic, and especially Dr. P. A. Cavell, who assisted in either one or both of the mass spectrometry and analytical chemistry.

R. Thorpe is thanked for permission to use unpublished data and for comments on the lead isotope data.

Fellow students B. St. Louis, C. Sayer, L. de St. Jorre, D. Fluet, M. Dufresne and C. Connolly provided encouragement to persevere at various stages in the course of the project.

Dr. R. Burwash came to my assistance on several occasions when Dr. Nesbitt was on sabattical, and his kindness is acknowledged.

Discussions on the regional geology with an enthusiastic J. King proved useful in attempting to place the thesis in a regional context.

R. Johnston and M. Dufresne deserve special thanks for editorial suggestions and discussions on iron formation hosted deposits. Discussions with D. Kristic helped in finding a new way to examine the lead isotopes.

My parents, brother, and especially my wife, Fiona, always supported my decision to return to university. Fiona endured the twists and turns of the emotional rollercoaster ride that this thesis, at times, inevitably became.

Financial support for the project was provided by an Industrial Postgraduate Scholarship from NSERC and Trigg, Woollett, Olson Consulting Ltd., a Postgraduate Scholarship from NSERC, and a Faculty of Graduate Studies and Research Scholarship. The Boreal Institute for Northern Studies provided funds for analytical work and other expenses. Echo Bay Mines Ltd. provided funds to pay for some of the polished thin sections used in this study.

TABLE OF CONTENTS

Chapter		Page
1.	**INTRODUCTION**	1
	A. Introduction to the thesis problem	1
	Epigenetic models	2
	Multistage models	2
	Synthesis of genetic models	3
	B. Previous research on gold deposits in iron formation in the Contwoyto Lake-Point Lake region	3
	C. Research methods	5
	D. References	6
2.	**GEOLOGY OF UNMINERALIZED AND GOLD-BEARING IRON FORMATION, CONTWOYTO LAKE-POINT LAKE REGION, NORTHWEST TERRITORIES, CANADA**	8
	A. Introduction	8
	B. Methods	9
	Field and petrographic techniques	9
	Analytical techniques	11
	C. Regional geology	12
	Pre-Yellowknife Supergroup rocks	12
	Yellowknife Supergroup	14
	Archean plutonic rocks	17
	Proterozoic rocks	18
	D. Metamorphism and deformation	18
	E. Unmineralized iron formation	20

Low metamorphic grade areas 21

Medium metamorphic grade areas 24

Summary 24

F. Small-scale gold occurrences in iron formation 26

Biotite zone 26

Garnet zone 29

Medium metamorphic grade 38

Summary: small-scale gold occurrences 40

G. Lupin 41

Mineralized iron formation 43

Unmineralized and weakly mineralized iron formation 45

Pelitic iron formation 46

Quartz veins 47

Calc-silicate rocks 48

Felsic dykes 49

Summary: Lupin 51

H. Discussion 51

Genetic models 51

Small-scale gold occurrences 52

Comparison of Lupin to the small-scale gold occurrences 56

Timing of the mineralization 58

I. Comparison of the Contwoyto Lake gold occurrences to other iron formation-hosted gold deposits 60

J. Summary and implications 62

K. References 64

3. MINERAL CHEMISTRY OF GOLD-BEARING MINERALIZED IRON FORMATION: EVIDENCE FOR EPIGENETIC SULPHIDATION, CONTWOYTO LAKE, NORTHWEST TERRITORIES, CANADA 71

A. Introduction 71

B. Methods 73

Analytical methods 73

Stoichiometric calculations 74

C. Geology 75

Regional geology 75

Geology of iron formation and gold occurrences 78

D. Esker Lake gold occurrence 80

Geology and mineralogy 80

Mineral chemistry 82

Sulphidation model 86

Other evidence for wallrock alteration 88

E. Fingers Lake gold occurrence 94

Geology and mineralogy 94

Mineral chemistry 95

Interpretation 95

F. Lupin 99

Geology and mineralogy 99

Mineral chemistry of iron formation 102

Mineral chemistry of pelitic iron formation 110

Mineral chemistry of calc-silicate rocks 111

Interpretation of the mineral assemblages 112

G. Discussion 112

H. Comparison of the mineral chemistry of the Homestake deposits to the Contwoyto Lake deposits 118

I. Summary 121

J. References 123

4. WHOLE ROCK GEOCHEMICAL EVIDENCE FOR EPIGENETIC HYDROTHERMAL ALTERATION AND GOLD MINERALIZATION, CONTWOYTO LAKE, NORTHWEST TERRITORIES, CANADA 126

A. Introduction 126

B. Methods 127

Sample preparation 127

C. Geology 129

Regional geology 129

Gold mineralization in iron formation 131

D. Immobile elements distribution patterns in iron formation 141

E. Alteration patterns in mineralized iron formation 146

Method of calculation 146

Weakly mineralized iron formation 152

Iron sulphide mineralized iron formation 152

Arsenide mineralized iron formation 153

Calc-silicate rocks 154

Average gains/losses for alteration at Contwoyto Lake 155

F. Alteration of pelitic iron formation 155

G. Discussion 159

Alteration of iron formation 159

Mass balance for the iron formation system 161

Comparisons to other Archean epigenetic and syngenetic deposits 162

H. Summary 165

I. References 166

5. LEAD AND STRONTIUM ISOTOPE GEOCHEMISTRY OF GOLD-BEARING IRON FORMATION, CONTWOYTO LAKE REGION, NORTHWEST TERRITORIES, CANADA 170

A. Introduction 170

B. Geology 171

Regional geology 171

Pre-Yellowknife Supergroup rocks 171

Yellowknife Supergroup 173

Archean plutonic rocks 173

Proterozoic rocks 174

Metamorphism and deformation 175

C. Gold mineralization in iron formation 175

D. Previous geochronology 180

E. Analytical techniques 183

F. Lead isotope data 185

Unmineralized whole rock samples 185

Mineralized whole rock samples 191

Mineral separates 192

Interpretation of lead isotopes 193

G. Strontium isotope data 197

Unmineralized whole rocks 197

Mineralized whole rocks and minerals 200

Interpretation 201

H. Discussion 205

Possible source regions 205

Comparisons to other Archean gold deposits 207

I. Conclusions 208

J. References 210

6. SUMMARY 216

A. Fieldwork and petrography 216

B. Mineral chemistry 217

C. Whole rock geochemistry 219

D. Lead and strontium isotope geochemistry 220

E. Major conclusions 221

F. References 223

APPENDICES 224

1. Summary of thin section and polished thin section mineralogy 225

2. Comparison of repeat electron microprobe analyses of the pyrope standard to accepted values 230

3. Electron microprobe analyses of silicate minerals 232

4. Comparison of whole rock geochemical analyses of duplicate samples and certified reference standards 261

LIST OF TABLES

Table		Page
2.1.	Duplicate gold analyses of samples by the lead fire assay technique.	13
3.1.	Representative electron microprobe analyses of amphiboles, chlorites, garnets and epidotes from the Esker Lake area.	83
3.2.	Representative electron microprobe analyses of amphiboles and chlorites from the Fingers Lake area.	96
3.3.	Representative electron microprobe analyses of amphiboles, chlorites, pyroxenes, garnets and epidotes from the Lupin mine area.	103
4.1.	Compositions of unmineralized and mineralized iron formation and associated rock types from Contwoyto Lake.	133
4.2.	Average compositions of unmineralized and mineralized iron formation and associated rock types in the Contwoyto Lake area.	148
4.3.	Average gains/losses in alteration of the various types of mineralized iron formation in the Contwoyto Lake area.	156
5.1.	Lead isotope data for rocks and minerals from Contwoyto Lake.	186
5.2.	Lead isotopic ratios for galenas from volcanogenic massive sulphide deposits of the Slave Province.	189
5.3.	Strontium and rubidium data for rocks and minerals from the Contwoyto Lake area.	198

LIST OF FIGURES

Figure		Page
2.1.	Geology of the Contwoyto Lake-Point Lake region. Modified after Bostock (1980) and others.	10
2.2.	*A.* Photomicrograph of unmineralized grunerite iron formation from the Lupin iron formation northeast of the end of the East Zone. *B.* Photomicrograph of weakly mineralized iron formation from the Lupin iron formation northeast of the end of the East Zone (reflected light).	23
2.3.	Pyrite (py) replacing magnetite (m) from the Fingers Lake gold occurrence (reflected light).	28
2.4.	Sketch of mineralization adjacent to a quartz vein in a hand specimen from the Fingers Lake gold occurrence.	30
2.5.	Sketch map of the Esker Lake gold occurrence showing the zonation of gold values and sulphides adjacent to a quartz vein in the nonpelitic portion of the iron formation.	32
2.6.	Photomicrographs and hand specimen photographs from the Esker Lake gold occurrence. *A.* and *B.*	33
2.6.	continued. *C.* and *D.*	35
2.6.	continued. *E.* and *F.*	36
2.6.	continued. *G.* and *H.*	37
2.7.	*A.* Outcrop photograph of quartz-hedenbergite veining and alteration of banded grunerite-rich iron formation at the Sik gold occurrence. *B.* Photomicrograph of zoned alteration adjacent to a quartz-hedenbergite veinlet.	39
2.8.	Geology map of the Lupin area showing the ore zones and other localized areas of gold mineralization.	42

2.9. Mineralized iron formation from Lupin. *A.* Hand specimen of ore from the West Zone. *B.* Photomicrograph of hornblende-rich iron formation from the Centre Zone. 44

2.10. Calc-silicate rocks from the East Zone of the Lupin mine. *A.* Photomicrograph of calc-silicate rock. *B.* Photomicrograph of a veinlet of pyrrhotite, hornblende and actinolite cutting across coarse grained hedenbergite. 50

2.11. Schematic summary diagram of the relationships between quartz veining and gold mineralization in iron formation in the Contwoyto Lake-Point Lake region. 54

3.1. Geology of the Contwoyto Lake-Point Lake region. Modified after Bostock (1980) and others. 76

3.2. Sketch map of the Esker Lake gold occurrence showing the zonation of gold values and sulphides adjacent to a quartz vein in the nonpelitic portion of the iron formation. 81

3.3. $(Al_2O_3 + Fe_2O_3)$ - (MgO) - (FeO) ternary diagram of minerals from the Esker Lake iron formation. 85

3.4. X_{Fe} values of coexisting grunerite and hornblende from the Esker Lake gold occurrence. 89

3.5. $(Al_2O_3 + Fe_2O_3)$ - (CaO) - (FeO + MgO) ternary diagram of minerals from the Esker Lake iron formation. 91

3.6. Zoning in garnets from unaltered and possibly altered pelitic iron formation at Esker Lake. 93

3.7. $(Al_2O_3 + Fe_2O_3)$ - (MgO) - (FeO) ternary diagram of minerals from the Fingers Lake iron formation. 97

3.8. Geology map of the Lupin area showing the ore zones and other localized areas of gold mineralization. 100

3.9. $(Al_2O_3 + Fe_2O_3)$ - (MgO) - (FeO) ternary diagram of minerals from the Lupin iron formation. 106

3.10. X_{Fe} of hornblende versus distance from a quartz vein in the East Zone of the Lupin mine. 109

3.11. $(Al_2O_3 + Fe_2O_3)$ - (CaO) - (FeO + MgO) ternary diagram of minerals from Lupin iron formation. 113

3.12. Summary histogram of the X_{Fe} values in amphiboles in iron formation at Lupin, Esker Lake and Fingers Lake. 115

3.13. X_{Fe} values in silicate minerals in iron formation from the Homestake Mine, South Dakota. 120

4.1. Geology of the Contwoyto Lake-Point Lake region. Modified after Bostock (1980) and others. 130

4.2. Geology map of the Lupin area showing the ore zones and other localized areas of gold mineralization. 137

4.3. Schematic summary diagram of the relationships between quartz veining and gold mineralization in iron formation in the Contwoyto Lake-Point Lake region. 140

4.4. Immobile element X-Y plots for iron formation and associated rock types. *A* . TiO_2 versus Al_2O_3. *B* . Zr versus TiO_2. *C* . Zr versus Al_2O_3. *D* . Zr versus Y. *E* . Sc versus Al_2O_3. 143

4.5. Percentage gains and losses in alteration of unmineralized iron formation in the different types of mineralized iron formation at Lupin and small-scale occurrences. *A.* Pyrite or pyrrhotite-rich mineralized iron formation and weakly mineralized iron formation. 150

4.5. continued. *B.* Calc-silicate rocks and arsenide-rich mineralized iron formation. 151

5.1. Geology of the Contwoyto Lake-Point Lake region. Modified after Bostock (1980) and others. 172

5.2. Schematic summary diagram of the relationships between quartz veining and gold mineralization in iron formation in the Contwoyto Lake-Point Lake region. 177

5.3. A $^{206}Pb/^{204}Pb$ versus $^{207}Pb/^{204}Pb$ plot of data for whole rocks and minerals from Contwoyto Lake. 188

5.4. A $^{206}Pb/^{204}Pb$ versus $^{207}Pb/^{204}Pb$ plot of calculated initial lead isotopic compositions of whole rocks and minerals at 2670 Ma. 195

5.5. Plots of $^{87}Rb/^{86}Sr$ atomic ratio versus $^{87}Sr/^{86}Sr$ (measured) for whole rocks and minerals. *A.* All data. *B.* Selected data at an expanded scale. 199

5.6. Plots of $1/^{86}Sr$ ppm versus $^{87}Sr/^{86}Sr$ (corrected to 2550 Ma) for whole rocks and minerals. *A.* All data. *B.* Selected data at an expanded scale. 203

5.7. Possible source regions of lead and strontium in mineralized iron formation. *A.* Lead isotopes. *B.* Strontium isotopes. 206

1. INTRODUCTION

A. Introduction to the thesis problem

The central objective of this thesis is to determine the process or processes that led to gold mineralization in iron formation at the Lupin mine and in the Contwoyto Lake-Point Lake region. The thesis also examines the timing of these processes in the evolution of the greenstone belt. Currently, genetic models for gold mineralization hosted by iron formation can be grouped into three main types: a syngenetic model in which deposition of gold is simultaneous with deposition of the iron formation; an epigenetic model in which gold is introduced to the iron formation during a later event; and a multistage model in which gold is an original component of the iron formation, but is remobilized during later events.

Syngenetic models

Syngenetic models for gold deposition came into prominence when the volcanogenic-exhalative model for base metal, massive sulphide deposits was applied to gold-bearing, carbonate iron formation of the Kirkland Lake-Larder Lake area of Ontario by Ridler (1970, 1976). Fripp (1976) applied a syngenetic model to the gold deposits of Zimbabwe that are hosted by sulphide or sulphide-carbonate iron formation. Both authors rely heavily on the stratabound nature of the deposits and the association of the gold with sulphides (pyrrhotite, pyrite and arsenopyrite), which are sometimes banded, to support their interpretation of a syngenetic model of gold concentration.

Epigenetic models

Epigenetic models were predominant prior to the syngenetic emphasis of the 1970's and have once again come into prominence in the last few years. Phillips *et al.* (1984) state that replacement of magnetite by pyrrhotite adjacent to structurally controlled, quartz-pyrrhotite veins, as well as the alteration of silicate minerals in iron formation adjacent to the veins, is evidence for an epigenetic origin for the Water Tank Hill deposit in Australia. They further suggest that a similar model may be applicable to the Zimbabwe gold deposits studied by Fripp (1976). Phillips *et al.* (1984) report that envelopes of gold-bearing arsenopyrite exist around quartz veins in Zimbabwe and imply that arsenopyrite replaces magnetite. Macdonald (1983) proposes that at Geraldton, Ontario, gold deposits hosted by oxide iron formation are epigenetic. Supporting evidence for his argument includes structural control of the gold-bearing zones and transgressive quartz veins associated with gold-bearing sulphides.

Multistage models

A multistage model was suggested by Rye and Rye (1974) for the economically important Homestake deposit in South Dakota. Iron formation at Homestake comprises sideroplesite (magnesian siderite) or cummingtonite schist which is locally chloritized and mineralized with gold, arsenopyrite and pyrrhotite. Rye and Rye (1974) suggest that because the sulphur and oxygen isotope ratios show a formational dependence they are indigenous to the Homestake Formation and the same is probably true for gold as well. Their model comprises a syngenetic concentration of gold in iron formation which was modified and upgraded to economic mineralization during metamorphism. Hallager (1984) suggested a similar model for gold mineralization at Jardine,

Montana based upon a whole rock geochemical study. Neither Rye and Rye (1974) nor Hallager (1984) clearly state on what scale remobilization has taken place.

Synthesis of genetic models

In a simplified sense, the proponents of the syngenetic theory rely heavily on the stratabound nature of the gold mineralization and the sometimes banded nature of the sulphides associated with the gold to support their model. The proponents of the epigenetic theory centre their arguments on: the spatial association of gold mineralization with veins and other transgressive structural features; textures indicating that the sulphides are replacing preexisting minerals; and the presence of alteration adjacent to the veins. These features are given as proof of epigenesis. The multistage model greatly complicates the use of all of the above criteria because it predicts that syngenetic deposits will be overprinted by epigenetic features.

In this thesis, in addition to using criteria based largely on fieldwork and petrographic data, geochemical data are used to examine the genesis of iron formation-hosted gold deposits.

B. Previous research on gold deposits in iron formation in the Contwoyto Lake-Point Lake region

At present, relatively few data are available on the gold deposits in iron formation in the Contwoyto Lake-Point Lake region; however, previous workers invariably suggest that the gold deposits are syngenetic. Kerswill (1986) states that the stratiform nature of the mineralization and the uniform dissemination of the gold at Lupin are suggestive of syngenetic deposition. Gardiner (1986), in a

structural study of the Lupin mine, states that gold is confined to the iron formation and no significant remobilization can be demonstrated for either the gold or the sulphides. He also suggests that the gold mineralization preceded the formation of the quartz veins. Bostock (1980) believed that the gold and arsenic were concentrated by syngenetic processes. Padgham (1984) uses the banding of the sulphides and the fact that the gold is greatly enriched in certain sulphide-bearing beds to infer that the gold is syngenetic. Franklin and Thorpe (1982) state that the Lupin deposit is the most convincing example of syngenetic gold mineralization in Canada. The characteristics used by Franklin and Thorpe to support a syngenetic model are: the strict stratigraphic control of ore; the lack of zoning; the similar metamorphic assemblages in ore and remote country rock; the absence of wallrock alteration; and the uniform distribution of the gold. Ridler (1976) lists the Contwoyto Lake deposits as an example of a gold-rich exhalite.

It is important to note that the preexisting database on the area is confined to fieldwork, petrographic and structural studies. This is also largely true of research on iron formation-hosted deposits elsewhere. Very few studies have examined the geochemistry of these types of deposits. Notable exceptions are Rye and Rye (1974), Rye *et al.* (1974), Chinn (1969) and Hallager (1984). However, these studies tend to be restricted to the gold-bearing portions of the iron formation and often do not adequately consider geochemistry of unmineralized iron formation or the transition between the mineralized iron formation and unmineralized iron formation.

C. Research methods

Since the region of interest is large and geologically complex, it was decided to select a number of relatively restricted areas containing mineralized and unmineralized iron formation for study. The study areas were chosen to represent the geology of the region over the range of metamorphic grades. At each area field observations were made on: the primary lithologies and structures; metamorphism and deformation; distribution of the gold and sulphides with special emphasis on the nature of the transition between the mineralized and unmineralized zones; and epigenetic features such as veining and alteration. These observations along with transmitted and reflected light microscopy and gold assay data are presented in Chapter 2.

Chapters 3 through 5 examine the geochemistry of Lupin and three other gold occurrences hosted by iron formation.

Specifically, Chapter 3 presents the results of electron microprobe analyses of silicate minerals in unmineralized and mineralized iron formation.

Chapter 4 contains whole rock major, minor, and trace element geochemical data on unmineralized and mineralized iron formation and associated rock types. These data are used to calculate the gains and losses of elements during the inferred epigenetic gold mineralization event.

Chapter 5 examines the lead and strontium isotopic systematics of unmineralized and mineralized iron formation and associated rock types. These data are used to further constrain genetic models for the gold mineralization.

Chapter 6 summarizes the results of the thesis.

D. References

Bostock, H. H. 1980. Geology of the Itchen Lake area, District of Mackenzie. Geological Survey of Canada, Memoir 391.

Chinn, W. 1969. Structural and mineralogical studies at the Homestake Mine, Lead, South Dakota. Ph.D. thesis, University of California, Berkeley, California. Available from University Microfilms International, Ann Arbour, Michigan.

Franklin, J. M., and Thorpe, R. I. 1982. Comparative metallogeny of the Superior, Slave and Churchill Provinces. *In* Precambrian sulphide deposits. *Edited by* R. W. Hutchinson, C. D. Spence, and J. M. Franklin. Geological Association of Canada, Special Paper 25, pp. 3-90.

Fripp, R. E. P. 1976. Stratabound gold deposits in Archean banded iron formation, Rhodesia. Economic Geology, **71**: 58-75.

Gardiner, J. J. 1986. Structural geology of the Lupin gold mine, Northwest Territories. M.Sc. thesis, Acadia University, Wolfville, Nova Scotia.

Hallager, W. S. 1984. Geology of gold-bearing metasediments near Jardine, Montana. *In* Gold'82: the geology, geochemistry of gold deposits. *Edited by* R. P. Foster, Geological Society of Zimbabwe Special Publication 1, pp. 191-218.

Kerswill, J. A. 1986. Gold deposits hosted by iron formation in the Contwoyto Lake area, Northwest Territories. *In* Gold'86 Poster Paper Abstracts. *Edited by* A. M. Chater, Geological Association of Canada, Mineral Deposits Division, pp. 82-85.

Macdonald, A. J. 1983. The iron formation-gold association evidence from the Geraldton area. *In* The geology of gold in Ontario. *Edited by* A. C. Colvine, Ontario Geological Survey, Miscellaneous Paper 110, pp. 75-83.

Padgham, W. A. 1984. Gold deposits of N. W. T. ; Classes, styles, genesis, exploration methods and success probabilities. Contributions to the geology of the Northwest Territories, **1**: 121-129.

Phillips, G. N., Groves, D. I., and Martyn, J. E. 1984. An epigenetic origin for Archean banded-iron-formation-hosted gold deposits. Economic Geology, **79**: 162-171.

Ridler, R. H. 1976. Stratigraphic keys to the gold metallogeny of the Abitibi Belt. Canadian Mining Journal, **97**: 81- 90.

Ridler, R. H. 1970. Relationships of mineralization to volcanic stratigraphy in the Kirkland-Larder Lakes area, Ontario. Geological Association of Canada Proceedings, **21**: 33-42.

Rye, D. M., and Rye, R. O. 1974. Homestake Gold Mine, South Dakota: I. Stable isotope studies. Economic Geology, **69**: 293-317.

Rye, D. M., Doe, B. R., and Deleveaux, M. H. 1974. Homestake Gold Mine, South Dakota: II. Lead isotopes, mineralization ages, and source of lead in ores of the Northern Black Hills. Economic Geology, **69**: 814-822.

2. GEOLOGY OF UNMINERALIZED AND GOLD-BEARING IRON FORMATION, CONTWOYTO LAKE-POINT LAKE REGION, NORTHWEST TERRITORIES, CANADA

A. Introduction

Gold deposits associated with iron formation are of importance worldwide. Some of the better known examples include the Homestake deposit in the United States (Rye and Rye 1974, and references therein) and the Morro Velho deposit in Brazil (Gair 1962) as well as other examples in Western Australia (Groves *et al.* 1987), South Africa (Fripp 1976) and India (Hamilton and Hodgson 1986). Genetic models for gold deposits associated with iron formation can be grouped into three main types: a syngenetic model in which gold is deposited simultaneously with deposition of the iron formation (Fripp 1976; Ridler 1970); an epigenetic model in which gold is introduced into the iron formation during a later event (Phillips *et al.* 1984; Macdonald 1983; Groves *et al.* 1987); and a multistage or remobilization model in which gold is a primary component of the iron formation and is remobilized and concentrated during later events (Rye and Rye 1974; Sawkins and Rye 1974).

Previous studies of gold deposits hosted by iron formation have concentrated largely on the gold deposits, often without examining the relationships between the gold-bearing portion of the iron formation and the laterally continuous host iron formation. One objective of this study is to describe both the unmineralized and the gold-bearing portions of the iron formations and the relationships between them. Another important aspect of this study is that not only is the economic mineralization described, but similar mineralization, of much smaller areal extent, is described. The processes of mineralization at small-scale occurrences are often easier to study and

understand than the ore deposit. Where the data supports a common origin for the mineralization, the characteristics and processes documented at the small-scale occurrences, can be scaled up to aid in understanding the ore deposit.

At present, relatively little is known about the gold-bearing iron formations in the region of interest. Archean iron formations, in the northern part of the Slave Province of the Canadian Shield between Contwoyto and Point Lakes, host over 100 gold occurrences and one major gold deposit, the Lupin mine (Fig. 2.1). Lupin is a major deposit that has produced 28.25 tonnes of gold (905,800 troy ounces) between startup in 1982 and the end of 1987 at an average grade of 11.12 ppm. As of the end of 1987 Lupin contained proven and probable ore reserves of 3,396,400 tonnes at an average grade of 11.38 ppm for a reserve of 38.65 tonnes of gold. The only detailed published work is that of Gardiner (1986). Other publications are less detailed or of a more regional nature (Lhotka and Nesbitt 1987a,b; Kerswill 1986, 1985a,b, 1984; Padgham 1984; Gibbins 1981; Franklin and Thorpe 1982; and Bostock 1980).

The data generated by this study are used to develop a genetic model for gold mineralization. A model involving epigenetic gold mineralization can account for all of the characteristics of the known gold occurrences.

B. Methods

Field and petrographic techniques

Five months of fieldwork was performed over the course of two seasons. The fieldwork was conducted in conjunction with exploration by Echo Bay Mines Ltd., the owner of the Lupin mine, and exploration data including geological mapping, diamond drilling, assays and geophysical data were freely available for study. Detailed data from Lupin, comprising geological mapping and assays, were also available for examination.

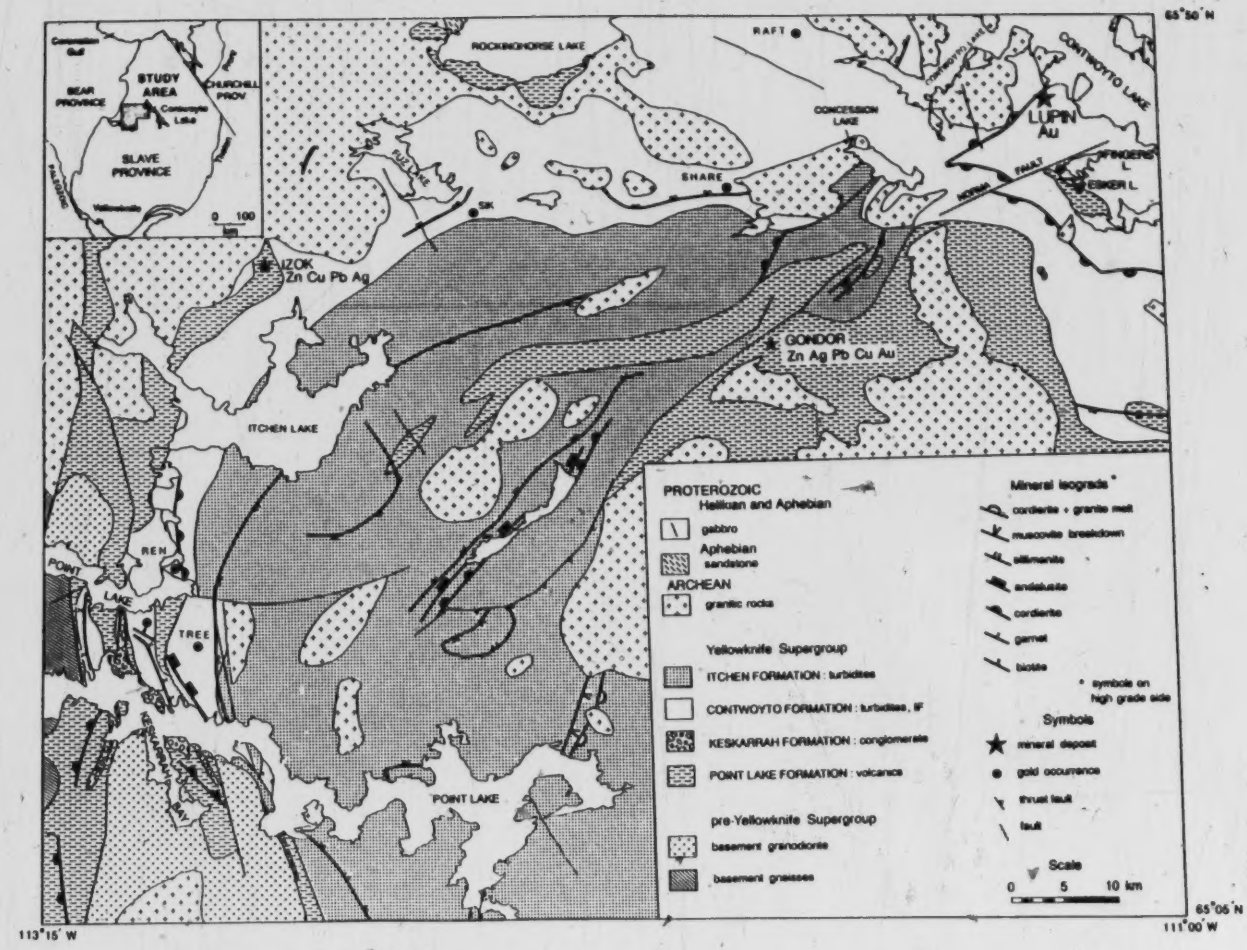

Fig. 2.1. Geology of the Contwoyto Lake-Point Lake region. Modified after Bostock (1980) and others.

The fieldwork comprised detailed mapping, description and sampling of outcrops and diamond drill cores at various study areas. At Lupin, detailed studies were done on core, and on surface and underground exposures. Initially, twenty areas in the region that contain gold-bearing and unmineralized iron formation at various metamorphic grades were selected for study. At these areas, observations were made on the distribution of sulphides and gold, quartz veining, and mineralogy of the iron formation. From this large group of study areas several representative study areas were selected for more detailed fieldwork and laboratory studies.

Petrographic descriptions are based on the examination of hundreds of hand specimens, and 180 polished thin sections and thin sections that were studied in transmitted and reflected light. A summary table of the thin section mineralogy is included as Appendix 1. X-ray powder diffraction techniques (XRD) were used to confirm the mineralogy of selected samples.

Analytical techniques

Samples for assay, collected in the course of this study, were prepared at the University of Alberta. Representative samples of about 2 kg were jaw crushed to less than 1 cm diameter. The whole sample was then ground in a disc mill fitted with alumina plates. At this point, the entire sample was rolled on paper and split by coning and quartering until about 150 g of sample were isolated. This subsample was then ground in a motorized agate mortar and pestle. Finally, the sample was again rolled and coned and quartered to separate an aliquot of about 35 g. This sample was sent to the Lupin Assay Laboratory of Echo Bay Mines for gold assay by the conventional lead fire assay technique: the entire aliquot was assayed. The detection limit of the technique, as practised at Lupin, is 0.03 ppm Au (J. German personal

communication 1986). Analyses of duplicate samples that were submitted indicate that the reproducibility of the analyses is good (Table 2.1).

C. Regional geology

The Contwoyto Lake-Point Lake region is predominantly underlain by Archean rocks of the Slave Province. Small outliers of Aphebian clastic sedimentary rocks are exposed near the margins of the area (Fig. 2.1). Bostock (1980) mapped the region at a scale of 1:250,000. More detailed mapping has been done by King *et al.* (1988), Jackson (1982), Easton *et al.* (1981), King *et al.* (1980), Bau *et al.* (1979a,b,c,d,e,f), Henderson and Easton (1977a) and Tremblay (1976). Data from all of these sources as well as unpublished company data were used to revise Bostock's map (Fig. 2.1).

Archean rocks can be subdivided into: pre-Yellowknife Supergroup rocks that comprise granitic rocks and gneisses; Yellowknife Supergroup supracrustal metavolcanic and metasedimentary units; and syn- and post-Yellowknife Supergroup granitic rocks. All but the late plutons have been metamorphosed to some degree; however, premetamorphic rock terminology is generally used hereinafter.

Pre-Yellowknife Supergroup rocks

Stockwell (1933) first noted that a sheared, chloritic granitic rock is unconformably overlain by conglomerate at Keskarrah Bay on Point Lake (Fig. 2.1). Subsequent work by Henderson (1975, 1981) describes the nature of the unconformity. U/Pb geochronology on zircons from the basement granitic rocks by Krogh and Gibbins (1978) gives an age of 3155 Ma which was later confirmed by Henderson *et al.* (1982). Although the Yellowknife Supergroup

Table 2.1. Duplicate gold analyses of samples by the lead fire assay technique. All values in ppm.

samples	duplicates
0.03	0.03
<0.03	0.03
1.58	1.27
34.29	33.77
87.40	81.87

has not been successfully dated in the Point Lake area (Wanless and Loveridge 1978), it is probable that it is of a similar age to other supracrustal rocks elsewhere in the Slave that have been dated at about 2670 Ma by the U/Pb method on zircons (Henderson *et al.* 1982). This indicates that the basement is about 500 Ma older than the supracrustal rocks.

Other rock units present in the Point Lake area have been suggested to constitute basement units by Henderson and Easton (1977b), and more recently by Easton (1985), and Easton *et al.* (1981). These units are gneissic (Fig. 2.1) and although the contacts with the less deformed supracrustals are faulted or mylonitized, there are several lines of field evidence that suggest the gneisses are older than the supracrustals (Easton *et al.* 1981).

Yellowknife Supergroup

The term Yellowknife Supergroup was defined by Henderson (1970) to include all of the supracrustal rocks in the Slave Province. Bostock (1980) subdivided the supergroup into four formations in the Contwoyto Lake-Point Lake region as follows: the Point Lake Formation which comprises mafic to felsic volcanic rocks; the Keskarrah Formation which comprises conglomerates and lithic sandstones; the Contwoyto Formation which comprises greywacke and mudstone beds with lenses and beds of iron formation; and the Itchen Formation which comprises greywacke and mudstone beds lacking iron formation (Fig. 2.1).

Age relationships between these formations are equivocal due in part to faulting of the contacts and intense folding in the sedimentary formations. Bostock (1980) considers the Keskarrah Formation to be a facies equivalent to the upper part of the Point Lake Formation. He believes the Contwoyto Formation is a facies equivalent to a late phase of Point Lake volcanism and

that the Itchen Formation is younger than the other three formations. On the basis of detailed mapping at Point Lake, Henderson and Easton (1977b) concluded that all four formations are essentially contemporaneous.

Lithologically the Point Lake Formation is a highly variable unit comprised mainly of mafic flows and tuffs, but also including felsic volcanic rocks and calcareous sedimentary rocks (Bostock 1980). A northerly trending belt of volcanics, informally known as the Western volcanic belt, is exposed in the western part of the area (Fig. 2.1). Much of this belt is comprised of pillowed mafic flows metamorphosed to low or medium grade. The Central volcanic belt is a westerly trending belt in the central part of the area that is more highly metamorphosed and is comprised of mafic to felsic tuffs and flows. A previously unmapped part of the Point Lake Formation, discovered by exploration geologists, exists south of Fingers Lake near Contwoyto Lake (Fig. 2.1). This unit is informally known as the Shallow Bay volcanics and is comprised of epiclastic volcanic rocks of intermediate composition that are generally fine grained but locally have fragments up to 10 cm diameter.

Two major undeveloped volcanogenic massive sulphide deposits containing Cu, Zn, Pb and lesser amounts of Ag and Au occur in the Point Lake Formation. The Izok deposit is described by Bostock (1980) and the Gondor deposit is described by Bubar and Heslop (1985).

The conglomerates and lithic sandstones of the Keskarrah Formation are restricted in areal extent to a small area near Point Lake (Fig. 2.1). The conglomerate is comprised predominantly of granitic and mafic volcanic clasts in variable proportions (Henderson and Easton 1977b), but locally includes gneissic clasts (Easton 1985) and felsic volcanic clasts (Bostock 1980). Lithic sandstone interbedded with conglomerate is fine grained and is crossbedded at medium to large scales suggesting a subaerial depositional environment

(Henderson and Easton 1977b). Fluvial deposition is suggested by the presence of well rounded clasts in a clast supported framework. Lenses of Keskarrah Formation conglomerates in the Contwoyto Formation at Point Lake are matrix supported and are probably sediment gravity flows. It is likely that the Keskarrah Formation represents portions of both a subaerial alluvial fan and a submarine turbidite fan.

The Contwoyto Formation comprises greywacke, mudstone and iron formation. Bostock (1980), Henderson and Easton (1977b), and Easton (1985) all conclude that the greywackes and mudstones were deposited as turbidites on a submarine fan. Observations made during the course of this study suggest that the greywacke beds are generally a few centimetres to 2m in thickness and may be massive or normally graded. Mudstone beds are generally a few centimetres to a few metres in thickness. Typical turbidites are AE in the terminology of Bouma (1962) and only rarely are B, C or D divisions recognized. Although mudstone and greywacke are typically present in subequal proportions both mudstone and greywacke dominant regions exist. Iron formations are found in both the mudstone and greywacke dominant regions. The iron formations range in thickness from a few centimetres to 20 m. Although gold occurrences are common in iron formation throughout the region, the majority of iron formation is not enriched in gold and does not contain visible sulphide mineralization. Available data suggest that the Contwoyto Formation represents turbidites and iron formation that accumulated on depositional lobes of a submarine fan or fans as defined by Walker (1978).

The Itchen Formation is similar to the Contwoyto Formation but lacks iron formation. Although, in general, the Itchen Formation appears to be thicker bedded and more arenaceous than the Contwoyto Formation, no obvious

differences in grain size, bedding thickness or composition were noted that could be correlated with the lack of iron formation.

Archean plutonic rocks

Bostock (1980) grouped the Archean plutonic rocks in the area into three age groups based on field relationships as follows: an older group of plutons possibly representing basement to the supracrustals; Early Kenoran (Archean) plutons that are essentially coeval with the Point Lake Formation; and Late Kenoran (Archean) plutons that are intrusive into all of the supracrustal formations. The first group consists of the granitic rocks at Keskarrah Bay and is in fact pre-Yellowknife Supergroup as was described above. Recent work by King *et al.* (1988) in the area south and east from Rockinghorse Lake to Contwoyto Lake (Fig. 2.1) has subdivided Bostock's (1980) second and third groups of plutons into six groups. These six groups are divided based on their compositions and interpreted timing of emplacement. The first four groups of plutons (King *et al.* 1988) have all been affected by the major Archean deformations and metamorphism. The fifth and sixth groups are later and are only affected by minor Archean deformation. The fifth group is apparently coincident with peak metamorphism and the sixth group slightly postdates peak metamorphic conditions. Compositions of the plutons evolved with time from early hornblende-diorite and tonalite through to biotite tonalite and granodiorite to monzogranite and syenogranite (King *et al.* 1988).

The majority of the geochronological studies completed in the region on the plutonic rocks are K-Ar determinations, on biotite or muscovite, or Rb-Sr whole rock isochrons. Most of the ages are too young to represent Archean crystallization ages and probably represent final cooling after peak metamorphism (King 1982; Easton 1984). In addition, there may be partial

resetting of Archean isotopic systems by events in the adjacent younger Bear Province to the west (Easton 1983). It is probable the late plutons (fifth and sixth groups) crystallized between about 2600 Ma and 2500 Ma as has been determined for similar plutons elsewhere in the Slave Province (Padgham 1985).

Proterozoic rocks

Aphebian sedimentary rocks including sandstone, argillite and minor dolomite are exposed at Rockinghorse Lake, and northeast of Contwoyto Lake (Fig. 2.1). These rocks are subhorizontally dipping, gently folded and are apparently unmetamorphosed, or metamorphosed to very low grade (Tremblay 1976, Bostock 1980).

Both the Aphebian sedimentary rocks and the Archean rocks are intruded by Proterozoic gabbro and diabase dykes and sills of several ages (Bostock 1980).

D. Metamorphism and deformation

Detailed structural and metamorphic studies have been completed at four areas within the present region of interest. Gardiner (1986) examined a small area around the Lupin mine (Fig. 2.1). Jackson (1984, 1982) mapped and studied the area between the arms of Point Lake. King (1982) and King and Helmstaedt (in press) studied the eastern Point Lake region. Kusky (1987) reports preliminary results of a study in progress at Keskarrah Bay on Point Lake. Early results of a mapping project currently underway in the Contwoyto Lake area are presented by King *et al.* (1988). Additional studies of importance outside the area of interest, or of a more regional nature, include work by Fyson

(1987, 1982) and Thompson (1978). The following description of the metamorphism and deformation is applicable to the region of interest and is drawn mainly from King *et al.* (1988) and Thompson (1978).

Archean structures are complex and comprise (King *et al.* 1988) two phases of isoclinal folding (D_2 and D_3) with associated penetrative cleavage followed by open folding, shearing and fracture cleavage (D_4). Proterozoic structures are not readily recognizable at the outcrop scale in the Archean rocks but do affect the Archean rocks on a regional scale. Fold interference patterns are produced by the intersection of F_2 and F_3 folds (King *et al.* 1988). Metamorphic isograds (Fig. 2.1) are defined in the pelitic sediments by the first appearance of the characteristic minerals biotite, garnet, cordierite, andalusite, sillimanite, and the breakdown of muscovite + quartz to form K-feldspar + sillimanite + H_2O. Garnet is present only in iron-rich beds associated with iron formation. These minerals are characteristic of a low pressure trajectory path in P-T space (Thompson 1978).

The distribution of the isograds suggests that the thermal highs are spatially associated with the fifth group of tonalite plutons (King *et al.* 1988). North of Lupin, the cordierite isograd cuts across F_3 folds, indicating that peak metamorphism probably slightly postdates F_3 folding. The relationship between the fifth group of tonalites, the cordierite isograd and the F_3 folds suggests that the peak metamorphic conditions are coincident in time with, or slightly postdate, the D_3 event. Granodiorite to syenodiorite plutons of the sixth group cut D_3 structures but are affected by D_4 structures (King *et al.* 1988). This implies that these plutons were emplaced after peak metamorphic conditions (King *et al.* 1988).

E. Unmineralized iron formation

The term iron formation is used in the recommended sense of Trendall (1983) for a sedimentary rock whose principal geochemical characteristic is an anomalously high concentration of iron. Also following the recommendations of Trendall (1983) the term "facies" is not used because of the confusion as to whether the mineralogical varieties of iron formation do in fact represent depositional environments and processes. This seems particularly advisable in the present area where variable metamorphic "facies" may have been superimposed on the depositional "facies" and also affected by hydrothermal alteration "facies". The term unmineralized iron formation is used here for iron formation that contains either trace or no visible iron sulphide. Unmineralized iron formation assayed for this study, and for exploration in the area, contains gold values at or near the detection limit of the fire-assay technique.

Since the mineralogy of metamorphosed iron formation is at least in part a function of metamorphic grade (Klein 1983), the descriptions of iron formations are subdivided into low and medium grade areas. Following the convention used in the Slave Province by Thompson (1978), which parallels the usage of Winkler (1979), the cordierite isograd separates low grade slates and metagreywackes from medium grade knotted schists. The low grade areas can be further subdivided into a sub-biotite isograd area, a biotite grade area, and finally a garnet grade area. The breakdown of muscovite + quartz to form K-feldspar + sillimanite + H_2O marks the division between the medium grade schists and the high grade gneisses and migmatites.

Low metamorphic grade areas

Sub-biotite isograd, iron formation is known only between the arms of Point Lake (Fig. 2.1). An outcrop of complexly folded iron formation, located 5 km southwest of the Tree gold occurrence, consists of interbedded oxide- and carbonate-rich beds. Oxide and carbonate iron formation is very fine grained and is well banded at the 1-2 cm scale. Petrographic and XRD work indicates that the grey weathering, oxide iron formation is comprised largely of quartz and magnetite, but often contains lesser amounts of siderite. Reddish-brown weathering, carbonate-rich iron formation contains abundant quartz and siderite, and sometimes, lesser amounts of ankerite. Minor amounts of an iron-rich chlorite are present in both rock types. Interbedded with iron formation is a massive, fine grained, greenish slatey rock comprising iron-rich chlorite (14 Å) and quartz with lesser amounts of carbonates, albite and iron-rich biotite. The abundance of aluminous phases suggests that this iron-rich rock type includes both chemical and fine grained detrital pelitic components; such rocks will be referred to as pelitic iron formation. Iron formation that is comprised largely of silicate minerals, which lacks a pelitic component, is common elsewhere in the region, but is apparently absent at this outcrop and was not seen anywhere in the sub-biotite area. Although biotite is present in the iron formation it is absent in the adjacent pelites which comprise albite, chlorite, quartz, muscovite, graphite and ilmenite. Sulphides are rare; occasional traces of fine grained pyrite are disseminated in oxide and carbonate iron formation.

Iron formation above the biotite isograd, but below the garnet isograd, was examined at the Fingers Lake area (Fig. 2.1), 7 km south of Lupin. Unmineralized iron formation is mainly comprised of iron-rich silicate minerals although bands with up to 20 % disseminated magnetite are common. Silicate iron formation is predominantly comprised of grunerite and quartz but contains

minor amounts of hornblende, stilpnomelane, ilmenite and graphite. Iron-rich chlorite may be present in trace amounts or, in more pelitic parts of the iron formation, may be abundant. Trace amounts of disseminated siderite (XRD) are occasionally noted in magnetite-bearing iron formation; however, minor amounts of siderite are also present in crosscutting quartz veins and the disseminated siderite may represent alteration adjacent to the veins.

Unmineralized iron formation in the garnet grade area is present at Lupin, at Esker Lake south of Lupin, and at Point Lake. Mineralogically, the iron formation in the garnet zone is similar to that in the biotite zone except for the appearance of reddish garnets in pelitic iron formation beds within and adjacent to iron formation. The garnets are typically associated with chlorite-bearing portions of the iron formation. Electron microprobe analyses by Bostock (1977) have shown the garnets to be about 80 % almandine with minor pyrope, grossular and andradite components.

In the garnet zone at Point Lake (Fig. 2.1) unmineralized iron formation, near an unnamed gold occurrence, is comprised of grunerite + quartz ± magnetite with lesser amounts of hornblende and rarely garnet. The differences in the mineralogy of this iron formation to the iron formation 3 km to the south in the sub-biotite zone, which lacks grunerite and contains abundant siderite are significant; however, because of overburden it is not known whether the two areas represent portions of the same iron formation or unrelated beds.

An unmineralized portion of the Lupin iron formation, intersected in drillholes about 220 m north of the East Zone of the Lupin orebody, is typical grunerite, quartz ± magnetite iron formation with minor amounts of hornblende (Fig. 2.2*A*). A sample of this material contains 0.07 ppm Au. Trace amounts of pyrrhotite replace magnetite in a similar, but weakly mineralized, sample from the same drillhole that contains 0.45 ppm Au (Fig. 2.2*B*).

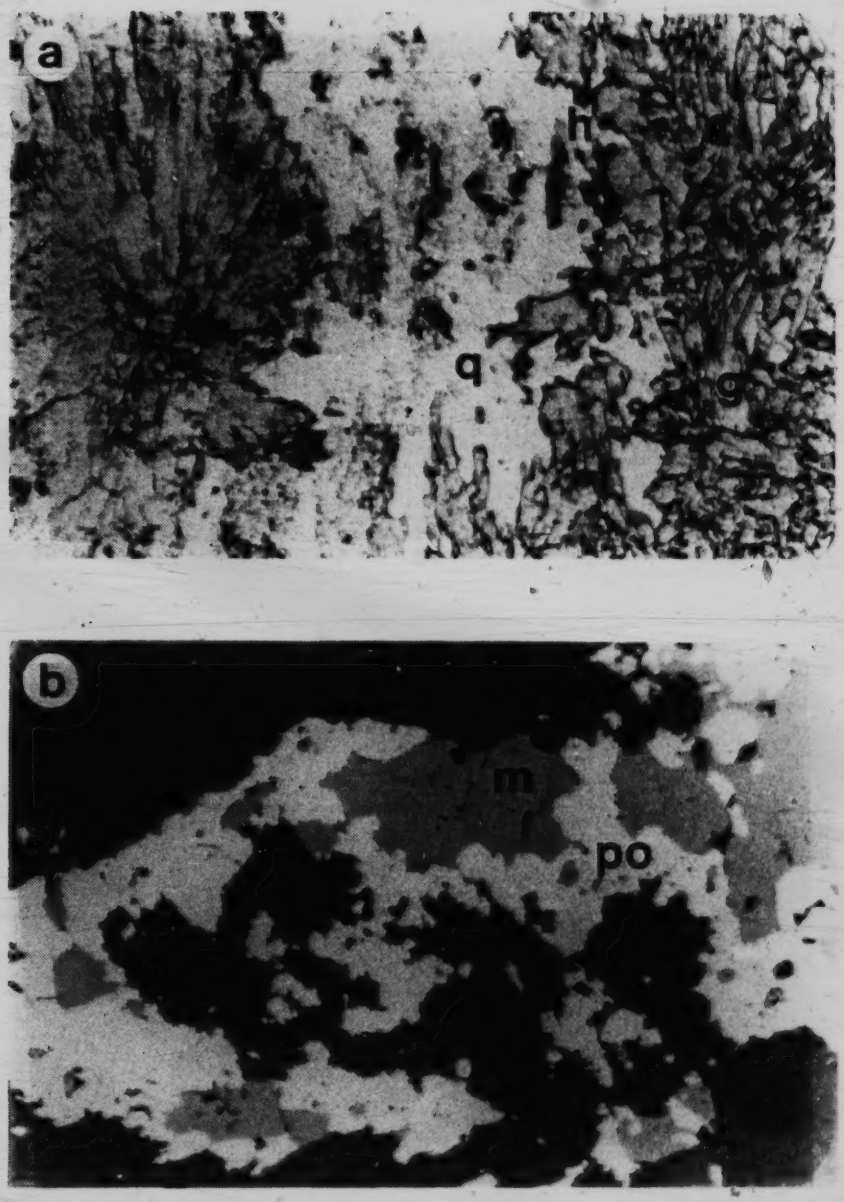

Fig. 2.2. *A.* Photomicrograph of unmineralized grunerite iron formation from the Lupin iron formation northeast of the end of the East Zone (plane polarized light). Grunerite (g) and quartz (q) with minor amounts of hornblende (h) in the quartz rich area. This sample contains 0.07 ppm Au. The base of the photomicrograph is 2.5 mm long. *B.* Photomicrograph of weakly mineralized iron formation with pyrrhotite (po) replacing magnetite (m) from the Lupin iron formation northeast of the end of the East Zone (reflected light). This sample contains 0.45 ppm Au. The base of the photomicrograph is 0.7 mm long.

Medium metamorphic grade areas

Unmineralized iron formation at medium metamorphic grade was examined near the Sik and Share gold occurrences south of Rockinghorse Lake (Fig. 2.1). At both locations iron formation is largely comprised of iron-silicates. In the Sik area magnetite is only rarely present; however, it is common and locally abundant at Share. Silicate iron formation comprises grunerite and quartz with lesser amounts of hornblende, graphite and ilmenite. Four representative samples of silicate ± magnetite iron formation from Sik contain <0.03, <0.03, 0.03 and 0.10 ppm Au. Pelitic iron formation beds contain almandine garnet, chlorite and biotite in addition to the minerals present in silicate iron formation. Although Klein (1983) and references therein state that clinopyroxenes and orthopyroxenes are often present in silicate iron formation at these metamorphic grades, pyroxene is absent in the Contwoyto Lake region except adjacent to quartz veins. All of the pyroxene is clinopyroxene that approaches end member hedenbergite in composition (unpublished electron microprobe data). This hedenbergite is always coarse grained and forms an alteration that is symmetrically zoned about quartz veins. Hedenbergite is therefore not considered to be part of the regional metamorphic assemblage. Fayalitic olivine is rarely present in iron formation where it forms equigranular intergrowths with grunerite and hornblende. Olivine is often mantled by magnetite. Elsewhere, olivine is common in iron formations metamorphosed to medium and high grades (Klein 1983).

Summary

Unmineralized iron formation below the biotite isograd lacks the grunerite, which is present at higher metamorphic grades. This observation is consistent with the detailed study of Haase (1982) and the review paper of Klein

(1983), in which both conclude that the first appearance of grunerite in iron formation is approximately coincident with the first appearance of biotite in adjacent pelites. Numerous metamorphic reactions have been proposed for the formation of grunerite (Klein 1983); however, in view of the abundance of siderite in the lowest grade area it is likely that most of the grunerite was produced by a reaction such as:

$$7 \text{ siderite} + 8 \text{ quartz} + H_2O \rightarrow 1 \text{ grunerite} + 7CO_2 . \quad (1)$$

The presence of minor amounts of hornblende associated with grunerite may be explained by the involvement in the reaction of minor amounts of a calcium-bearing phase (ankerite) and an aluminous phase (chlorite?), which would contain the required Ca and Al to form hornblende. A reaction of this type is proposed by Haase (1982) for the Negaunee Iron Formation in Michigan.

The abundance of magnetite is highest in the sub-biotite isograd area at Point Lake, but magnetite is present, in highly variable amounts, at metamorphic grades up to and including the sillimanite zone. It is uncertain from the present work whether the abundance of magnetite can be directly related to depositional environment, or to metamorphic grade, or other factors.

Thus, the typical iron formation throughout the region, except within the sub-biotite grade area, comprises grunerite and quartz ± magnetite with minor amounts of hornblende. This type of iron formation grades into pelitic iron formation, a mixed rock of chemical sedimentary and pelitic components, which comprises the above minerals plus almandine garnet, chlorite and biotite. Neither of these rock types contain concentrations of iron sulphides greater than trace amounts, and arsenides are entirely absent. Mineralogically, the unmineralized iron formation is similar to typical silicate iron formation described in the literature (Klein 1983).

F. Small-scale gold occurrences in iron formation

Numerous gold occurrences, virtually all of which are hosted by iron formation, are known throughout most of the region. Gold occurrences are spatially associated with increased concentrations of sulphides and arsenides in iron formation at metamorphic grades ranging from the biotite zone to the sillimanite zone. Although the iron formation of the sub-biotite isograd area was prospected and sampled by exploration crews (Keisman 1984), no gold occurrences were discovered, and nearly all of the iron formation samples contained ≤ 0.03 ppm Au. All of the known gold occurrences in iron formation, except Lupin, are small-scale occurrences, many of which contain ore grade gold values, within volumes of mineralized rock too small to be economic. At the small-scale occurrences, gold is associated with increased concentrations of sulphides, which are in turn spatially associated with quartz veins (Kerswill 1985a). Rather than attempting to describe many small-scale occurrences, detailed descriptions of a few well studied occurrences, which are believed to be representative, are presented. These occurrences will be described separately from Lupin.

Biotite zone

The Fingers Lake gold occurrence is within the biotite metamorphic zone 7 km south of Lupin (Fig. 2.1). The occurrence comprises localized concentrations of pyrite and arsenides in iron formation exposed in outcrop, trenches and drillholes. The concentrations of sulphides are erratic along the strike of the iron formation with well mineralized portions of the iron formation limited to a few metres of strike length. Sulphide-poor portions of the iron

formation contain grunerite + quartz ± magnetite with minor amounts of hornblende. The sulphide-rich areas are spatially associated with white to light grey, translucent to opaque quartz veins, with or without siderite. The veins range from centimetres to a few tens of centimetres in width. Quartz in the veins is medium grained, strained, and has wavy or sutured grain boundaries. The veins themselves generally contain trace amounts of pyrite and arsenides; very rarely they contain small specks of visible gold. Exploration assays (Dudek and Woollett 1983) indicate that gold values are erratic and generally low in the veins. In the sulphide-bearing wallrock gold values tend to increase as the concentrations of sulphides increase (Dudek and Woollett 1983).

Arsenides form euhedral crystals that only occur immediately adjacent to veins. In polished thin section the arsenides comprise crystals of arsenopyrite, a few of which contain cores of loellingite. Pyrite is present in more extensive haloes about the veins where it forms fine grained disseminations, sometimes with a banded appearance, and less commonly, coarser grained aggregates or veinlets. Concentrations of pyrite may reach 30 % but are generally less than 5 %. Pyrite can often be seen to replace magnetite (Fig. 2.3), and also may replace amphiboles. Trace amounts of chalcopyrite are associated with pyrite. Tiny inclusions of pyrrhotite occur in magnetite.

Where the iron formation contains abundant sulphides the iron formation is hornblende-rich. Hornblende replaces grunerite leaving isolated islands of grunerite in hornblende. In some samples little or no grunerite is preserved. As distance from the well mineralized part of the iron formation increases, the concentrations of sulphides and hornblende decrease and the concentration of grunerite increases.

A large sample of a typical small, quartz veinlet, that cuts across the banding of the adjacent iron formation, was sawn into three parts and assayed

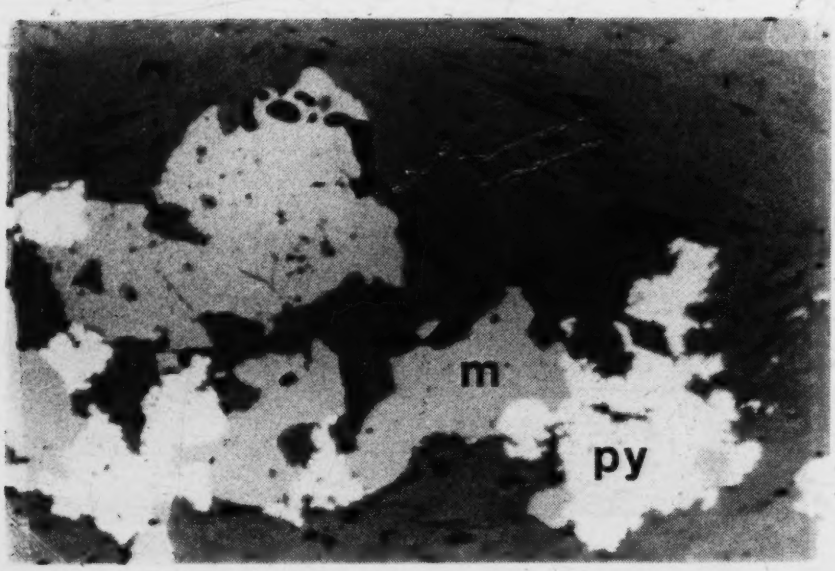

Fig. 2.3. Pyrite (py) replacing magnetite (m) from the Fingers Lake gold occurrence (reflected light). The base of the photomicrograph is 0.7 mm long.

for gold (Fig. 2.4). The 3 cm wide veinlet comprises quartz with some hornblende and traces of pyrite and arsenopyrite. It contains 0.41 ppm Au (Fig. 2.4). The adjacent 2 cm wide hornblende-rich, grunerite-poor iron formation contains magnetite that is partially replaced by pyrite (this sample is shown in Fig. 2.3) which totals about 1 %. A trace of arsenopyrite is also present in this zone which contains 4.53 ppm Au. The remaining portion of the sample, most distant from the vein, comprises grunerite and magnetite with less abundant hornblende. About 0.5 % pyrite is present replacing magnetite and this sample contains 0.69 ppm Au. A sample of grunerite + magnetite iron formation with traces of pyrite from this area, but further from known veins, contains 0.10 ppm Au

Although detailed studies have not been made, observations suggest that more than one generation of quartz veins is present at Fingers Lake. Early, bedding parallel veins and early crosscutting veins are clearly folded and do not have sulphide mineralization associated with them. The veins with associated sulphide enrichment are not obviously folded; however, quartz within them is strained. It appears probable that these veins were emplaced relatively late in the deformational history.

Field observations at other nearby gold occurrences are consistent with those at Fingers Lake. Gold is associated with increased concentrations of pyrite and arsenides that are spatially associated with quartz-veined portions of iron formation. Pyrrhotite, as far as is known, is never the predominant iron sulphide in biotite zone gold occurrences.

Garnet zone

The Esker Lake gold occurrence is about 3 km southeast of the Fingers Lake gold occurrence (Fig. 2.1). Overburden separates the two areas, but

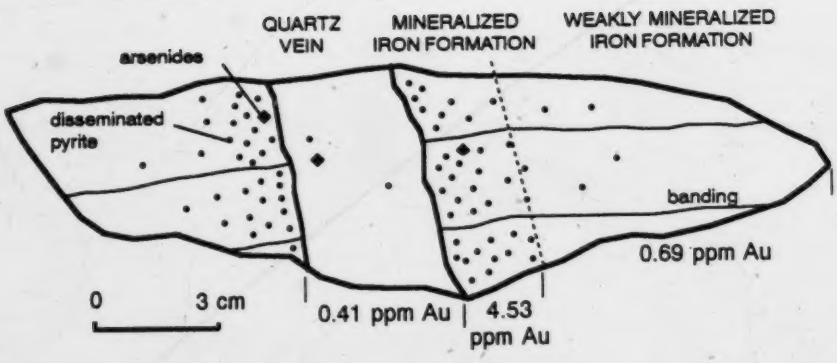

Fig. 2.4. Sketch of mineralization adjacent to a quartz vein in a hand specimen from the Fingers Lake gold occurrence. Gold values were determined on slabs sawn from the sample.

detailed mapping and geophysical surveys by exploration personnel suggest that the two occurrences may be part of the same iron formation. At Esker Lake, most of the iron formation is pelitic and comprises abundant almandine garnet, grunerite and chlorite, but lacks visible sulphides.

Sulphides and gold are restricted to a small portion of the iron formation where a 15 cm wide light grey, glassy quartz vein cuts the 2 m wide iron formation at a right angle (Fig. 2.5). The vein itself contains little or no sulphides and comprises strained, sutured quartz, hornblende and apatite: a sample of the vein assays 0.17 ppm Au. Where the vein crosses the pelitic iron formation, the pelitic iron formation adjacent to the vein lacks macroscopically visible sulphides; however, where the vein intersects a 15 cm wide series of bands of iron formation lacking garnet, these bands contain abundant sulphides. Immediately adjacent to the vein is an arsenide-rich zone that extends for 15 cm from the vein (Fig. 2.6*A*). This zone contains about 40 % coarse grained, diamond-shaped, aggregate porphyroblasts of arsenopyrite intergrown with pyrrhotite. The arsenopyrite grains contain cores of loellingite. Microscopic grains of visible gold often occur on the grain boundaries between the two arsenides. Similar textures of arsenides and gold are clearly seen in excellent photomicrographs of Bostock (1980; Figures 56 to 59) from Lupin and another small-scale gold occurrence that Bostock studied. A sample of the arsenide-rich zone contains 34.29 ppm Au. Other minerals present in the arsenide-rich zone include quartz, hornblende and minor to trace amounts of actinolite and apatite.

At 15 cm from the vein the arsenide-rich zone grades rapidly into a well-banded pyrrhotite-rich zone with occasional, isolated, arsenide porphyroblasts. A sample from the 15 cm to 30 cm interval contains about 40 % pyrrhotite (Fig. 2.6*B*). In thin section the sample comprises abundant pyrrhotite with trace amounts of chalcopyrite, arsenopyrite, loellingite, ilmenite and gold. Other

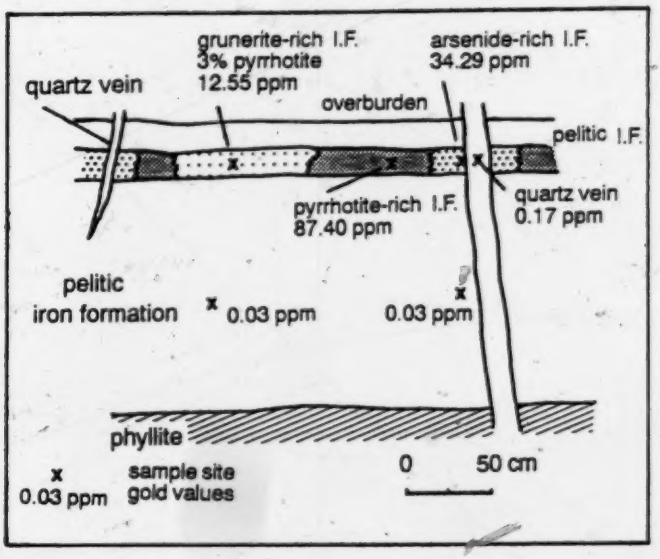

Fig. 2.5. Sketch map of the Esker Lake gold occurrence showing the zonation of gold values and sulphides adjacent to a quartz vein in the nonpelitic portion of the iron formation. Pelitic iron formation is not mineralized adjacent to the vein.

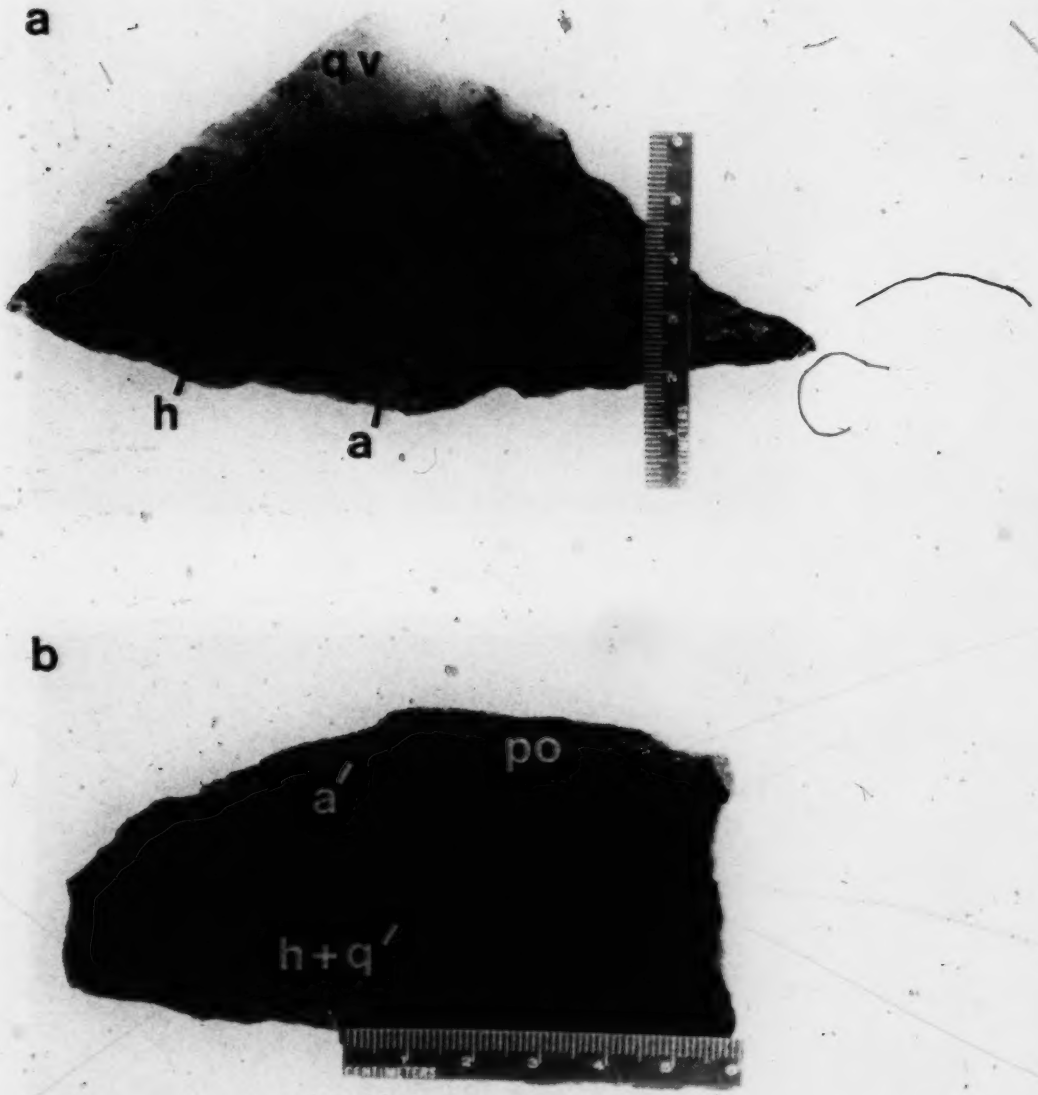

Fig. 2.6. Photomicrographs and hand specimen photographs from the Esker Lake gold occurrence (see Fig. 2.5 for locations of the rock types). *A.* Hand specimen of arsenide-rich mineralization (a) adjacent to quartz vein (qv) with coarse grained hornblende (h). *B.* Hand specimen of pyrrhotite-rich iron formation (po) with minor amounts of arsenides (a), hornblende (h) and quartz (q).

minerals present are abundant quartz and hornblende (Fig. 2.6*C*). Pyrrhotite replaces hornblende in this sample (Fig. 2.6*D*). Minor amounts of grunerite are present as cores in grains of hornblende. The sample of this interval contains 87.40 ppm Au.

As the distance from the vein increases the abundance of pyrrhotite decreases until a distance of 150 cm: a sample of the iron formation from this location contains just 3 % pyrrhotite (Fig. 2.6*E*). In thin section this well-banded sample comprises abundant grunerite, with subordinate hornblende, about 2 % magnetite, traces of arsenopyrite, loellingite, chalcopyrite and ilmenite, and contains 12.55 ppm Au (Fig. 2.6*F*). Fig. 2.6*G* shows that pyrrhotite replaces both grunerite and hornblende, and Fig. 2.6*H* shows that hornblende replaces grunerite in this sample.

Further along strike from the vein the abundance of pyrrhotite begins to increase again as another small crosscutting quartz vein is approached (Fig. 2.5). Thus, there is a well developed zonation to the distribution of gold, sulphides and silicates which is spatially associated with quartz veins that cut the silicate iron formation. The change from dark greenish-black, hornblende-rich iron formation to light yellowish-green, grunerite-rich iron formation is recognizable in hand specimen.

Microscopic examination of garnetiferrous, pelitic iron formation adjacent to the vein shows that the pelitic iron formation contains traces of arsenopyrite and pyrrhotite near the vein which are absent further away. There are no visible changes in the silicate mineralogy that may be related to the vein. Pelitic iron formation has uniformly low gold values both near and far from the veins (Fig. 2.5).

In one location, a few metres away from the gold occurrence, iron formation is visibly altered to a bright green colour adjacent to a quartz vein.

Fig. 2.6. continued. *C.* Photomicrograph (plane polarized light) of pyrrhotite-rich (po) iron formation with abundant hornblende (h), pyrrhotite (po) and quartz (q). The base of the photomicrograph is 2.5 mm long. *D.* Close-up (plane polarized light) of 6*C* showing pyrrhotite replacing hornblende. The base of the photomicrograph is 0.6 mm long.

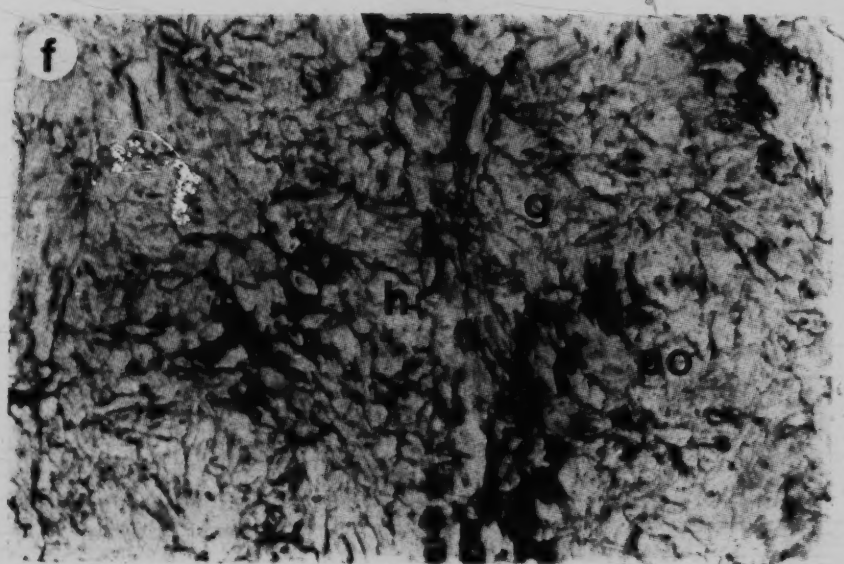

Fig. 2.6. continued. *E.* Hand specimen of weakly mineralized grunerite-rich iron formation with abundant grunerite (g), and lesser hornblende (h), pyrrhotite (p) and arsenides (a). *F.* Photomicrograph of grunerite-rich iron formation (plane polarized light) with grunerite (g), hornblende (h) and pyrrhotite (po). The base of the photomicrograph is 2.5 mm long.

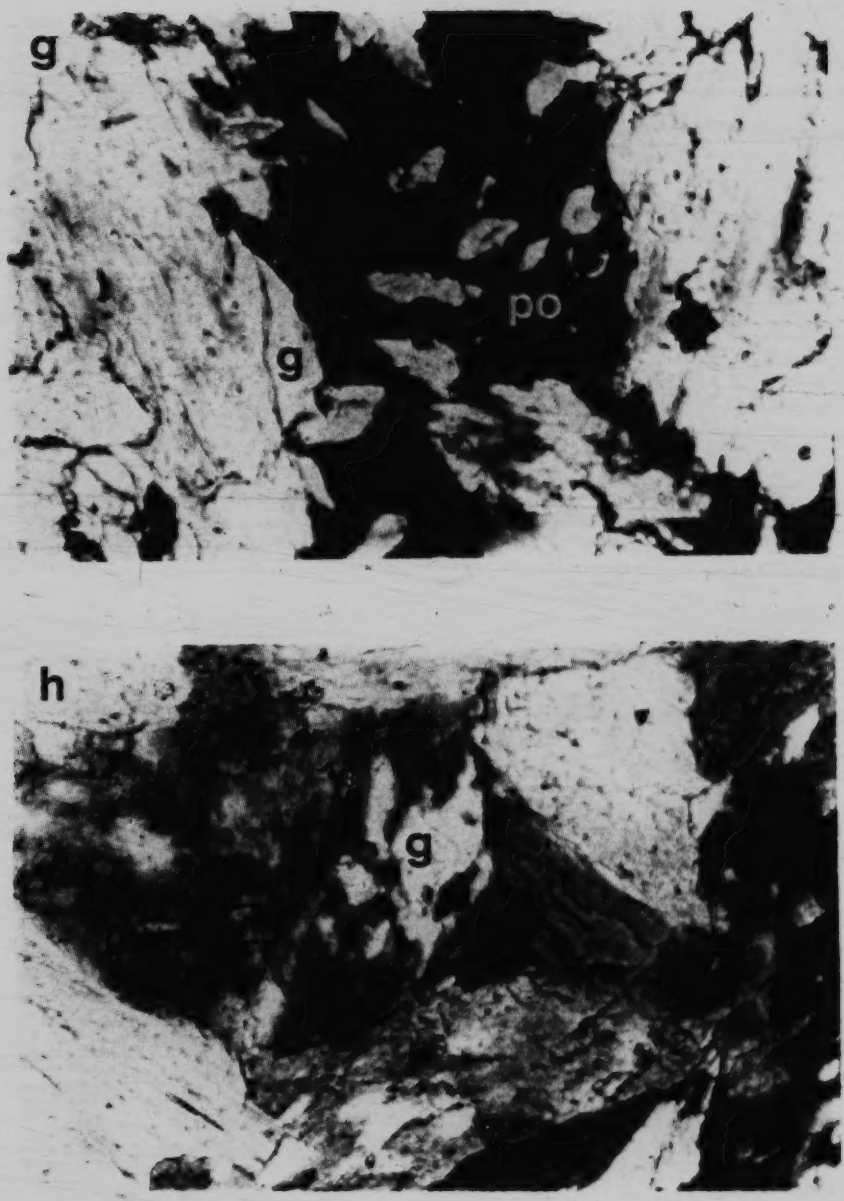

Fig. 2.6. continued. *G.* Close-up (plane polarized light) of 6*F.* showing pyrrhotite (po) replacing grunerite (g) and hornblende (h). The base of the photomicrograph is 0.6 mm long. *H.* Close-up (plane polarized light) from the same thin section as 6*F* . showing hornblende replacing grunerite leaving islands of grunerite (g) in hornblende (h). The base of the photomicrograph is 0.6 mm long.

This rock comprises quartz, epidote and hornblende. Abundant actinolite, that appears to pseudomorph coarse grained pyroxene, is present. Minor and trace phases present include apatite, zircon, pyrrhotite and arsenopyrite. The presence of altered pyroxene and epidote may be significant because these minerals are common in mineralized iron formation at Lupin but are absent in unmineralized iron formation away from quartz veins in the region as a whole.

Medium metamorphic grade

Gold-bearing iron formation in the andalusite zone is very well exposed in a glacially polished outcrop that was stripped clean by exploration crews at the Sik gold occurrence (Fig. 2.1). Examination of exploration assay data from detailed surface sampling and diamond drilling (Dudek and Woollett 1984) in conjunction with detailed mapping of the outcrop indicates that gold is associated with hornblende- and sulphide-bearing portions of a predominantly grunerite-rich iron formation. Numerous discontinuous mineralized zones, that are generally less than a few square metres in plan area, are irregularly distributed within the iron formation. These mineralized zones are spatially associated with quartz veins.

Small crosscutting veinlets of quartz ± hedenbergite have a zoned sequence of alteration adjacent to them (Fig. 2.7*A*). Immediately adjacent to the veinlets is a zone of dark-green to blackish-green alteration of the lighter green iron formation. Banding parallel quartz veins related to the crosscutting veins also have this alteration adjacent to them. Recognition of these banding parallel veins as veins would be difficult without the bordering alteration. Veins associated with alteration range in width from <1 cm to about 2 m, The veins vary in plan view from simple linear forms to irregular masses. In thin section, quartz within the veins is strained and has wavy or sutured grain boundaries.

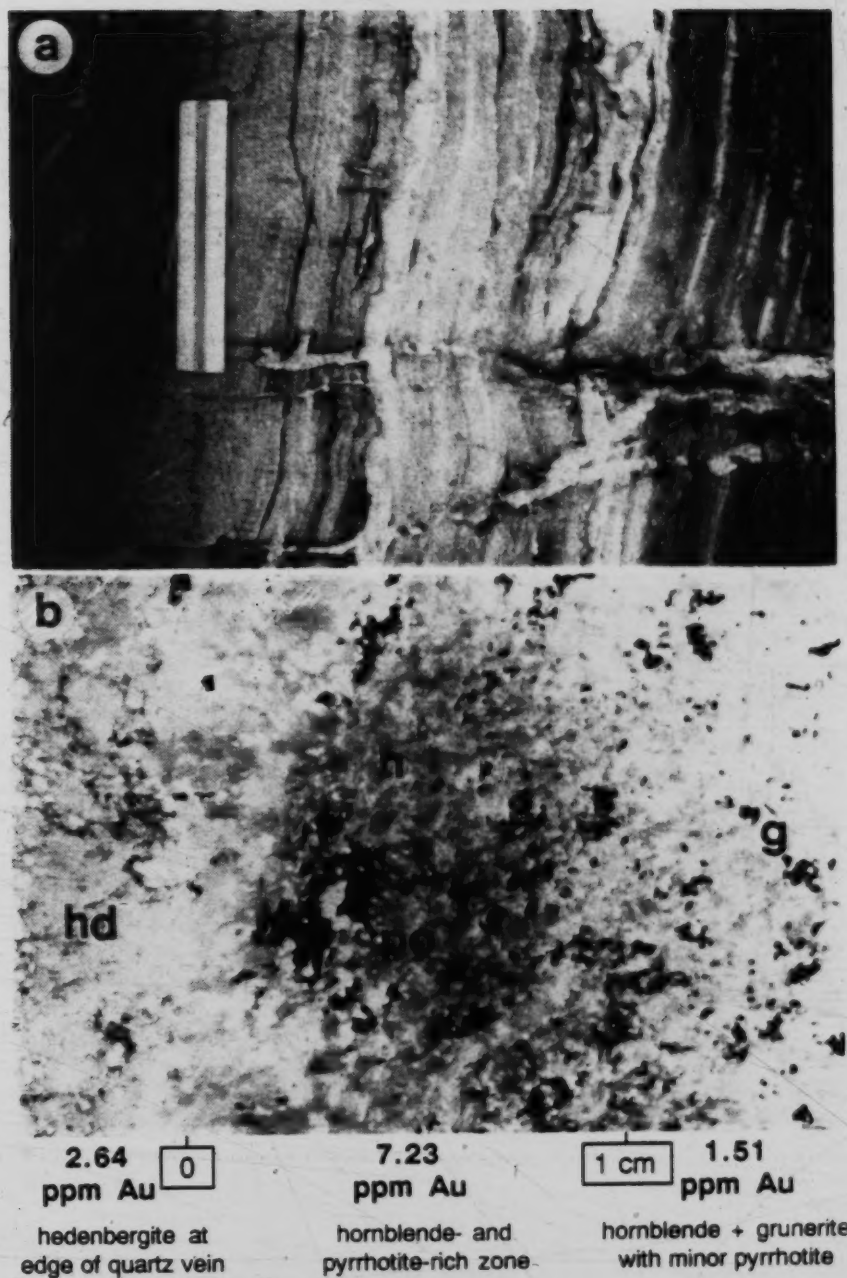

Fig. 2.7. *A.* Outcrop photograph of quartz-hedenbergite veining and alteration of banded grunerite-rich iron formation at the Sik gold occurrence. Note the dark colored alteration adjacent to the vein near the lower end of the scale (scale is 15 cm long). The dark color is due to the abundance of hornblende. Alteration is also present adjacent to small banding-parallel veinlet to the right of the middle of the scale. *B.* Photomicrograph of zoned alteration adjacent to a quartz-hedenbergite veinlet (plane polarized light). The photograph shows the hedenbergite (hd) at the left. In the middle portion of the photo micrograph abundant hornblende (h) and pyrrhotite (po) are present. On the right hand side of the photomicrograph the hornblende-rich zone contains less pyrrhotite and some grunerite (g) is present. Gold values for the zones are indicated. A sample from a distance of 2-4 cm (outside the field of view) contains 0.86 ppm.

Microscopic examination of a typical veinlet indicates that the veinlet comprises quartz and hedenbergite with minor amounts of pyrrhotite (Fig. 2.7*B*). A sample of this veinlet contains 2.64 ppm Au. The 1 cm wide, dark coloured zone of alteration adjacent to the veinlet comprises iron formation with abundant hornblende, and little or no grunerite. This 1 cm wide zone contains 5 % fine grained disseminated pyrrhotite and 7.23 ppm Au. As the distance from the veinlet increases, the abundance of gold, sulphides and hornblende decreases, and the abundance of grunerite increases (Fig. 2.7*B*). A sample of the interval 1-2 cm from the quartz vein margin contains 1.51 ppm Au and a sample of the 2-4 cm interval contains 0.86 ppm Au. Four samples of unmineralized grunerite-rich iron formation from this outcrop contain <0.03, <0.03, 0.03 and 0.10 ppm Au. As at Esker Lake, mineralization is absent in pelitic iron formation adjacent to quartz veins, suggesting that there is a lithologic control on mineralization associated with veining.

Summary: small-scale gold occurrences

At all of the small-scale gold occurrences concentrations of gold are associated with sulphide- and hornblende-rich zones in silicate ± magnetite iron formation. These hornblende-rich zones are spatially associated with quartz veins that cut iron formation and are interpreted as an alteration product of unmineralized, grunerite-rich iron formation. In the biotite metamorphic zone the iron sulphide is predominantly pyrite; at higher metamorphic grades the predominant iron sulphide is pyrrhotite. Iron sulphides replace both magnetite and iron silicates. The arsenides, arsenopyrite and loellingite, form porphyroblasts in which loellingite forms cores to arsenopyrite. Microscopic grains of gold often occur at the arsenopyrite-loellingite grain boundaries. Calc-silicate mineral assemblages of hedenbergite ± epidote are associated with

quartz veins in the garnet zone and higher metamorphic grade zones, but are apparently absent at lower grades.

Many of these characteristics suggest that the sulphides and gold were introduced into the iron formations at the time of vein formation.

G. Lupin

Most of the bedrock geology surrounding Lupin is poorly exposed. Figure 2.8 is a simplified version of a map compiled by company geologists from outcrop, drillhole and geophysical data. In the mine, and to the northwest, beds of iron formation define tight to isoclinal anticlines and synclines (F_3 in the terminology of King *et al.* 1988), with near vertical limbs, that plunge northwesterly at 65-70°. South of the shaft at L-18 and L-16 similar folds plunge to the southeast at about 85°. Although Gardiner (1986) mapped two major faults that parallel the West Zone of the mine, and he inferred about 3.5 km of sinistral offset, based on mapping and geophysical correlations to the southeast, it appears unlikely that there could be any major offset. This is because the traces of iron formations northwest of the mine are not offset (Fig. 2.8). The surface trace of the cordierite isograd cuts across the major folds north of Lupin and intersects the mine workings at depth, thereby defining a southeast dip to the isograd surface (R. Bullis personal communication, 1987). Granitic plutons intrude the folded sedimentary sequence about 1.5 km north of, and 1.5 km southwest of the shaft. Proterozoic gabbro dykes intrude all of the above rock types, but do not occur in the immediate mine area (Fig. 2.8).

The Lupin orebody is divided into three zones, the West, Centre and East Zones, which are actually the limbs of a continuous anticline-syncline pair defined by the Lupin iron formation. All of the gold mined to date at Lupin comes

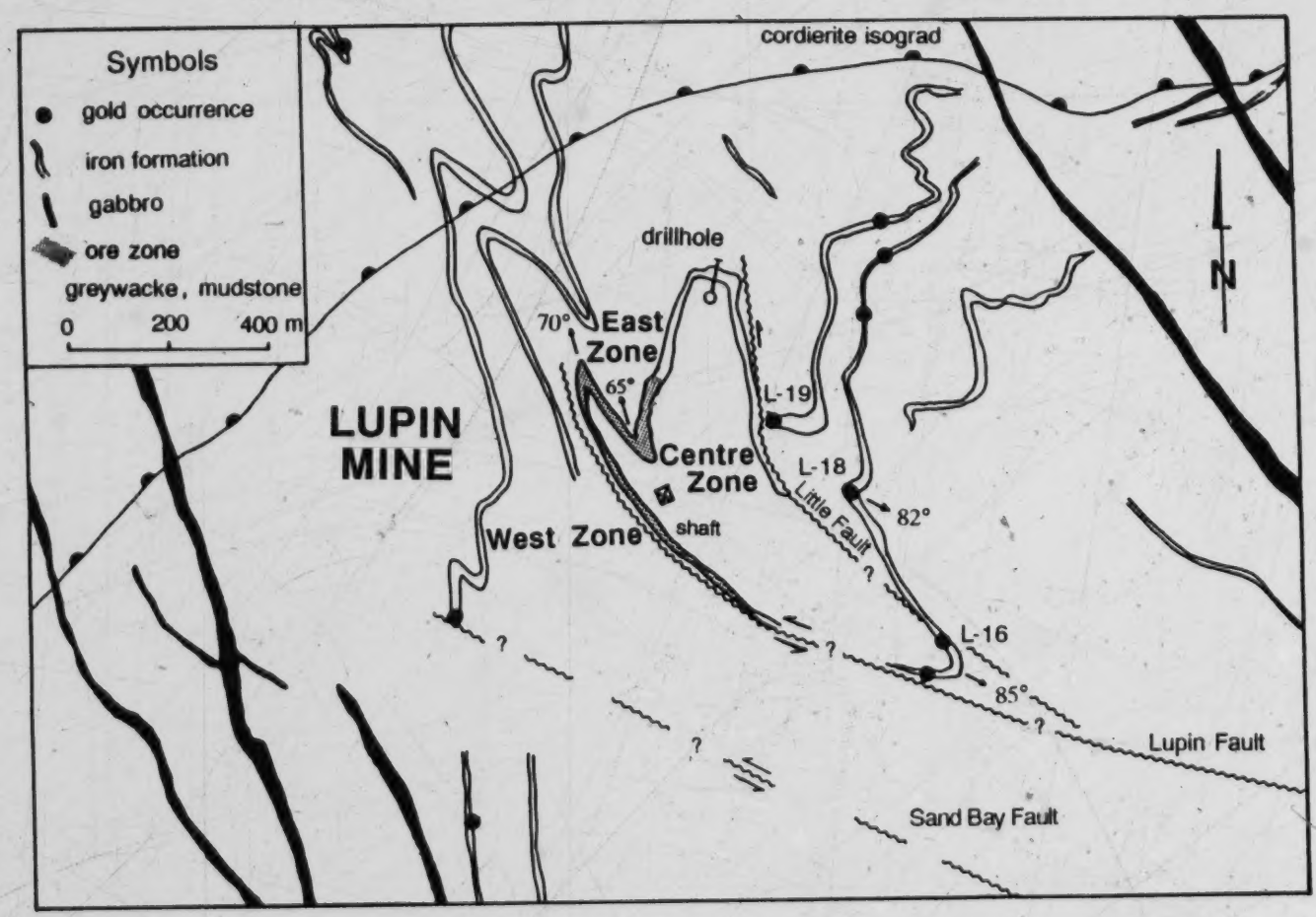

Fig. 2.8. Geology map of the Lupin area showing the ore zones and other localized areas of gold mineralization. Faults and possible faults modified after Gardiner (1986).

from these three zones. Gold mineralization is also present at the L-19, L-18 and L-16 and other occurrences. The L-19 occurrence contains mineable reserves. South of the Centre Zone and underlying the iron formation is a thick sequence of massive arenaceous greywacke. A thin unit of mudstone separates the iron formation from the greywacke. Overlying the iron formation, the clastic sediments are predominantly mudstones, but contain thin, beds of graded greywacke. The grading in the greywacke beds indicates that the sedimentary sequence is upright (R. Bullis personal communication, 1987).

The iron formation unit varies in thickness from about 1 m to about 20 m with the unit being thickest in the East and Centre Zones, and thinner in the West Zone. The unit comprises iron formation, which can be subdivided into mineralized and unmineralized or weakly mineralized varieties depending on the abundance of sulphides, pelitic iron formation, and minor amounts of mudstone and fine grained greywacke. Although the orebody, as mined, contains all of these rock types only the sulphide-rich mineralized iron formation contains economically significant gold values. These rock types are intimately interbedded and range in thickness from a few centimetres up to 2 m. Mapping of the lithologies is difficult because gradational differences exist between mineralized and unmineralized iron formation, between iron formation and pelitic iron formation, and between pelitic iron formation and mudstone.

Mineralized iron formation

Sulphide-rich mineralized iron formation constitutes the principal gold-bearing lithology in the mine. This rock type comprises abundant, fine grained, disseminated grains of pyrrhotite (both hexagonal and monoclinic polytypes) that together with quartz and amphibole commonly form bands in the iron formation (Fig. 2.9). Hornblende is the predominant amphibole and is much

Fig. 2.9. Mineralized iron formation from Lupin. *A*. Hand specimen of pyrrhotite (po) and arsenide-rich (a) ore from the West Zone. Matrix to the sulphides is dark colored due to the abundance of hornblende (h). *B*. Photomicrograph (plane polarized light) of hornblende-rich iron formation from the Centre Zone. Hornblende (h) is intergrown with pyrrhotite (po) and quartz (q). The base of the photomicrograph is 2.5 mm long.

more abundant than grunerite, which never predominates where pyrrhotite is abundant. In well mineralized samples grunerite is often absent. Where grunerite is present it forms the core to grains of hornblende. Coarse grained hedenbergite is often present, and may locally be abundant. Actinolite replaces hedenbergite along fractures and sometimes rims hornblende. Other minor or trace phases include epidote, chalcopyrite, which is intergrown with pyrrhotite, ilmenite and graphite. Pyrite is very rare throughout the deposit except in parts of the West Zone where it locally replaces pyrrhotite.

Adjacent to late quartz veins, 1 cm diameter porphyroblasts of arsenopyrite, containing cores of loellingite, overgrow pyrrhotite. Arsenides are abundant only immediately adjacent to the veins and are absent at distances of greater than about 2 m from veins (Fig. 2.9). Microscopically visible gold is commonly present at the arsenopyrite-loellingite grain boundary (Bostock 1980), but is also present in contact with pyrrhotite, and interstitially to silicates (Kerswill 1986). Although there is generally a positive correlation between the abundance of sulphides and gold, it is difficult to predict gold values from visual estimates of sulphide abundance alone. Representative samples of pyrrhotite-rich iron formation collected for this study contain 9.84, 24.69 and 48.17 ppm Au, while samples of arsenide-rich iron formation contain 7.75, 37.58 and 47.49 ppm Au.

Unmineralized and weakly mineralized iron formation

Unmineralized iron formation, that is iron formation with trace or less than trace amounts of visible sulphide, is rarely present within ore grade portions of the Centre and West Zones, but is more abundant in relatively gold-poor parts of the East Zone. This rock type comprises well banded grunerite and quartz. In thin section, grunerite is the predominant amphibole. Hornblende forms rims to

grains of grunerite and varies from a minor proportion of the total amphibole up to about 50 %. Minor amounts of ilmenite, graphite and pyrrhotite are also present, but arsenides are absent. In weakly mineralized iron formation hornblende and pyrrhotite are more abundant than in unmineralized iron formation. Detailed mapping in the northern part of the East Zone (Fig. 2.8), near the edge of the orebody on the 130 m level, was able to trace weakly mineralized grunerite iron formation into pyrrhotite-rich, hornblende iron formation, and finally into arsenide-rich, hornblende iron formation. This transition occurs along the strike of the banding, as a late quartz vein was approached over a distance of 2.5 m. Representative samples of these three rock types from this location contain 0.10, 9.84 and 7.75 ppm Au, respectively.

Beyond the end of the East Zone (Fig. 2.8) unmineralized grunerite-rich iron formation is the predominant type of iron formation and mineralized iron formation is absent or present only as narrow zones adjacent to quartz veins.

Pelitic iron formation

Pelitic iron formation forms thin, generally <1 m wide, lenses or beds within the Lupin iron formation. Almandine garnet, grunerite, chlorite and quartz comprise the pelitic iron formation. Garnet forms sieve-textured crystals of up to about 5 mm diameter. Grunerite and chlorite are present in highly variable proportions. Where the rock is chlorite-rich, it is often a crenulated schist in which almandine garnet overgrows the early foliation, but predates the late cleavage (Gardiner 1986). Hornblende and biotite are sometimes present, as are trace amounts of ilmenite, graphite, allanite, zircon, and rarely, pyrrhotite and arsenopyrite. Where chlorite-rich pelitic iron formation is intersected by large quartz veins, the grain size of almandine garnet may increase to 2 cm in diameter without any other apparent changes in mineralogy.

Examination of assays of detailed underground channel sampling together with geological maps shows that pelitic iron formation has consistently low gold values. Two representative samples of this rock type from the East Zone contain 0.03 and 0.21 ppm Au.

Quartz veins

At least two generations of quartz veins cut the iron formation unit at Lupin. Early quartz veins are up to a few centimetres wide and are obviously tightly folded. They do not have any visible alteration adjacent to them and will not be discussed further.

Late quartz veins range in width from a few centimetres to about 2 m. These veins are common in iron formation and greywacke, but are less common in the more ductile pelites. Most of the late quartz veins are not obviously folded and form a systematic set as described in detail by Gardiner (1986). He recognized that in the West and Centre Zones the veins consistently strike between 006° and 032° and dip nearly vertically. In the East Zone he found the veins are much less abundant and have more variable orientations that cluster into two sets. One of the sets strikes and dips about 038°/76° SE, which is similar to the orientation of the veins in the West and Centre Zones, and the second set strikes and dips about 101°/77°N. As Gardiner (1986) first noted, there are minor sinistral offsets of up to 1 m of the northerly striking quartz veins along graphitic slip surfaces in the West Zone, and to a lesser degree, in the Centre Zone.

The frequency of late quartz veins is difficult to estimate; however, an indication of the abundance of veins was obtained by using maps prepared by company geologists on what is believed to be a typical portion of the Centre Zone at the 130 m level. Fifty-two veins are indicated on the map over a strike

length of 150 m for an average spacing of about 3 m between veins. Nowhere within the 150 m is there a gap between mapped veins of greater than 8.5 m. Detailed mapping during this study suggests that this estimate of vein density is a minimum estimate because veins of less than about 20 cm in width are commonly not shown on these maps.

In thin section, the veins comprise strained quartz with sutured grain boundaries. Trace amounts of hedenbergite, hornblende, actinolite, pyrrhotite, pyrite, arsenopyrite, loellingite, scheelite, and rarely, visible gold, generally comprise <2 % of the vein material. These veins clearly control the distribution of arsenides which are only present where pyrrhotite-rich, iron formation is intersected by the veins.

Calc-silicate rocks

Sulphide-poor, calc-silicate rocks form a volumetrically minor, but important part, of the Lupin orebody. In hand specimen, they are recognized by their lack of banding and the abundance of coarse grained hedenbergite. The calc-silicate rocks form irregular zones that are often spatially associated with the late quartz vein set. These zones sometimes border the veins, but also form tabular units that parallel the banding in iron formation as well as irregular masses that truncate the banding in iron formation. These zones may be up to 2 m wide and several metres long; however, their abundance and distribution is not well known because they have not been mapped as a separate unit by mine geologists. Calc-silicate rocks occur in the East, Centre and West Zones and from surface to a depth of 410 m, the deepest level examined as part of this study.

Traverses underground with an ultraviolet lamp showed that most of the scheelite present at Lupin is in the calc-silicate rocks. Lesser amounts of

scheelite were noted in sulphide-rich iron formation adjacent to calc-silicate zones, and at the margins of late quartz veins.

Calc-silicate rocks comprise hedenbergite and quartz as the major phases. Epidote is commonly present as a minor component; however, in some samples intergrown epidote and grossular-rich garnet (up to 81 % grossular from electron microprobe analyses) are abundant (Fig. 2.10*A*). Minor phases present include calcite, sphene, apatite, ilmenite and graphite. Microveinlets of hornblende, actinolite, pyrrhotite, arsenopyrite, loellingite and gold cut across and replace hedenbergite in calc-silicate rocks (Fig. 2.10*B*). Assays of three representative calc-silicate rock samples, lacking sulphide microveinlets, all contain ≤0.03 ppm Au, whereas two similar samples with sulphide microveinlets contain 0.48 and 8.95 ppm Au.

The calc-silicate rocks are interpreted to represent alteration zones within the iron formation. Since they are spatially associated with the late quartz veins, and can be seen to cut across small-scale folds, they cannot represent early seafloor alteration of iron formation that has subsequently been metamorphosed.

Felsic dykes

Unlike many other Archean gold deposits (Hodgson and MacGeehan 1982) felsic porphyry dykes are not abundant at Lupin or in the vicinity of other gold occurrences. Only two or three such dykes have been discovered in all of the underground workings (R. Bullis personal communication 1987). The dykes are felsic to intermediate in composition. Age relationships between the dykes and the late quartz vein set have not determined.

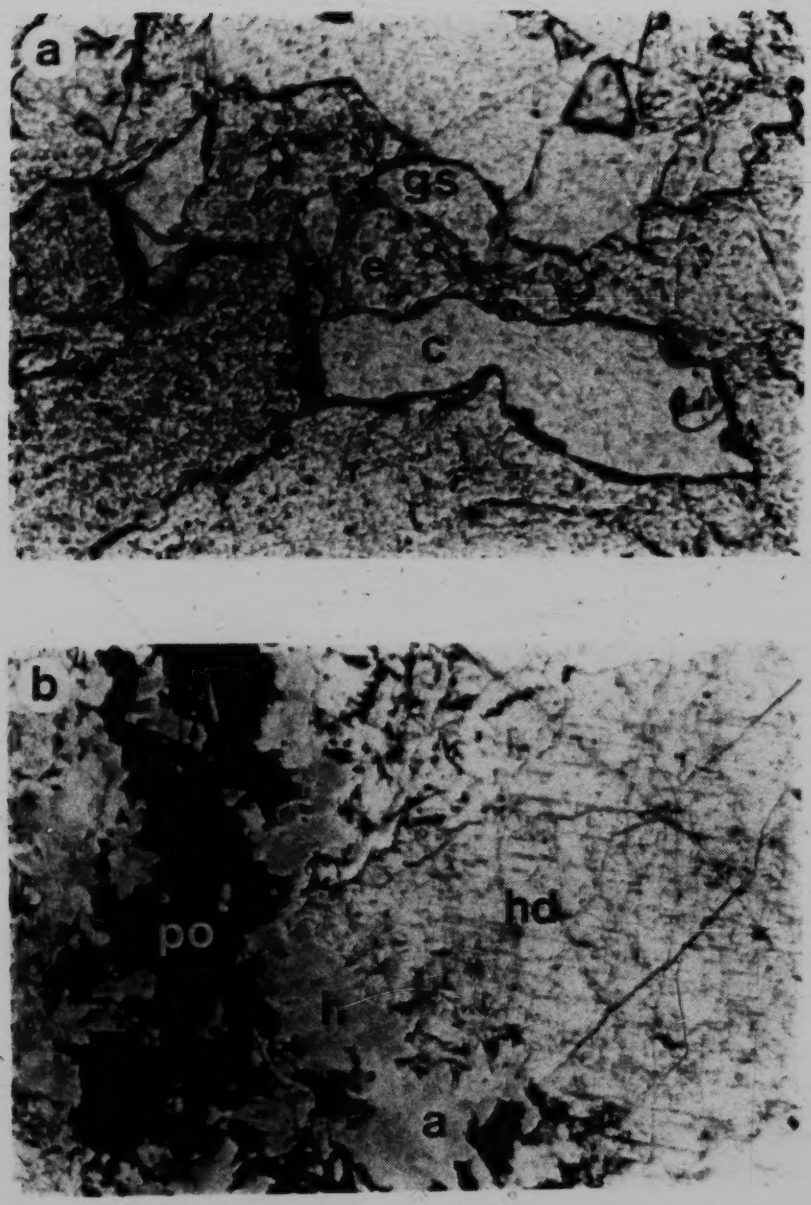

Fig. 2.10. Calc-silicate rocks from the East Zone of the Lupin mine. *A.* Photomicrograph (plane polarized light) of calc-silicate rock. Low relief mineral is calcite (c). The highest relief mineral is scheelite (s). The remainder of the field of view comprises intergrown epidote (e) and grossular garnet (gs) that are difficult to distinguish from each other in this photo. The base of the photomicrograph is 0.6 mm long. *B.* Photomicrograph (plane polarized light) of a veinlet of pyrrhotite (po), hornblende (h) and actinolite (a) cutting across coarse grained hedenbergite (hd). The base of the photomicrograph is 2.5 mm long.

Summary: Lupin

Gold at Lupin is present in pyrrhotite ± arsenide-rich iron formation in which hornblende is the predominant amphibole. Late quartz veins are abundant in the mineralized zones and they obviously control the distribution of arsenides. The timing of the emplacement of the late quartz veins postdates isoclinal folding, but minor deformation has affected the veins. Calc-silicate rocks that represent hydrothermal alteration of iron formation are spatially and temporally associated with the late quartz veins. At the margins of the orebody, in the East Zone, weakly mineralized iron formation, predominantly comprised of grunerite, can be traced along strike into mineralized iron formation, predominantly comprised of hornblende, towards quartz veins. Textures indicate that hornblende replaces grunerite. Unmineralized iron formation along strike from the orebody is grunerite-rich iron formation that is gold poor.

H. Discussion

Genetic models

As stated earlier, three genetic models have been previously proposed to explain the timing and manner in which gold was concentrated in iron formation. Syngenetic models require that the gold was concentrated at an early stage during the deposition of the iron formation on the seafloor. Epigenetic models require that the gold was concentrated at some later time, and that the processes of gold concentration are not related to the deposition of iron formation. Multistage or remobilization models invoke concentration of gold in iron formation on the seafloor followed by further concentration during later geological events.

Whichever model is chosen it must account for three general characteristics of gold deposits associated with iron formation that are present

in the Contwoyto Lake area and are common in many iron formation-hosted deposits worldwide. These general characteristics are:

(1) There is a close spatial association between gold and iron formation. Rock types adjacent to mineralized iron formation often lack gold mineralization.

(2) The gold-bearing zones coincide with sulphide-bearing portions of the iron formation.

(3) The sulphides often, but not always, conform to the banding in the iron formation.

These three general characteristics are often used to support a syngenetic model of gold mineralization but it will be shown that they are also compatible with an epigenetic model.

In the following sections the detailed characteristics of the small-scale occurrences and Lupin will be considered separately and used to build a genetic model for gold mineralization in the area.

Small-scale gold occurrences

An appropriate genetic model that can explain the concentration of gold at the small-scale occurrences must be compatible with the following specific characteristics:

(1) The concentrations of gold coincide with sulphide-bearing zones that are associated with late quartz veins cutting iron formation.

(2) The sulphide mineralogy associated with the gold comprises pyrrhotite, or pyrite in the biotite metamorphic zone, and arsenopyrite, loellingite, and minor amounts of chalcopyrite. The sulphides are generally disseminated and may be concentrated in specific bands within the iron formation.

(3) Pyrrhotite and pyrite replace magnetite and amphiboles.

(4) The predominant amphibole in mineralized iron formation is hornblende, with little or no grunerite. Where both amphiboles are present grunerite is partially replaced by hornblende.

(5) Along strike from the mineralized zones the sulphide-bearing, hornblende-rich mineralized iron formation passes into sulphide and gold-poor unmineralized iron formation that is comprised of grunerite + quartz ± magnetite ± minor amounts of hornblende.

(6) Calc-silicate minerals, such as hedenbergite, sometimes form alteration zones in iron formation associated with the late quartz veins.

(7) Pelitic iron formation, interbedded with the mineralized iron formation is not significantly enriched in sulphides and gold, even where it is immediately adjacent to late quartz veins.

These characteristics, together with the typical abundances of gold in the different rock types, are summarized in a schematic diagram (Fig. 2.11). The diagram does not include a scale because the scales of the various features show extreme variability. For example, the sulphide and gold-bearing zone adjacent to a veinlet at Sik is about 1 cm in width (Fig. 2.7*B*), but a similar zone at Esker Lake is greater than 1 m in width (Fig. 2.5).

An important fact is that symmetrical zonal patterns are developed in the mineralogy and gold abundance adjacent to the quartz veins. The fact that this zonation is developed adjacent to veinlets suggests that the transition from sulphide-bearing iron formation to unmineralized iron formation is not a depositional or diagenetic facies change. This observation and many of the listed characteristics do not support a simple syngenetic model for the concentration of gold at the small-scale occurrences. The relationship between quartz veining, sulphides and gold mineralization strongly suggests that these are epigenetic, or possibly, highly remobilized gold occurrences.

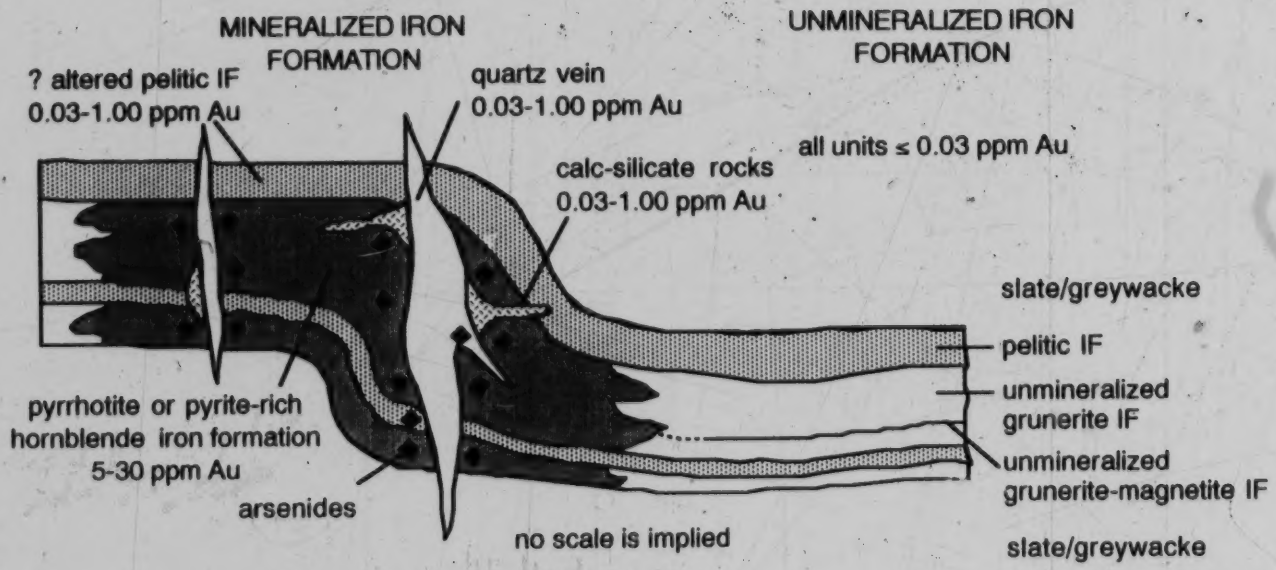

Fig. 2.11. Schematic summary diagram of the relationships between quartz veining and gold mineralization in iron formation in the Contwoyto Lake-Point Lake region. The mineralogy and typical gold values of iron formation and associated units are shown. A scale is not indicated because the relationships occur at scales ranging from a hand specimen to an ore zone.

An epigenetic model implies that gold, and the associated elements S and As, were added to mineralized iron formation from a source external to the iron formation. In addition, the abundance of hornblende (a Ca-bearing mineral) in mineralized iron formation suggests that Ca may also have been added during mineralization. If a model involving local remobilization is to be applied, it assumes that the Au, S, As and Ca were derived from nearby iron formation and concentrated adjacent to the vein during vein formation.

Previously proposed models that invoke local remobilization such as Rye and Rye (1974) for the Homestake deposit, and Hallager (1984) for the Jardine deposit, are generally vague as to the scale of remobilization and the mechanism by which components are remobilized. Low analytical values for gold, the absence of S- and As-rich phases, and the presence of only minor amounts of Ca-bearing minerals away from the veins, suggests that these elements are not regionally enriched in iron formation. These observations make a local remobilization model, in which transport of components on the scale of a few metres, or tens of metres, an unlikely scenario the feasibility of which is yet to be proven.

An epigenetic model is favoured in which the quartz veins represent infillings of fractures that allowed hydrothermal fluids to flow into the iron formation. These fluids deposited silica in the veins and Au, As and S in the adjacent wallrock. This model can account for the observed zonal pattern in sulphide and silicate mineralogy associated with the quartz veins and the textures of sulphides replacing preexisting minerals. It can also account for the formation of new calcic mineral assemblages adjacent to the veins.

The observation that iron oxide and iron silicate minerals are selectively replaced by sulphides is critical because of the close association between sulphides and gold. Such selective replacement implies that the original

distribution of iron-rich phases can control the distribution of epigenetic sulphides. Selective replacement of bands of iron-rich minerals can explain the abundance of sulphides adjacent to the vein at Esker Lake in iron formation, while the pelitic iron formation adjacent to the vein lacks sulphides and gold (Fig. 2.5). This suggests that selective replacement occurs on two scales: first on the scale of the individual iron-rich mineral grains producing the disseminated or banded distribution of sulphides that mimics the original banding of the iron-rich minerals; and second, on the scale of individual beds of iron-rich lithologies that will, together with the frequency of fractures, control the thickness and lateral extent of the mineralized zone.

A simple, single stage epigenetic model of mineralization in which Au and the associated elements S, As and Ca were added to iron formation from an external source is consistent with the available data and is therefore favoured for the small-scale occurrences. This model has also been proposed by Kerswill (1985a) for some of these occurrences.

Comparison of Lupin to the small-scale gold occurrences

It is important to realize that all seven of the characteristics that were used to support an epigenetic model for gold concentration at the small-scale occurrences are also present at Lupin.

The main differences between Lupin and the small-scale occurrences include:

(1) The much greater size and continuity of the sulphide and gold-bearing zones at Lupin.

(2) The calc-silicate alteration zones are absent or weakly developed at some of the small-scale gold occurrences relative to Lupin.

The differences in the size of the mineralized zone and continuity of mineralization at Lupin can be explained by a greater intensity of fracturing, veining and alteration at Lupin that resulted in more extensive sulphidation of the iron formation. It should be emphasized that in a relatively weakly mineralized part of the mine, weakly mineralized grunerite-rich iron formation with low gold values could be traced into ore grade, mineralized, hornblende-rich iron formation as a quartz vein was approached over a distance of 2.5m. This situation is directly comparable with the transition at the small-scale occurrences. The other difference between Lupin and the small-scale occurrences is the greater abundance of calc-silicate alteration zones at Lupin. This can also be explained by an epigenetic model in which these zones represent the most intense alteration of iron formation. This would be expected where the mineralization, and presumably alteration, were the greatest. It is therefore valid to use Fig. 2.11 as a model for both Lupin and the small-scale occurrences.

Two characteristics of Lupin, the banding of sulphides and the fact that gold is greatly enriched in sulphide-bearing beds within the iron formation have been interpreted to be due to syngenetic deposition of sulphides and gold (Kerswill 1986, 1985a,b, 1984; Padgham 1984; Franklin and Thorpe 1982). The distribution of the sulphides can be explained by selective sulphidation of iron-rich minerals and iron-rich beds. If gold is transported as an aqueous gold-sulphide complex then deposition of gold will coincide with the deposition of sulphides (Phillips and Groves 1983).

Conversely a syngenetic model cannot explain the zonation of sulphide and silicate mineralogy adjacent to quartz veins. The syngenetic model also cannot explain the presence of the calc-silicate rocks at Lupin which are evidence for Ca enrichment of the iron formation that postdates early

deformation and is apparently associated with the late quartz veining. The increase in the abundance of Ca-bearing silicates like hornblende in the mineralized iron formation is consistent with the development of the calc-silicate rocks.

Like the small-scale occurrences, the Lupin iron formation, beyond the end of the East Zone and within a weakly mineralized portion of the East Zone, comprises weakly mineralized grunerite-rich iron formation, lacking enriched gold concentrations. This suggests that a local remobilization model is not appropriate for Lupin either. It is therefore clear that an epigenetic model of gold mineralization can explain all of the critical characteristics of Lupin and the small-scale occurrences. The compositions and abundances of minerals associated with gold at Lupin, suggest that like the small-scale occurrences Au, S, As and Ca were added during epigenetic mineralization. The presence of scheelite in these calc-silicate rocks indicates that W was also introduced into iron formation during this alteration.

Timing of the mineralization

Since an epigenetic model is favoured for all of the gold occurrences in iron formation in the area it is important to examine the timing of the emplacement of the late quartz veins. Detailed work by Gardiner (1986) at Lupin suggests that the veins were emplaced after early isoclinal folding, but preceeding the final Archean deformation. This has resulted in systematically oriented, sheet-like veins, that show little sign of folding, but comprise strained and sutured quartz. Observations on the late quartz veins at small-scale occurrences are limited, but are consistent with these data.

Observations on quartz veining have also been made during the course of regional mapping by King *et al.* (1988). King *et al.* 's (1988) descriptions of

the quartz veins associated with the D_3 deformation indicate that they are the same vein set described by Gardiner (1986) at Lupin, and described here at small-scale occurrences, that are referred to here as the "late" quartz veins. King *et al.* (1988) state that these veins are present regionally but are best developed in iron formation and greywacke lithologies. They further state that these veins form arrays of conjugate veins that are symmetrically oriented about the S_3 cleavage, but in any given outcrop one member of the set is generally dominant. This last observation is consistent with the pattern of veining at Lupin described by Gardiner (1986). Since these veins are interpreted to have been emplaced during the D_3 event (King *et al.* 1988) and the peak metamorphism is interpreted to be coincident or slightly postdating D_3, the veins must have been emplaced at near peak thermal conditions.

Alteration mineral assemblages associated with the late quartz vein set vary according to the regional metamorphic grade. For example, hedenbergite is absent in the biotite grade areas and pyrite is the predominant iron sulphide whereas at higher metamorphic grades hedenbergite is abundant and pyrrhotite is the predominant iron sulphide. These variations can be interpreted as either the result of different temperatures of hydrothermal alteration in different areas that coincide with variations in the metamorphic grade, or as overheating of hydrothermal alteration assemblages developed at lower metamorphic grades by subsequent higher grade metamorphism.

To summarize, the evidence suggests that the introduction of the gold into iron formation occurred at the time of quartz vein formation, which postdates early regional deformation (D_2 of King *et al.* 1988). Quartz veining and alteration is coincident with later deformation (D_3) and near peak metamorphic conditions.

I. Comparison of the Contwoyto Lake gold occurrences to other iron formation-hosted gold deposits

Many of the features described here have been noted in other gold deposits in iron formation where they have been interpreted to be the result of epigenetic mineralization. For example, the genetic association between mineralization and quartz veining has been noted in several Australian gold deposits (Phillips *et al.* 1984; Groves *et al.* 1987) and at the Vubachikwe Mine in Zimbabwe (Fuchter and Hodgson 1986; Phillips *et al.* 1984). Macdonald (1983), and Anglin and Franklin (1985) have demonstrated that epigenetic gold mineralization, with associated sulphidation, occurs adjacent to quartz veins in iron formation at Geraldton in northern Ontario. Phillips *et al.* (1984) describe the replacement of magnetite by pyrrhotite near quartz-pyrrhotite veinlets at the Water Tank Hill deposit. Similar relationships exist at the Fingers Lake gold occurrence, where pyrite replaces magnetite, and along strike from the Lupin deposit, where pyrrhotite replaces magnetite.

Phillips and Groves (1983), Phillips *et al.* (1984) and Macdonald and Fyon (1986) have previously noted that sulphidation of iron formation is an efficient way of depositing gold from hydrothermal fluids. Sulphidation promotes deposition of gold by the breakdown of aqueous gold-sulphide complexes to form iron sulphide minerals thereby decreasing the amount of aqueous sulphide available to complex gold. This reaction can explain the close association between the distribution of gold and sulphides. Iron-rich rocks are very reactive with sulphides-bearing fluids and are the most favourable host rocks for the deposition of gold by sulphidation (Phillips and Groves 1983). This fact, together with to fact that quartz veins are commonly well developed in iron formations, predicts that iron formations are likely to be mineralized by this sulphidation process.

The elemental association of Au, As, S and W, found in the mineralized Contwoyto Lake iron formations, is typical of iron formation-hosted gold deposits and Archean epigenetic gold deposits in general, regardless of their host rock type (Phillips and Groves 1983).

One significant difference between the Contwoyto Lake deposits and other iron formation-hosted deposits is the predominance of silicate mineral alteration assemblages at Contwoyto Lake. In many localities carbonatization is the principal form of alteration associated with gold mineralization in iron formation (Macdonald 1983; Anglin and Franklin 1985); however, Phillips *et al.* (1984) report that at the Nevoria Mine in Western Australia diopsidic clinopyroxene and Fe-rich actinolite are associated with the mineralization. Cummingtonite, of unspecified composition, is the predominant silicate mineral of the iron formation away from mineralization. Pyrrhotite replaces cummingtonite and possibly also magnetite. This alteration is very similar to the alteration at the small-scale gold occurrences, and Lupin, where hornblende, and sometimes hedenbergite and actinolite, are associated with veining and mineralization. Minor amounts of siderite that are present in and adjacent to quartz veins at the Fingers Lake gold occurrence probably represent carbonate alteration. It is possible that evidence of silicate alteration assemblages exists at other areas but has been overlooked by researchers concentrating on the sulphide mineralogy.

McConnell (1964) pointed out that there are several similarities between the Contwoyto Lake gold deposits and the famous Homestake deposits in South Dakota. The similarities McConnell listed include: the regional metamorphic grade and structural geology; the lithologies of the iron formation and adjacent rocks; the association between gold, pyrrhotite and arsenopyrite; and the presence of quartz veins. One major difference that is present in the

mineralogy of the iron formation in the two areas is that at Homestake, in the biotite metamorphic grade portion of the mine, Mg-bearing siderite (commonly referred to as sideroplesite) is common in the iron formation (Rye and Rye 1974). In the garnet zone the Homestake iron formation includes abundant cummingtonite. In the Contwoyto Lake area carbonates are not present in mineralized iron formation except for trace amounts of calcite in the calc-silicate rocks at Lupin, and minor amounts of siderite at the Fingers Lake occurrence.

Gold mineralization at Homestake occurs in chloritized portions of the sideroplesite and cummingtonite iron formation that are associated with increased concentrations of pyrrhotite, pyrite, arsenopyrite and quartz veining (Rye and Rye 1974 and references therein). The Homestake deposits have been variously interpreted as remobilized syngenetic exhalative deposits (Rye and Rye 1974), and as epigenetic deposits of Precambrian to Tertiary age (Noble 1950 and references therein).

J. Summary and Implications

This study has shown that an epigenetic model can account for all of the characteristics of all of the known gold deposits hosted by iron formation in the Contwoyto Lake-Point Lake region. In addition to Au the elements S, As, Ca and W were also added to iron formation during the epigenetic mineralization.

Observations suggest that the quartz veining and associated hydrothermal alteration occurred after early Archean deformation and may have accompanied peak metamorphism. It is noteworthy that the sub-biotite zone area, the lowest metamorphic grade area, contains iron formation, but is unusual in that it lacks any known gold occurrences. This may indicate that the late thermal metamorphism is an integral part of gold mineralization, an idea

previously proposed by Padgham (1986), for vein-gold deposits, hosted by greywacke and mudstone turbidites, in the southern Slave Province.

Thus it seems that several criteria must be simultaneously satisfied in order to form an iron formation-hosted gold deposit of economic size. The iron formation must be of sufficient size to contain an economic deposit. The iron formation must have sufficient structurally induced permeability to allow circulation of hydrothermal fluids to a significant portion of the iron formation. The gold-bearing hydrothermal fluids must efficiently deposit their gold in conjunction with deposition of sulphides. If mineralization is related to the late thermal metamorphism then there may be a lower limit to the metamorphic grade in which gold deposits could form.

K. References

Anglin, C. D., and Franklin, J. M. 1985. Gold mineralization in the Beardmore-Geraldton area of northwestern Ontario: Structural considerations and the role of iron formation. *In* Current research, part A, Geological Survey of Canada, paper 85-1A, pp.193-201.

Bau, A. F. S. 1979a. Geological map of 86H/9 District of Mackenzie: Department of Indian Affairs and Northern Development, Geology Division, Preliminary Geological Map EGS-1979-2A.

Bau, A. F. S. 1979b. Geological map of 86H/10 District of Mackenzie: Department of Indian Affairs and Northern Development, Geology Division, Preliminary Geological Map EGS-1979-2B.

Bau, A. F. S. 1979c. Geological map of 86H/11 District of Mackenzie: Department of Indian Affairs and Northern Development, Geology Division, Preliminary Geological Map EGS-1979-2C.

Bau, A. F. S. 1979d. Geological map of 86H/14 District of Mackenzie: Department of Indian Affairs and Northern Development, Geology Division, Preliminary Geological Map EGS-1979-4A.

Bau, A. F. S. 1979e. Geological map of 86H/15 District of Mackenzie: Department of Indian Affairs and Northern Development, Geology Division, Preliminary Geological Map EGS-1979-4B.

Bau, A. F. S. 1979f. Geological map of 86H/16 District of Mackenzie: Department of Indian Affairs and Northern Development, Geology Division, Preliminary Geological Map EGS-1979-4C.

Bostock, H. H. 1980. Geology of the Itchen Lake area, District of Mackenzie. Geological Survey of Canada, Memoir 391.

Bostock, H. H. 1977. The composition of hornblende, grunerite, and garnet in Archean iron formation of the Itchen Lake area, District of Mackenzie, Canada. Canadian Journal of Earth Sciences, **14**: 1740-1752.

Bouma, A. H. 1962. Sedimentology of some flysch deposits. Elsevier, Amsterdam, The Netherlands.

Bubar, D. S., and Heslop, J. B. 1985. Geology of the Gondor volcanogenic massive sulphide deposit. Slave Province, N.W.T. Canadian Institute of Mining and Metallurgy, **78**: Number 876, 52-60.

Dudek, D. P., and Woollett, G. N. 1984. Exploration-1984. SIK 1 mineral claim, Contwoyto Lake, Northwest Territories. Unpublished report prepared for Echo Bay Mines Ltd.

Dudek, D. P., and Woollett, G. N. 1983. Exploration-1983. BRI 1, DER 1, PEN 1 mineral claims, Contwoyto Lake, Northwest Territories. Unpublished report prepared for Echo Bay Mines Ltd.

Easton, R. M. 1985. The nature and significance of pre-Yellowknife Supergroup rocks in the Point Lake area, Slave Structural Province, Canada. *In* Evolution of Archean Supracrustal Sequences. *Edited by* L. D. Ayres, P. C. Thurston, K. D. Card, and W. Weber, Geological Association of Canada, Special Paper 28, pp. 153-167.

Easton, R. M. 1984. Compilation of geochronologic data for the Yellowknife greenstone belt (85 J/8, 85 J/9) and vicinity, District of Mackenzie, N.W.T. Contributions to geology of the Northwest Territories, **1**: 1-20.

Easton, R. M. 1983. Regional resetting of Rb-Sr and K-Ar isotopic systems at ca. 1770 Ma in the Bear and Western Slave Provinces, N.W.T. Geological Association of Canada, Program with Abstracts, **8**: A19.

Easton, R. M., Boodle, R. L., Zalusky, L., Eiche, G., and McKinnon, D. 1981. Geology of 86H/3, H/4, H/5 and H/6, District of Mackenzie: Department of Indian Affairs and Northern Development, Geology Division, Preliminary Geological Map EGS-1981-5.

Franklin, J. M., and Thorpe, R. I. 1982. Comparative metallogeny of the Superior, Slave and Churchill Provinces. *In* Precambrian sulphide deposits. *Edited by* R. W. Hutchinson, C. D. Spence, and J. M. Franklin. Geological Association of Canada, Special Paper 25, pp. 3-90.

Franklin, J. M., Lyndon, J. W., and Sangster, D. F. 1981. Volcanic-associated massive sulfide deposits. *In* Economic Geology 75th Anniversary Volume. *Edited by* B. J. Skinner, Econmic Geology, pp. 485-627.

Fripp, R. E. P. 1976. Stratabound gold deposits in Archean banded iron formation, Rhodesia. Economic Geology, **71**: 58-75.

Fuchter, W. A. H., and Hodgson, C. J. 1986. Gold deposits of the North Western Mining Camp, Gwanda Greenstone Belt, Zimbabwe. *In* Gold'86 Proceedings Volume. *Edited by* A. J. Macdonald, Gold'86, pp. 255-269.

Fyson, W. K. 1987. A succession of quartz veins in Archean metaturbidites, Yellowknife Bay, Slave Province, Canada. Canadian Journal of Earth Sciences, **24**: 698-710.

Fyson, W. K. 1982. Complex evolution of folds and cleavages in Archean rocks, Yellowknife, N.W.T. Canadian Journal of Earth Sciences, **19**: 878-893.

Gair, J. E. 1962. Geology and ore deposits of the Nova Lima and Rio Acima Quadrangles Minas Gerais, Brazil. United States Geological Survey Professional Paper 341-A.

Gardiner, J. J. 1986. Structural geology of the Lupin gold mine, Northwest Territories. M.Sc. thesis, Acadia University, Wolfville, Nova Scotia.

Gibbins, W. 1981. Gold and Precambrian iron formation in the Northwest Territories. *In* Proceedings of the Gold Workshop, Yellowknife, 1979. *Edited by* R. D. Morton, Yellowknife Gold Workshop Committee, pp. 258-287.

Groves, D. I., Phillips, G. N., Falconer, L. J., Houstoun, S. M., Ho, S. E., Browning, P., Dahl, N., and McNaughton, N. J. 1987. Evidence for an epigenetic origin for BIF-hosted gold deposits in the greenstone belts of the Yilgarn Block, Western Australia. *In* recent advances in understanding Precambrian gold depsoits. *Edited by* S. E. Ho and D. I. Groves, Geology Department & University Extension, University of Western Australia, Publication II, pp. 167-179.

Haase, C. S. 1982. Metamorphic petrology of the Negaunee Iron Formation, Marquette District, Northern Michigan: Mineralogy, metamorphic reactions, and phase equilibria. Economic Geology, **77**: 60-81.

Hallager, W. S. 1984. Geology of gold-bearing metasediments near Jardine, Montana. *In* Gold'82: the geology, geochemistry of gold deposits. *Edited by* R. P. Foster, Geological Society of Zimbabwe Special Publication 1, pp. 191-218.

Hamilton, J. V., and Hodgson, C. J. 1986. Mineralization and structure of the Kolar gold field, India. *In* Gold'86 Proceedings Volume. *Edited by* A. J. Macdonald, Gold'86, pp. 270-283.

Henderson, J. B. 1981. Archaean Basin Evolution in the Slave Province, Canada. *In* Plate Tectonics in the Precambrian. *Edited by* A. Kroner. Elsevier, Amsterdam, The Netherlands, pp. 216-236.

Henderson, J. B. 1975. Sedimentological studies of the Yellowknife Supergroup in the Slave Structural Province. *In* Current research, part A. Geological Survey of Canada, paper 75-1A, pp. 325-330.

Henderson, J. B. 1970. Stratigraphy of the Yellowknife Supergroup, Yellowknife Bay; Prosperous Lake area, District of Mackenzie. Geological Survey of Canada, paper 70-26.

Henderson, J. B., and Easton, R. M. 1977a. Archean supracrustal-basement rock relationships in the Keskarrah Bay map-area, Slave Structural Province, District of Mackenzie. Geological Survey of Canada, Open File 447.

Henderson, J. B., and Easton, R. M. 1977b. Archean supracrustal-basement rock relationships in the Keskarrah Bay map-area, Slave Structural Province, District of Mackenzie. *In* Current research, part A. Geological Survey of Canada, paper 77-1A, pp. 217-221.

Henderson, J. B., Loveridge, W. D., and Sullivan, R. W. 1982. A U-Pb study of zircon from granitic basement beneath Yellowknife Supergroup, Point Lake, District of Mackenzie. *In* Current research, part C. Geological Survey of Canada, paper 82-1C, pp. 173-178.

Hodgson, C. J., and MacGeehan, P. J. 1982. A review of the geological characteristics of "gold-only" deposits in the Superior Province of the Canadian Shield. *In* Geology of Canadian Gold Deposits. *Edited by* R. W. Hodder and W. Petruk, Canadian Institute of Mining and Metallurgy Special Volume 24, pp. 211-229.

Jackson, V. A. 1984. Structure and metamorphism of the Keskarrah Bay area, Point Lake, N.W.T., Second preliminary report. Contributions to the geology of the Northwest Territories, **1**: pp. 47-54.

Jackson, V. A. 1982. Preliminary geological map of the Keskarrah Bay area, Slave Structural Province, District of Mackenzie, N.W.T., (86 H/2w, 6e and 7w). Department of Indian Affairs and Northern Development, Geology Division, preliminary geological map, EGS 1982-4.

Kerswill, J. A. 1986. Gold deposits hosted by iron formation in the Contwoyto Lake area, Northwest Territories. *In* Gold'86 Poster Paper Abstracts. *Edited by* A. M. Chater, Geological Association of Canada, Mineral Deposits Division, pp. 82-85.

Kerswill, J. A. 1985a. Gold, Sulphur, and Arsenic in metamorphosed iron formation of the Contwoyto Lake area, Northwest Territories, Canada. Geological Society of America, Abstracts with Program, Annual Meeting, Orlando, Florida, pp. 627.

Kerswill, J. A. 1985b. Gold metallogeny of Archean iron formation in the Contwoyto Lake area, N.W.T. Geological Association of Canada, Program with Abstracts, **10**: A31.

Kerswill, J. A. 1984. The Lupin gold deposit, Contwoyto Lake area, N.W.T; Styles of gold distribution and possible genetic models. Geological Association of Canada, Program with Abstracts, **9**: 78.

Kissman, B. 1984. Exploration 1984, P claims, Point Lake, Northwest Territories, NTS 86H/6,7. Unpublished report by Echo Bay Mines Ltd.

Kimball, K. L., and Spear, F. S. 1984. Metamorphic petrology of the Jackson County iron formation, Wisconsin. Canadian Mineralogist, **22**: 605-619.

King, J. E. 1982. Low pressure regional metamorphism and progressive deformation in the eastern Point Lake area, Slave Province, N.W.T. M.Sc. thesis, Queen's University, Kingston, Ontario.

King, J. E., and Helmstaedt H. In press. Deformational history of an Archean fold belt, eastern Point Lake area, Slave Structural Province, N.W.T. Canadian Journal of Earth Sciences

King, J. E., Boodle, R. L., and St-Onge, M. R. 1980. Geological map of 86 H/1, H/8, H/2 E1/2 and H/7 E1/2, District of Mackenzie: Department of Indian Affairs and Northern Development, Geology Division, Preliminary Geological Map, EGS-1980-10.

King, J. E., Davis, W. J., Relf, C., and Avery, R. W. 1988. Deformation and plutonism in the western Contwoyto Lake map area, central Slave Province, District of Mackenzie, N.W.T. *In* Current research part C. Geological Survey of Canada, paper 88-1C, pp. 161-176.

Klein, C. 1983. Diagenesis and metamorphism of Precambrian banded iron-formations. *In* Iron formations: Facts and problems. *Edited by* A. F. Trendall, Elsevier, New York, New York.

Krogh, T. E., and Gibbins, W. 1978. U-Pb isotopic ages of basement and supracrustal rocks in the Point Lake area of the Slave Structural Province, Canada. Joint meeting of the Geological Association of Canada, Mineralogical Association of Canada and Geological Association of America, program with abstracts, pp. 438.

Kusky, T. M. 1987. An Archean fold-and-thrust belt at Point Lake, N. W. T. Geological Association of Canada Summer Field Meeting, Program with Abstracts.

Lhotka, P. G., and Nesbitt, B. E. 1987a. An epigenetic origin for gold in iron formation in and around the Lupin mine, N.W.T. Geological Association of Canada, Annual General Meeting, Saskatoon, Saskatchewan, Program with Abstracts, **12**: p.67.

Lhotka, P. G., and Nesbitt, B. E. 1987b. Epigenetic gold hosted by iron formation at the Lupin mine, Contwoyto Lake, N.W.T. Geological Association of Canada, Summer Field Meeting, Yellowknife, N.W.T., Program with Abstracts.

Macdonald, A. J. 1983. The iron formation-gold association evidence from the Geraldton area. *In* The geology of gold in Ontario. *Edited by* A. C. Colvine, Ontario Geological Survey, Miscellaneous Paper 110, pp. 75-83.

Macdonald, A. J., and Fyon, J. A. 1986. Sulphidation the key to gold mineralization in banded iron formation. *In* Gold'86 Poster Paper Abstracts. *Edited by* A. M. Chater, Geological Association of Canada, Mineral Deposits Division, pp. 96-97.

McConnell, G. W. 1964. Notes on the similarities between some Canadian gold deposits and the Homestake deposits of South Dakota. Economic Geology, **59**: 719-720.

Noble, J. A. 1950. Ore mineralization in the Homestake gold mine, Lead, South Dakota. Geological Society of America Bulletin, **61**: 221-252.

Padgham, W. A. 1986. Turbidite-hosted gold-quartz veins in the Slave Structural Province,N.W.T. *In* Turbidite-hosted gold deposits. *Edited by* J.D. Keppie, R.W. Boyle and S.J. Haynes, Geological Association of Canada, Special Paper 32, pp. 119-134.

Padgham, W. A. 1985. Observations and speculations on supracrustal successions in the Slave Structural Province. *In* Evolution of Archean Supracrustal Sequences. *Edited by* L. D. Ayres, P. C. Thurston, K. D. Card, and W. Weber, Geological Association of Canada, Special Paper 28, pp. 133-151.

Padgham, W. A. 1984. Gold deposits of N. W. T. ; Classes, styles, genesis, exploration methods and success probabilities. Contributions to the geology of the Northwest Territories, **1**: 121-129.

Phillips, G. N., and Groves, D. I. 1983. The nature of Archean gold-bearing fluids as deduced from gold deposits of Western Australia. Journal of the Geological Association of Australia, **30**: 25-39.

Phillips, G. N., Groves, D. I., and Martyn, J. E. 1984. An epigenetic origin for Archean banded-iron-formation-hosted gold deposits. Economic Geology, **79**: 162-171.

Ridler, R. H. 1970. Relationships of mineralization to volcanic stratigraphy in the Kirkland-Larder Lakes area, Ontario. Geological Association of Canada Proceedings, **21**: 33-42.

Rye, D. M., and Rye, R. O. 1974. Homestake Gold Mine, South Dakota: I. Stable isotope studies. Economic Geology, **69**: 293-317.

Sawkins, F. J., and Rye, D. M. 1974. Relationship of Homestake type gold deposits to iron-rich Precambrian sedimentary rock. Institute of Mining and Metallurgy, Transactions, Section B, **84**: pp. B37-B38.

Stockwell, C. H. 1982. Proposals for time classification and correlation of Precambrian rocks and events in Canada and adjacent areas of the Canadian Shield. Part A . Geological Survey of Canada, paper 80-19.

Stockwell, C. H. 1933. Great Slave Lake-Coppermine River area, Northwest Territories. Geological Survey of Canada, Summary Report 1932, Part C, pp.37-63.

Thompson, P. H. 1978. Archean regional metamorphism in the Slave Structural Province-a new perspective on some old rocks. Geological Survey of Canada, paper 78-10, pp. 85-102.

Tremblay, L. P. 1976. Geology of northern Contwoyto Lake area, District of Mackenzie. Geological Survey of Canada, Memoir 381.

Trendall, A. F. 1983. Introduction. *In* Iron Formation: Facts and Problems. *Edited by* A. F. Trendall and R. C. Morris. Elsevier, Amsterdam, The Netherlands.

Walker, R. G. 1978. Deep-water sandstone facies and ancient submarine fans: models for exploration for stratigraphic traps. American Association of Petroleum Geologists Bulletin, **62**: 932-966.

Wanless, R. K., and Loveridge, W. D. 1978. Rubidium-strontium isotopic age studies, Report 2 (Canadian Shield). Geological Survey of Canada paper 77-14.

Winkler, H. J. F. 1979. Petrogenesis of metamorphic rocks. Springer-Verlag, Berlin.

3. MINERAL CHEMISTRY OF GOLD-BEARING MINERALIZED IRON FORMATION: EVIDENCE FOR EPIGENETIC SULPHIDATION, CONTWOYTO LAKE, NORTHWEST TERRITORIES, CANADA

A. Introduction

Important gold deposits associated with iron formation, such as the Homestake deposit in the United States, Morro Velho in Brazil, and the Lupin mine in the Northwest Territories, Canada, are found worldwide. Their origin has been debated for many years with current models ranging from syngenetic (Fripp 1976; Ridler 1970) to epigenetic (Groves *et al.* 1987; Macdonald 1983) and including multistage or remobilization models (Rye and Rye 1974).

Recently, Groves *et al.* (1987), Phillips *et al.* (1984), Phillips and Groves (1983) and Macdonald and Fyon (1986) have emphasized the importance of sulphidation as a process in the formation of epigenetic gold mineralization of iron formation and other iron-rich host rocks. Evidence for sulphidation in these studies is based on textural observations and the abundances of sulphides adjacent to quartz veins. However, since these iron formations are often comprised of iron-rich silicate minerals, which exhibit compositional variations, it is reasonable to assume that if sulphidation is an important process in gold mineralization, the chemistry of these phases will reflect the sulphidation process. Independent confirmation of the process of sulphidation is a key piece of data in support of epigenetic models of gold mineralization because the deposition of the gold is believed to be linked to the deposition of the sulphides.

In other lines of research in economic geology the compositions of silicate minerals have been valuable in understanding the metamorphism of ores and ore genesis. For example, Nesbitt (1982) used the compositions of silicate minerals to explain the variations in mineral assemblages surrounding the metamorphosed massive sulphide deposits at Ducktown, Tennessee.

Silicate mineral compositions have also been useful in understanding wallrock alteration and ore genesis in skarn deposits (Einaudi *et al.* 1981).

Surprisingly, there has been only one comprehensive study of the chemistry of iron silicate minerals associated with gold deposits in iron formation. This study was done on the Homestake deposit by Chinn (1969). Additional, less comprehensive studies include a few analyses on the iron silicates from the deposits at Jardine Montana by Hallager (1984). In the Contwoyto Lake area, a few analyses of silicate minerals, from the ore zones at Lupin, have been done by Gardiner (1986). Bostock (1977) published analyses of silicate minerals from the Contwoyto Lake region from widely scattered occurrences of iron formation. These less comprehensive studies do not contain sufficient data to establish whether sulphidation may have occurred.

This study represents a systematic examination of the compositions of silicate minerals in gold-bearing iron formation and laterally continuous, unmineralized iron formation, as well as in the transition zone between mineralized and unmineralized iron formation. The chemistry of silicate minerals from iron formation, as determined by electron microprobe analyses, is examined at three study areas in the Contwoyto Lake region. Two of these study areas are small-scale, uneconomic gold occurrences and the third is the Lupin mine. Lupin is a major deposit that has produced 28.25 tonnes of gold between startup in 1982 and the end of 1987 from 2,669,400 tonnes of ore at an average grade of 11.12 ppm. The results of this study show that the process of sulphidation can be recognized by variations in the chemistry of iron silicate minerals. These data strongly suggest that sulphidation did occur and therefore support an epigenetic model for the gold mineralization.

B. Methods

Analytical methods

The majority of the electron microprobe analyses were done at the University of Alberta on an ARL-SEMQ microprobe fitted with an ORTEC EEDS energy dispersive spectrometer and four crystal spectrometers. Operating conditions for the standards and samples were 15 kV operating voltage, 4 nA probe current, and a 240 second counting time. Most of the analyses were performed by energy dispersive analysis (EDA) alone; however, some combined EDA and wavelength dispersive analyses (WDA) were also conducted. When EDA was shown to produce high quality analyses, WDA was discontinued. When combined EDA and WDA analyses were done, the EDA and WDA data were collected simultaneously. Areas for analysis were selected by backscattered electron (BSE) imagery. The 240 second count time represents the sum of eight, 30 second analyses, from nearby spots of a portion of a mineral grain. A point beam was used when combined EDA/WDA analyses were being performed; a rastered beam, with an area of about 10 μm^2, was used for those samples analysed by EDA alone. Data were processed by the EDATA2 program of Smith and Gold (1979). The detection limit by EDA is 0.05 weight %. Relative errors, calculated from the statistical uncertainties at the 99 % confidence level , range from <1 % for abundant elements (oxide weight percent > 10 %) up to 6 % at low concentrations (oxide weight percent of 0.5 %). Repeat analyses of a pyrope standard during analytical runs were used to monitor the quality of the analytical data. The pyrope standard was analysed as an unknown and the resulting data were compared to the accepted values for the standard. A summary of these analyses is included as Appendix 2.

Some additional WDA analyses were done at the University of Calgary on an ARL-SEMQ microprobe with eight crystal spectrometers. The operating

conditions for these analyses were 15 kV operating voltage, 0.15 μA probe current, and counting times of 20 seconds per spot. An analysis represents the average of five to eight spots from a grain. Beam diameter was about 1μm. Analyses of the same samples on both microprobes indicate that the data from the two microprobes are comparable. All of the analytical data are included as Appendix 3.

Stoichiometric calculations

Since the oxidation state of Fe can not be determined directly from microprobe analyses, the results of amphibole, chlorite, stilpnomelane, biotite and pyroxene analyses are based on the assumption that all of the Fe is present as Fe^{2+}. The stoichiometries calculated are based on the respective number of anhydrous oxygens in the various mineral formulae. This procedure gives reasonable stoichiometries, which suggests that the assumption is valid. Hawthorne (1983) states that in amphiboles estimates of Fe^{3+}/Fe^{2+} based on stoichiometric considerations show no relationship to the actual measured Fe^{3+}/Fe^{2+}.

Calculation of epidote, and some garnet, analyses using the assumption that all of the iron is Fe^{2+} results in low stoichiometric coefficients for oxygen, indicating that these minerals contain significant Fe^{3+}. The stoichiometries of these phases were therefore based upon the assumption that the cations sum to 8. In garnet, it was assumed that, if the sum of Ca, Mn and Mg is less than 3, then the required Fe^{2+} is added to equal 3, and the remainder of the Fe, if any, is Fe^{3+}. Epidote stoichiometries were calculated in a similar manner assuming that if the sum of Ca, Mn and Mg is less than 2, then the required Fe^{2+} is added to equal 2, and any remaining Fe is assumed to be Fe^{3+}. This procedure results in reasonable stoichiometries for the garnets. Some of the epidotes have

unusual chemistries and unusual stoichiometries regardless of how they are calculated. EDA spectra show that rare earth element concentrations are very low and could not account for the observed chemistry. Repeated analyses of these epidotes, during runs that gave good results for other minerals, showed that the unusual chemistry of the epidotes is repeatable. X-ray powder diffraction studies confirmed that the epidotes are minerals of the epidote-clinozoisite series.

C. Geology

Regional geology

The following description of the regional geology is summarized from Chapter 2. The descriptions are based largely on the work of Bostock (1980), Thompson (1978) and King *et al.* (1988). The Contwoyto Lake-Point Lake region is predominantly underlain by Archean rocks of the Slave Province (Fig. 3.1). Archean rocks can be subdivided into: pre-Yellowknife Supergroup rocks that comprise granitic rocks and gneisses; Yellowknife Supergroup supracrustal metavolcanic and metasedimentary units; and syn- and post-Yellowknife Supergroup granitic rocks. All but the late plutons have been metamorphosed to some degree; however, premetamorphic rock terminology is generally used hereinafter.

The Yellowknife Supergroup (Henderson 1970) is subdivided (Bostock 1980) into four formations in the Contwoyto Lake-Point Lake region as follows: the Point Lake Formation which comprises mafic to felsic volcanic rocks; the Keskarrah Formation which comprises conglomerates and lithic sandstones; the Contwoyto Formation which comprises greywacke and mudstone beds with lenses and beds of iron formation; and the Itchen Formation which comprises greywacke and mudstone beds lacking iron formation (Fig. 3.1).

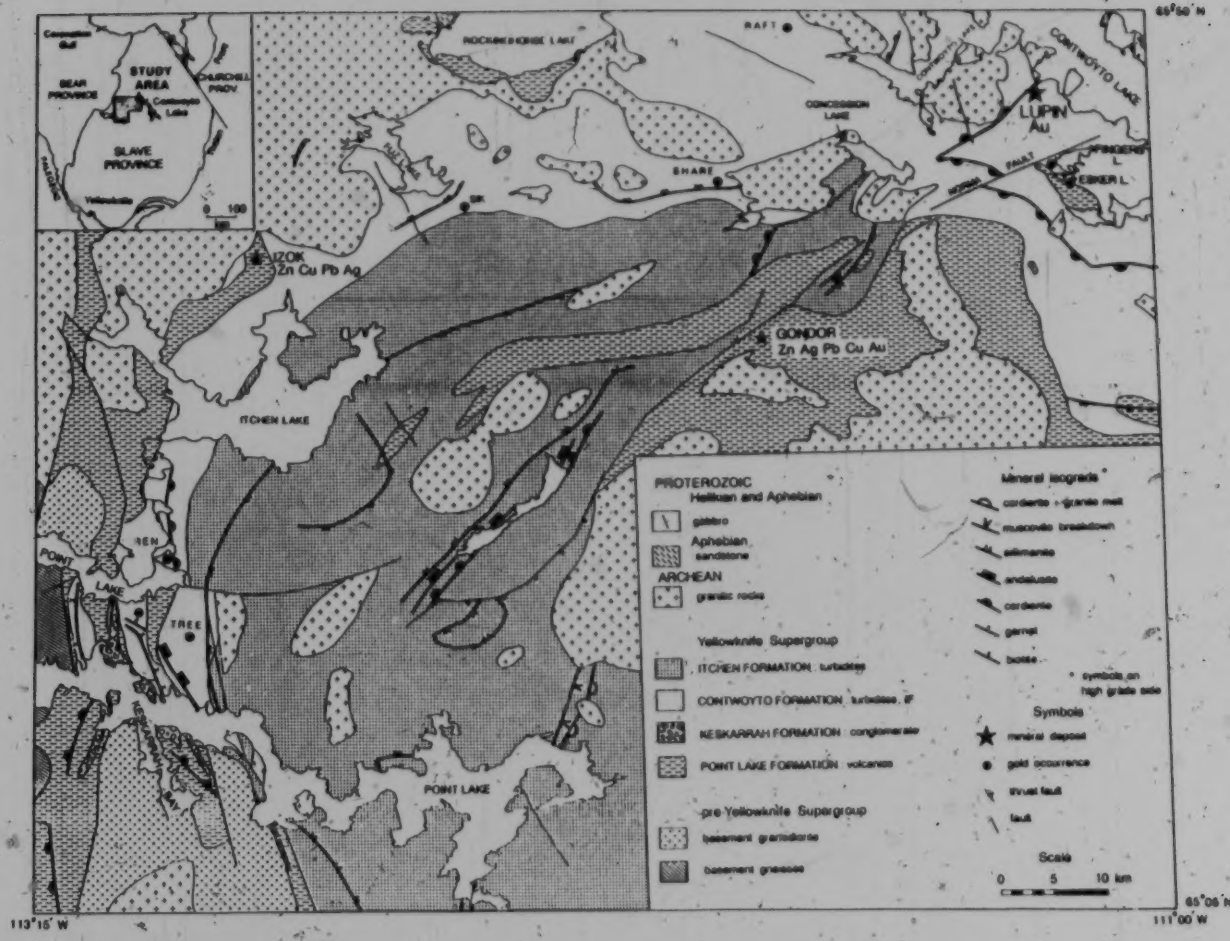

Fig. 3.1. Geology of the Contwoyto Lake-Point Lake region. Modified after Bostock (1980) and others.

The Contwoyto Formation is important because it contains the iron formations that host most of the known gold occurrences and the Lupin mine. The iron formations range in thickness from a few centimetres to 20 m. Although gold occurrences are common in iron formation throughout the region, the majority of iron formation is not enriched in gold and does not contain visible sulphide mineralization.

Archean rocks have been deformed and metamorphosed by Archean tectonic events. Archean structures comprise complexly interfering isoclinal folds with associated penetrative fabrics (King *et al.* 1988). Metamorphic isograds are defined in the pelitic sediments by the first appearance of the characteristic minerals biotite, garnet, cordierite, andalusite, sillimanite, and the breakdown of muscovite + quartz to form K-feldspar + sillimanite (Fig. 3.1). Garnet is present only in iron-rich beds associated with iron formation. These minerals are characteristic of a low pressure trajectory path in P-T space (Thompson 1978). The distribution of the isograds generally suggests that the thermal highs are spatially associated with the fifth group of granitic plutons of King *et al.* (1988). Isograds cut across some of the folds indicating that peak metamorphism postdated at least some of the early deformation.

Two pairs of coexisting biotite and almandine-rich garnet, in which the two minerals were in direct contact, were analysed from a sample of pelitic iron formation. The sample was collected from a drillhole near, but on the low grade side of, the cordierite isograd 220 m north of Lupin (Fig. 3.1). The resulting data were used to calculate metamorphic temperatures based on the partitioning of Fe and Mg into the two minerals using the geothermometer of Perchuk and Laverent'eva (1982). The calculations were done with the assumption that all of the Fe is Fe^{2+} and that the pressure equals 3 Kbars. Results of the calculations suggest that the garnet and biotite pairs equilibrated at 600°C.

These data indicate somewhat higher temperatures than the work of Thompson (1978). The proximity of the sample to the cordierite isograd suggests that the isograd represents temperatures of slightly above 600°C in this area. Thompson (1978), on the basis of experimentally calibrated mineral reactions and mineral assemblages in the Point Lake area, concluded that the first appearance of cordierite occurs at about 575°C.

Aphebian and later geological events have had little or no effect on Archean mineral assemblages except immediately adjacent to Proterozoic gabbro dykes.

Geology of iron formation and gold occurrences

On the basis of detailed fieldwork and petrographic studies (Chapter 2), iron formation has been subdivided into unmineralized iron formation, containing trace or no visible iron sulphide minerals, and mineralized iron formation, containing abundant iron sulphide minerals. Enhanced gold values are only associated with the mineralized iron formation. The following geological descriptions are summarized from Chapter 2.

Unmineralized iron formation in most of the region is comprised largely of grunerite + quartz ± magnetite with minor amounts of hornblende. This rock type, comprised largely of chemical sediment, is interbedded with a rock of mixed parentage that is referred to as pelitic iron formation. Pelitic iron formation is a mixture of chemical and fine grained, detrital sediment which, following metamorphism, comprises chlorite (14 Å), quartz, ilmenite ± almandine garnet ± grunerite ± hornblende. Unmineralized iron formation and interbedded pelitic iron formation generally contain ≤0.03 ppm Au (Chapter 2).

Mineralized iron formation in the Contwoyto Lake area comprises iron sulphides ± arsenides (arsenopyrite and loellingite) in iron formation that is

predominantly comprised of hornblende and quartz with little or no grunerite. In the sub-garnet metamorphic zone, the iron sulphide is pyrite, whereas at higher metamorphic grades it is pyrrhotite. Gold values of mineralized iron formation are generally between about 5 and 30 ppm (Chapters 2 and 4). Pelitic iron formation is interbedded with mineralized iron formation but does not contain more than trace amounts of sulphide or enhanced gold values.

At small-scale gold occurrences, the distribution of mineralized iron formation is clearly controlled by late quartz veins. Mineralized iron formation only occurs adjacent to veins and grades into unmineralized grunerite iron formation along strike. Textural evidence suggests that those minerals that predominate in mineralized iron formation replace those minerals that predominate in unmineralized iron formation: hornblende replaces grunerite and iron sulphides replace amphiboles and magnetite.

Lupin is the only known economic gold deposit in the area (Fig. 3.1). It differs from the small-scale occurrences in its much larger size and continuity of the mineralized zones, and the fact that unmineralized grunerite-rich iron formation is rare or absent within the deposit. Abundant quartz veining is present in the gold-bearing zones, which are comprised of mineralized iron formation that is pyrrhotite- and hornblende-rich. Arsenides are found only immediately adjacent to the veins; pyrrhotite is more evenly distributed and is abundant between closely spaced veins. Along strike, to the northeast of the deposit, the laterally continuous Lupin iron formation is comprised of unmineralized grunerite ± magnetite iron formation with few quartz veins.

These observations suggest that sulphidation of iron formation and wallrock alteration, which produces hornblende-rich iron formation, are important processes in gold mineralization at the small-scale occurrences and probably at Lupin as well. Such evidence supports an epigenetic model of gold

mineralization (Chapter 2). In the following section, results of analytical work on the compositions of iron silicates in unmineralized iron formation and mineralized iron formation, will be used to test the sulphidation and wallrock alteration model of gold mineralization.

D. Esker Lake gold occurrence

Geology and mineralogy

The Esker Lake gold occurrence is about 10 km southeast of Lupin in the garnet metamorphic zone (Fig. 3.1). The geology and mineralogy described here is a summary of data presented in Chapter 2. Most of the iron formation at Esker Lake is pelitic iron formation that lacks sulphides and gold. Mineralized iron formation containing abundant sulphides and gold is present adjacent to a quartz vein where the vein cuts a nonpelitic portion of iron formation (Fig. 3.2).

Immediately adjacent to the quartz vein the mineralized iron formation comprises about 40 % porphyroblasts of arsenopyrite, containing cores of loellingite, with lesser amounts of pyrrhotite (Fig. 3.2). The arsenide-rich iron formation is hornblende-rich and has trace amounts of grunerite and actinolite. At 30 cm from the vein, the arsenides comprise <1 %, but pyrrhotite comprises about 40 % of the hornblende-rich rock. Further away from the vein the abundances of pyrrhotite and hornblende decrease until at 150 cm from the vein the iron formation contains 3 % pyrrhotite in a grunerite-rich iron formation with minor amounts of hornblende. Petrographic studies have shown that hornblende replaces grunerite, and that pyrrhotite replaces hornblende and grunerite (Chapter 2). Pelitic iron formation contains traces of arsenopyrite and pyrrhotite only near the vein. Most of the sulphides that are present in pelitic iron formation occur in fractures in garnet. The distributions of sulphides and gold, the change from hornblende-rich iron formation to grunerite-rich iron formation,

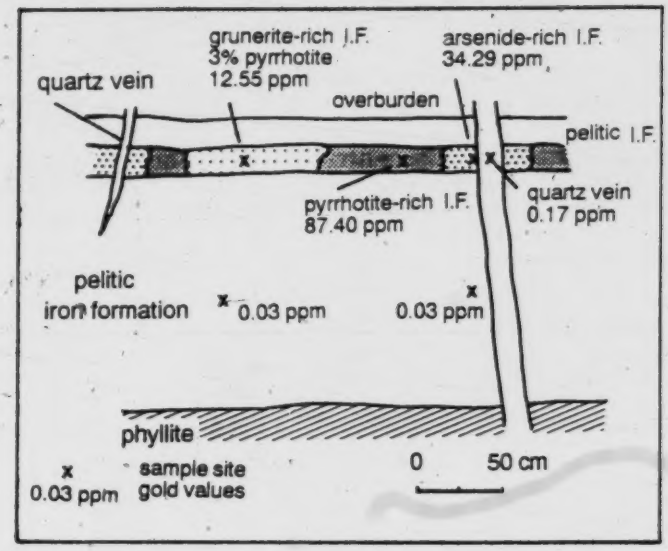

Fig. 3.2. Sketch map of the Esker Lake gold occurrence showing the zonation of gold values and sulphides adjacent to a quartz vein in the nonpelitic portion of the iron formation. Pelitic iron formation is not mineralized adjacent to the vein.

and the textural evidence suggest that the mineralization was introduced into the iron formation by hydrothermal fluids associated with the quartz veining.

Mineral chemistry

Representative analyses of the 113 mineral analyses from the Esker Lake gold occurrence are included in Table 3.1. Figs. 3.3*A* and 3.3*B* show the compositions of minerals from iron formation and pelitic iron formation respectively on a ternary diagram with the appices $(Al_2O_3+Fe_2O_3)$ - (FeO) - (MgO).

The first important point to note is that pelitic iron formation is comprised of phases rich in MgO and $(Al_2O_3+Fe_2O_3)$ relative to phases present in iron formation (Figs. 3.3*A* and 3.3*B*). This is consistent with the field observations that suggest that the pelitic iron formation is a mixture of chemical and pelitic sedimentary components and therefore has a different bulk composition to iron formation. Thus, in order to examine changes in the chemistry of iron formation, which may be related to sulphidation or wallrock alteration, it is important to examine iron formation and pelitic iron formation separately.

In Fig 3.3*A* it is apparent that the X_{Fe} values of the coexisting grunerite and hornblende are related to the abundance of sulphides. Where the concentration of sulphides is the highest (in mineralized iron formation), the amphiboles have the lowest X_{Fe} values [X_{Fe} is defined as $Fe^{2+}/(Fe^{2+}+Mg^{2+})$]. As the concentration of pyrrhotite ± arsenides decreases, the amphiboles have progressively higher X_{Fe} values (weakly mineralized iron formation). This relationship results in a pattern of lower X_{Fe} amphibole values near the veins, where sulphides are abundant, and higher X_{Fe} amphibole values at greater distances from the veins, where sulphides are less abundant. These changes occur laterally in one narrow series of bands and are therefore not likely to be

Table 3.1 Representative electron microprobe analyses of amphiboles, chlorites, garnets and epidotes from the Esker Lake area.

sample	4C020	4C020	4C018	4C018	4C011	4C011	4C007	4C007	4C007	4C006	4C006	4C020	4C019
rock type	3	3	4	4	6	6	7	7	7	8	8	3	4
analysis	grun 1	hbl 1	grun 1	hbl 1	grun 2	hbl 2	act 1	grun 1	hbl 1	grun 3	hbl 3	chlor 1	chlor 1
SiO_2	51.02	40.76	50.74	41.61	48.55	43.10	49.92	49.28	45.67	49.35	40.85	23.24	23.48
Al_2O_3	0.52	16.96	0.39	15.17	0.20	8.79	1.01	0.16	6.15	0.55	15.27	20.38	21.03
Cr_2O_3	0.00	0.00	0.00	0.00	0.00	0.00	0.00	0.00	0.00	0.00	0.00	0.09	0.00
TiO_2	0.00	0.11	0.00	0.19	0.00	0.00	0.00	0.00	0.15	0.00	0.00	0.10	0.00
MgO	8.09	3.37	6.36	3.31	0.74	0.61	3.19	2.92	2.42	4.32	2.06	6.48	6.92
FeO+	38.38	24.12	40.63	25.54	48.97	34.87	32.98	44.82	32.17	43.22	27.38	37.93	37.75
MnO	0.00	0.00	0.00	0.00	0.00	0.00	0.00	0.15	0.00	0.14	0.00	0.00	0.00
CaO	0.38	10.78	0.55	10.90	0.66	10.90	10.76	1.05	10.99	0.50	10.93	0.00	0.00
Na_2O	0.00	0.48	0.00	1.66	0.00	0.89	0.00	0.00	0.32	0.00	0.88	0.00	0.39
K_2O	0.00	0.36	0.00	0.46	0.00	0.27	0.00	0.00	0.16	0.00	0.35	0.00	0.00
Cl	0.00	0.00	0.00	0.00	0.00	0.00	0.00	0.00	0.00	0.00	0.00	0.00	0.00
TOTAL	98.40	96.95	98.66	98.83	99.12	99.42	97.85	98.38	98.02	98.07	97.72	88.22	89.57
H2O(dif)	1.60	3.05	1.34	1.17	0.88	0.58	2.15	1.62	1.98	1.93	2.28	11.78	10.43
	amphiboles: cations based on anhydrous O + Cl =23											chlorites: cations based on 28 oxygens	
Si	7.954	6.286	7.981	6.373	7.964	6.860	7.892	7.986	7.238	7.943	6.372	5.243	5.200
Al iv	0.046	1.714	0.019	1.627	0.036	1.140	0.108	0.014	0.762	0.057	1.628	2.757	2.800
Al vi	0.049	1.370	0.054	1.110	0.003	0.509	0.080	0.016	0.386	0.047	1.180	2.660	2.691
Cr	0.000	0.000	0.000	0.000	0.000	0.000	0.000	0.000	0.000	0.000	0.000	0.016	0.000
Ti	0.000	0.013	0.000	0.022	0.000	0.000	0.000	0.000	0.018	0.000	0.000	0.017	0.000
Mg	1.881	0.775	1.491	0.754	0.180	0.144	0.751	0.706	0.571	1.035	0.478	2.178	2.286
Fe	5.004	3.112	5.345	3.271	6.717	4.641	4.361	6.074	4.263	5.817	3.572	7.154	6.994
Mn	0.000	0.000	0.000	0.000	0.000	0.000	0.000	0.021	0.000	0.020	0.000	0.000	0.000
Ca	0.064	1.781	0.092	1.788	0.116	1.858	1.822	0.183	1.865	0.086	1.826	0.000	0.000
Na	0.000	0.145	0.000	0.491	0.000	0.274	0.000	0.000	0.099	0.000	0.268	0.000	0.167
K	0.000	0.071	0.000	0.091	0.000	0.054	0.000	0.000	0.032	0.000	0.069	0.000	0.000
SUM	14.998	15.266	14.982	15.527	15.016	15.479	15.014	14.999	15.235	15.005	15.392	20.024	20.138
Cl	0.000	0.000	0.000	0.000	0.000	0.000	0.000	0.000	0.000	0.000	0.000	0.000	0.000
Fe/(Fe+Mg)	0.7268	0.8006	0.7818	0.8126	0.9739	0.9699	0.8531	0.8959	0.8819	0.8489	0.8819	0.7666	0.7537

Table 3.1 continued.

sample	4C017	4C017	5C012	5C012	4C018	4C018	5C009
rock type	3	3	3	3	4	4	9
analysis	gar rim	gar core	gar core	gar rim	gar rim	gar core	epi
SiO_2	37.01	36.92	36.94	36.85	37.14	36.99	38.38
Al_2O_3	21.54	21.62	21.48	21.46	21.45	21.30	26.44
TiO_2	0.00	0.00	0.00	0.00	0.00	0.00	0.00
Cr_2O_3	0.00	0.00	0.00	0.00	0.00	0.00	0.00
$Fe_2O_3^*$	0.90	0.88	0.74	0.71	0.59	1.15	9.61
FeO^*	37.58	37.64	37.46	40.18	35.94	36.49	0.00
MgO	1.33	1.26	1.08	1.30	1.04	1.15	0.34
MnO	0.00	0.00	1.01	0.00	0.00	0.00	0.00
CaO	4.14	4.19	3.64	1.92	5.71	5.18	24.30
K_2O	0.00	0.00	0.00	0.00	0.00	0.00	0.00
Na_2O	n.a.	n.a.	n.a.	n.a.	n.a.	n.a.	n.a.
TOTAL	102.49	102.50	102.35	102.41	101.87	102.26	99.06
H_2O (dif)							0.94
			garnet and epidote: cations normalized to 8				
Si	2.934	2.928	2.940	2.940	2.954	2.938	2.972
Al	2.013	2.020	2.016	2.018	2.011	1.993	2.413
Ti	0.000	0.000	0.000	0.000	0.000	0.000	0.000
Cr	0.000	0.000	0.000	0.000	0.000	0.000	0.000
Fe^{3+}	0.054	0.052	0.044	0.043	0.035	0.069	0.562
Fe^{2+}	2.492	2.496	2.494	2.681	2.391	2.423	0.000
Mg	0.157	0.148	0.128	0.155	0.123	0.136	0.039
Mn	0.000	0.000	0.068	0.000	0.000	0.000	0.000
Ca	0.352	0.356	0.310	0.164	0.486	0.441	2.016
O	11.967	11.964	11.970	11.970	11.977	11.969	12.461
$Fe^{2+}/(Mg+Fe^{2+})$	0.9409	0.9439	0.9512	0.9454	0.9510	0.9470	0.0000
$Fe^{2+}/(Fe^{2+}+Fe^{3+})$	0.9788	0.9796	0.9827	0.9842	0.9856	0.9723	0.0000

Notes: FeO+ = total iron as FeO; Fe2O3* and FeO* estimated by stoichiometry (see text for method). n.a.= not analysed; 0.000= not detected; H_2O (dif)= H_2O by difference from 100%. Rock types 3= pelitic IF; 4= possibly altered pelitic IF; 5= unmineralized IF; 6= weakly mineralized IF; 7= pyrrhotite mineralized IF; 8= arsenide mineralized IF; 9= calc-silicate rocks.

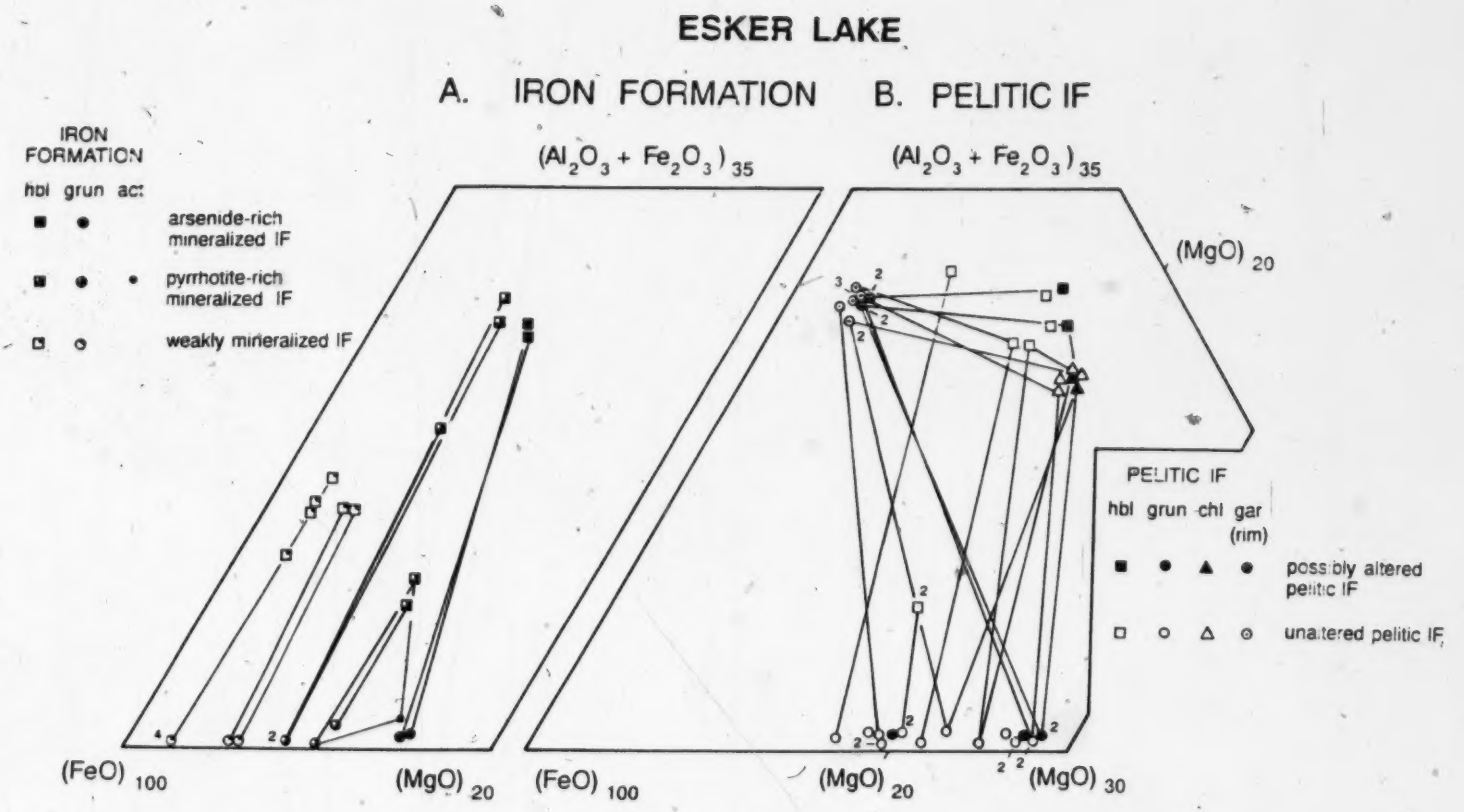

Fig. 3.3. (Al_2O_3 + Fe_2O_3) - (MgO) - (FeO) ternary diagram of minerals from the Esker Lake iron formation. *A.* Iron formation. *B.* Pelitic iron formation. Abbreviations for this figure and Figs. 3.6, 3.7, and 3.9: hbl= hornblende; grun= grunerite; act= actinolite; chl= chlorite; gar= almandine-rich garnet; bio= biotite.

due to variations in the original bulk rock composition (Fig. 3.2). These data strongly suggest that sulphidation of the iron formation occurred adjacent to quartz veins.

Pelitic iron formation is sulphide-poor and does not have any obvious differences in mineralogy related to the veins; it was therefore grouped into "possibly altered" samples, located near veins and "unaltered" samples, located distant from the veins. There are no systematic differences in the compositions of the minerals between the two groups in Fig. 3.3*B* . The minor variations in chemistry are probably due to slight differences in the bulk compositions of the individual samples.

Sulphidation model

If a sulphidation model is valid, then it must explain the observed changes in the chemistries of the amphiboles in iron formation, related to the veining. The following reaction shows how a decrease in the X_{Fe} of grunerite can accompany sulphidation:

$$2Fe_{6.5}Mg_{0.5}Si_8O_{22}(OH)_2 + 8H_2S + 1/2O_2 \rightarrow Fe_{6.0}Mg_{1.0}Si_8O_{22}(OH)_2 + 8SiO_2 + Fe_7S_8 + 9H_2O. \quad (1)$$

It is worth noting that a similar reaction can be written, in which As is substituted for S, and loellingite ($FeAs_2$) is formed instead of pyrrhotite. This reaction will also produce lower X_{Fe} values in the grunerite. Thus, the term sulphidation is defined to include addition of sulphur and/or arsenic hereinafter except where specific references are made to the element sulphur.

A more representative reaction for the Esker Lake occurrence must also account for the change in the composition of the amphibole from grunerite to

hornblende, as well as the decrease in the X_{Fe} of the amphiboles, as the following qualitative reaction does:

$$\text{grunerite} + H_2S + O_2 + Ca + Al \rightarrow \text{hornblende} + \text{quartz} + H_2O + \text{pyrrhotite.} \quad (2)$$

To further evaluate whether the sulphidation model is correct, the amount of sulphur added to the iron formation can be calculated from the estimated abundances of the amphiboles and their measured chemistry assuming that there is no net gain or loss of iron or magnesium from the system. The calculation assumes that a rock comprised of 80 weight % grunerite with an X_{Fe} of 0.97 (49 % FeO) is altered to form a rock comprised of 60 weight % hornblende with an X_{Fe} of 0.85 (27 % FeO). If the iron liberated when grunerite is converted to hornblende combines with sulphur to form pyrrhotite then about 11 weight % sulphur can be consumed. The 11 weight % sulphur will form 29 weight % pyrrhotite. This result is in reasonable agreement with the observation that the visually estimated abundance of pyrrhotite is about 3 % in the grunerite-rich iron formation and about 40 % in the hornblende-rich iron formation: a difference of about 37 volume %, which converts to about 46 weight % pyrrhotite.

The good correlation between the X_{Fe} of the silicates and the abundances of sulphides and gold is compatible with an epigenetic sulphidation model. Phillips and Groves (1983) have previously proposed the following reaction to explain the association between sulphides and gold where gold is transported in solution as an aqueous gold-sulphide complex and is deposited due to sulphidation (sulphur only):

$$FeO \text{ (in silicates)} + HAu(HS)_2 + 1/4O_2 \rightarrow Au + FeS_2 + 3/2\ H_2O \qquad (3)$$

This reaction is similar to reaction (2). Together reactions (2) and (3) show how the chemistry of the amphiboles can change as sulphides and gold are deposited. The observed change in the X_{Fe} values of amphiboles, in a single series of bands of variably mineralized iron formation, is strong evidence in favour of the epigenetic sulphidation of gold-bearing iron formation adjacent to quartz veins at Esker Lake.

It is interesting that the amphiboles in the pelitic iron formation (Fig. 3.3*B*) have lower X_{Fe} values than the amphiboles in mineralized iron formation even where sulphidation has lowered the X_{Fe} values of the amphiboles (Fig. 3.3*A*). This is shown in Fig. 3.4 where the trend of sulphidation is plotted together with the compositions of coexisting amphiboles in iron formation and pelitic iron formation. The fact that pelitic iron formation is characterized by lower X_{Fe} amphiboles than mineralized iron formation may help to explain why pelitic iron formation is not sulphidized adjacent to the quartz veins. Apparently, the pelitic iron formation has X_{Fe} values of amphiboles, which are equal to or less than, X_{Fe} values of amphiboles in equilibrium with the hydrothermal fluid.

Other evidence for wallrock alteration

In addition to the changes in the X_{Fe} values of amphiboles due to sulphidation, the alteration of unmineralized grunerite-rich iron formation to mineralized hornblende-rich iron formation implies that there may be other chemical changes in the mineralized iron formation adjacent to the veins. The bulk rock chemistry of these rocks types in the system $(Al_2O_3+Fe_2O_3)$ - (FeO) - (MgO) can be crudely modelled by the compositions of the predominant amphibole. This is because there are no other mineral phases except for quartz

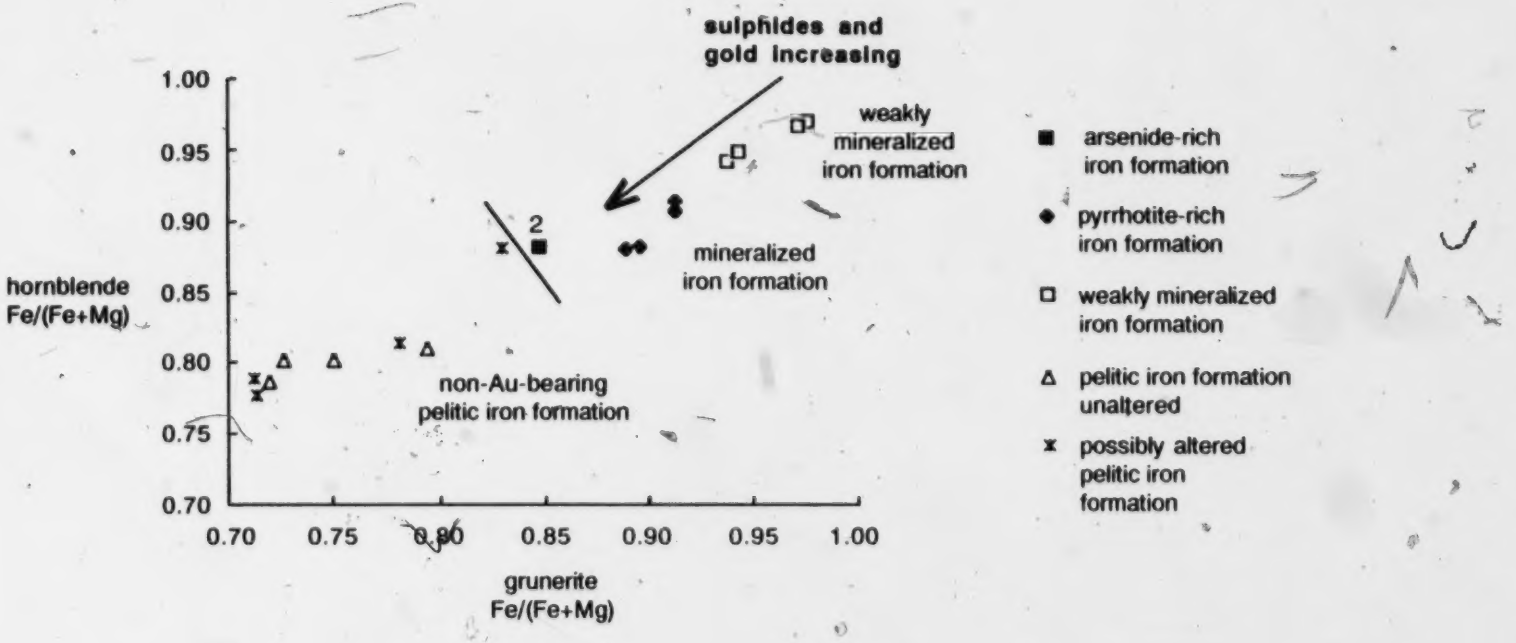

Fig. 3.4. X_{Fe} values of coexisting grunerite and hornblende from the Esker Lake gold occurrence.

and sulphides. Thus, the change from unmineralized grunerite-rich iron formation to mineralized hornblende-rich iron formation suggests that Al has been added (Fig. 3.3*A*). This is consistent with equation (2), which suggests that Al may have been added during the sulphidation event. The suggestion that Al may be mobile in this setting is unusual in that Al is generally regarded as an immobile element under most conditions (Grant 1986). However, in this situation it is impossible for the hornblende-rich rocks to have been produced from grunerite-rich rocks, which lack Al-bearing phases, without the addition of Al unless the sulphidation was accompanied by major volume reductions, for which there is no field evidence.

Figure 3.5 shows the compositions of the iron formation minerals in terms of the components (CaO) - (MgO + FeO) - (Al_2O_3+Fe_2O_3). In this diagram grunerite, the phase characteristic of unmineralized iron formation, plots at the (MgO + FeO) apex while chlorite and almandine garnet, the phases characteristic of pelitic iron formation, plot towards more (Al_2O_3+Fe_2O_3)-rich compositions. This trend, indicated by an arrow in Fig. 3.5, is suggestive of the previously mentioned hypothesis that the pelitic iron formation represents a mixture of clastic and chemical sediment. The minerals hornblende and actinolite, which are present in mineralized iron formation derived from the grunerite iron formation, plot towards more (Al_2O_3+Fe_2O_3)- and (CaO)-rich compositions. This implies that the mineralized iron formation is altered by the addition of Al and Ca.

Although epidote and hedenbergite are not common at Esker Lake, in one location on the same outcrop, epidote and actinolite, pseudomorphing hedenbergite, are present adjacent to a quartz vein. Epidote and hedenbergite are absent in unmineralized iron formation and pelitic iron formation in the region as a whole, but are common in mineralized iron formation at Lupin. If

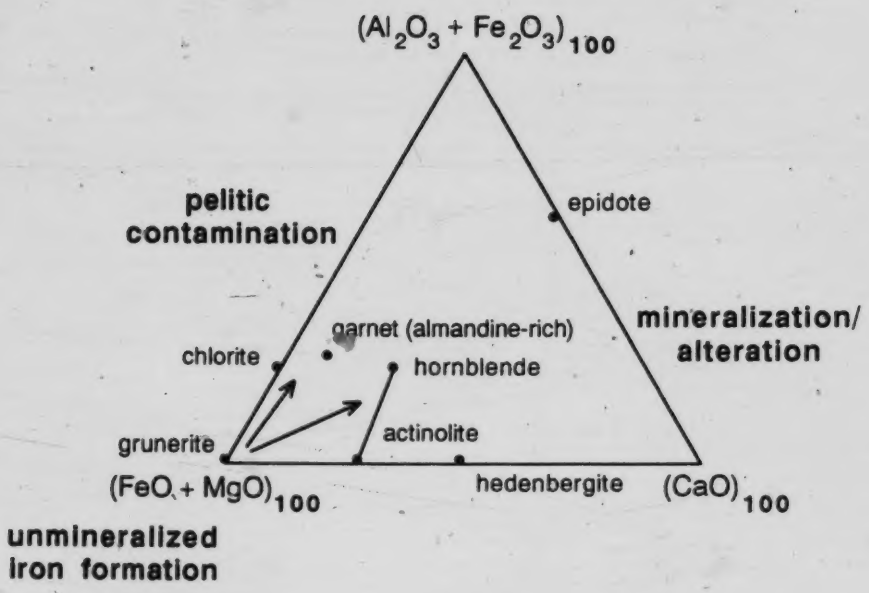

Fig. 3.5. $(Al_2O_3 + Fe_2O_3)$ - (CaO) - (FeO + MgO) ternary diagram of minerals from the Esker Lake iron formation.

these phases do represent alteration associated with the quartz veining and mineralization, then their compositions are consistent with the trend to more Ca- and Al-rich minerals associated with mineralization (Fig. 3.5).

The lack of obvious changes in the compositions of minerals in pelitic iron formation related to veins suggests that pelitic iron formation is not altered adjacent to the veins (Fig. 3.3 *B*). A detailed examination of the compositions of the garnets in pelitic iron formation does, however, indicate that there is some evidence of alteration. Analyses of the cores and rims of the garnets show that although the garnets are not optically zoned, there are slight compositional variations. These analyses are plotted in Fig. 3.6. An indication of the precision of the data, based upon four analyses of the same spot of one garnet grain analysed on four different runs, is shown for reference. In samples distant from the veins (unaltered), the garnets have MnO- and CaO-rich cores and FeO-rich rims (Fig. 3.6). This zoning is typical of garnets in regionally metamorphosed sedimentary rocks (Deer *et al.* 1978). Garnets from possibly altered samples adjacent to the veins have cores that are similar in composition to the cores of the unaltered garnets. However, the rims of the possibly altered garnets are CaO-rich, a trend which is opposite to the zoning in the unaltered garnets and opposite to the common zonation in metamorphic garnets. The CaO-rich rims are best interpreted as resulting from Ca-metasomatism adjacent to the veins. Fig. 3.6 *B* shows that the variations in FeO, MgO and MnO are very small. This confirms that the major variation is in the abundance of CaO.

Thus, there is considerable evidence in the mineral chemistries to suggest that wallrock alteration is present in the mineralized zones of the iron formation associated with quartz veining. This alteration is present to a minor degree in the pelitic iron formation and to a much greater degree in the non-pelitic iron formation.

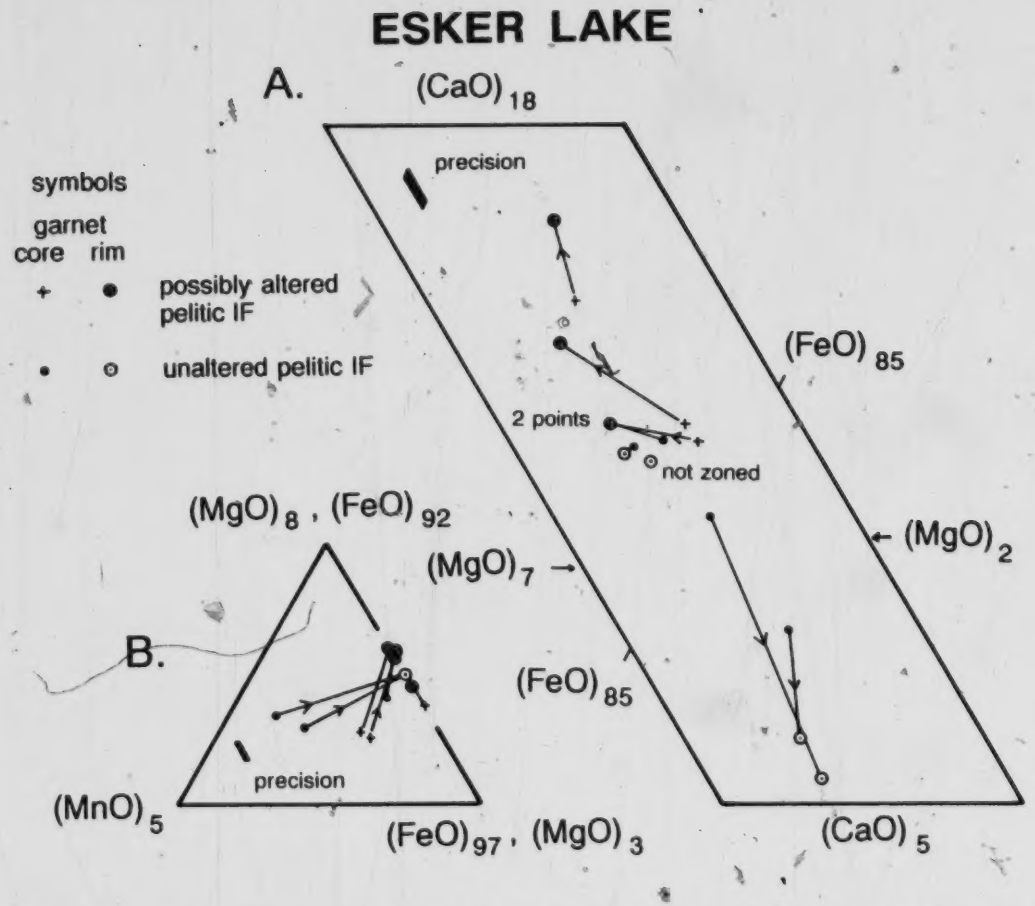

Fig. 3.6. Zoning in garnets from unaltered and possibly altered pelitic iron formation at Esker Lake. *A.* (CaO) - (FeO) -(MgO) ternary plot. *B.* (MgO) - (FeO) - (MnO) ternary plot. See text for explanation of the analytical precision.

E. Fingers Lake gold occurrence

Geology and mineralogy

The Fingers Lake gold occurrence is about 3 km northwest of the Esker Lake gold occurrence in the biotite metamorphic zone (Fig.3.1). Like the Esker Lake gold occurrence, mineralization at Fingers Lake is spatially associated with quartz veins; however, at Fingers Lake the mineralization comprises arsenides and pyrite, instead of arsenides and pyrrhotite. The Fingers Lake gold occurrence has been described in detail in Chapter 2.

The distribution of sulphides at Fingers Lake is like that at Esker Lake in that arsenides occur nearest to the veins and pyrite forms more extensive haloes surrounding the vein. In the mineralized iron formation, pyrite replaces magnetite and may also replace amphiboles. Again, the predominant amphibole in mineralized iron formation is hornblende, and hornblende replaces grunerite.

As the abundance of sulphides decreases away from the veins, the proportion of hornblende decreases and the proportion of grunerite increases. Away from quartz veined areas, the iron formation is comprised of grunerite + quartz ± magnetite, stilpnomelane and minor amounts of hornblende. The amount of magnetite is variable, but, unlike Esker Lake, magnetite is common at Fingers Lake and often comprises up to 20 % of the unmineralized iron formation.

Minor amounts of pelitic iron formation are present at Fingers Lake. Due to the lower metamorphic grade, garnet is absent in these rocks and they are comprised of chlorite (14Å) and grunerite with or without minor amounts of hornblende, stilpnomelane, ilmenite and graphite. Pelitic iron formation does not contain enhanced sulphide abundances or gold values, even near quartz veins.

Mineral chemistry

Representative analyses of the 89 mineral analyses from Fingers Lake are included in Table 3.2. and the analytical data are shown in Fig. 3.7. Grunerite and chlorite in pelitic iron formation from Fingers Lake (Fig. 3.7) are relatively iron-rich compared to grunerite and chlorite in pelitic iron formation from Esker Lake (Fig. 3.3*A*). The higher X_{Fe} values of grunerite and chlorite could indicate that pelitic iron formation at Fingers Lake has a higher bulk X_{Fe} value than pelitic iron formation at Esker Lake. However, it is probable that the difference in compositions is at least partly due to the absence of almandine garnet at Fingers Lake because of the lower metamorphic grade. The absence of almandine garnet, with an X_{Fe} of about 0.95, would allow the other iron silicates to have higher X_{Fe} values.

In Fig. 3.7 there is poor correlation between the composition of coexisting grunerite and hornblende and the abundance of sulphides in iron formation. Grunerite and hornblende, in unmineralized iron formation, have X_{Fe} values of 0.90 to 0.96. These values are comparable to the Esker Lake data for the same rock type. Grunerite and hornblende in mineralized iron formation have X_{Fe} values between 0.89 and 0.96. These values overlap with the X_{Fe} values in unmineralized iron formation.

Interpretation

The data from Fingers Lake are not compatible with the sulphidation model for Esker Lake in which iron silicates are sulphidized resulting in lower X_{Fe} values for the remaining iron silicates. This, however, does not mean that sulphidation did not occur at Fingers Lake. Petrographic data have shown that

Table 3.2 Representative electron microprobe analyses of amphiboles and chlorites from the Fingers Lake area.

sample	5B039	5B039	5B071	5B004	5B004	5B005	5B005	5B046	5B046	5B073	5B073	5B039	5B071
rock type	3	3	4	5	5	6	6	7	7	8	8	3	4
analysis	grun 2	hbl 2	hbl 1	grun 1	hbl 1	grun 1	hbl 1	grun 1	hbl 1	grun 2	hbl 2	chlor 2	chlor 1
SiO_2	49.96	41.41	40.80	49.15	39.88	48.22	40.21	48.59	40.49	48.61	40.04	23.26	23.65
Al_2O_3	0.53	14.00	15.04	0.41	14.92	0.25	11.50	0.30	12.60	0.48	13.65	19.28	19.06
Cr_2O_3	0.00	0.00	0.00	0.00	0.00	0.00	0.00	0.00	0.00	0.08	0.00	0.00	0.00
TiO_2	0.12	0.12	0.00	0.00	0.15	0.00	0.00	0.00	0.00	0.00	0.17	0.12	0.00
MgO	5.21	2.56	3.05	3.03	1.35	1.01	0.63	1.39	0.80	2.84	1.47	4.52	5.30
FeO+	42.11	27.91	25.80	46.03	29.20	48.42	32.73	47.52	31.13	45.36	29.97	41.43	39.74
MnO	0.14	0.00	0.08	0.00	0.00	0.00	0.00	0.00	0.00	0.15	0.00	0.00	0.00
CaO	0.45	10.54	11.27	0.38	10.97	0.49	10.98	0.45	11.10	0.46	10.59	0.09	0.07
Na_2O	0.00	0.76	1.08	0.00	1.01	0.00	0.86	0.00	0.81	0.00	0.88	0.00	0.00
K_2O	0.00	0.35	0.39	0.00	0.44	0.00	0.40	0.00	0.35	0.00	0.42	0.00	0.00
Cl	0.00	0.00	0.00	0.00	0.00	0.00	0.00	0.00	0.00	0.00	0.00	0.00	0.00
TOTAL	98.52	97.65	97.51	98.98	97.91	98.39	97.31	98.26	97.28	97.97	97.18	88.70	87.83
H_2O (dif)	1.48	2.35	2.49	1.02	2.09	1.61	2.69	1.74	2.72	2.03	2.82	11.30	12
	amphiboles: cations based on anhydrous O + Cl= 23											chlorites: cations based on 28 oxygens	
Si	7.946	6.473	6.351	7.937	6.291	7.955	6.517	7.982	6.495	7.932	6.387	5.327	5.419
Al iv	0.054	1.527	1.649	0.063	1.709	0.045	1.483	0.018	1.505	0.068	1.613	2.673	2.581
Al vi	0.045	1.052	1.111	0.014	1.065	0.004	0.713	0.040	0.878	0.025	0.954	2.531	2.566
Cr	0.000	0.000	0.000	0.000	0.000	0.000	0.000	0.000	0.000	0.010	0.000	0.000	0.000
Ti	0.014	0.014	0.000	0.000	0.017	0.000	0.000	0.000	0.000	0.000	0.020	0.020	0.000
Mg	1.236	0.596	0.709	0.728	0.318	0.248	0.153	0.339	0.191	0.691	0.348	1.542	1.809
Fe	5.600	3.647	3.358	6.217	3.852	6.681	4.436	6.529	4.176	6.189	3.998	7.935	7.614
Mn	0.019	0.000	0.010	0.000	0.000	0.000	0.000	0.000	0.000	0.020	0.000	0.000	0.000
Ca	0.076	1.765	1.880	0.065	1.854	0.086	1.907	0.080	1.908	0.080	1.809	0.023	0.018
Na	0.000	0.230	0.326	0.000	0.308	0.000	0.270	0.000	0.251	0.000	0.273	0.000	0.000
K	0.000	0.070	0.077	0.000	0.088	0.000	0.082	0.000	0.072	0.000	0.085	0.000	0.000
SUM	14.990	15.373	15.470	15.024	15.502	15.020	15.561	14.988	15.476	15.016	15.487	20.050	20.007
Cl	0.000	0.000	0.000	0.000	0.000	0.000	0.000	0.000	0.000	0.000	0.000	0.000	0.000
Fe/(Fe + Mg)	0.8192	0.8596	0.8258	0.8952	0.9237	0.9642	0.9667	0.9506	0.9564	0.8995	0.9198	0.8373	0.8080

Notes: FeO^+ = total iron as FeO; n.a.= not analysed; 0.000= not detected; H_2O (dif)= H_2O by difference from 100%. Rock types 3= pelitic IF; 4= possibly altered pelitic IF; 5= unmineralized IF; 6= weakly mineralized IF; 7= pyrite mineralized IF; 8= arsenide mineralized IF.

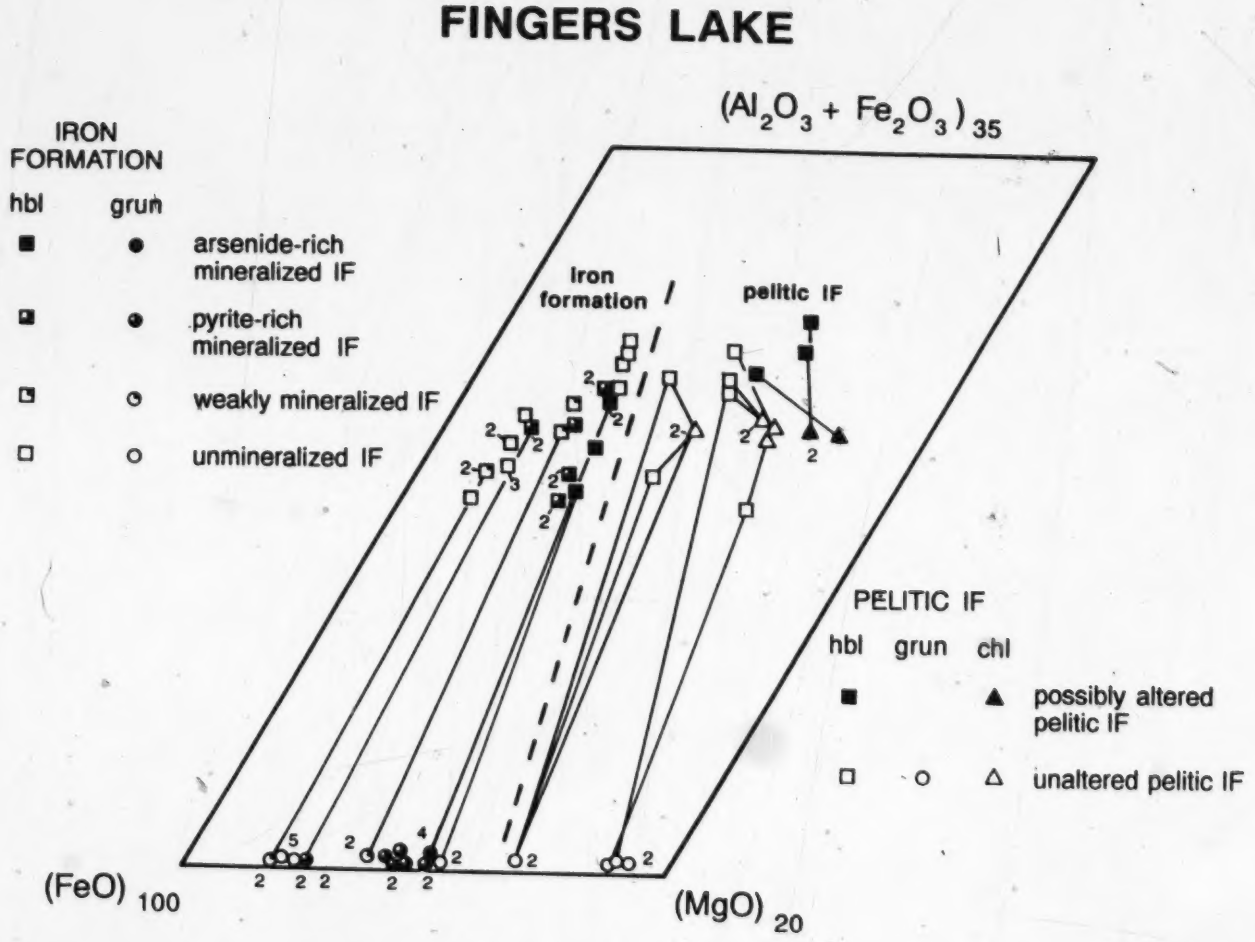

Fig. 3.7. $(Al_2O_3 + Fe_2O_3)$ - (MgO) - (FeO) ternary diagram of minerals from the Fingers Lake iron formation.

magnetite is abundant at Fingers Lake and that it is often replaced by pyrite (Chapter 2). The following reaction represents this process:

$$Fe_3O_4 + 6H_2S + O_2 \rightarrow 3\ FeS_2 + 6H_2O. \qquad (4)$$

This reaction will not directly affect the compositions of the amphiboles but is equally as effective as reaction (3) in depositing gold complexed by aqueous sulphide. Therefore, if much of the iron that forms the iron sulphides is derived by the breakdown of magnetite then the amphiboles would not be expected to have lower X_{Fe} values where sulphides are abundant. This interpretation is consistent with the petrographic observations that magnetite is abundant and is commonly replaced by pyrite.

The presence of pyrite, rather than pyrrhotite, also has an effect on the magnitude of the changes in X_{Fe} in silicates due to sulphidation. This is because pyrite is a disulphide and pyrrhotite is a monosulphide and therefore twice as much sulphur would have to be added to the iron formation to cause the same change in the X_{Fe} values of the silicates.

It is noteworthy that at Fingers Lake, as at Esker Lake, mineralization does not occur in pelitic iron formation adjacent to quartz veins. The mineralization is limited to portions of the iron formation that apparently had the highest bulk X_{Fe} values. This is also consistent with the sulphidation model.

In conclusion, the data from Fingers Lake are compatible with a sulphidation model in which most of the iron incorporated into the sulphides is derived by the breakdown of magnetite. Petrographic data suggest that magnetite contributed most of the iron in the sulphides.

F. Lupin

Geology and mineralogy

The geology of the Lupin mine has previously been described by Kerswill (1984, 1985a,b, 1986), Lhotka and Nesbitt (1987a,b) and Gardiner (1986). The following description is summarized from Chapter 2. Fig. 3.8 is a simplified version of the geology at Lupin. In the mine and to the northwest, beds of iron formation define tight to isoclinal anticlines and synclines, with near vertical limbs, that plunge northwesterly at 65-70°. Southeast of the shaft at L-18 and L-16 large folds plunge to the southeast at about 85°. The surface trace of the cordierite isograd cuts across the major folds north of Lupin and intersects the mine workings at depth, thereby defining a southeast dip to the isograd surface (R. Bullis personal communication, 1987). Granitic plutons intrude the folded sedimentary sequence about 1.5 km north of, and 1.5 km southwest of the shaft.

The Lupin orebody is divided into three zones, the West, Centre and East Zones, which are actually the limbs of a continuous anticline-syncline pair defined by the Lupin iron formation. All of the gold mined to date at Lupin comes from these three zones. The iron formation can be subdivided into mineralized and unmineralized varieties, pelitic iron formation, and minor amounts of mudstone and fine grained greywacke.

Mineralized iron formation, that is sulphide-rich iron formation, constitutes the principal gold-bearing lithology in the mine. This rock type comprises abundant, fine grained disseminated pyrrhotite that together with quartz and amphibole commonly form bands in the iron formation. Hornblende is the predominant amphibole and is much more abundant than grunerite, which never predominates where pyrrhotite is abundant. In well mineralized samples grunerite is often absent. Where grunerite is present it forms the core to grains

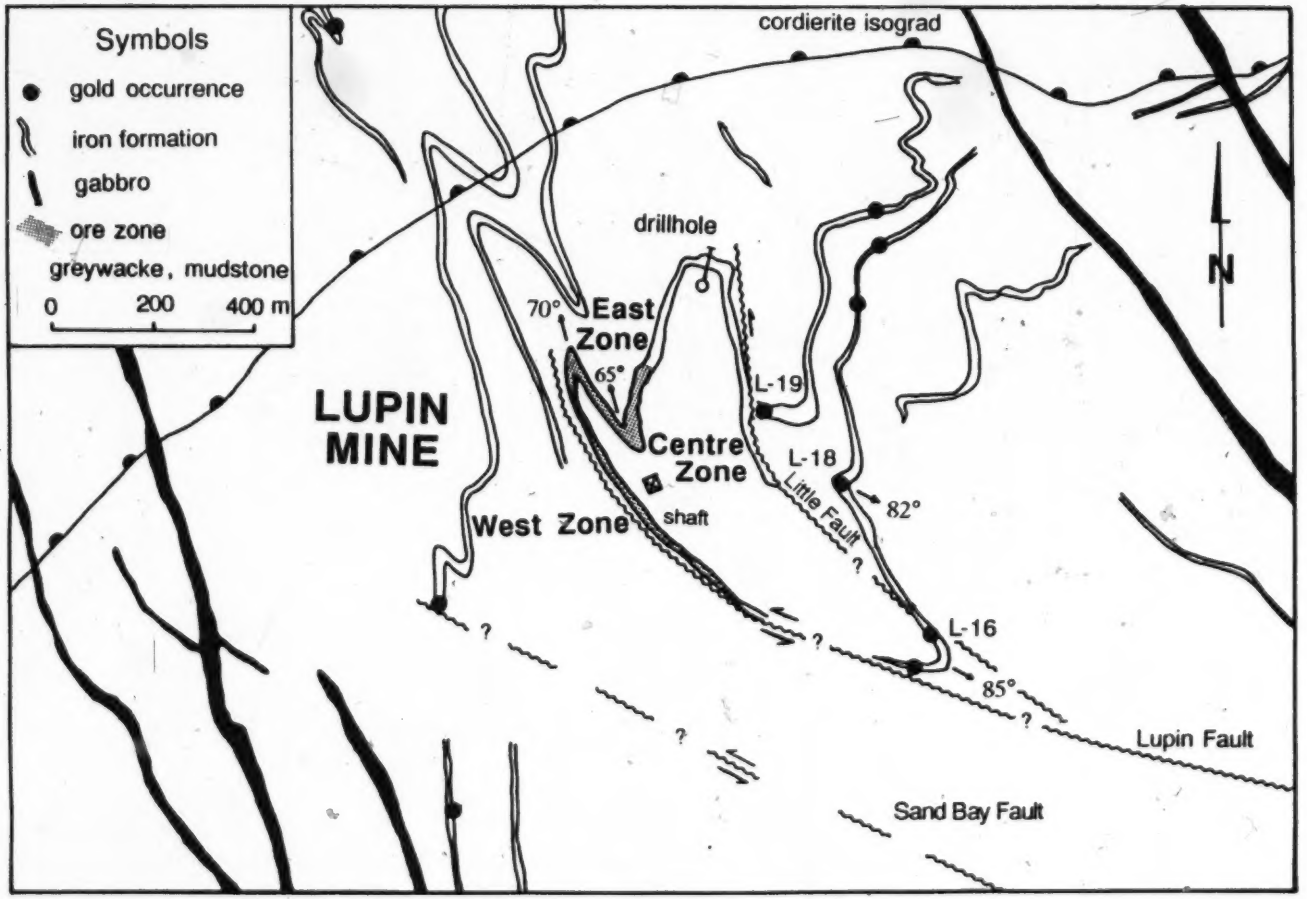

Fig. 3.8. Geology map of the Lupin area showing the ore zones and other localized areas of gold mineralization. Faults and possible faults modified after Gardiner (1986).

of hornblende. Coarse grained hedenbergite is often present, and may locally be abundant. Actinolite and sometimes hornblende replace hedenbergite along fractures. Actinolite also sometimes rims coarse grained hornblende. Actinolite and hornblende occurrences of this type may be paragenetically late and are referred to as retrograde hereinafter. Other minor or trace phases in mineralized iron formation include epidote, chalcopyrite, ilmenite, pyrite and graphite.

Adjacent to late quartz veins porphyroblasts of arsenopyrite, which contain cores of loellingite, overgrow pyrrhotite in mineralized iron formation. The quartz veins comprise strained quartz with sutured grain boundaries. Trace amounts of hedenbergite, hornblende, actinolite, pyrrhotite, pyrite, arsenopyrite, loellingite, scheelite, and rarely, visible gold, generally comprise <2 % of the vein material. These veins clearly control the distribution of arsenides in the mineralized iron formation.

Unmineralized iron formation, that is iron formation with trace or less than trace amounts of visible sulphide, is rarely present within ore grade portions of the Centre and West Zones, but is more common in relatively gold-poor parts of the East Zone. This rock type comprises well banded grunerite and quartz. In thin section, grunerite is the predominant amphibole. Hornblende forms rims to grains of grunerite and varies from a minor proportion of the total amphibole up to about 50 %. Minor amounts of ilmenite, graphite and pyrrhotite are also present, but arsenides are absent. In weakly mineralized iron formation hornblende and pyrrhotite are more abundant than in unmineralized iron formation. Detailed mapping in the northern part of the East Zone (Fig. 3.8), near the edge of the orebody on the 130 m level, was able to trace weakly mineralized grunerite iron formation into pyrrhotite-rich, hornblende iron formation, and finally into arsenide-rich, hornblende iron formation. This transition occurs along the strike of the banding, as a late quartz vein is

approached over a distance of 2.5 m. Beyond the end of the East Zone (Fig. 3.8) unmineralized grunerite-rich iron formation is the predominant type of iron formation and mineralized iron formation is absent or present only as narrow zones adjacent to quartz veins.

Pelitic iron formation forms thin, generally <1 m wide, lenses or beds within the Lupin iron formation. Almandine-rich garnet, grunerite, chlorite and quartz comprise the pelitic iron formation. Hornblende and biotite are sometimes present, as are trace amounts of ilmenite, graphite, allanite, zircon, and rarely, pyrrhotite and arsenopyrite.

Sulphide-poor, calc-silicate rocks form a volumetrically minor, but important, part of the Lupin orebody. Calc-silicate rocks comprise hedenbergite and quartz as the major phases. Epidote is commonly present as a minor component; however, in some samples intergrown epidote and grossular-rich garnet are abundant. Minor phases present include scheelite, calcite, sphene, apatite, ilmenite and graphite. Microveinlets of hornblende, actinolite, pyrrhotite, arsenopyrite, loellingite and gold cut across and replace hedenbergite in calc-silicate rocks. The calc-silicate rocks are interpreted to represent alteration zones within the iron formation.

Mineral chemistry of iron formation

Electron microprobe analyses were performed on samples from the ore zones of the Lupin mine and from a drillhole that intersects the continuation of the Lupin iron formation unit about 220 m north of the East Zone (Fig. 3.8). Representative examples of electron microprobe analyses of the 174 mineral analyses from the Lupin iron formation unit are included in Table 3.3. The compositions of minerals from iron formation and pelitic iron formation are shown on ternary diagrams (Fig. 3.9*A*,*B*) with the appices (Al_2O_3+Fe_2O_3) -

Table 3.3 Representative electron microprobe analyses of amphiboles, chlorites, pyroxenes,garnets and epidotes from the Lupin mine area.

sample	5A105	5A069	5A120	5A120	5A057	5A057	5A017	5A024	5A062
rock type	3	4	5	5	6	6	7	7	7
analysis	hbl 1	grun 1	grun 2	hbl 2	grun 2	hbl 2	hbl 5	hbl 3	hbl 1
SiO_2	40.25	51.05	48.22	42.21	48.32	39.80	41.25	42.08	43.77
Al_2O_3	19.34	0.35	0.39	9.07	0.52	16.62	15.64	14.47	10.11
Cr_2O_3	0.09	0.00	0.00	0.00	0.00	0.00	n.a.	n.a.	0.00
TiO_2	0.12	0.39	0.00	0.16	0.00	0.16	0.21	0.17	0.17
MgO	3.58	7.56	1.64	1.14	1.96	1.01	3.32	2.57	2.21
FeO+	21.94	39.07	46.27	32.60	46.37	28.01	25.64	27.20	29.99
MnO	0.00	0.00	0.00	0.00	0.00	0.00	n.a.	n.a.	0.00
CaO	11.02	0.63	0.70	10.76	0.48	10.95	11.80	12.05	11.25
Na_2O	1.07	0.00	0.00	0.52	0.00	0.46	0.56	0.53	0.49
K_2O	0.42	0.00	0.00	0.42	0.00	0.35	0.25	0.26	0.22
Cl	0.00	0.00	0.00	0.00	0.00	0.00	n.a.	n.a.	0.00
TOTAL	97.82	99.06	97.22	96.88	97.64	97.36	98.66	99.32	98.19
H_2O (dif)	2.18	0.94	2.78	3.12	2.36	2.64	1.34	0.68	1.81
	amphiboles: cations based on anhydrous O + Cl =23								
Si	6.100	7.937	7.977	6.838	7.951	6.246	6.317	6.445	6.863
Al iv	1.900	0.063	0.023	1.162	0.049	1.755	1.683	1.555	1.137
Al vi	1.555	0.002	0.054	0.571	0.052	1.320	1.140	1.056	0.731
Cr	0.011	0.000	0.000	0.000	0.000	0.000	0.000	0.000	0.000
Ti	0.013	0.046	0.000	0.020	0.000	0.019	0.024	0.020	0.020
Mg	0.808	1.752	0.405	0.275	0.480	0.236	0.756	0.587	0.516
Fe	2.780	5.079	6.401	4.418	6.381	3.676	3.284	3.485	3.932
Mn	0.000	0.000	0.000	0.000	0.000	0.000	0.000	0.000	0.000
Ca	1.789	0.105	0.124	1.868	0.085	1.841	1.935	1.978	1.890
Na	0.315	0.000	0.000	0.162	0.000	0.140	0.168	0.157	0.148
K	0.081	0.000	0.000	0.087	0.000	0.070	0.050	0.052	0.043
SUM	15.351	14.984	14.984	15.400	14.998	15.303	15.356	15.334	15.278
Cl	0.000	0.000	0.000	0.000	0.000	0.000	0.000	0.000	0.000
Fe/(Fe+Mg)	0.7749	0.7435	0.9405	0.9414	0.9300	0.9396	0.8128	0.8558	0.8841

Table 3.3 continued.

sample	5A020	5A064	5A064	5A062	5A062	5A105	5A069	5A105	5A062	5A056	5A041
rock type	8	8	8	9	9	3	4	3	7	9	9
analysis	hbl 5	act 2 retro	hbl 2 retro	act 1 retro	hbl 1 retro	bio 1	chlor 1	chlor 1	hed 1	hed 1	hed 1
SiO_2	42.55	49.46	46.58	48.94	43.44	34.28	24.04	24.21	47.93	48.84	49.15
Al_2O_3	13.28	0.79	6.19	0.47	7.83	18.08	19.74	21.29	0.53	0.38	0.21
Cr_2O_3	n.a.	0.00	0.00	0.00	0.00	0.00	0.13	0.11	0.00	0.09	0.08
TiO_2	0.16	0.00	0.14	0.00	0.09	2.08	0.19	0.22	0.00	0.00	0.00
MgO	3.07	2.01	3.48	0.65	0.84	6.63	6.56	9.69	0.65	2.25	1.13
FeO+	27.96	34.44	30.41	35.34	31.91	24.85	38.78	33.29	28.60	26.13	27.10
MnO	n.a.	0.00	0.00	0.00	0.00	0.00	0.00	0.00	0.08	0.07	0.00
CaO	11.29	11.16	11.14	11.44	11.14	0.00	0.12	0.10	22.15	22.72	22.80
Na_2O	0.52	0.00	0.31	0.00	0.33	0.13	0.12	0.27	0.00	n.a.	n.a.
K_2O	0.24	0.00	0.09	0.07	0.21	8.56	0.00	0.08	0.00	0.00	0.00
Cl	n.a.	0.00	0.00	0.18	0.00	0.00	0.00	0.00	n.a	n.a	n.a
TOTAL	99.07	97.87	98.34	97.09	95.80	94.61	89.69	89.25	99.94	100.47	100.46
H_2O (dif)	0.93	2.13	1.66	2.91	4.20	5.39	10.32	10.75			
	amphiboles cations: based on anhydrous O + Cl =23			chlorite: cations based on 28 oxygens biotite: cations based on 22 oxygens					pyroxenes: cations based based on 6 oxygens		
Si	6.545	7.895	7.276	7.962	7.076	5.391	5.347	5.246	1.977	1.979	1.999
Al iv	1.455	0.105	0.724	0.038	0.925	2.610	2.653	2.755	0.026	0.018	0.010
Al vi	0.953	0.045	0.417	0.052	0.579	0.741	2.522	2.684	0.003	0.000	0.009
Cr	0.000	0.000	0.000	0.000	0.000	0.000	0.024	0.013	0.000	0.003	0.003
Ti	0.018	0.000	0.016	0.000	0.011	0.246	0.032	0.036	0.000	0.000	0.000
Mg	0.703	0.479	0.810	0.156	0.205	1.554	2.176	3.129	0.040	0.136	0.068
Fe	3.597	4.597	3.974	4.808	4.347	3.269	7.213	6.034	0.986	0.885	0.922
Mn	0.000	0.000	0.000	0.000	0.000	0.000	0.000	0.000	0.003	0.002	0.000
Ca	1.861	1.908	1.865	1.993	1.945	0.000	0.029	0.024	0.979	0.966	0.993
Na	0.155	0.000	0.094	0.000	0.104	0.041	0.051	0.111	0.000	n.a.	n.a.
K	0.048	0.000	0.018	0.014	0.044	1.716	0.000	0.022	0.000	0.000	0.000
SUM	15.335	15.029	15.193	15.025	15.235	15.566	20.046	20.057	4.010	4.010	3.995
Cl	0.000	0.000	0.000	0.050	0.000	0.000	0.000	0.000	n.a.	n.a.	n.a.
Fe/(Fe + Mg)	0.8364	0.9056	0.8306	0.9685	0.9550	0.6778	0.7683	0.6585	0.9609	0.8668	0.9309

Table 3.3 continued.

sample	5A105	5A105	5A069	5A069	4A031	5A056	5A041	5A041	5A056	5A056
rock type	3	3	4	4	9	9	9	9	9	9
analysis	gar core	gar rim	gar 1 core 1	gar 1 rim 1	gar rim	gar 1	epi 1 low z	epi 1 high z	epi high z	epi low z
SiO_2	36.64	36.73	36.36	36.47	38.60	38.55	39.98	41.08	40.36	38.22
Al_2O_3	21.52	21.47	21.28	21.21	19.27	19.40	25.35	24.48	25.03	25.88
TiO2	0.00	0.09	0.00	0.00	0.00	0.00	0.00	0.00	0.00	0.00
Cr_2O_3	0.00	0.10	0.00	0.00	0.00	0.00	0.08	0.00	n.a.	n.a.
Fe_2O_3*	0.49	0.52	0.95	0.92	4.35	5.22	7.69	6.83	7.49	9.91
FeO*	35.53	36.53	36.84	36.96	4.26	1.69	2.48	4.72	3.51	0.00
MgO	1.55	1.76	1.63	1.67	0.08	0.19	0.42	0.46	0.49	0.46
MnO	1.35	0.39	0.00	0.00	0.11	0.00	0.00	0.00	0.00	0.00
CaO	3.97	3.78	3.78	3.63	32.64	35.00	21.26	19.50	20.40	24.06
K_2O	0.00	0.00	n.a.	n.a.	0.00	0.00	0.00	0.00	0.00	0.00
Na_2O	n.a.	n.a.	n.a.	n.a.	n.a.	n.a.	n.a.	n.a.	0.00	0.00
TOTAL	101.06	101.37	100.83	100.87	99.31	100.05	97.26	97.06	97.28	98.55
H_2O (dif)							2.74	2.94	2.72	1.45
					garnet and epidote cations normalized to 8					
Si	2.937	2.935	2.925	2.934	2.989	2.950	3.167	3.280	3.206	2.979
Al	2.034	2.022	2.017	2.011	1.758	1.749	2.367	2.304	2.343	2.377
Ti	0.000	0.005	0.000	0.000	0.000	0.000	0.000	0.000	0.000	0.000
Cr	0.000	0.007	0.000	0.000	0.000	0.000	0.005	0.000	0.000	0.000
Fe^{3+}	0.030	0.031	0.058	0.055	0.253	0.301	0.453	0.401	0.441	0.583
Fe^{2+}	2.383	2.441	2.478	2.487	0.276	0.108	0.146	0.277	0.206	0.000
Mg	0.185	0.209	0.196	0.201	0.010	0.022	0.050	0.054	0.058	0.054
Mn	0.091	0.026	0.000	0.000	0.007	0.000	0.000	0.000	0.000	0.000
Ca	0.341	0.324	0.326	0.313	2.708	2.870	1.805	1.668	1.736	2.009
O	11.969	11.970	11.962	11.967	11.994	11.975	12.572	12.617	12.587	12.461
$Fe^{2+}/(Mg + Fe^{2+})$	0.9278	0.9210	0.9267	0.9253	0.9664	0.8322	0.7449	0.8369	0.7803	0.0000
$Fe^{2+}/(Fe^{2+} + Fe^{3+})$	0.9877	0.9873	0.9773	0.9783	0.5214	0.2645	0.2435	0.4086	0.3188	0.0000

Notes: FeO+ = total iron as FeO; Fe2O3* and FeO* estimated by stoichiometry (see text for method). n.a.= not analysed; 0.000= not detected; H_2O (dif)= H_2O by difference from 100% ; z= relative average atomic number determined by backscattered electron imagery. Rock types 3= pelitic IF; 4= possibly altered pelitic IF; 5= unmineralized IF; 6= weakly mineralized IF; 7= pyrrhotite mineralized IF; 8= arsenide mineralized IF; 9= calc-silicate rocks.

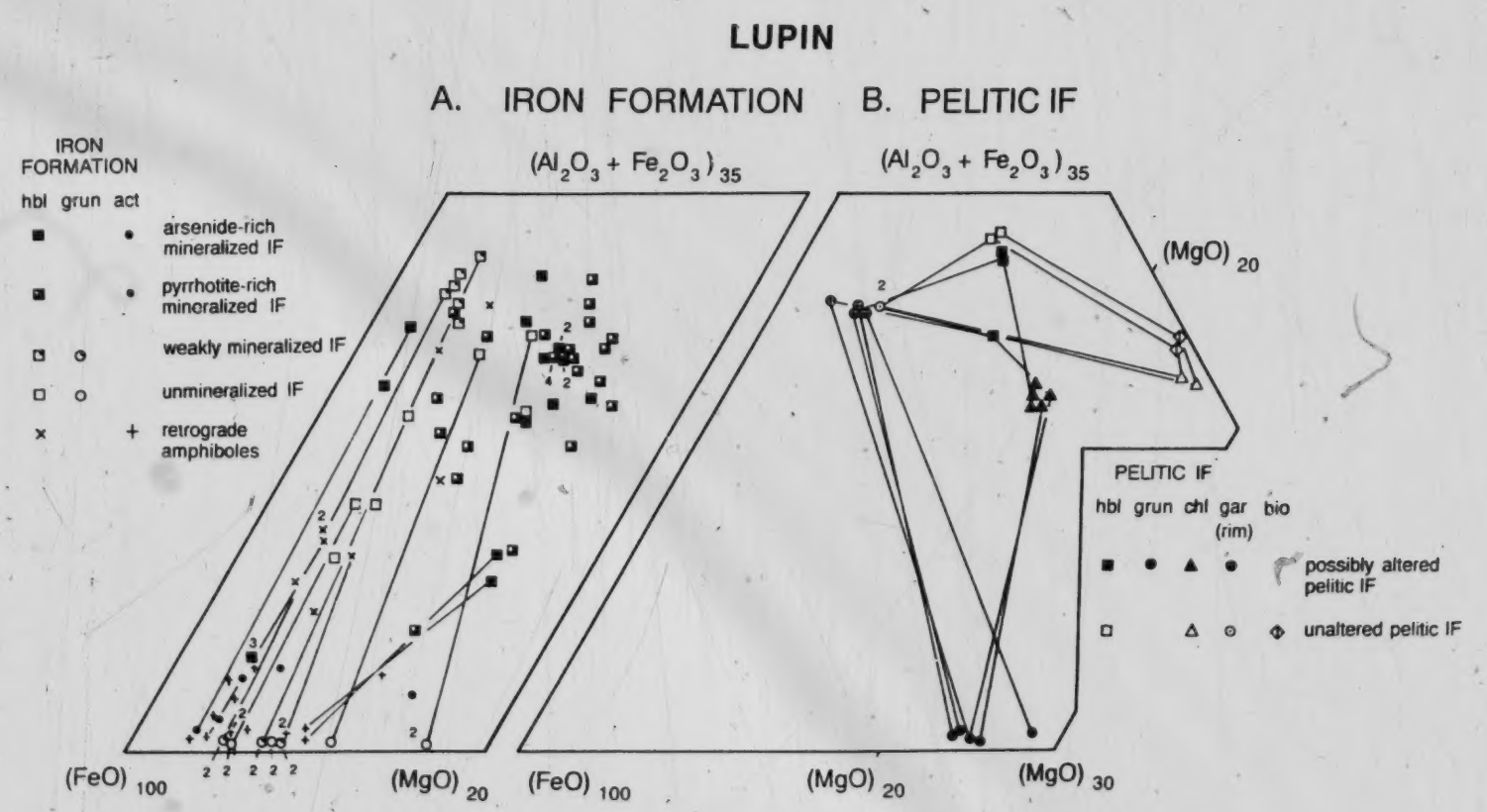

Fig. 3.9. (Al_2O_3 + Fe_2O_3) - (MgO) - (FeO) ternary diagram of minerals from the Lupin iron formation. *A.* Iron formation. *B.* Pelitic iron formation.

(FeO) - (MgO). As expected, when the mineral chemistry of pelitic iron formation is compared to that of the iron formation, the iron silicates in pelitic iron formation tend to have lower X_{Fe} values (Fig. 3.9).

When the compositions of amphiboles in iron formation are plotted together with the abundance of sulphides (Fig. 3.9 *A*), it is evident that the amphiboles from mineralized iron formation tend to have lower X_{Fe} values than amphiboles from unmineralized and weakly mineralized iron formation. There is, however, some overlap between the groups. Retrograde actinolite and hornblende in mineralized iron formation and in calc-silicate rocks tend to have higher X_{Fe} values than the typical amphiboles in mineralized iron formation. Tie lines joining some of the retrograde actinolites to the non-retrograde hornblendes in the same sample, clearly indicate that the retrograde actinolites are not in equilibrium with the non-retrograde hornblendes (Fig. 3.9 *A*).

One possible reason for the imperfect correlation between the sulphide abundance and the X_{Fe} compositions of the amphiboles is the possibility that there are significant variations in the bulk composition of unmineralized iron formation. In order to minimize the effect of this possibility, three samples of iron formation from the 130 m level of the East zone were analysed. These samples were collected along strike in iron formation as a quartz vein was approached over a distance of 250 cm. The sample furthest from the vein is weakly mineralized, grunerite-rich iron formation with minor amounts of hornblende and trace amounts of pyrrhotite. The sample collected at a distance of 60 cm from the vein contains abundant pyrrhotite and is hornblende-rich with minor amounts of hedenbergite, epidote and no grunerite. The sample collected 30 cm from the vein contains abundant pyrrhotite and arsenides and is hornblende-rich with minor amounts of hedenbergite and trace amounts of grunerite. In both mineralized samples hedenbergite is partially replaced by

retrograde hornblende and actinolite. The analyses of hornblendes in these three samples, with the exception of the retrograde hornblendes in hedenbergite, have a good correlation between the X_{Fe} values of the amphiboles, distance from the vein, and abundance of sulphides and gold (Fig. 3.10). The retrograde hornblendes have higher X_{Fe} values than do the coarse grained hornblendes intergrown with sulphides and are not in equilibrium with them. The pattern and magnitude of the variation in amphibole compositions at this location is very similar to the Esker Lake data (Fig. 3.4), where a similar sampling pattern was employed. This suggests that sulphidation of iron silicates occurred at this location in the Lupin mine.

With this evidence for sulphidation in mind, the data in Fig. 3.9*A* can be reexamined. All of the data points for unmineralized iron formation lacking sulphides are from the drillhole north of the East Zone. Hornblendes from these rocks range from X_{Fe} 0.80 to 0.98, although most of the X_{Fe} values are near 0.94. Since these samples contain no appreciable sulphides, this variation is not due to sulphidation and is probably due to variations in the bulk X_{Fe} values of the samples. It is important to note that the weakly mineralized sample from the East Zone described above, which contains only traces of pyrrhotite, has hornblende with an X_{Fe} composition of 0.94 to 0.95. This suggests that the bulk X_{Fe} value of weakly mineralized iron formation within the mine is similar to the typical bulk X_{Fe} value of unmineralized iron formation along strike from the mine. The tendency of amphiboles from mineralized samples to have lower X_{Fe} values due to sulphidation is thus superimposed on the previously existing variations in the bulk composition of the iron formation. These two factors combine to produce the overlapping distribution of data in Fig. 3.9*A*.

Amphiboles, which do not follow the trend of lower X_{Fe} values as the abundance of sulphide mineralization increases, come primarily from the

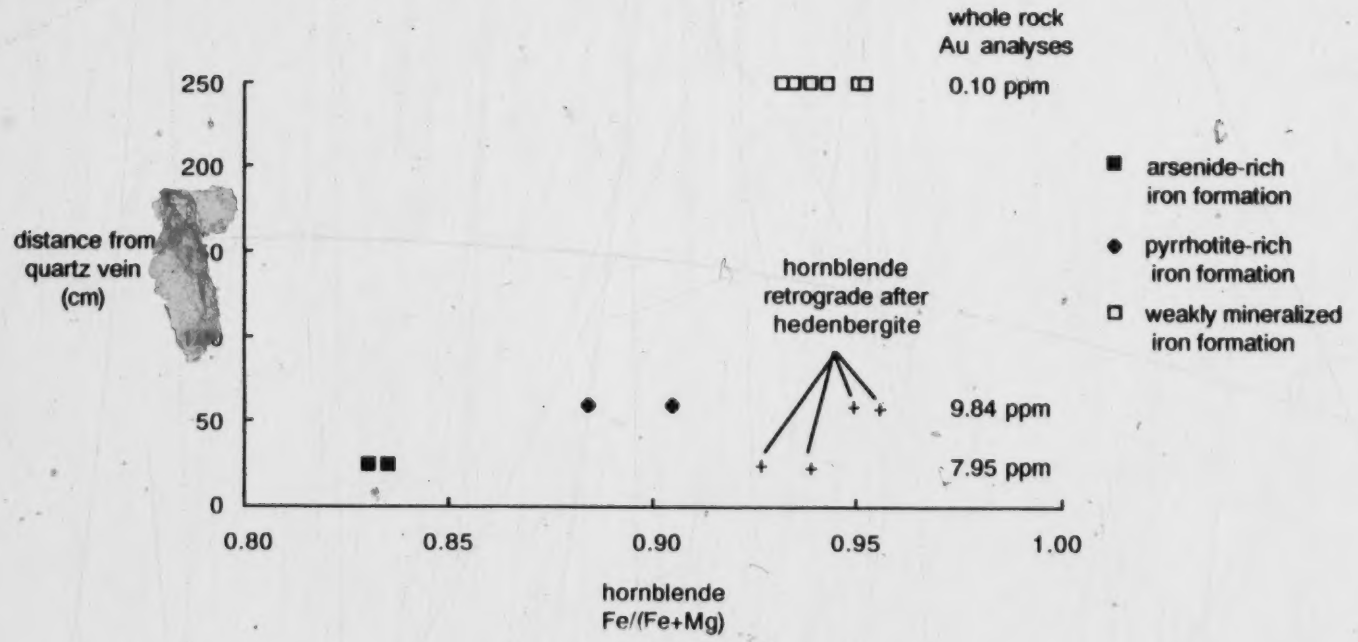

Fig. 3.10. X_{Fe} of hornblende versus distance from a quartz vein in the East Zone of the Lupin mine.

arsenide-rich mineralized iron formation and not from the pyrrhotite-rich mineralized iron formation (Fig. 3.9*A*). This may be due to the arsenide-rich and pyrrhotite-poor nature of some of these samples. Arsenide-rich rocks would be expected to have somewhat higher amphibole X_{Fe} values than pyrrhotite-rich rocks because the arsenides arsenopyrite and loellingite are disulphide minerals instead of monosulphide minerals like pyrrhotite. Thus, the effect of arsenides on the X_{Fe} values is similar to the effect of pyrite previously noted in the discussion of the Fingers Lake data.

Another possible explanation for the higher X_{Fe} values of the amphiboles in the arsenide-rich mineralized iron formation is that these amphiboles may have partially or completely equilibrated with the fluids that produced the retrograde amphiboles.

Mineral chemistry of pelitic iron formation

Minerals were analysed from samples of pelitic iron formation from within the Lupin mine and the drillhole north of the East Zone (Fig. 3.9*B*). The sample of unaltered pelitic iron formation from the drillhole is somewhat unusual in that it lacks grunerite, and contains biotite in addition to almandine-rich garnet, chlorite and hornblende. The sample was examined because it contains coexisting biotite and garnet. The mineral chemistry of the phases in this sample are distinctive in that chlorite and garnet are significantly more MgO-rich than chlorites and garnets in any other pelitic iron formation analysed as part of this study. The hornblende in this sample is also very Al_2O_3-rich. These data suggest that this sample contains a higher proportion of pelitic, detrital material than the other pelitic iron formations. The coexistence of almandine-rich garnet and biotite in this sample is also unusual; textures of these two minerals suggest that they are in equilibrium.

The chemistry of minerals in possibly altered pelitic iron formation from Lupin (Fig. 3.9*B*) is very similar to the chemistry of minerals in unaltered and possibly altered pelitic iron formation at Esker Lake (Fig. 3.3*B*). This suggests that these pelitic iron formations have similar bulk chemistries. One difference does however exist in the chemistry of the almandine-rich garnets. At Lupin analyses of the cores and rims of the almandine-rich garnets have similar compositions. The minor variations that were found are much smaller than at Esker Lake (Fig. 3.6) and there is no pattern in the variations that can be related to the proximity of veining or mineralization.

Mineral chemistry of calc-silicate rocks

The calc-silicate rocks have a significantly different mineralogy than other rocks at Lupin. These rocks are characterized by the minerals hedenbergite ± epidote ± grossular-rich garnet. These minerals contain large amounts of Ca ± Al. Representative analyses of these phases (Table 3.3) show the marked difference in the chemistry of the grossular-rich garnets in comparison to the previously described almandine-rich garnets. Zoning was not found in the grossular-rich garnets and no grains were found that contain both garnet varieties. Hedenbergite has X_{Fe} values of 0.81 to 0.96. A pattern has not been recognized in the X_{Fe} values of hedenbergite. The johannsenite molecule accounts for <1% of the pyroxene.

Epidotes comprise inhomogeneous grains which are not systematically zoned. Examination of the epidote grains by backscattered electron imagery revealed differences in the chemistry and the analysed areas were selected to determine the maximum variation within a grain or group of grains. Although the analytical totals remain constant at reasonable values, the concentrations of Si,

Fe, Ca and Al vary considerably. Further work would have to be performed to explain these variations in the epidote chemistry.

Interpretation of the mineral assemblages

Compositions of the calc-silicate minerals are plotted together with the minerals present in the other rock types at Lupin in Fig. 3.11. Petrographic and field evidence indicates that the mineralized hornblende-rich iron formation is derived by alteration of the grunerite-rich iron formation associated with quartz veining. This suggests that Ca and Al were added to the iron formation during the alteration and mineralization event. The calc-silicate rocks, which are present at Lupin, represent the extension of this trend, indicated by an arrow in Fig. 3.11, to increasingly Ca- and Al-rich bulk compositions. The calc-silicate rocks are therefore best interpreted as the most highly altered portion of the iron formation. This interpretation is consistent with the known distribution of the calc-silicate rocks as being spatially associated with quartz veined and mineralized portions of the iron formation and not with unmineralized grunerite-rich iron formation. The trends in the inferred changes in the bulk composition of iron formation at Lupin, due to mineralization and pelitic contamination, are identical to the trends at Esker Lake (Fig. 3.5). In both cases it appears that mineralization of iron formation involves addition of Ca and Al by epigenetic processes.

G. Discussion

In the previous sections specific conclusions were made on the data for the Esker Lake and Fingers Lake occurrences and the Lupin mine. The data from these areas are used here to develop more generalized conclusions, and

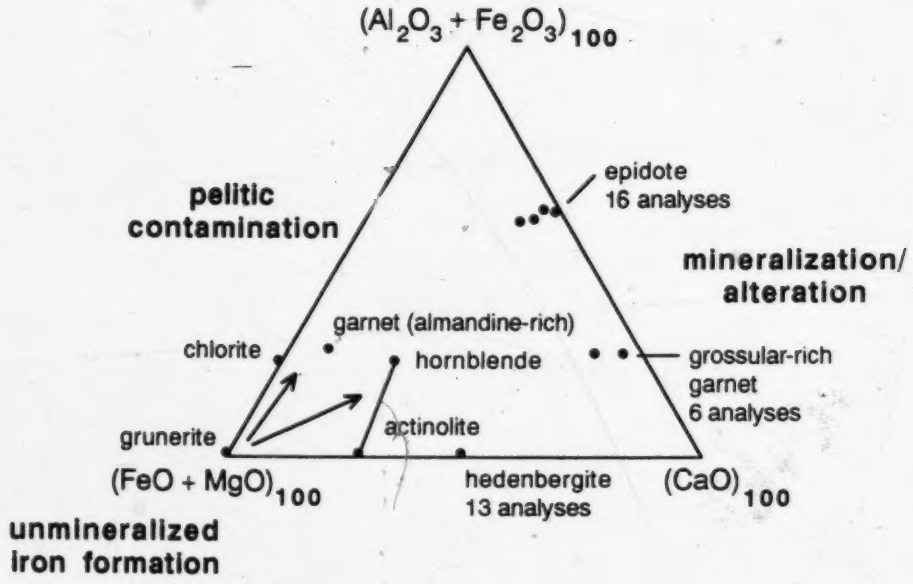

Fig. 3.11. $(Al_2O_3 + Fe_2O_3)$ - (CaO) - (FeO + MgO) ternary diagram of minerals from Lupin iron formation.

to build upon the previously proposed epigenetic model of the gold mineralization (Chapter 2).

Fig. 3.12 depicts the X_{Fe} values of amphiboles from Lupin, Esker Lake and Fingers Lake. The histograms in Fig. 3.12 show that amphiboles from samples of unmineralized and weakly mineralized iron formation, from all three areas, tend to have X_{Fe} values between 0.88 and 0.98. A few amphiboles from these rock types have X_{Fe} values as low as 0.80. Amphiboles in pelitic iron formation have X_{Fe} values that are typically between 0.70 and 0.82, although a few amphiboles with X_{Fe} values of as high as 0.90 were found. The similarity in the respective X_{Fe} values of amphiboles in pelitic iron formation, unmineralized iron formation and weakly mineralized iron formation, between the Lupin, Esker Lake and Fingers Lake areas, indicates that these rock types are comparable in the different areas. The lower X_{Fe} values of amphiboles from pelitic iron formation in all areas is due to the lower bulk X_{Fe} value of the pelitic iron formation. All of these rock types contain trace amounts of sulphide and low gold values.

Amphiboles in arsenide-rich and pyrrhotite- or pyrite-rich mineralized iron formation, at all three areas, typically have lower X_{Fe} values than the unmineralized and weakly mineralized iron formation. At Fingers Lake, the X_{Fe} values of amphiboles in these rocks range from 0.84 to 0.96 with most of the values near 0.90. At Esker Lake, the X_{Fe} values of amphiboles in mineralized iron formation range from 0.84 to 0.90. At Lupin, the X_{Fe} values of amphiboles in pyrrhotite-rich mineralized iron formation range from 0.78 to 0.94; most of the values are between 0.80 and 0.86. In the arsenide-rich mineralized iron formation at Lupin there is an indication that the amphiboles have a bimodal distribution with one group having X_{Fe} values of 0.82 to 0.86. This group of values is similar to the typical X_{Fe} values in pyrrhotite-rich mineralized iron

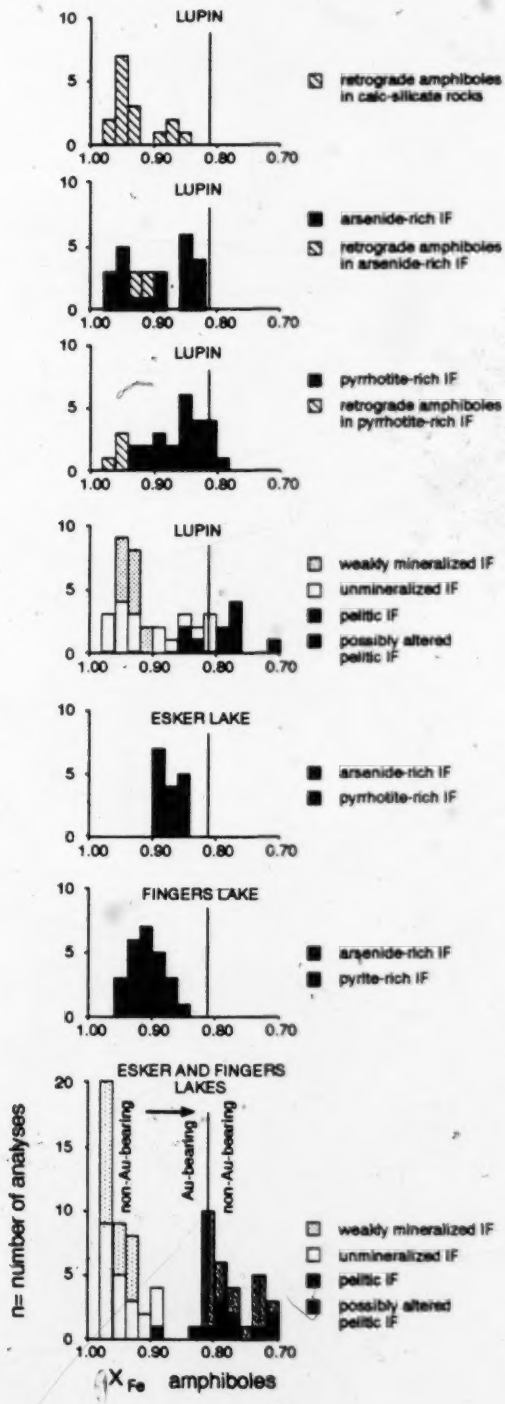

Fig. 3.12. Summary histogram of the X_{Fe} values in amphiboles in iron formation at Lupin, Esker Lake and Fingers Lake.

formation. The second group of X_{Fe} values in arsenide-rich mineralized iron formation at Lupin range from 0.88 to 0.98. This group of amphibole X_{Fe} values has a similar distribution to that of the retrograde amphiboles in calc-silicate rocks, and retrograde amphiboles in arsenide-rich and pyrrhotite-rich mineralized iron formation.

The histograms from all three areas indicate that there is a definite trend in the amphiboles from high X_{Fe} values in unmineralized and weakly mineralized iron formation to lower X_{Fe} values in mineralized iron formation. It has been shown in two locations, one at Esker Lake and the other within the Lupin mine, that this trend to lower X_{Fe} values occurs as the abundance of sulphides increases towards a quartz vein. These spatial relationships confirm that the trend to lower amphibole X_{Fe} values in mineralized iron formation is due to epigenetic sulphidation of the iron formation. Assay data in Figs 3.2 and 3.10 indicate that gold values increase as the X_{Fe} values in amphiboles decrease. This trend is shown on the bottom histogram of Fig. 3.12, but it applies to all of the histograms.

Another important observation is that at all three areas there is a well defined boundary, at an X_{Fe} of about 0.81, between the amphibole X_{Fe} values of mineralized iron formation and pelitic iron formation (Fig. 3.12). Amphiboles from pelitic iron formation and possibly altered pelitic iron formation typically have X_{Fe} values lower than 0.81. These rock types are not mineralized and do not have elevated gold values. As the amphibole X_{Fe} of mineralized iron formation approaches the 0.81 boundary, from typical high X_{Fe} values, the amount of sulphide and gold increases. This pattern suggests that the 0.81 value represents the X_{Fe} value of the amphiboles in mineralized rocks in equilibrium with the hydrothermal fluid that caused mineralization by the sulphidation process. This model implies that rocks with amphiboles with the

highest original X_{Fe} values have the greatest potential to become sulphidized. Conversely, rocks with amphiboles with X_{Fe} values less than 0.81 do not have the potential to become sulphidized because the amphiboles in these rocks are already below the X_{Fe} value, which is in equilibrium with the hydrothermal fluid. This explains why pelitic iron formation adjacent to a quartz vein is not mineralized while grunerite-rich unmineralized iron formation is sulphidized adjacent to the same vein.

Phillips and Groves (1983) have pointed out that sulphidation reactions are extremely important in depositing gold in many rock types including iron formation. This is because work by Seward (1973) has shown that gold is efficiently complexed by sulphur in hydrothermal fluids at temperatures of 300 to 400°C and near neutral pH. Since the solubility of gold is directly related to the solubility of sulphur, a decrease in the activity of sulpur will cause deposition of gold. Thus, sulphidation of iron formation adjacent to quartz veins will cause gold deposition. Rocks which are not sulphidized, like pelitic iron formation, will therefore not contain gold.

Another significant observation resulting from this work is that although hornblende replaces grunerite, analyses of these amphiboles almost invariably have parallel tie lines (eg. Fig 3.3*A*) suggesting that these amphiboles are in equilibrium despite textural evidence to the contrary.

The different zoning patterns in the almandine-rich garnets adjacent to veins and distant from veins at Esker Lake indicates that the Ca-enrichment in mineralized iron formation occurred during garnet growth and not prior to garnet growth. This is important because it suggests that the Ca-rich minerals associated with sulphidation and gold mineralization reflect alteration coincident in time with the emplacement of the quartz veining and peak metamorphic temperatures. These data are consistent with the conclusions of

King *et al.* (1988) who state that the late quartz veining is temporally related to the thermal peak of metamorphism.

The compositions of the predominant silicate minerals in unmineralized iron formation, mineralized iron formation, and calc-silicate rocks suggest a trend towards more Ca- and Al-rich mineral assemblages, which is interpreted as being due to metasomatic additions of Ca and Al, as well as Au, S, As.

H. Comparison of the mineral chemistry of the Homestake deposits to the Contwoyto Lake deposits

As mentioned in the introduction very little research has been done on the compositions of silicate minerals in gold-bearing iron formation except for a study by Chinn (1969) on the Homestake deposits of South Dakota. The important parts of Chinn's (1969) study are summarized here because Chinn's data are analagous to the data from this study.

Chinn's study was based upon analyses of samples from the Main, 5, 7, and 9 Ledges. He analysed biotite, chlorite, cummingtonite, hornblende, garnet and carbonates for their major elements. Chinn's main conclusions are as follows:

1) The mineral assemblages are iron-rich and the only significant variations discovered were in the iron and magnesium contents of the minerals.

2) The covariance of X_{Fe} in coexisting minerals suggests that the minerals reached equilibrium despite evidence of complex and contradictory textural relationships.

3) The X_{Fe} of a particular mineral is a function of the coexisting mineral assemblage.

4) The X_{Fe} values of biotite, chlorite and cummingtonite in cummingtonite-bearing assemblages that contain free gold and arsenopyrite are lower than the X_{Fe} values of these minerals in cummingtonite-bearing assemblages in which gold and arsenopyrite are absent .

5) The lowest X_{Fe} biotite and chlorite compositions are found in muscovite-bearing assemblages. (None of Chinn's muscovite-bearing samples contain arsenopyrite or gold.)

Chinn also pointed out some pertinent petrographic features of the Homestake deposits such as the ores being associated with chloritized portions of the Homestake Formation. One feature he notes that is similar to the Contwoyto Lake area, but is not commonly reported by other workers at Homestake, is that hornblende is closely associated with cummingtonite and that hornblende partially, to nearly completely, replaces cummingtonite. As other authors (Noble 1950; Rye and Rye 1974) have pointed out, Chinn states that the gold-bearing zones are essentially confined to the iron-rich Homestake Formation where increased concentrations of arsenopyrite and pyrrhotite are found. Quartz veining is often abundant in the gold-bearing zones (Noble 1950).

Data on the mineral chemistry of cummingtonite, chlorite and biotite, the important phases for which Chinn provides data, are replotted in Fig. 3.13. Chinn divided these minerals into two groups, which are based on the presence or absence of arsenopyrite and gold. The data exhibit a consistent trend whereby the silicates associated with arsenopyrite and gold mineralization have lower X_{Fe} values than the silicates from unmineralized iron formation. He interpreted this trend to lower X_{Fe} values as the result of Fe/Mg-exchange reactions between the hydrothermal ore fluid and the Fe/Mg-silicates in the wallrock through which the fluid was migrating. These reactions were triggered

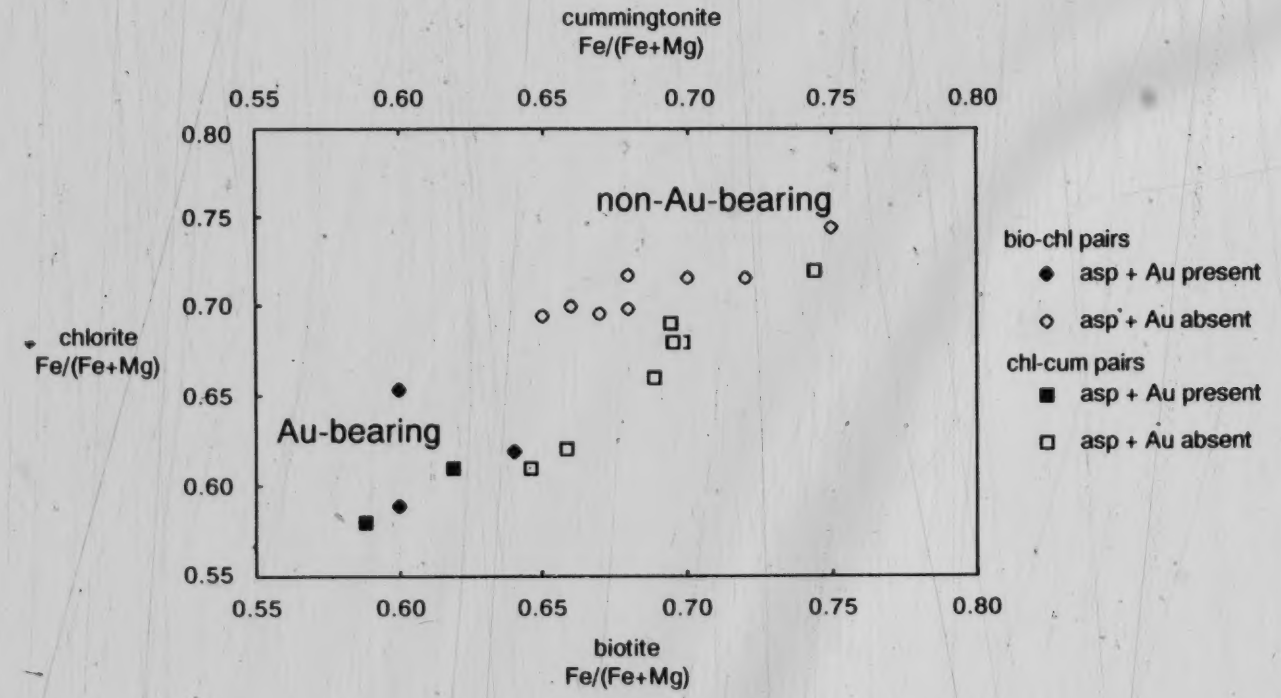

Fig. 3.13. X_{Fe} values in silicate minerals in iron formation from the Homestake Mine, South Dakota. Plotted from data in Chinn (1969).

by the precipitation of arsenopyrite which removed iron, sulphur, and arsenic from solution which caused the removal of Fe from the Fe/Mg-silicates. His interpretation is identical to the interpretation of the Contwoyto Lake data in this study.

Chinn did not state an explanation for the lower X_{Fe} values of biotite and chlorite in non-ore-bearing assemblages with muscovite, and in non-ore-bearing assemblages where cummingtonite is absent (neither of which are replotted here). The lower X_{Fe} values in these sulphide-poor samples, together with their mineral assemblages, suggest that they may represent a lithology like the pelitic iron formation at Contwoyto Lake. The X_{Fe} values of biotite and chlorite in these samples are lower than or equal to the X_{Fe} values of these minerals in the ore-bearing assemblages, a pattern which is consistent with the Contwoyto Lake data.

In summary, Chinn's (1969) data show that mineral assemblages in unmineralized iron formation have high X_{Fe} values, while mineralized iron formation with the same silicate mineral assemblages have lower X_{Fe} values. However, he does not present data to show whether these variations are spatially associated with quartz veins as has been shown at Contwoyto Lake. His data are entirely consistent with the epigenetic sulphidation model developed from the Contwoyto Lake data and may indicate that similar processes occurred at Homestake.

I. Summary

This study has provided independent evidence showing that sulphidation occurs adjacent to quartz veins at small-scale occurrences and at the Lupin mine. The evidence for sulphidation is the decrease in the X_{Fe} values of

amphiboles as the abundance of sulphides increases. The decrease in amphibole X_{Fe} values occurs as quartz veins are approached along strike within the iron formation.

The compositions of the common silicate minerals associated with mineralized iron formation suggest that in addition to Au, S and As that Ca and Al were added to iron formation during alteration associated with sulphidation. These data are consistent with earlier field and petrographic evidence that indicate that the gold mineralization in iron formation at Contwoyto Lake is epigenetic (Chapter 2). Zoning in almandine-rich garnets from the Esker Lake supports the hypothesis (Chapter 2) that mineralization and alteration occurred at or near peak metamorphic conditions. This is consistent with a study by King *et al.* (1988) that concluded that the quartz veins associated with the mineralization were emplaced relatively late in the Archean deformation event at peak thermal conditions.

A reexamination of data from the Homestake deposit is consistent with the model derived from the Contwoyto Lake area; however, further work would have to be done at Homestake to confirm whether the spatial variations in mineral chemistry are related to quartz veining.

J. References

Bostock, H. H. 1980. Geology of the Itchen Lake area, District of Mackenzie. Geological Survey of Canada, Memoir 391.

Bostock, H. H. 1977. The composition of hornblende, grunerite, and garnet in Archean iron formation of the Itchen Lake area, District of Mackenzie, Canada. Canadian Journal of Earth Sciences, **14**: 1740-1752.

Chinn, W. 1969. Structural and mineralogical studies at the Homestake Mine, Lead, South Dakota. Ph.D. thesis, University of California, Berkeley, California. Available from University Microfilms International, Ann Arbour, Michigan.

Deer, W. A., Howie, R. A., and Zussman, J. 1978. An Introduction to the rock forming minerals. Longman Group Limited, London, England.

Einaudi, M. T., Meinert, L. D., and Newberry, R. J. 1981. Skarn deposits. *In* Economic Geology Seventy-fifth Anniversary Volume. *Edited by* B. J. Skinner, pp. 317-391.

Fripp, R. E. P. 1976. Stratabound gold deposits in Archean banded iron formation, Rhodesia. Economic Geology, **71**: 58-75.

Gardiner, J. J. 1986. Structural geology of the Lupin gold mine, Northwest Territories. M.Sc. thesis, Acadia University, Wolfville, Nova Scotia.

Grant, J. A. 1986. The isocon diagram- A simple solution to Gresens' equation for metasomatic alteration. Economic Geology, **81**: 1976-1982.

Groves, D. I., Phillips, G. N., Falconer, L. J., Houstoun, S. M., Ho, S. E., Browning, P., Dahl, N., and McNaughton, N. J. 1987. Evidence for an epigenetic origin for BIF-hosted gold deposits in the greenstone belts of the Yilgarn Block, Western Australia. *In* recent advances in understanding Precambrian gold depsoits. *Edited by* S. E. Ho and D. I. Groves, Geology Department & University Extension, University of Western Australia, Publication II, pp. 167-179.

Hallager, W. S. 1984. Geology of gold-bearing metasediments near Jardine, Montana. *In* Gold'82: the geology, geochemistry of gold deposits. *Edited by* R. P. Foster, Geological Society of Zimbabwe Special Publication 1, pp. 191-218.

Hawthorne, F. C. 1983. The crystal chemistry of the amphiboles. Canadian Mineralogist, **21**: 173-480.

Henderson, J. B. 1970. Stratigraphy of the Yellowknife Supergroup, Yellowknife Bay; Prosperous Lake area, District of Mackenzie. Geological Survey of Canada, paper 70-26.

Kerswill, J. A. 1986. Gold deposits hosted by iron formation in the Contwoyto Lake area, Northwest Territories. *In* Gold'86 Poster Paper Abstracts. *Edited by* A. M. Chater, Geological Association of Canada, Mineral Deposits Division, pp. 82-85.

Kerswill, J. A. 1985a. Gold, Sulphur, and Arsenic in metamorphosed iron formation of the Contwoyto Lake area, Northwest Territories, Canada. Geological Society of America, Abstracts with Program, Annual Meeting, Orlando, Florida, pp. 627.

Kerswill, J. A. 1985b. Gold metallogeny of Archean iron formation in the Contwoyto Lake area, N.W.T. Geological Association of Canada, Program with Abstracts, **10**: A31.

Kerswill, J. A. 1984. The Lupin gold deposit, Contwoyto Lake area, N.W.T; Styles of gold distribution and possible genetic models. Geological Association of Canada, Program with Abstracts, **9**: 78.

King, J. E., Davis, W. J., Relf, C., and Avery, R. W. 1988. Deformation and plutonism in the western Contwoyto Lake map area, central Slave Province, District of Mackenzie, N.W.T. *In* Current research part C. Geological Survey of Canada, paper 88-1C, pp. 161-176.

Lhotka, P. G., and Nesbitt, B. E. 1987a. An epigenetic origin for gold in iron formation in and around the Lupin mine, N.W.T. Geological Association of Canada, Annual General Meeting, Saskatoon, Saskatchewan, Program with Abstracts, **12**: p.67.

Lhotka, P. G., and Nesbitt, B. E. 1987b. Epigenetic gold hosted by iron formation at the Lupin mine, Contwoyto Lake, N.W.T. Geological Association of Canada, Summer Field Meeting, Yellowknife, N.W.T., Program with Abstracts.

Macdonald, A. J. 1983. The iron formation-gold association evidence from the Geraldton area. *In* The geology of gold in Ontario. *Edited by* A. C. Colvine, Ontario Geological Survey, Miscellaneous Paper 110, pp. 75-83.

Macdonald, A. J., and Fyon, J. A. 1986. Sulphidation the key to gold mineralization in banded iron formation. *In* Gold'86 Poster Paper Abstracts. *Edited by* A. M. Chater, Geological Association of Canada, Mineral Deposits Division, pp. 96-97.

Nesbitt, B. E. 1982. Metamorphic sulfide-silicate equilibria in the massive sulfide deposits at Ducktown, Tennessee. Economic Geology, **77**: 364-378.

Noble, J. A. 1950. Ore mineralization in the Homestake gold mine, Lead, South Dakota. Geological Society of America Bulletin, **61**: 221-252.

Perchuk, L. L., and Laverent'eva, I. V. 1982. Experimental investigation of exchange equilibria in the system cordierite-garnet-biotite. *In* Advances in physical geochemistry. Volume II. *Edited by* S. K. Saxena. Springer-Verlag, New York, NY, pp. 199-239.

Phillips, G. N., and Groves, D. I. 1983. The nature of Archean gold-bearing fluids as deduced from gold deposits of Western Australia. Journal of the Geological Association of Australia, **30**: 25-39.

Phillips, G. N., Groves, D. I., and Martyn, J. E. 1984. An epigenetic origin for Archean banded-iron-formation-hosted gold deposits. Economic Geology, **79**: 162-171.

Ridler, R. H. 1970. Relationships of mineralization to volcanic stratigraphy in the Kirkland-Larder Lakes area, Ontario. Geological Association of Canada Proceedings, **21**: 33-42.

Rye, D. M., and Rye, R. O. 1974. Homestake Gold Mine, South Dakota: I. Stable isotope studies. Economic Geology, **69**: 293-317.

Seward, T. M. 1973. Thio-complexes of gold and the transport of gold in hydrothermal ore solutions. Geochimica et Cosmochimica Acta, **37**: 379-399.

Smith, D. G. W., and Gold, C. M. 1979. EDATA2: a Fortran iv computer program for processing wavelength- and/or energy-dispersive electron microprobe analyses. *In* Proceedings of the 14th Annual Conference-Microbeam Analysis Society, San Antonio, Texas. *Edited by* D. E. Newbury, pp. 272-278.

Thompson, P. H. 1978. Archean regional metamorphism in the Slave Structural Province-a new perspective on some old rocks. Geological Survey of Canada, paper 78-10, pp. 85-102.

4. WHOLE ROCK GEOCHEMICAL EVIDENCE FOR EPIGENETIC HYDROTHERMAL ALTERATION AND GOLD MINERALIZATION, CONTWOYTO LAKE, NORTHWEST TERRITORIES, CANADA

A. Introduction

The origin of gold deposits hosted by iron formation has been debated for many years with current models ranging from syngenetic (Fripp 1976; Ridler 1970) to epigenetic (Groves *et al.* 1987; Macdonald 1983) and including multistage or remobilization models (Rye and Rye 1974). Recently, Groves *et al.* (1987), Phillips *et al.* (1984), Phillips and Groves (1983) and Macdonald and Fyon (1986) have emphasized the epigenetic characteristics of gold mineralization in iron formation. Fieldwork and mineralogical studies in the Contwoyto Lake area (Chapters 2 and 3) have shown that there is evidence for epigenetic gold mineralization and wallrock alteration adjacent to quartz veins in the iron formation-hosted gold deposits in the area.

The objective of this study is to examine the major and trace element geochemistry of unmineralized and mineralized iron formation and to quantify the elemental fluxes, which occurred during hydrothermal alteration. The approach used here involves comparing the chemistry of the apparently least altered samples to their altered equivalents by the method of Gresens (1967). Gresens' principal assumption is that during alteration some elements are likely immobile. If these elements can be identified, then their abundances can be used to determine the amount of volume change, if any, due to alteration and to quantify the gains and losses of mobile elements during alteration.

Many studies of this type have been done on Archean lode gold deposits (Robert and Brown 1986; Ludden *et al.* 1984; Kerrich and Watson 1984). Although there are some published data on the geochemistry of gold deposits

hosted by iron formation (Hallager 1984; Fripp 1976), apparently no studies have attempted to quantify the elemental fluxes during epigenetic mineralization of iron formation. Inferences by Phillips and Groves (1983), based on the mineralogy of gold deposits in iron formation, suggest that alteration patterns in iron formation-hosted gold deposits are similar to other types of lode gold deposits. They suggest that lode gold deposits contain a distinctive suite of trace elements (Au, As S, Sb, W and others) regardless of their host rock type.

This study shows that major and trace element geochemistry does in fact support the previous field and petrographic evidence for epigenetic gold mineralization and wallrock alteration adjacent to quartz veins in iron formation at Contwoyto Lake (Chapters 2 and 3). It also shows that the principal elements added to iron formation during alteration are Au, S, As, Ca, Al and W.

B. Methods

Sample preparation

Representative samples of about 2 kg were crushed in a steel jaw crusher to less than 1 cm diameter. The whole sample was then ground in a disc mill fitted with alumina plates. At this point, the entire sample was rolled on paper and split by coning and quartering until about 150 g of sample were isolated. This subsample was then ground in a motorized, agate mortar and pestle. Finally, the sample was again rolled and coned and quartered to separate two aliquots of about 35 g. One aliquot of sample was sent to the Lupin Assay Laboratory of Echo Bay Mines for gold assay by the conventional lead fire assay technique: the entire aliquot was assayed. The detection limit of the technique, as practised at Lupin, is 0.03 ppm Au (J. German personal communication 1986).

Another aliquot of each sample was sent to Midlands Earth Science Associates (MESA) of Nottingham, United Kingdom for X-ray fluorescence (XRF) analysis. Trace elements, with a few exceptions, were analysed by the pressed powder method. Major elements were analysed by the fusion bead method with the exception of Na, which was analysed by the pressed powder method. The fusion bead method could not be used on major elements in the As-rich samples due to problems in obtaining a proper fusion. In As-rich samples SiO_2, TiO_2, MgO, CaO, K_2O, MnO and P_2O_5 were analysed by the pressed powder method and Fe_2O_3 and Al_2O_3 were analysed by instrumental neutron activation analysis (INAA) at the University of Alberta Slowpoke Facility by M. J. M. Duke. Comparisons of pressed powder, fusion bead, and INAA results with duplicate samples and certified reference standards indicate that the data set is internally consistent, (Appendix 4). Most of the U values are at or below the detection limits. Bi, La, and W are often at or near the detection limits in unmineralized iron formation but are significantly enriched in mineralized iron formation. Results of the whole rock analyses are given in Table 4.1.

Due to unusually high concentrations of S and As in some of the iron formation samples, a correction was made to the analysed Fe_2O_3 in order to account for the Fe present as sulphides and arsenides. Fe_2O_3 in iron formation samples with >0.5 % As + S was recalculated, based on the known sample mineralogy, to separate the Fe into Fe associated with sulphides and the remaining Fe, which is expressed as FeO. Totals for these samples were recalculated to reflect this change and include major elements plus As and S. Fe_2O_3, in iron formation samples with <0.5 % As + S, was also recalculated as FeO and the total was adjusted. This was done because the mineralogy of the samples suggests that most of the iron is Fe^{2+}. Loss on ignition (LOI) was also corrected to account for the oxidation of Fe^{2+} to Fe^{3+}.

The use of alumina plates in the disc mill undoubtedly caused some Al contamination to the samples during preparation. However, because all of the iron formation samples were ground under the same conditions, and the samples have similar hardnesses, this will not bias the comparisons between different groups of iron formation samples. This is because all samples are similarly affected.

For statistical purposes, where elements were reported as less than a specified value, the value used in calculations was equal to one half of the detection limit.

C. Geology

Regional geology

The Contwoyto Lake-Point Lake region is predominantly underlain by Archean rocks of the Slave Province (Fig. 4.1). The following description of the regional geology is summarized from Chapter 2. The descriptions are based largely on the work of Bostock (1980), Thompson (1978) and King *et al.* (1988). Archean rocks can be subdivided into: pre-Yellowknife Supergroup rocks that comprise granitic rocks and gneisses; Yellowknife Supergroup supracrustal metavolcanic and metasedimentary units; and syn- and post-Yellowknife Supergroup granitic rocks.

The Yellowknife Supergroup (Henderson 1970) is subdivided (Bostock 1980) into four formations in the Contwoyto Lake-Point Lake region as follows: the Point Lake Formation which comprises mafic to felsic volcanic rocks; the Keskarrah Formation which comprises conglomerates and lithic sandstones; the Contwoyto Formation which comprises greywacke and mudstone beds with lenses and beds of iron formation; and the Itchen Formation which comprises greywacke and mudstone beds lacking iron formation (Fig. 4.1).

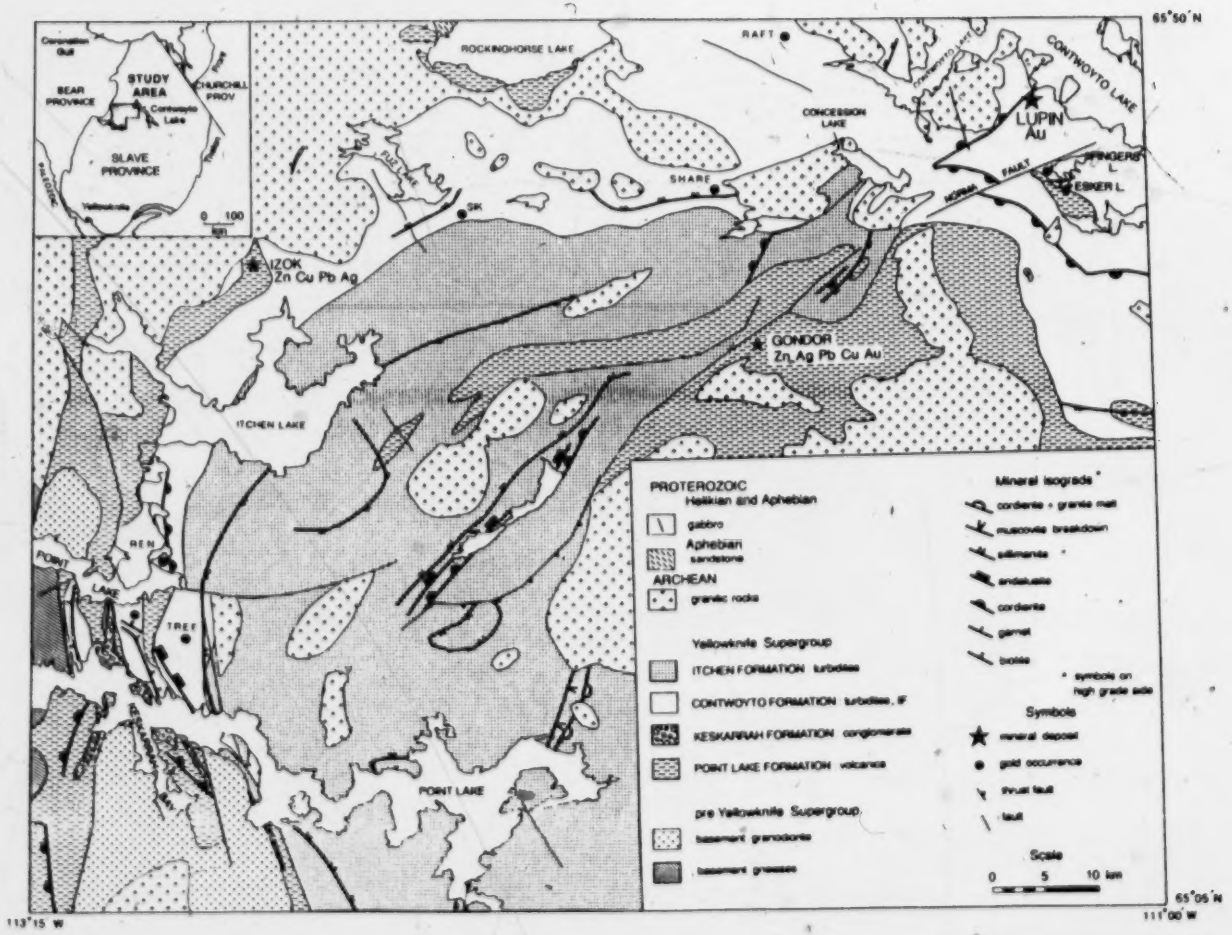

Fig. 4.1. Geology of the Contwoyto Lake-Point Lake region. Modified after Bostock (1980) and others.

The Contwoyto Formation is important because it contains the iron formations that host most of the known gold occurrences and the Lupin mine. The iron formations range in thickness from a few centimetres to 20 m. Although gold occurrences are common in iron formation throughout the region, the majority of iron formation is not enriched in gold and does not contain visible sulphide mineralization.

Archean rocks have been deformed and metamorphosed by Archean tectonic events. Archean structures comprise complexly interfering isoclinal folds with associated penetrative fabrics (King *et al.* 1988). Metamorphic isograds are defined in the pelitic sediments by the first appearance of the characteristic minerals biotite, garnet, cordierite, andalusite, sillimanite, and the breakdown of muscovite + quartz to form K-feldspar + sillimanite + H_2O (Fig. 4.1). Garnet is present only in iron-rich beds associated with iron formation. These minerals are characteristic of a low pressure trajectory path in P-T space (Thompson 1978). The distribution of the isograds generally suggests that the thermal highs are spatially associated with one of the later groups of granitic plutons (King *et al.* 1988). Isograds cut across some of the folds indicating that peak metamorphism postdated at least some of the early deformation. Aphebian and later geological events have had little or no effect on Archean mineral assemblages except immediately adjacent to Proterozoic gabbro dykes.

Gold mineralization in iron formation

On the basis of detailed fieldwork and petrographic studies (Chapter 2), iron formation has been subdivided into unmineralized iron formation, containing trace or no visible iron sulphide minerals, and mineralized iron formation, containing abundant iron sulphide and/or arsenide minerals.

Enhanced gold values are associated only with the sulphide mineralized iron formation. The following geological descriptions are summarized from Chapter 2.

Unmineralized iron formation in most of the region is comprised largely of grunerite + quartz ± magnetite with minor amounts of hornblende. This rock type, comprised largely of chemical sediment, is interbedded with a rock of mixed parentage, which is referred to as pelitic iron formation. Pelitic iron formation is a mixture of chemical and fine grained detrital sediment which, following metamorphism, comprises chlorite, quartz, ilmenite ± almandine garnet ± grunerite ± hornblende. Unmineralized iron formation and interbedded pelitic iron formation generally contains ≤0.03 ppm Au (Table 4.1).

All of the known gold occurrences in iron formation, except Lupin, are small-scale gold occurrences, many of which contain ore grade gold values, within volumes of mineralized rock too small to be economic. At the small-scale occurrences, gold is associated with increased concentrations of sulphides, which are in turn spatially associated with quartz veins (Kerswill 1985a; Lhotka and Nesbitt 1987a,b; Chapter 2). Pelitic iron formation is interbedded with the mineralized iron formation but does not generally contain more than trace amounts of sulphide or greatly enhanced gold values.

At the small-scale gold occurrences, the distribution of mineralized iron formation is clearly controlled by late quartz veins (Chapter 2). Mineralized iron formation is comprised of iron sulphides ± arsenides (arsenopyrite and loellingite) in iron formation that is predominantly comprised of hornblende with little or no grunerite. In the sub-garnet metamorphic zone the iron sulphide is usually pyrite, whereas at higher metamorphic grades, it is usually pyrrhotite. If present, arsenides always occur immediately adjacent to the vein and are enveloped by a larger halo of iron sulphides. Gold values of mineralized iron

TABLE 4.1 Compositions of mineralized and unmineralized iron formation and associated rock types from Contwoyto Lake. Major elements in weight percent, trace elements in ppm.

Sample	5A084	5A094	5B085	4E022a	5A074	5A095	5B086	4E022b	5A085	5A105	5A114	5B006	5B039	4C020	5C015a	4E026	5A058	5A065	5B071	4C018a	4C018b
rock type	greywacke				mudstone				unaltered pelitic iron formation								possibly altered pelitic iron formation				
SiO_2	69.41	68.98	63.21	72.61	58.31	59.57	55.67	54.48	55.21	49.80	61.07	42.43	38.21	49.70	39.91	49.07	40.68	53.51	42.34	48.73	47.57
Al_2O_3	13.97	9.59	13.39	12.35	16.96	16.44	16.87	21.67	10.48	14.09	8.92	10.33	10.97	11.93	13.33	13.46	10.82	7.58	12.44	10.63	7.41
TiO_2	0.45	0.60	0.71	0.48	0.71	0.65	0.62	0.82	0.41	0.56	0.34	0.40	0.39	0.46	0.45	0.59	0.40	0.29	0.36	0.37	0.24
Fe_2O_3[1]	3.98	10.41	9.45	3.76	9.49	8.66	11.06	7.87	21.71	23.27	21.25	37.06	38.33	29.51	40.74	26.13	39.19	27.24	29.17	33.19	38.62
FeO[2]	n.c.	n.c.	n.c.	n.c.	n.c.	n.c.	n.c.	n.c.	16.25	20.94	19.12	33.35	34.49	26.55	36.66	23.51	35.26	24.51	26.25	29.86	30.26
MgO	1.70	2.98	2.85	1.63	3.67	3.14	3.42	3.61	4.09	4.74	3.08	3.61	3.54	2.62	2.00	5.21	4.05	3.27	2.66	2.36	2.45
CaO	1.65	0.75	3.64	2.34	0.20	1.80	0.37	1.69	0.16	2.34	1.79	0.82	1.55	3.45	3.36	0.80	1.92	3.21	6.48	3.54	3.34
Na_2O	4.74	1.04	1.24	2.82	0.23	3.26	0.50	3.22	0.01	0.01	0.04	0.01	0.02	0.04	0.01	0.05	0.01	0.09	0.27	0.09	0.12
K_2O	1.55	2.90	1.14	1.58	4.51	3.48	3.39	2.84	0.05	1.56	0.13	0.02	0.05	0.07	0.01	2.78	0.03	0.07	0.23	0.06	0.06
MnO	0.05	0.06	0.13	0.07	0.05	0.05	0.09	0.10	0.09	0.06	0.06	0.06	0.06	0.10	0.12	0.07	0.07	0.03	0.16	0.06	0.07
P_2O_5	0.10	0.13	0.09	0.11	0.11	0.12	0.10	0.09	0.10	0.33	0.08	0.13	0.19	0.12	0.08	0.08	0.11	0.13	0.16	0.13	0.21
LOI[3]	2.71	2.38	3.75	2.52	5.97	2.70	7.65	3.20	9.52	5.60	5.18	8.84	10.33	4.82	4.21	4.67	6.11	7.39	8.76	4.29	5.07
TOTAL[4]	99.93	99.71	100.10	100.20	100.20	100.00	100.00	100.10	100.80	100.10	99.78	100.00	99.82	99.88	100.10	100.30	99.57	100.30	100.10	100.20	100.30
Au	<0.03	<0.03	0.03	<0.03	0.03	<0.03	0.03	0.10	<0.03	n.a.	0.03	0.07	<0.07	0.03	0.03	<0.03	0.03	0.21	0.21	0.03	0.14
Ag	<1	<1	<1	<1	<1	<1	<1	<1	2	3	3	7	7	5	6	4	6	1	4	4	8
As	28	6	12	25	9	13	4	48	4	8	7	6	8	97	116	42	42	332	26	274	83
Ba	644	591	361	249	2609	827	1147	769	46	1003	91	35	52	23	30	302	106	104	40	30	21
Bi	<1	2	<1	<1	3	<1	<1	4	2	<1	4	<1	<1	2	<1	<1	6	1	<1	<1	<1
Ce	48	117	29	60	41	43	41	28	36	50	10	72	64	63	60	79	44	48	92	47	65
Co	17	25	26	10	20	30	26	32	32	31	19	26	21	22	24	30	29	19	26	24	17
Cr	112	154	197	145	190	171	182	246	138	163	99	151	174	172	176	168	119	90	73	129	100
Cu	32	136	71	52	1	47	5	3	532	6	3	4	7	5	6	6	13	13	4	12	54
La	23	64	21	30	18	20	23	18	18	24	9	27	24	28	6	72	19	13	30	31	11
Ni	43	44	74	28	76	67	84	98	47	82	30	50	67	68	43	82	41	38	42	53	22
Pb	20	11	19	14	13	19	10	23	8	16	7	6	6	5	10	10	12	13	5	4	8
Rb	70	147	44	65	116	166	117	102	4	108	14	2	6	5	4	306	6	4	5	6	5
S	147	9082	4196	937	139	2178	361	309	16746	199	119	179	214	167	218	271	1139	1665	278	501	13701
Sc	14	12	19	13	23	17	18	26	11	13	6	14	14	13	12	12	11	10	15	12	7
Sr	358	81	233	222	181	240	62	312	2	40	36	23	47	5	4	232	343	550	40	7	8
U	2	4	<1	2	3	<1	2	3	<1	<1	4	1	<1	1	2	<1	3	<1	6	<1	<1
V	72	76	142	74	140	125	126	156	90	110	49	59	85	94	60	126	105	59	73	81	72
W	<2	<2	<2	<2	8	<2	3	<2	<2	<2	<2	<2	<2	<2	<2	<2	<2	<2	<2	8	<2
Y	18	19	22	18	16	26	20	21	28	22	9	18	20	17	16	18	20	16	43	19	17
Zn	54	83	114	42	60	83	65	91	108	85	55	30	49	43	27	101	68	41	42	30	49
Zr	153	249	128	161	112	120	116	138	84	113	93	76	78	78	79	99	94	59	239	78	48
Al/Ti	27	14	17	23	24	22	24	23	23	21	23	23	25	23	26	20	24	23	31	25	27
Ti/Zr	18	14	33	18	38	32	32	36	29	31	22	32	30	35	34	36	26	29	9	28	30
Zr/Sc	11	21	7	12	5	7	6	5	8	9	16	5	6	6	7	8	9	6	16	7	7
Zr/Y	9	13	6	9	7	5	6	7	3	5	10	4	4	5	5	6	5	4	6	4	3

TABLE 4.1 continued.

Sample rock type	5A122	5B095	5C015Bb	4E025	4E029	5E003	5E015	5A057	5A101	5A120	5B005	5B020	5B031c	4C011	4E019d	5A017	5A024	5A062	5B046	4C007	4E019b	4E019c
			unmineralized iron formation							weakly mineralized iron formation							iron sulphide mineralized iron formation					
SiO_2	66.83	45.52	47.50	55.49	59.99	53.04	47.61	53.43	49.20	41.89	46.60	46.04	42.03	43.37	53.57	53.63	51.91	57.53	49.89	36.02	51.59	52.07
Al_2O_3	1.64	2.35	2.57	2.04	2.66	2.76	2.20	2.45	1.75	2.11	2.06	3.41	2.00	1.11	2.84	4.19	4.90	1.66	2.58	1.40	1.93	2.36
TiO_2	0.10	0.09	0.11	0.06	0.17	0.11	0.10	0.09	0.06	0.09	0.07	0.09	0.06	0.04	0.07	0.10	0.10	0.05	0.05	0.04	0.09	0.06
Fe_2O_3[1]	25.54	44.94	44.20	37.38	30.66	40.41	44.66	39.25	44.75	48.91	45.39	44.61	48.49	53.16	36.42	31.98	28.66	28.94	38.71	47.13	36.40	38.90
FeO[2]	22.98	40.44	39.77	33.63	27.77	36.36	37.26	33.50	40.27	42.66	40.84	40.14	42.91	43.62	31.48	5.42	10.61	8.24	26.09	0.00	25.05	31.30
MgO	1.64	2.03	2.31	1.33	1.82	1.51	1.06	1.11	0.53	1.30	0.50	1.17	1.11	0.51	1.25	0.84	1.04	0.59	0.86	0.69	1.05	1.19
CaO	2.12	2.18	1.87	2.17	2.66	1.31	2.79	2.18	2.53	3.97	1.96	2.48	2.39	1.93	3.87	3.56	8.42	5.51	2.33	2.52	3.46	3.49
Na_2O	0.05	0.09	0.05	0.10	0.06	0.01	0.04	0.04	0.05	0.02	0.07	0.06	0.10	0.02	0.07	0.02	0.05	0.03	0.06	0.04	0.06	0.06
K_2O	0.05	0.18	0.05	0.10	0.15	0.01	0.13	0.06	0.05	0.06	0.07	0.13	0.06	0.04	0.06	0.05	0.08	0.04	0.06	0.02	0.06	0.06
MnO	0.04	0.22	0.06	0.06	0.04	0.04	0.06	0.04	0.04	0.05	0.06	0.06	0.04	0.04	0.06	0.03	0.03	0.02	0.07	0.01	0.06	0.06
P_2O_5	0.06	0.10	0.18	0.07	0.44	0.15	0.07	0.19	0.30	0.14	0.19	0.19	0.11	0.12	0.07	0.21	0.19	0.12	0.23	0.12	0.07	0.07
LOI[3]	4.30	6.70	5.34	4.66	3.71	4.63	5.35	4.56	5.05	5.89	5.19	6.26	6.67	4.85	5.03	4.39	5.40	3.80	7.83	9.39	5.51	4.84
TOTAL[4]	100.20	99.89	100.10	100.10	99.91	100.30	100.50	99.99	100.30	99.95	99.93	100.30	100.70	101.10	100.10	102.90	102.40	100.90	103.35	105.69	101.16	100.42
Au	0.07	0.10	<0.03	<0.03	<0.03	0.03	0.10	0.10	0.21	0.45	0.38	0.17	0.69	12.55	0.66	48.17	24.69	9.84	0.45	87.40	7.23	1.51
Ag	4	9	9	7	4	6	9	8	9	9	7	10	9	8	6	9	7	7	8	20	8	8
As	89	10	4	20	<1	25	7	71	202	181	13	3	18	725	58	3792	1155	2164	20	600	47	103
Ba	37	23	12	104	143	448	27	101	27	58	32	23	19	9	46	26	26	51	22	12	38	41
Bi	<1	<1	<1	<1	<1	3	<1	4	<1	<1	<1	1	<1	2	<1	8	3	<1	1	<1	4	1
Ce	<7	23	50	10	26	22	<7	33	33	40	20	55	<7	22	20	32	31	16	31	<7	12	23
Co	10	27	18	19	25	18	19	16	16	22	12	19	21	19	17	6	9	7	16	13	13	14
Cr	28	37	45	26	46	34	30	21	37	31	12	55	71	20	34	43	27	20	28	105	53	41
Cu	10	14	41	15	7	15	81	15	29	28	28	17	24	82	9	149	101	83	113	355	61	28
La	14	5	<4	4	9	<4	<4	5	<4	<4	7	<4	5	<4	<4	<4	<4	<4	<4	<4	<4	<4
Ni	21	13	28	12	17	28	11	21	14	22	2	24	25	18	6	6	3	5	12	9	9	12
Pb	9	10	4	6	5	4	5	9	6	6	6	3	13	6	6	8	12	7	27	<2	12	7
Rb	5	4	5	5	7	2	4	2	5	4	5	5	4	3	5	3	3	2	6	6	4	4
S	4069	166	2270	3524	190	3339	15027	9283	4491	6849	3210	2494	6409	21463	6557	118894	77354	90656	60196	219377	48436	18654
Sc	4	4	6	4	5	3	<1	5	4	6	3	4	3	1	6	5	6	4	3	7	4	6
Sr	50	9	14	121	170	81	134	423	99	186	46	46	83	12	179	380	332	382	90	23	168	177
U	2	<1	1	<1	3	2	2	3	<1	2	<1	<1	<1	<1	2	2	<1	<1	<1	<1	<1	<1
V	17	24	62	18	16	17	22	23	20	22	31	19	19	9	12	33	32	10	8	15	17	16
W	<2	<2	<2	<2	<2	<2	<2	<2	5	<2	<2	<2	<2	2	<2	<2	164	5	<2	<2	<2	<2
Y	14	14	14	11	18	12	7	14	13	11	11	13	9	11	11	13	17	11	10	10	9	9
Zn	17	15	49	14	20	13	26	10	19	15	18	19	12	6	25	24	34	20	17	10	25	22
Zr	30	23	25	31	41	31	26	24	29	24	16	34	18	15	19	29	27	15	21	23	23	23
Al/Ti	14	23	21	23	15	22	19	24	19	21	26	33	29	24	36	37	43	33	46	31	19	26
Ti/Zr	20	23	26	15	25	21	23	22	17	22	26	16	20	16	22	21	22	20	14	10	23	21
Zr/Sc	8	6	4	8	8	10	-	5	7	4	5	9	6	15	3	6	5	4	7	3	6	4
Zr/Y	2	2	2	3	2	3	4	2	2	2	1	3	2	1	2	2	2	1	2	2	3	3

Table 4.1 continued.

Sample rock type	5A010	5A020	5A064	5B031b	5B073	4C006	4E015	4E033	4A031	5A015	5A041	5A056	5A060	5C009	4E019a	5A040	5B031a	4C005
			arsenide-rich mineralized iron formation								calc-silicate rocks						quartz veins	
SiO_2	44.56	26.17	47.26	35.76	30.65	11.67	34.65	47.83	49.78	55.59	59.85	49.59	60.63	53.57	61.89	90.46	89.46	92.12
Al_2O_3	2.06	3.03	3.66	2.44	3.33	2.04	3.76	3.81	12.31	1.33	1.14	8.98	3.95	11.15	1.66	1.21	0.26	0.16
TiO_2	0.06	0.09	0.09	0.07	0.09	0.02	0.16	0.11	0.09	0.04	0.04	0.13	0.08	0.17	0.05	<0.01	<0.01	0.01
Fe_2O_3[1]	29.96	38.08	38.62	49.94	43.88	49.64	47.85	39.76	13.58	25.79	26.30	16.84	17.34	17.60	26.23	6.00	6.35	2.90
FeO[2]	10.46	6.30	14.86	43.95	28.67	1.43	33.55	12.23	12.22	17.86	18.05	15.15	15.60	15.84	20.00	2.75	5.71	0.94
MgO	0.32	0.59	0.19	0.85	1.24	0.25	1.87	0.69	0.46	0.61	0.53	1.16	1.17	1.44	0.76	0.37	0.30	0.08
CaO	3.91	4.27	3.00	3.48	2.22	2.05	3.17	1.76	18.47	12.18	11.06	22.32	14.88	12.20	6.69	0.33	0.46	0.05
Na_2O	0.09	0.09	0.08	0.11	0.07	0.08	0.04	<0.01	0.02	0.03	<0.01	0.01	0.01	0.16	0.07	0.01	0.01	0.01
K_2O	0.05	0.08	0.05	0.07	0.06	0.05	0.07	0.01	0.01	0.03	0.01	0.02	0.01	0.13	0.05	0.02	0.02	0.01
MnO	0.02	0.02	<0.01	0.05	0.06	0.02	0.09	0.07	0.10	0.08	0.06	0.05	0.10	0.09	0.07	0.00	0.04	<0.01
P_2O_5	0.14	1.09	0.14	0.11	0.11	0.26	0.30	0.54	0.40	0.59	0.06	0.05	0.48	0.25	0.05	0.01	0.03	<0.01
LOI[3]	1.34	1.01	1.65	6.33	12.68	0.46	6.09	6.53	5.96	5.46	2.86	1.94	2.79	5.12	4.66	2.07	3.27	4.60
TOTAL[4]	98.40	95.94	102.10	95.04	97.63	94.20	95.96	104.00	99.88	100.80	100.90	99.43	99.73	100.40	100.60	100.60	99.84	100.20
Au	47.49	37.58	7.75	4.53	9.29	34.29	0.82	1.58	0.03	0.48	8.95	<0.03	<0.03	0.07	2.84	0.03	0.41	0.17
Ag	17	19	8	9	9	27	9	8	3	7	5	5	3	2	4	<1	<1	<1
As	150690	183438	57985	2689	8896	215385	1891	1002	33	1243	374	55	72	35	63	33	62	57
Ba	50	33	51	25	14	<8	63	44	<8	18	44	16	13	10	35	40	12	<8
Bi	18	<1	<1	3	2	25	<1	3	<1	<1	<1	<1	<1	<1	3	<1	<1	<1
Ce	26	<7	13	7	11	<7	41	49	26	31	13	53	55	41	9	13	8	<7
Co	46	60	31	18	20	117	18	20	6	6	16	5	12	11	11	<2	5	<2
Cr	76	52	51	29	60	103	61	37	19	25	28	34	23	60	26	4	4	3
Cu	174	349	171	42	127	2121	55	133	7	41	30	13	12	20	21	7	2	6
La	<4	<4	<4	<4	<4	<4	<4	22	14	<4	<4	16	25	11	<4	<4	<4	<4
Ni	113	112	37	3	25	486	13	16	12	11	2	14	12	25	8	<2	6	4
Pb	6	12	11	7	28	10	2	3	23	8	9	10	17	9	4	5	7	4
Rb	7	9	6	5	3	8	5	4	2	4	3	3	<1	3	5	2	2	<1
S	74934	131401	97910	7578	90943	207327	47464	120129	332	27177	28636	277	446	2952	18382	13513	795	8531
Sc	2	5	3	1	2	5	6	2	9	6	4	12	9	10	5	2	<1	2
Sr	203	315	119	91	53	25	189	222	2278	657	569	1596	3651	183	213	286	16	1
U	5	<1	<1	<1	6	<1	2	<1	<1	<1	<1	<1	<1	<1	<1	<1	<1	<1
V	11	20	22	13	19	14	26	24	15	13	10	38	13	40	9	6	<2	<2
W	5	2	7	<2	6	<2	<2	<2	608	7	21	871	3	95	<2	<2	<2	<2
Y	14	20	10	12	17	6	17	13	15	15	10	45	27	18	14	4	6	3
Zn	74	72	46	7	12	36	33	27	22	11	15	23	13	27	11	4	<2	<2
Zr	21	21	26	25	34	19	38	34	22	21	20	25	28	35	21	12	8	10
Al/Ti	30	30	36	31	33	90	21	31	121	29	25	61	44	58	30	-	-	18
Ti/Zr	17	28	21	17	16	6	25	19	25	11	12	31	17	29	14	-	-	6
Zr/Sc	11	4	9	25	17	4	6	17	2	4	5	2	3	4	4	6	-	5
Zr/Y	2	1	3	2	2	2	2	3	1	1	2	1	1	2	2	3	1	3

Notes: The second character of the sample identifier denotes the sample location as follows: A= Lupin; B= Fingers Lake; C= Esker Lake; E= Silk.

Abbreviations: n.c.= not calculated; n.a.= not analyzed.

[1] All Fe expressed as Fe_2O_3.

[2] In rock types 3 to10 FeO represents the corrected, nonsulphide portion of the Fe, expressed as FeO : see text for method of calculation.

[3] In rock types 3 to10 LOI = loss on ignition corrected for oxidation of Fe : see text for method of calculation.

[4] In rock types 3 to10 total equals the total of major elements plus As + S and corrected FeO : see text for method of calculation.

formation are typically between about 5 and 30 ppm (Table 4.1). Mineralized iron formation grades into unmineralized grunerite iron formation along strike. Textural evidence suggests that those minerals that predominate in mineralized iron formation replace those minerals that predominate in unmineralized iron formation: thus, hornblende replaces grunerite and iron sulphides replace amphiboles and magnetite (Chapter 2). Samples of mineralized iron formation from small-scale occurrences analysed in this study are from the Esker Lake, Fingers Lake and Sik occurrences (Fig.4.1). These occurrences have been described individually in Chapters 2 and 3. Unmineralized iron formation samples were collected in the vicinity of these occurrences and along strike from the Lupin mine away from areas of known mineralization.

Lupin is the only known economic gold deposit. It differs from the small-scale occurrences in its much larger size and continuity of the mineralized zones, and the fact that unmineralized grunerite iron formation is rare within the deposit. The geology of the Lupin mine has previously been described by Kerswill (1984, 1985a,b, 1986), Lhotka and Nesbitt (1987a,b) and Gardiner (1986). The following description is summarized from Chapter 2.

The Lupin orebody is divided into three zones, the West, Centre and East Zones, which are actually the limbs of a continuous anticline-syncline pair defined by the Lupin iron formation (Fig. 4.2). All of the gold mined to date at Lupin comes from these three zones. The iron formation unit can be subdivided into unmineralized and mineralized iron formation, pelitic iron formation, and minor amounts of mudstone and fine grained greywacke.

Mineralized iron formation constitutes the principal gold-bearing lithology in the mine. This rock type comprises abundant, fine grained, disseminated grains of pyrrhotite which, together with quartz and amphibole, commonly form bands in the iron formation. Hornblende is the predominant amphibole and is

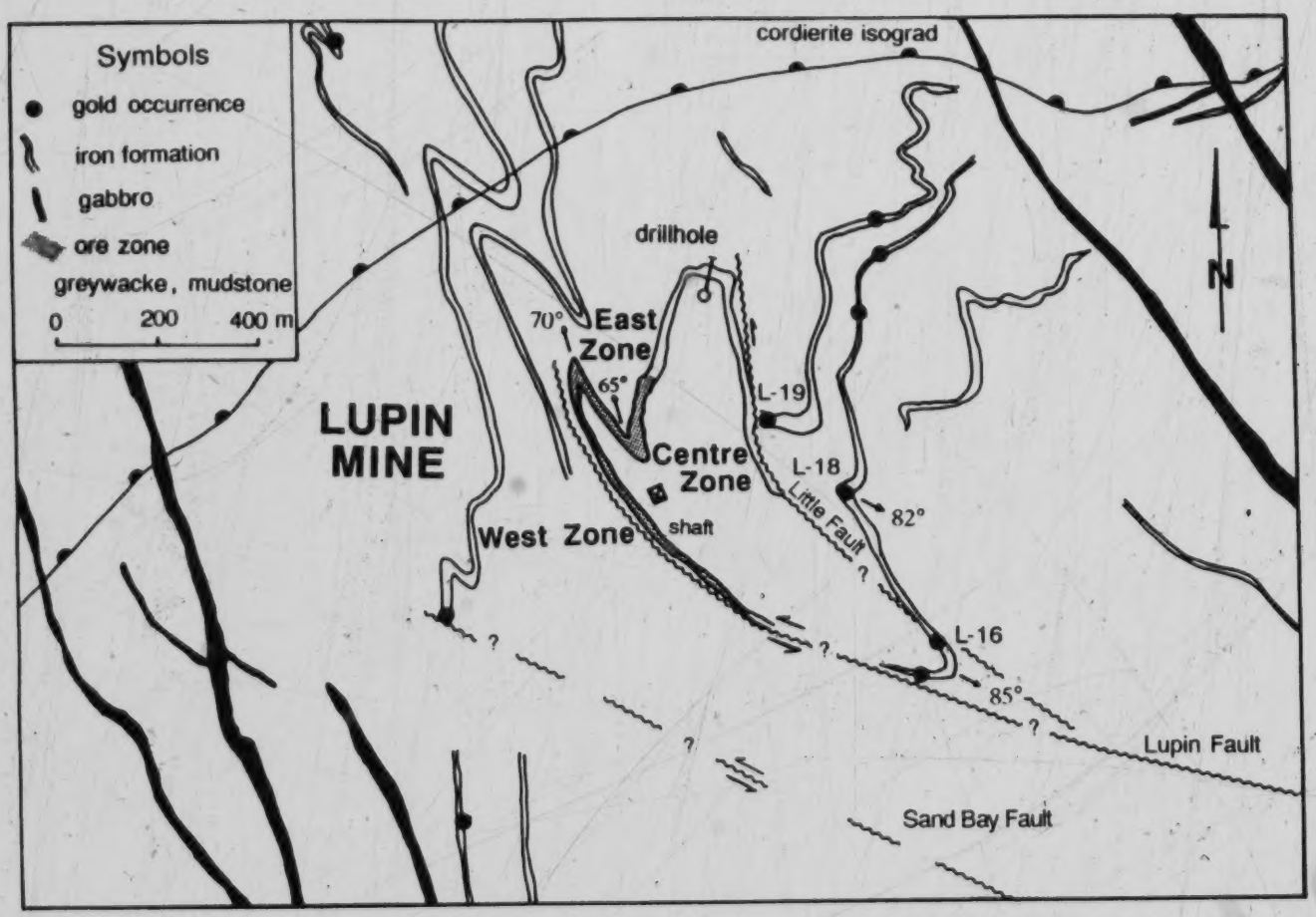

Fig. 4.2. Geology map of the Lupin area showing the ore zones and other localized areas of gold mineralization. Faults and possible faults modified after Gardiner (1986).

much more abundant than grunerite, which never predominates where pyrrhotite is abundant. In well mineralized samples grunerite is often absent. Where grunerite is present it forms the core to grains of hornblende. Coarse grained hedenbergite is often present, and may locally be abundant. Actinolite replaces hedenbergite along fractures and sometimes rims hornblende. Other minor or trace phases include epidote, chalcopyrite, ilmenite, pyrite and graphite.

Adjacent to late quartz veins, 1 cm diameter porphyroblasts of arsenopyrite, containing cores of loellingite, overgrow pyrrhotite in sulphide-rich iron formation. The veins comprise strained quartz with sutured grain boundaries. Trace amounts of hedenbergite, hornblende, actinolite, pyrrhotite, pyrite, arsenopyrite, loellingite, scheelite, and rarely, visible gold, generally comprise <2% of the vein material. These veins clearly control the distribution of arsenides, which are only present where pyrrhotite-rich, iron formation is intersected by the vein.

Unmineralized or weakly mineralized iron formation is rarely present within ore grade portions of the Centre and West Zones, but is more abundant in relatively gold-poor parts of the East Zone. This rock type comprises well banded grunerite and quartz. In thin section, grunerite is the predominant amphibole. Hornblende forms rims to grains of grunerite and varies from a minor proportion of the total amphibole to up to about 50 %. Minor amounts of ilmenite, graphite and pyrrhotite are also present, but arsenides are absent. In the northern part of the East Zone (Fig. 4.2), near the edge of the orebody on the 130 m level, gold- and sulphide-poor, grunerite iron formation can be traced into gold- and pyrrhotite-rich, hornblende iron formation, and finally into gold- and arsenide-rich, hornblende iron formation. This transition occurs along the strike of the banding, as a late quartz vein is approached over a distance of 2.5

m. Beyond the end of the East Zone (Fig. 4.2), unmineralized grunerite-rich iron formation is the predominant type of iron formation and mineralized iron formation is absent or present only as narrow zones adjacent to quartz veins.

Pelitic iron formation forms thin, generally <1 m wide, lenses or beds within the Lupin iron formation. Almandine-rich garnet, grunerite, chlorite and quartz comprise the pelitic iron formation. Hornblende and biotite are sometimes present, as are trace amounts of ilmenite, graphite, allanite, zircon, and rarely, pyrrhotite and arsenopyrite.

Sulphide-poor, calc-silicate rocks form a volumetrically minor, but important, part of the Lupin orebody. Calc-silicate rocks comprise hedenbergite and quartz as major phases. Epidote is commonly present as a minor component; however, in some samples intergrown epidote and grossular-rich garnet are abundant. Minor phases present include scheelite, calcite, sphene, apatite, ilmenite and graphite. Microveinlets of hornblende, actinolite, pyrrhotite, arsenopyrite, loellingite and gold cut across and replace hedenbergite in calc-silicate rocks. The principal significance of the calc-silicate rocks is that they are spatially associated with the quartz veins and are interpreted to represent alteration zones within the iron formation.

These observations suggest that sulphidation of iron formation and walirock alteration, which produces hornblende-rich iron formation, are important processes in the gold mineralization at the small-scale occurrences and probably at Lupin as well. The field observations and petrographic data for the small-scale occurrences and Lupin have been summarized into a scaleless schematic diagram to show the critical features of the gold-bearing zones (Fig. 4.3). The evidence supports an epigenetic model of gold mineralization.

In the following sections the whole rock geochemistry of unmineralized and mineralized iron formation and associated lithologies will be examined at

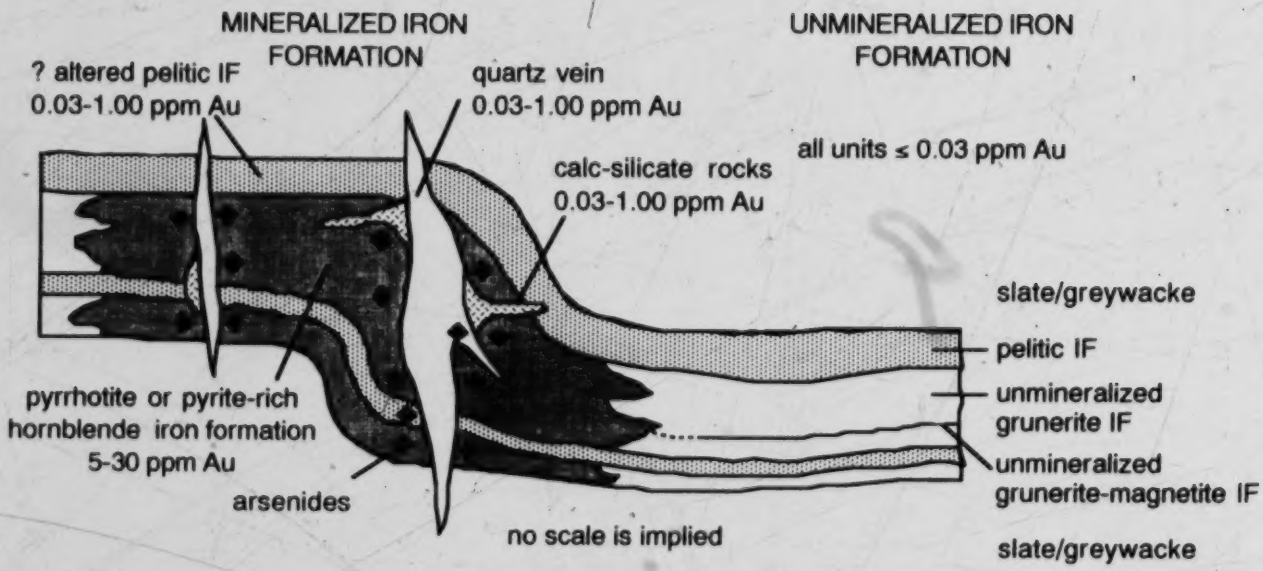

Fig. 4.3. Schematic summary diagram of the relationships between quartz veining and gold mineralization in iron formation in the Contwoyto Lake-Point Lake region. The mineralogy and typical gold values of iron formation and associated units are shown. A scale is not indicated because the relationships occur at scales ranging from a hand specimen to an ore zone.

the small-scale gold occurrences and at Lupin. The field and petrographic studies have contributed several pieces of data that are critical to the method of examining and interpreting the geochemical data:

1) Pelitic iron formation probably represents a mixture of a chemical sedimentary component and a pelitic detrital component.

2) Mineralized iron formation with abundant gold, sulphides, and hornblende probably represents an alteration of gold- and sulphide-poor, grunerite-rich iron formation. This alteration is spatially and genetically related to the late quartz veining.

3) The unusual calc-silicate rocks probably represent alteration of iron formation which is spatially and genetically associated with late quartz veining and thus is related to the alteration event that mineralized iron formation.

4) Structural observations have shown that the late quartz veins postdate early regional deformation and accompany the later regional deformation, which is coincident, or nearly coincident, with peak thermal metamorphism. Thus the unusual calc-silicate rocks associated with the veins cannot represent seafloor alteration at the time of chemical sedimentation.

D. Immobile elements distribution patterns in iron formation

In order to quantify the gains and losses of elements during hydrothermal alteration, the unaltered or least altered equivalent rock type must be first identified on the basis of field relationships and petrology. The rationale for interpreting that the unmineralized grunerite ± magnetite iron formation is in fact the unaltered equivalent of the mineralized iron formation is summarized above and is presented in its entirety in Chapter 2. Once this decision is made the

chemistries of the unaltered and altered rock types are compared by assuming either that there has been no volume change (sometimes stated as mass change) during alteration, or that some elements have remained immobile during the alteration (Gresens 1967).

In some situations it is possible to geologically estimate the volume changes during alteration based on structural considerations or modal proportions of phenocrysts (Ludden *et al.* 1984) or other geological parameters. However, in the present case this is not possible and the only constraint on the possible volume changes is that there is no obvious field evidence for extreme volume changes. Thus, in order to quantify the gains and losses, some elements must be identified which can be considered to be immobile. In this study Al, Ti, Zr, Y and Sc are examined as possibly immobile elements. Selected binary plots of the abundances of these elements in 54 samples of unmineralized and mineralized iron formation and associated rock types from Lupin and the small-scale occurrences are shown in Fig. 4.4.

Using Fig. 4.4*A* as an example, several important features are evident in the binary plots. First, with the exception of 3 data points for calc-silicate rocks, there is a strong, positive, linear correlation between the abundances of Ti and Al with the mudstones having the highest concentrations of the these elements and the samples of iron formation having the lowest concentrations. This pattern is strong evidence that the Ti and Al are detrital components and are not chemical sedimentary components of the system. Thus, the concentrations of Al and Ti, to a first approximation for most samples, represent the amount of detrital contamination of the chemical sedimentary component of the iron formation. Sirnilar observations and conclusions were made by Hallager (1984) in his study of the iron formations at Jardine, Montana and have been noted elsewhere in other chemical sediments (Robinson 1984; Kerrich *et al.* 1981). A

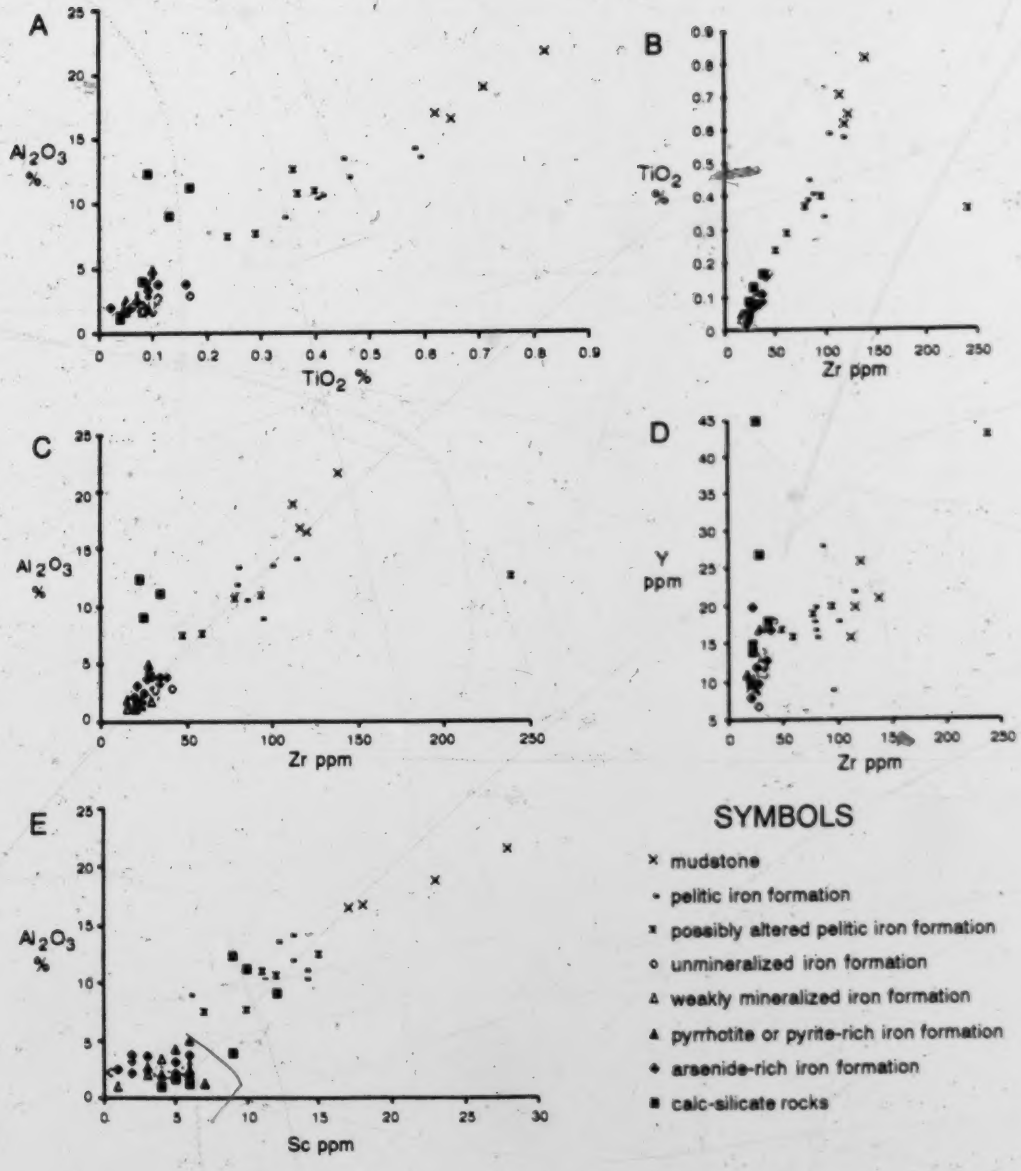

Fig. 4.4. Immobile element X-Y plots for iron formation and associated rock types. *A*. TiO_2 versus Al_2O_3. *B*. Zr versus TiO_2. *C*. Zr versus Al_2O_3. *D*. Zr versus Y. *E*. Sc versus Al_2O_3.

cursory examination of the rest of the plots in Fig. 4.4 shows that all of the possibly immobile elements Al, Ti, Zr, Y and Sc fit this pattern, at least to a first approximation.

Another important feature of the distribution of the group of commonly immobile elements in Fig. 4.4 is that when the samples of unmineralized iron formation are compared to the samples of the mineralized varieties of iron formation and the calc-silicate rocks, the rock types have very similar concentrations of the immobile elements (one exception to this pattern is that some of the samples of calc-silicate rocks have higher concentrations of Al, Sc and Y). This general similarity in concentrations suggests that if the unmineralized iron formation is in fact the unaltered equivalent of the mineralized types of iron formation, and these elements are assumed to be immobile, then major volume changes have not occurred during the alteration.

Closer examination of the distribution of the commonly immobile elements in the calc-silicate rocks shows that these rocks tend not to fit the simple model of contamination of a chemical sediment by detrital sediment (Fig. 4.4). Since geological evidence suggests that these rocks may represent highly altered portions of the iron formation, it seems likely that the deviations in the patterns of the elements in these rocks are due to mobility of at least some of the commonly immobile elements. In Fig. 4.4*B* the calc-silicate rocks have the same concentrations of Ti and Zr as do the remainder of the mineralized and unmineralized iron formation samples. This fact and the excellent correlation of the two elements suggest that Ti and Zr are truly immobile. Plots of Al versus Ti (Fig. 4.4*A*) and Al versus Zr (Fig 4.4*C*) show that some of the calc-silicate rocks tend to be enriched in Al relative to the other types of iron formation. This suggests that Al was added to some of the calc-silcate rocks. Petrographic examinations of the samples with high Al show that these samples have

abundant epidote and sometimes contain grossular garnet, two phases that are notably rich in Al. Interestingly, when Sc is plotted against Al (Fig. 4.4*E*), the plot indicates that the calc-silicate rocks, which are enriched in Al, are also enriched in Sc. This results in these calc-silicate rocks having similar concentrations of Al and Sc to samples of pelitic iron formation. This could be interpreted as indicating that these samples contain a significant detrital component, as do the pelitic iron formation samples. However, the plot of Zr versus Ti strongly suggests that these samples do not have a large detrital component and it is therefore likely that these calc-silicate rocks were in fact enriched in both Al and Sc during alteration of the iron formation. The plot of Zr versus Y (Fig. 4.4*D*) also indicates that Y is enriched in some of the calc-silicate rocks and is evidence for the mobility of this element as well.

Samples from beds of pelitic iron formation hosted by unmineralized iron formation and pelitic iron formation within mineralized iron formation, which may therefore be hydrothermally altered, are plotted separately in Fig. 4.4. These samples generally have similar concentrations of the commonly immobile elements, which appear, with the exception of one sample, to fit the trend of variable contamination of a chemical sediment by detrital sediment. The one sample of possibly altered pelitic iron formation which does not fit is greatly enriched in Zr and Y, but has normal concentrations of Al, Ti and Sc. Petrographic examination of this sample shows that it contains anomalously abundant allanite and zircon. This sample has apparently experienced mobility of Zr and Y.

In summary, in examining the patterns of the commonly immobile elements Al, Ti, Zr, Y and Sc, it is apparent that Ti and Zr are the least mobile. Significant mobility is indicated for Al, Sc and Y in at least some of the calc-silicate rocks. Any calculations of mass balances therefore must assume that Ti

and Zr are immobile. In addition, it is important that the geochemistry of iron formation is interpreted separately from pelitic iron formation because of the evidence that suggests that these rock types, represent respectively, nearly pure chemical sediment, and a mixture of chemical sediment and detrital sediment.

E. Alteration patterns in mineralized iron formation

Method of calculation

Quantitative comparisions of the chemistry of unmineralized iron formation and the various types of mineralized iron formation are done here using the method of Grant (1986), which is a simple method of calculating gains and losses using a rearrangement of Gresens' (1967) equations. In Grant's rearrangement, the volume changes in Gresens' equations have been restated as mass changes, and gain or loss of a component or mass of the sample is calculated by the formula:

$$(\Delta C_i/C^o_i) = (M^a/M^o)\,(C^a_i/C^o_i) - 1 \qquad (1)$$

where ΔC_i = change in concentration of component i

C^o_i = concentration of component i in the original (unaltered) rock

C^a_i = concentration of component i in the altered rock

M^a = mass of the altered rock

M^o = reference mass of the original rock

The factor (M^a/M^o) corrects the changes in concentration of an element for changes in the mass of the sample during alteration. Thus, if it is assumed that there is no mass change, the factor (M^a/M^o) equals unity. Alternatively, when the

mass of the sample is allowed to vary and a specific element such as Ti is assumed to be immobile then the gains or losses of the mobile elements are calculated by the related formula:

$$(\Delta C_i/C^o_i) = (C^a_{Ti}/C^o_{Ti})\,(C^a_i/C^o_i) - 1 \qquad (2)$$

and the change in mass of the sample is equal to:

$$(M^a/M^o) = (C^a_{Ti}/C^o_{Ti}) \qquad (3)$$

In this study, both Zr and Ti are used as immobile elements and the factor (M^a/M^o) equals a best fit, straight line through the concentrations of Ti and Zr in the altered sample, the unaltered sample, and the origin. This line of equal concentration is known as the isocon (Grant 1986). Once the slope of the isocon is determined the gain or loss of a mobile component is easily calculated from equation (1).

In the following calculations the average composition of seven samples of unmineralized iron formation was used to represent the original unaltered rock. This average composition is given in Table 4.2 together with the standard deviations of the averages. As expected, the standard deviations of the averages are quite large because of the often documented variability in the chemistry of iron formation and the difficulty in sampling this rock type (eg. Klein 1983). It is important to consider this fact when the chemistry of the unaltered and altered rock types are compared so that where small gains or losses are indicated, they are not given undue significance. In Ludden *et al.* (1984), a stated limit of interpretation of ± 20 % was deemed reasonable when the analytical errors (< 10 %) and the inhomogeneity of the unaltered rocks were

TABLE 4.2. Average compositions of iron formation and associated rock types in the Contwoyto Lake area. Major elements in weight percent, trace elements in ppm.

average (n)	grey-wacke 4	mud-stone 4	pelitic IF 8	? alt. pelitic IF 5	unimineralized iron formation aver. 7	std. dev.	weakly min. IF 8	po/py min. IF 7	arsenide min. IF 8	calc-silicate rock 7	quartz vein 3	Algoma oxide IF 352
SiO_2	68.55	56.51	48.18	46.57	53.71	(7.72)	47.27	50.38	34.82	55.84	90.68	50.50
Al_2O_3	12.33	18.49	11.69	9.78	2.35	(0.43)	2.22	2.75	3.02	5.79	0.55	3.00
TiO_2	0.56	0.70	0.45	0.33	0.11	(0.03)	0.07	0.07	0.09	0.09	<0.01	0.14
Fe_2O_3[1]	6.90	9.27	29.75	33.08	38.29	(7.56)	45.12	36.10	42.19	20.53	5.08	41.10
FeO[2]	0.00	0.00	26.36	29.23	34.03	(6.47)	39.43	15.53	18.95	16.39	3.13	-
MgO	2.29	3.46	3.61	2.96	1.67	(0.42)	0.94	0.90	0.75	0.88	0.25	1.53
CaO	2.10	1.02	1.78	3.70	2.19	(0.53)	2.66	4.18	2.99	13.97	0.28	1.51
Na_2O	2.46	1.80	0.02	0.12	0.06	(0.03)	0.06	0.05	0.07	0.04	0.01	0.31
K_2O	1.79	3.56	0.58	0.09	0.09	(0.06)	0.07	0.06	0.05	0.04	0.02	0.58
MnO	0.08	0.07	0.08	0.08	0.08	(0.06)	0.05	0.04	0.04	0.08	0.02	0.11
P_2O_5	0.11	0.11	0.13	0.15	0.15	(0.13)	0.16	0.14	0.34	0.27	0.02	0.21
LOI[3]	2.84	4.88	3.71	3.07	4.96	(0.96)	5.69	5.88	4.51	4.11	2.96	-
TOTAL[4]	99.98	100.08	100.21	100.16	100.13	(0.07)	100.30	102.39	97.91	100.26	99.90	-
Au	0.02	0.04	0.03	0.12	0.05	(0.04)	1.93	25.61	17.92	1.74	0.20	-
Ag	1	1	5	5	7	(2)	8	10	13	4	1	-
As	17	19	36	151	22	(31)	159	1126	77770	268	51	-
Ba	461	1338	198	60	58[5]	(53)	40	31	36	20	19	170
Bi	1	2	1	2	1	(1)	1	3	7	1	1	-
Ce	64	38	55	59	20	(16)	28	21	19	33	8	-
Co	20	27	26	23	19	(6)	18	11	42	10	2	38
Cr	152	197	155	102	35	(8)	35	45	59	31	4	78
Cu	73	14	71	19	26	(27)	29	127	397	21	5	96
La	35	20	26	21	5	(5)	3	2	5	10	2	-
Ni	47	81	59	39	19	(7)	16	8	101	12	4	83
Pb	16	16	9	8	6	(2)	7	11	10	11	5	-
Rb	82	125	56	5	5	(2)	4	4	6	3	2	-
S	3591	747	2264	3457	4084	(5073)	7595	90538	97211	11172	7613	2900
Sc	15	22	12	11	4	(2)	4	5	3	8	2	8
Sr	224	199	49	190	83	(62)	132	222	152	1307	101	98
U	2	2	1	2	2	(1)	1	1	2	1	1	-
V	91	137	84	78	25	(17)	19	19	19	20	3	97
W	1	3	1	2	1	(0)	2	25	3	229	1	-
Y	19	21	19	23	13	(3)	12	11	14	21	4	54
Zn	73	75	62	46	22	(13)	16	22	38	17	2	330
Zr	173	122	88	104	30	(6)	22	23	27	25	10	84

Notes: IF = iron formation; ?alt = possibly altered; po/py = pyrrhotite or pyrite; min. = mineralized; ( ) = standard deviation; - = not given. Algoma oxide iron formation data from Gross and McLeod (1980).

[1] All Fe expressed as Fe_2O_3.

[2] FeO represents the corrected, nonsulphide portion of the Fe, expressed as FeO : see text for method of calculation.

[3] LOI = loss on ignition corrected for oxidation of Fe : see text for method of calculation.

[4] Total equals the total of major elements plus As + S and corrected FeO : see text for method of calculation.

[5] Average does not include one very high value of 446 ppm Ba; with the high value the average is 113 ppm.

considered. In the present case, the inhomogeneity of the unaltered iron formation is obviously much greater than that of the feldspathic porphyry studied by Ludden *et al.* (1984) and it is suggested that a reasonable limit of interpretation is about ± 50 %. Although this may seem high, many elements have much larger gains and it seems wise to err on the side of conservatism.

Also shown in Table 4.2 is the average composition of 352 samples of iron formation from a compilation by Gross and McLeod (1980). The chemistry of the average unmineralized iron formation from Contwoyto Lake is very similar to Gross and McLeod's (1980) average iron formation. This suggests that unmineralized iron formation in the Contwoyto Lake region is not geochemically anomalous on a regional basis. Although the field and petrographic evidence presented in Chapter 2 and data on mineral chemistry in Chapter 3 suggest that Lupin and the small-scale gold occurrences formed by the same epigenetic process, previous workers (Kerswill 1986; Padgham 1984; and Franklin and Thorpe 1982) have suggested that Lupin is a syngenetic deposit and that both syngenetic and epigenetic gold deposits may be present in the Contwoyto Lake iron formations (Kerswill 1986). In view of this, the samples from Lupin and the small-scale gold occurrences are treated separately in this section.

Rather than comparing data from individual samples of mineralized iron formation to the average unmineralized iron formation as is commonly done, it was decided that comparisons of average values of samples, representative of the different varieties of mineralized iron formation, would be more meaningful. This should at least partially offset the prealteration heterogeneity of the iron formation and enable the recognition of true changes related to alteration. Thus the gains and losses in Fig. 4.5 represent the independently calculated metasomatic changes between average samples from Lupin and the small-scale occurrences when compared to the average unmineralized iron formation

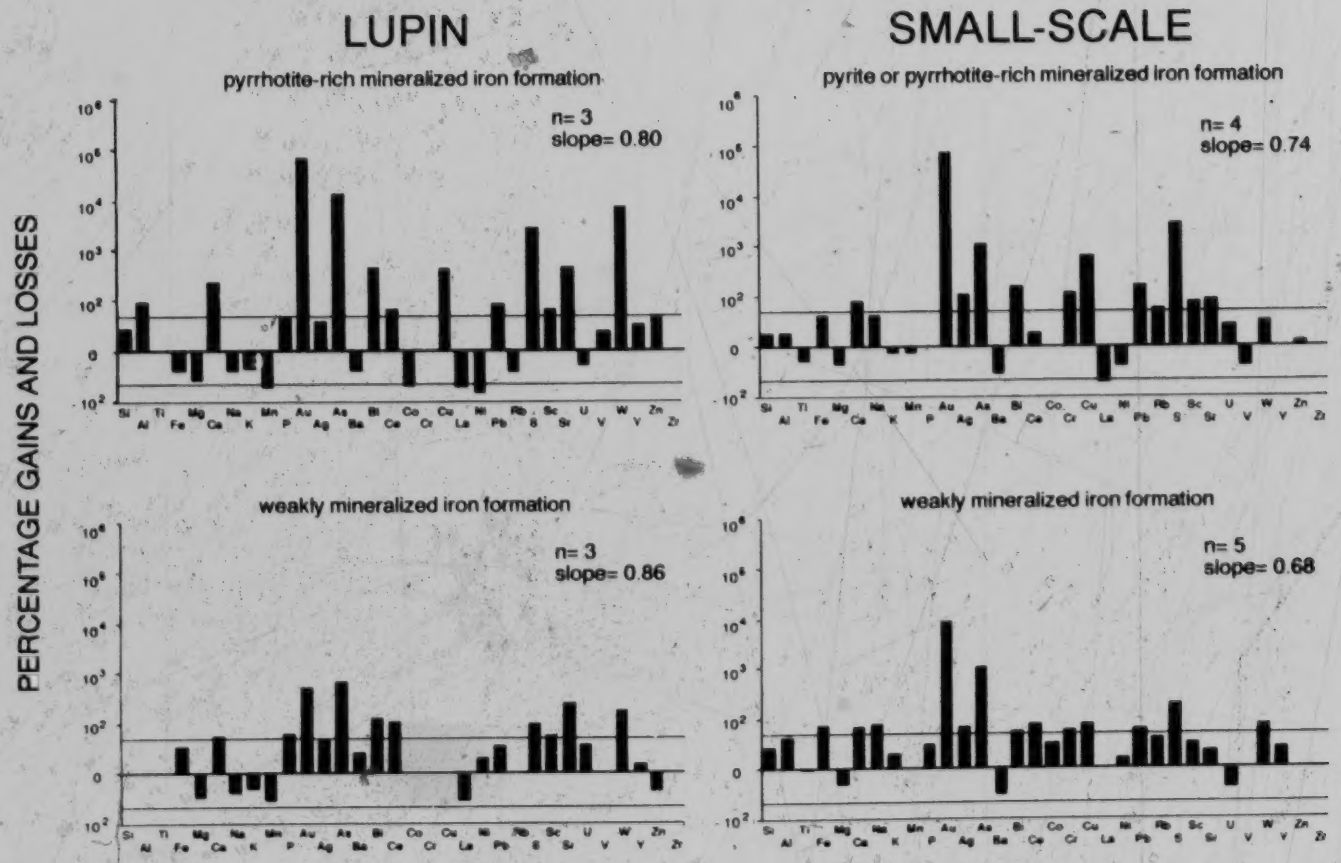

Fig. 4.5. Percentage gains and losses in alteration of unmineralized iron formation in the different types of mineralized iron formation at Lupin and small-scale occurrences. N= the number of samples the average is based upon. The slope indicated is the slope of the Zr-Ti isocon. Slopes less than one indicate mass increases. *A*. Pyrite or pyrrhotite-rich mineralized iron formation and weakly mineralized iron formation.

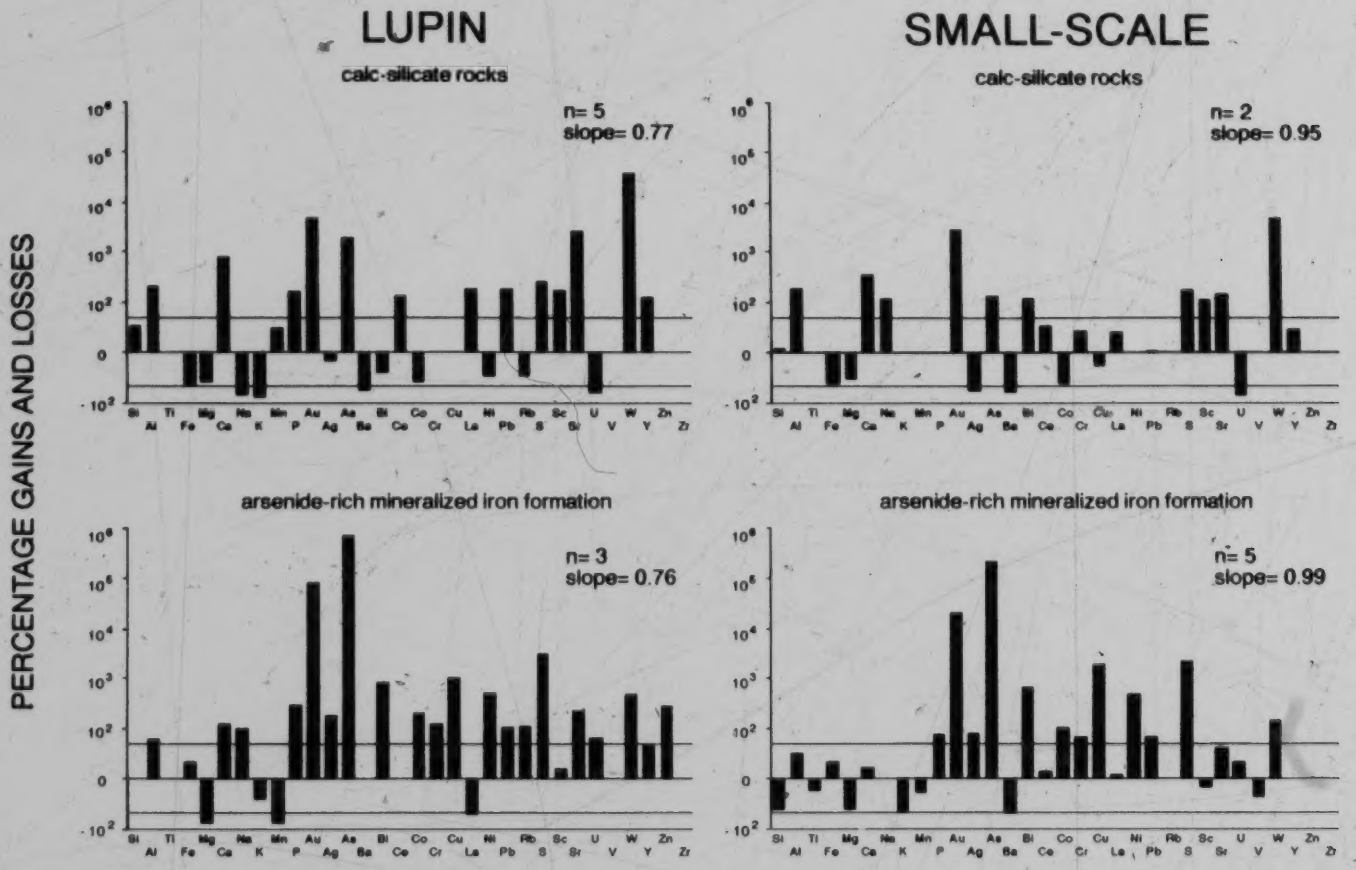

Fig. 4.5 continued. *B.* Calc-silicate rocks and arsenide-rich mineralized iron formation.

in Table 4.2. The number of samples used in each average is shown in Fig. 4.5. In addition, the slope of the Zr-Ti isocon is shown for each group of samples. Isocon slopes of less than one indicate mass increases. All of the groups of mineralized iron formation have negligible to moderate mass increases due to alteration (Fig. 4.5).

Weakly mineralized iron formation

When the elemental gains and losses of weakly mineralized iron formation samples from Lupin are compared with the weakly mineralized samples from the small-scale occurrences, it can be seen that the patterns of gains and losses are similar (Fig. 4.5*A*). In both cases the largest gains are in Au and As. The samples from Lupin also indicate gains of ≥ 50 % in Ca, P, Bi, Ce, S, Sc, Sr, and W, while at the small-scale occurrences gains of ≥ 50 % occur in Fe, Ca, Na, Ag, Bi, Ce, Cr, Cu, Pb, S, and W. Petrographically, the weakly mineralized iron formation samples from both types of gold occurrences are similar and are characterized by the occasional presence of arsenides, the increased abundance of iron sulphides, and the greater abundance of hornblende relative to grunerite when compared to unmineralized iron formation. The petrographic data are consistent with the calculated gains in Au, As, S and Ca.

Iron sulphide mineralized iron formation

The patterns of gains and losses, during alteration of unmineralized iron formation to iron sulphide mineralized iron formation, at Lupin and the small-scale gold occurrences, are geochemically similar. In both cases the greatest enrichments are in Au, As and S. The large average enrichment of W at Lupin is due to one sample that contains 164 ppm W, whereas, the remainder of the

samples from Lupin and the small-scale occurrences contain between <2 and 8 ppm W. Other elements with gains of ≥ 50 % at Lupin are Al, Ca, Bi, Ce, Cu, Pb, S, Sc and Sr and losses of ≥ 50 % are indicated for Mn, Co, La and Ni. At the small-scale occurrences gains of ≥ 50 % are present in Ca, Ag, Bi, Cr, Cu, Pb, Rb, Sc and Sr and losses of ≥ 50 % occur only in La. The similarity of the patterns of gains and losses between the samples from Lupin and the small-scale occurrences is striking. The opposed behavior of Ce and La in the Lupin samples is geochemically unlikely and probably represents analytical uncertainty due to low concentrations of La which are at or below the detection limit.

Petrographically, the iron sulphide mineralized iron formation is similar to the weakly mineralized iron formation, except for the greater intensity of the sulphide mineralization and the greater abundance of hornblende relative to grunerite. This is reflected in the similar but larger gains in Au, S, As and Ca in the iron sulphide mineralized iron formation relative to the weakly mineralized iron formation, as well as in the larger number of elements showing gains of ≥ 50 %.

Arsenide mineralized iron formation

Patterns of gains and losses in the samples of arsenide mineralized iron formation from Lupin and the small-scale occurrences are again similar (Fig. 4.5*B*). In both cases this lithology is characterized by large gains of As > Au > S. At Lupin, other elements with gains of ≥ 50 % include Al, Ca, Na, P, Ag, Bi, Co, Cr, Cu, Ni, Pb, Rb, S, Sr, U, W and Zn and losses of ≥ 50 % are indicated for Mg, Mn and La. Small-scale gold occurrences have gains of ≥ 50 % for P, Ag, Bi, Co, Cr, Cu, Ni, Pb and W and no elements with losses ≥ 50%. Groups of elements enriched in arsenide mineralized iron formation from Lupin and the

small-scale occurrences are similar to each other; however, they differ from the samples of iron sulphide mineralized iron formation in that they have much larger gains of As and are notably enriched in Co, Cr and Ni, elements commonly associated with As.

Calc-silicate rocks

Calc-silicate rocks are more abundant and better developed at Lupin than at the small-scale occurrences (Chapter 2). Because of this only two samples of calc-silicate rock were analysed from the small-scale occurrences and five samples were analysed from Lupin. At Lupin the calc-silicate rocks are characterized by gains of ≥ 50 % of Al, Ca, P, Au, As, Ce, La, Pb, S, Sc, Sr, W and Y and by losses of ≥ 50 % of Na, K, Ba and U. The small-scale occurrences are characterized by gains of ≥ 50 % of Al, Ca, Na, Au, As, As, Bi, S, Sc, Sr and W and losses of ≥ 50 % of Ag, Ba and U. In both Lupin and the small-scale occurrences the largest gains are in W and the gains in Au, As, and S are relatively low compared to the other types of mineralized iron formation. The similarity in the patterns of gains and losses at Lupin and the small-scale occurrences is again striking.

Gains in Ca, Al and W in the calc-silicate rocks reflect the unusual mineralogy of these rocks which are comprised of hedenbergite ± epidote ± grossular garnet ± scheelite. The lower enrichments of Au, As and S are due to the generally sulphide-poor nature of these rocks except where they are cut by late microveinlets of sulphides associated with hornblende and actinolite (Chapter 2). Three samples of calc-silicate rocks lacking the sulphide microveinlets from Lupin all contain ≤ 0.03 ppm Au, whereas two samples with sulphide microveinlets from Lupin contain 0.48 and 8.95 ppm Au (Table 4.1).

Average gains/losses for alteration at Contwoyto Lake

The high degree of similarity in the average gains and losses for the samples from Lupin and the small-scale occurrences strongly suggests that mineralization at the two different scales of gold occurrence originated from the same process. This indicates that a single genetic model is valid for all of the gold occurrences in the Contwoyto Lake iron formations.

The average gains and losses were recalculated using the data from both Lupin and the small-scale occurrences to define average gains and losses for the Contwoyto Lake gold mineralization as a whole. These average gains and losses are shown in Table 4.3. Also shown in Table 4.3 are the mass changes for the various rock types, which were calculated from the slopes of the isocons for Ti and Zr. All four types of mineralized iron formation have mass increases which range from 10 to 34 %. The differences in mass change for the rock types are not considered significant and the minor increases in mass indicated show that the gains and losses in Table 4.3 would not change substantially if the mass balance calculations had been based on constant mass instead of the Zr-Ti isocon. For example, if constant mass was assumed for the weakly mineralized iron formation, the percentage gain for Au would be 3800 instead of 5100. Since the indicated mass changes are greatest for this rock type, the changes in the gain/losses in other rock types would be proportionately smaller.

F. Alteration of pelitic iron formation

To this point the alteration of pelitic iron formation has not been considered. Unlike the iron formation proper, pelitic iron formation does not appear to undergo major mineralogical changes when it is traced from

TABLE 4.3. Average gains/losses in alteration of the various types of mineralized iron formation in the Contwoyto Lake area. Gains and losses are given in percentages relative to the average unmineralized iron formation and are based on immobile behavior of the isocon of Ti and Zr. Mass changes indicated by the assumption of constant Ti and Zr are shown.

	weakly mineralized iron formation	pyrrhotite/pyrite mineralized iron formation	arsenide mineralized iron formation	calc-silicate rock
n=	8	7	8	7
Isocon slope	0.747	0.765	0.906	0.826
Mass change %	34	30	10	21
SiO_2	18	23	-28	26
Al_2O_3	26	53	42	200
TiO_2	-9	-12	-12	-4
Fe[1]	58	23	22	-35
MgO	-25	-30	-51	-36
CaO	63	150	51	670
Na_2O	33	13	38	-10
K_2O	3	-18	-38	-52
MnO	-11	-32	-37	23
P_2O_5	43	23	142	110
Au	5100	68000	40000	4200
Ag	61	82	110	-27
As	860	6500	390000	1400
Ba	-8	-30	-32	-58
Bi	85	290	750	21
Ce	92	41	8	100
Co	22	-25	140	-39
Cr	34	68	84	6
Cu	48	540	1600	-5
La	-17	-52	-9	130
Ni	17	-44	500	-22
Pb	50	130	80	130
Rb	21	23	42	-22
S	150	2800	2500	230
Sc	41	73	-5	150
Sr	110	250	100	1800
U	1	7	36	-61
V	3	-3	-18	-5
W	120	3100	260	28000
Y	21	15	19	94
Zn	-6	29	92	-4
Zr	1	2	2	1

[1] Fe denotes total iron as Fe

unmineralized portions of the iron formation unit into mineralized portions of the iron formation unit (Fig. 4.3, Chapters 2 and 3). The average compositions of the unaltered pelitic iron formation and possibly altered pelitic iron formation are given in Table 4.2 and the distributions of the commonly immobile elements are presented graphically in Fig. 4.4.

Examination of Fig. 4.4 indicates that samples of possibly altered iron formation generally have lower concentrations of Ti, Zr and Al than the samples of unaltered pelitic iron formation. This is reflected in the lower average concentrations of these elements in these rock types in Table 4.2. Since Ti and Zr are apparently immobile during the alteration of iron formation, it is probable that these differences are due to a lower proportion of detrital material in the group of possibly altered samples. This is probably a chance occurrence due to the relatively small number of samples analysed, but because of this it would not be valid to calculate gains and losses in the same way as done for the mineralized iron formation. This is because the differences in the abundances of the immobile element concentrations would lead to large mass changes which are probably false. However, it is probably valid to assume that there are no significant changes in mass in the alteration of pelitic iron formation because none were indicated in the apparently more reactive iron formation. With this in mind, the average composition of the possibly altered pelitic iron formation can be compared directly to the average composition of unaltered pelitic iron formation in Table 4.2. The general similarity in the two average compositions indicates that there is relatively little alteration. Differences exist in the concentrations of Ca, Na, Au, Ba, Cu, Rb, Sr and S. Of these, the differences in K, Rb, Ba and Cu are caused by single samples with high concentrations of one of these elements (Table 4.1). These single sample anomalies strongly affect the averages and are not likely related to alteration. In contrast, the increases in

Ca, Na, Au, As, Sr, and S appear to be more uniform and probably do reflect alteration. In addition, most of the elements in this second group are elements that were shown to be enriched in alteration of mineralized iron formation. However, the degree of enrichment of Ca (200 %), Na (600 %), Au (400 %), As (420 %), Sr (390 %), and S (150 %) is much lower in the altered pelitic iron formation than in mineralized iron formation. In the various types of mineralized iron formation average gains for Ca (670 %), Na (38 %), Au (68000 %), As (390000 %), Sr (1800 %), and S (2800 %) are much higher (Table 4.3).

The relatively low degree of alteration in pelitic iron formation is best interpreted as the hydrothermal fluid being closer to equilibrium with the pelitic iron formation than with the unmineralized iron formation. This is reasonable since the stratigraphic sequence is dominated by pelitic rocks and the hydrothermal fluid would have had to traverse through, and interact with, the pelitic rocks. It is important to note that where the quartz veins associated with mineralization cut pelitic rocks or pelitic iron formation there is little or no mineralogical evidence of wallrock alteration (Chapters 2 and 3). This observation is consistent with the interpretation that the hydrothermal fluid was close to equilibrium with the pelitic rocks.

The increase in Na in the altered pelitic iron formation, but not in mineralized iron formation, is significant because in many lode gold deposits Na metasomatism is a common feature (Kerrich 1983). Groves *et al.* (1987) have suggested that alteration patterns for K in gold deposits hosted by iron formation may differ from gold deposits hosted by volcanic rocks because of the low concentrations of Al in iron formation, which does not allow the stabilization of the typical K-Al silicate alteration minerals. It is possible that a similar argument can be made for the lack of enrichment in Na in mineralized iron

formation in contrast with the enrichment of Na in the more aluminous, pelitic iron formation.

G. Discussion

Alteration of iron formation

Geological observations indicate that the mineralized varieties of iron formation form a zoned pattern centred on the quartz veins (Fig. 4.3; Chapter 2). Where present, the calc-silicate rocks are nearest to the veins followed by the arsenide-rich mineralized iron formation, iron-sulphide mineralized iron formation, weakly mineralized iron formation, and finally, unmineralized iron formation. The behavior of the group of commonly immobile elements (Al, Ti, Zr, Y, and Sc), shows that the mobility of Al, Y and Sc is the highest in the calc-silicate rocks (Table 4.3) and decreases towards the weakly mineralized iron formation. This suggests that this series of rock types represents differences in the water/rock ratio during the hydrothermal alteration of unmineralized iron formation. The highest water/rock ratio occurs in the calc-silicate rocks nearest the veins and the lowest water/rock ratio occurs in the weakly mineralized iron formation furthest from the veins.

If the elemental gains and losses for the different rock types are interpreted as arising from differences in water/rock ratio then several important features are apparent. The first is that the calc-silicate rocks are characterized by the largest gains of Al, Ca W, Sr, but have relatively low gains of Au, As, and S (Table 4.3). The generally low abundances of sulphides and gold in these rocks, except where they are cut by late sulphide microveinlets, indicates that Au, As and S were probably soluble at the high water/rock ratios experienced by the calc-silicate rocks. These elements were not deposited until the water/rock ratio decreased in the adjacent arsenide-rich mineralized iron

formation. Although gold grains coarser than about 100 microns in diameter are rare at Lupin, many of the coarser grains of gold occur at the contact of the calc-silicate rocks with the arsenide-rich mineralized iron formation. This observation supports the idea that gold was soluble during the alteration that produced the calc-silicate rocks and was deposited in the adjacent mineralized iron formation. Sulphide microveinlets in the calc-silicate rocks may represent a late stage of the hydrothermal alteration similar to that in metasomatic alteration in skarn deposits (Einaudi *et al.* 1981).

Arsenide-rich mineralized iron formation is characterized by massive enrichments in As and large enrichments in Au and S. It is significant that despite increases of 2 or nearly 3 orders of magnitude in the gains of As, in the arsenide mineralized iron formation relative to the iron sulphide mineralized iron formation, the gains in Au in these two rock types are similar. In fact, it appears that gains in Au more closely parallel the gains in S than the gains in As in all types of mineralized iron formation (Fig. 4.5, Table 4.3). This suggests that deposition of Au and S were closely linked and is consistent with the previously proposed model (Chapter 3), where Au is deposited from hydrothermal fluids in response to sulphidation of the iron formation. The sulphide precipitation forces deposition of Au by the breakdown of gold-sulphide complexes thereby depositing Au and S simultaneously.

The gains and losses of elements in weakly mineralized iron formation indicate that at the lowest water/rock ratio most elements do not exhibit much enrichment or depletion except for Au and As (Fig. 4.5,Table 4.3). Thus, there is an overall pattern of decreasing enrichment factors in mobile major and trace elements from the high water/rock ratios in the calc-silicate rocks to the low water/rock ratios in weakly mineralized iron formation. This

trend is accompanied by generally decreasing mobility of Al, Sc and Y (which are commonly considered immobile) as the inferred water/rock ratio decreases.

The calculations show that of the major element group, Ca and Al are the only elements that are markedly enriched during alteration of unmineralized iron formation to mineralized iron formation and calc-silicate rocks. This is consistent with the petrographic data that show that the major mineralogical difference between unmineralized iron formation and mineralized iron formation is that grunerite in unmineralized iron formation is replaced and altered to hornblende in mineralized iron formation (Chapter 2). In the calc-silicate rocks the silicate minerals hedenbergite + epidote ± grossular represent the extension of this trend to even more Ca- and Al-rich minerals.

Mass balance for the iron formation system

In order to quantify the mass balance of an element for alteration of the entire iron formation system, the abundances of the different rock types must be accurately known. This is because elements that are enriched in one rock type, or alteration zone such as Co and Ni in the arsenide-rich mineralized iron formation, may be depleted in other zones thereby not necessarily requiring a net gain of the elements to the iron formation system as a whole. Unfortunately, sufficiently detailed mapping of all of the rock types is not available for Lupin to permit calculation of net gains or losses of elements to the iron formation system as a whole. But if we assume that pelitic iron formation does not undergo any significant losses, then any elements that show gains in all of the four types of mineralized iron formation must have been introduced to the iron formation system from an external source during the alteration. Elements with gains in all four types of mineralized iron formation include Al, Ca, P, Au, As, Bi, Ce, Cr, Pb, S, Sr, W and Y (Tables 4.2 and 4.3). In addition, the large gains in Cu in all four

types of mineralized iron formation, except the calc-silicate rocks for which there is a slight loss, indicate that Cu was also added from an external source. All of these elements must therefore have been introduced into the iron formation during hydrothermal alteration associated with the the quartz veining.

The abundance of quartz veins in mineralized iron formation suggests that Si has been added to the iron formation system during alteration. Gains and losses of Si in Table 4.3 indicate that neither large gains nor losses exist in mineralized iron formation. Thus, although it is likely that Si was added to the iron formation system the actual gain cannot be calculated without accurate information on the abundance of quartz veins and other rock types.

Comparisons to other Archean epigenetic and syngenetic deposits

Other studies of undoubtedly epigenetic Archean gold deposits indicate that these deposits are enriched in a suite of elements during alteration, which is similar to the suite of elements enriched during alteration of iron formation at Contwoyto Lake. At the adjoining Sigma and Lamaque Mines in Quebec, alteration of feldspathic porphyry dykes is characterized by addition of Au, W, As, Rb, K, CO_2, P and S from an external source during gold mineralization (Ludden *et al.* 1984). Robert and Brown (1986) have shown that Ca, Na, Si and B were also introduced from an external source at Sigma. Colvine (1984), in a compilation of the characteristics of Canadian Archean gold deposits, states that the gold deposits typically have Au, S, As, W, Mo, Sb, CO_2 and K introduced during alteration and that Si, Na, Te, Se, Bi, Cr, B and Ba are sometimes introduced from external sources. The similarity of these suites of elements to the suite of elements added during alteration of the Contwoyto Lake iron formations is strong evidence that the Contwoyto Lake deposits formed from similar epigenetic processes.

Another feature characteristic of the Contwoyto Lake gold deposits is the very large enrichments of gold and the low enrichments of base metals. Average Cu/Au and Zn/Au for the Contwoyto Lake arsenide-rich mineralization are 22 and 2 respectively, and for the iron sulphide-rich mineralized iron formation are 5 and 0.9, respectively (Table 4.2). These values are typical of Archean lode gold deposits, but are in sharp contrast to even the most gold-rich, volcanogenic massive sulphide deposits (Kerrich and Hodder 1982). For example, the Horne Mine is a well known gold-rich syngenetic deposit and it has Cu/Au of about 5000 (calculated from data in Kerrich and Hodder 1982). Similarly, as pointed out by Groves *et al.* (1987) the gold-rich interflow sediments at Kambalda, Western Australia, which are interpreted as syngenetic exhalative sediments, have Cu/Au and Zn/Au of 12,000 and 33,000 (data from Bavington and Keays 1978, and Bavington 1981). Data from actively forming seafloor polymetallic sulphide deposits in the Pacific Ocean (Hannington *et al.* 1986) indicate that even relatively gold-rich deposits have Cu/Au and Zn/Au of about 900 and 4600, respectively and in many deposits both ratios often exceed 100,000.

Several papers have examined the separation of Au from the base metals Cu, Pb and Zn in lode gold deposits and the lack of similar separation in exhalative massive sulphide deposits and attempted to explain the process of separation (Kerrich 1983; Kerrich and Hodder 1982; Kerrich and Fryer 1981; Kerrich *et al.* 1981; Phillips and Groves 1983). These papers suggest that in lode gold deposits Au was complexed by sulphur in an H_2O-CO_2 hydrothermal fluid with low Cl concentrations. Such a fluid could leach gold preferentially, and upon deposition, produce the characteristically low Cu/Au and Zn/Au. This type of system is very different to the hydrothermal systems which produce syngenetic massive sulphide deposits. In these systems the hydrothermal fluid

is evolved seawater that is an H_2O-NaCl brine which is capable of transporting base metals and precious metals in similar proportions to their crustal abundances (Kerrich and Hodder 1982). The fundamental differences in these two hydrothermal systems indicate that they are not end members of a series. Instead, it appears they are independent systems.

Geological evidence indicates that the seafloor hydrothermal systems are, of course, predeformational (Franklin *et al.* 1981), while the lode gold systems are considered to be syn- or post-deformational (Colvine 1984). The early suggestion (Kerrich and Hodder 1982) that the same fluids that formed the epigenetic gold deposits could have vented to the seafloor and formed syngenetic gold-rich base metal-poor deposits is not consistent with the evidence that the epigentic deposits formed late in the deformational history (Colvine 1984). Instead, it appears the supposedly syngenetic lode gold deposits are in fact replacement deposits formed at the same time and from the same type of fluids as the epigenetic gold deposits (Phillips and Groves 1983).

The similarity of the base metal/gold ratios of the Contwoyto Lake deposits to the undoubtedly epigenetic lode gold deposits, is stong evidence that the Contwoyto Lake gold-deposits are epigenetic replacement deposits hosted by iron formation. The Contwoyto Lake deposits in iron formation also have a similar characteristic suite of trace elements that are enriched during alteration to the suite of elements enriched in epigenetic lode gold deposits hosted by other rock types. These data indicate that the Contwoyto Lake deposits in iron formation probably formed from a hydrothermal system similar to the hydrothermal systems that formed other Archean epigenetic lode gold deposits and not from hydrothermal systems like those which formed syngenetic, massive sulphide deposits.

H. Summary

Whole rock geochemical studies of unmineralized iron formation and mineralized iron formation, from Lupin and small-scale gold occurrences, have shown that gold mineralization at both scales of gold occurrence is similar. These data are consistent with the petrographic data that suggest that the mineralized iron formation and calc-silicate rocks are hydrothermal alteration products of unmineralized iron formation, which are spatially and genetically associated with a specific set of quartz veins that formed at or near peak metamorphic conditions. At high water/rock ratios the commonly immobile elements Al, Sc and Y are mobile and are added to the mineralized iron formation. The only major elements that are added to the iron formation system during alteration are Ca, Al and P. Trace elements added to the iron formation system during alteration include Au, As, Bi, Ce, Cr, Pb, S, Sr, W, and Y. This suite of elements, and the low base metal/gold ratios of the Contwoyto Lake gold mineralization, are similar to other undoubtedly epigenetic Archean gold deposits. These data, together with the evidence of mobility of relatively immobile elements, clearly indicate that the gold and sulphide mineralization was not a syngenetic component on the iron formation but was deposited during later hydrothermal alteration of the iron formation during quartz veining.

I. References

Bavington, O. A. 1981. The nature of sulfidic metasediments at Kambalda and their broad relationships with associated ultramafic rocks and nickel ores. Economic Geology, **76**: 1606-1628.

Bavington, O. A., Keays, R.R. 1978. Precious metal values from interflow sedimentary rocks for the komatiite sequence at Kambalda, Western Australia. Geochemica et Cosmochimica Acta, **44**: 639-648.

Bostock, H. H. 1980. Geology of the Itchen Lake area, District of Mackenzie. Geological Survey of Canada, Memoir 391.

Colvine, A. C. 1984. An integrated model for the origin of lode gold deposits. Ontario Geological Survey, open file report 5524, 98p.

Einaudi, M. T., Meinert, L. D., and Newberry, R. J. 1981. Skarn deposits. *In* Economic Geology Seventy-fifth Anniversary Volume. *Edited by* B. J. Skinner, pp. 317-391.

Franklin, J. M., and Thorpe, R. I. 1982. Comparative metallogeny of the Superior, Slave and Churchill Provinces. *In* Precambrian sulphide deposits. *Edited by* R. W. Hutchinson, C. D. Spence, and J. M. Franklin. Geological Association of Canada, Special Paper 25, pp. 3-90.

Franklin, J. M., Lyndon, J. W., and Sangster, D. F. 1981. Volcanic-associated massive sulfide deposits. *In* Economic Geology 75th Anniversary Volume. *Edited by* B. J. Skinner, Econmic Geology, pp. 485-627.

Fripp, R. E. P. 1976. Stratabound gold deposits in Archean banded iron formation, Rhodesia. Economic Geology, **71**: 58-75.

Gardiner, J. J. 1986. Structural geology of the Lupin gold mine, Northwest Territories. M.Sc. thesis, Acadia University, Wolfville, Nova Scotia.

Grant, J. A. 1986. The isocon diagram- A simple solution to Gresens' equation for metasomatic alteration. Economic Geology, **81**: 1976-1982.

Gresens, R. L. 1967. Composition-volume relationships of metasomatism. Chemical Geology, **2**: 47-65.

Gross, G. A., and McLeod, C. R. 1980. A preliminary assessment of the chemical composition of iron formations in Canada. Canadian Mineralogist, **18**: 223-229.

Groves, D. I., Phillips, G. N., Falconer, L. J., Houstoun, S. M., Ho, S. E., Browning, P., Dahl, N., and McNaughton, N. J. 1987. Evidence for an epigenetic origin for BIF-hosted gold deposits in the greenstone belts of the

Yilgarn Block, Western Australia. *In* recent advances in understanding Precambrian gold depsoits. *Edited by* S. E. Ho and D. I. Groves, Geology Department & University Extension, University of Western Australia, Publication II, pp. 167-179.

Hallager, W. S. 1984. Geology of gold-bearing metasediments near Jardine, Montana. *In* Gold'82: the geology, geochemistry of gold deposits. *Edited by* R. P. Foster, Geological Society of Zimbabwe Special Publication 1, pp. 191-218.

Hannington, M. D., Peter, J. M., and Scott, S. D. 1986. Gold in sea-floor polymetallic sulfide deposits. Economic Geology, **81**: 1867-1883.

Henderson, J. B. 1970. Stratigraphy of the Yellowknife Supergroup, Yellowknife Bay; Prosperous Lake area, District of Mackenzie. Geological Survey of Canada, paper 70-26.

Kerrich, R. 1983. Geochemistry of gold deposits in the Abitibi Greenstone Belt. Canadian Institute of Mining and Metallurgy, Special Volume 27.

Kerrich, R., and Fryer, B. J. 1981. The separation of rare elements from abundant base metals in Archean lode gold depsoits: implications of low water/rock source regions. Economic Geology, **76**, 160-166.

Kerrich, R., and Hodder, R. W. 1982. Archean lode gold and base metal deposits: Evidence for metal separation into independant hydrothermal systems. *In* Geology of Canadian gold deposits. *Edited by* R. W. Hodder and W. Petruk. Canadian Institute of Mining and Metallurgy, Special Volume 24, pp. 144-160.

Kerrich, R., and Watson, G. P. 1984. The Macassa Mine Archean lode gold deposit, Kirkland Lake, Ontario: Geology, patterns of alteration, and hydrothermal regimes. Economic Geology, **79**: 1104-1130.

Kerrich, R., Fryer, B. J., Milner, K. J., and Peirce, M. G. 1981. The geochemistry of gold-bearing chemical sediments, Dickenson Mine, Red Lake, Ontario: A reconnaissance study. Canadian Journal of Earth Sciences, **18**: 624-637.

Kerswill, J. A. 1986. Gold deposits hosted by iron formation in the Contwoyto Lake area, Northwest Territories. *In* Gold'86 Poster Paper Abstracts. *Edited by* A. M. Chater, Geological Association of Canada, Mineral Deposits Division, pp. 82-85.

Kerswill, J. A. 1985a. Gold, Sulphur, and Arsenic in metamorphosed iron formation of the Contwoyto Lake area, Northwest Territories, Canada. Geological Society of America, Abstracts with Program, Annual Meeting, Orlando, Florida, pp. 627.

Kerswill, J. A. 1985b. Gold metallogeny of Archean iron formation in the Contwoyto Lake area, N.W.T. Geological Association of Canada, Program with Abstracts, **10**: A31.

Kerswill, J. A. 1984. The Lupin gold deposit, Contwoyto Lake area, N.W.T; Styles of gold distribution and possible genetic models. Geological Association of Canada, Program with Abstracts, **9**: 78.

King, J. E., Davis, W. J., Relf, C., and Avery, R. W. 1988. Deformation and plutonism in the western Contwoyto Lake map area, central Slave Province, District of Mackenzie, N.W.T. *In* Current research part C. Geological Survey of Canada, paper 88-1C, pp. 161-176.

Klein, C. 1983. Diagenesis and metamorphism of Precambrian banded iron-formations. *In* Iron formations: Facts and problems. *Edited by* A. F. Trendall, Elsevier, New York, New York.

Lhotka, P. G., and Nesbitt, B. E. 1987a. An epigenetic origin for gold in iron formation in and around the Lupin mine, N.W.T. Geological Association of Canada, Annual General Meeting, Saskatoon, Saskatchewan, Program with Abstracts, **12**: p.67.

Lhotka, P. G., and Nesbitt, B. E. 1987b. Epigenetic gold hosted by iron formation at the Lupin mine, Contwoyto Lake, N.W.T. Geological Association of Canada, Summer Field Meeting, Yellowknife, N.W.T., Program with Abstracts.

Ludden, J. N., Daigneault, R., Robert, F., and Taylor, R. P. 1984. Trace element mobility in alteration zones associated with Archean Au lode deposits. Economic Geology, **79**: 1131-1141.

Macdonald, A. J. 1983. The iron formation-gold association evidence from the Geraldton area. *In* The geology of gold in Ontario. *Edited by* A. C. Colvine, Ontario Geological Survey, Miscellaneous Paper 110, pp. 75-83.

Macdonald, A. J., and Fyon, J. A. 1986. Sulphidation the key to gold mineralization in banded iron formation. *In* Gold'86 Poster Paper Abstracts. *Edited by* A. M. Chater, Geological Association of Canada, Mineral Deposits Division, pp. 96-97.

Padgham, W. A. 1984. Gold deposits of N. W. T. ; Classes, styles, genesis, exploration methods and success probabilities. Contributions to the geology of the Northwest Territories, **1**: 121-129.

Phillips, G. N., and Groves, D. I. 1983. The nature of Archean gold-bearing fluids as deduced from gold deposits of Western Australia. Journal of the Geological Association of Australia, **30**: 25-39.

Phillips, G. N., Groves, D. I., and Martyn, J. E. 1984. An epigenetic origin for Archean banded-iron-formation-hosted gold deposits. Economic Geology, **79**: 162-171.

Ridler, R. H. 1970. Relationships of mineralization to volcanic stratigraphy in the Kirkland-Larder Lakes area, Ontario. Geological Association of Canada Proceedings, **21**: 33-42.

Robert, F., and Brown, A. C. 1986. Archean gold-bearing veins at the Sigma Mine, Abitibi Greenstone Belt, Quebec: Part II. Vein paragenesis and hydrothermal alteration. Economic Geology, **81**: 593-616.

Robinson, D. J. 1984. Silicate facies iron-formation and stratabound alteration: tuffaceous exhalites derived by mixing-evidence from Mn garnet-stilpnomelane rocks at Redstone, Timmins, Ontario. Economic Geology, **79**: 1796-1817.

Rye, D. M., and Rye, R. O. 1974. Homestake Gold Mine, South Dakota: I. Stable isotope studies. Economic Geology, **69**: 293-317.

Thompson, P. H. 1978. Archean regional metamorphism in the Slave Structural Province-a new perspective on some old rocks. Geological Survey of Canada, paper 78-10, pp. 85-102.

5. LEAD AND STRONTIUM ISOTOPE GEOCHEMISTRY OF GOLD-BEARING IRON FORMATION, CONTWOYTO LAKE REGION, NORTHWEST TERRITORIES, CANADA

A. Introduction

Previous studies of gold deposits associated with iron formation have resulted in three main genetic models: a syngenetic model in which gold is deposited simultaneously with the deposition of the iron formation (Fripp 1976; Ridler 1970); an epigenetic model in which gold is introduced into the iron formation during a later event (Phillips *et al.* 1984; Macdonald 1983; Groves *et al.* 1987); and a multistage or remobilization model in which gold is a primary component of the iron formation and is remobilized and concentrated during later events (Rye and Rye; 1974, Sawkins and Rye, 1974). These studies have concentrated on the field, petrographic, structural, and, to a far lesser extent, stable and radiogenic isotopic aspects of these deposits.

Very few studies have examined the lead isotope systematics of gold deposits hosted by iron formation (Robertson 1973; Rye *et al.* 1974; Kramers and Foster 1984; Browning *et al.* 1987) and to the best of our knowledge no studies have investigated the strontium isotope systematics of these deposits. The objective of this study was to examine the lead and strontium isotope systematics of whole rocks and mineral separates from mineralized zones in iron formation and from laterally equivalent unmineralized iron formation in the Contwoyto Lake region and use the resulting data to constrain genetic models of the deposits. Archean iron formations, in the northern part of the Slave Province of the Canadian Shield between Contwoyto and Point Lakes, host over 100 gold occurrences and one major gold deposit, the Lupin mine (Fig. 5.1). Lupin is a major deposit that has produced 28.25 tonnes of gold (905,800

troy ounces) between startup in 1982 and the end of 1987 at an average grade of 11.12 ppm.

B. Geology

Regional geology

The Contwoyto Lake region is underlain predominantly by Archean rocks of the Slave Province. Small outliers of Aphebian, clastic sedimentary rocks are exposed near the margins of the area (Fig. 5.1). Bostock (1980) mapped the region at a scale of 1:250,000. More detailed mapping has been done by King *et al.* (1988), Jackson (1982), Easton *et al.* (1981), King *et al.* (1980), Bau *et al.* (1979a,b,c,d,e,f), Henderson and Easton (1977a) and Tremblay (1976). Data from all of these sources as well as unpublished company data were used to revise Bostock's map (Fig. 5.1).

Archean rocks can be subdivided into: pre-Yellowknife Supergroup rocks that comprise granitic rocks and gneisses; Yellowknife Supergroup supracrustal metavolcanic and metasedimentary units; and syn- and post-Yellowknife Supergroup granitic rocks. All but the late plutons have been metamorphosed to some degree; however, premetamorphic rock terminology is generally used hereinafter.

Pre-Yellowknife Supergroup rocks

Stockwell (1933) first noted that a sheared, chloritic granitic rock (basement) is unconformably overlain by conglomerate at Keskarrah Bay on Point Lake (Fig. 5.1). Other rock units present in the Point Lake area have been suggested to constitute basement units by Henderson and Easton (1977b), and more recently by Easton (1985), and Easton *et al.* (1981). These units are

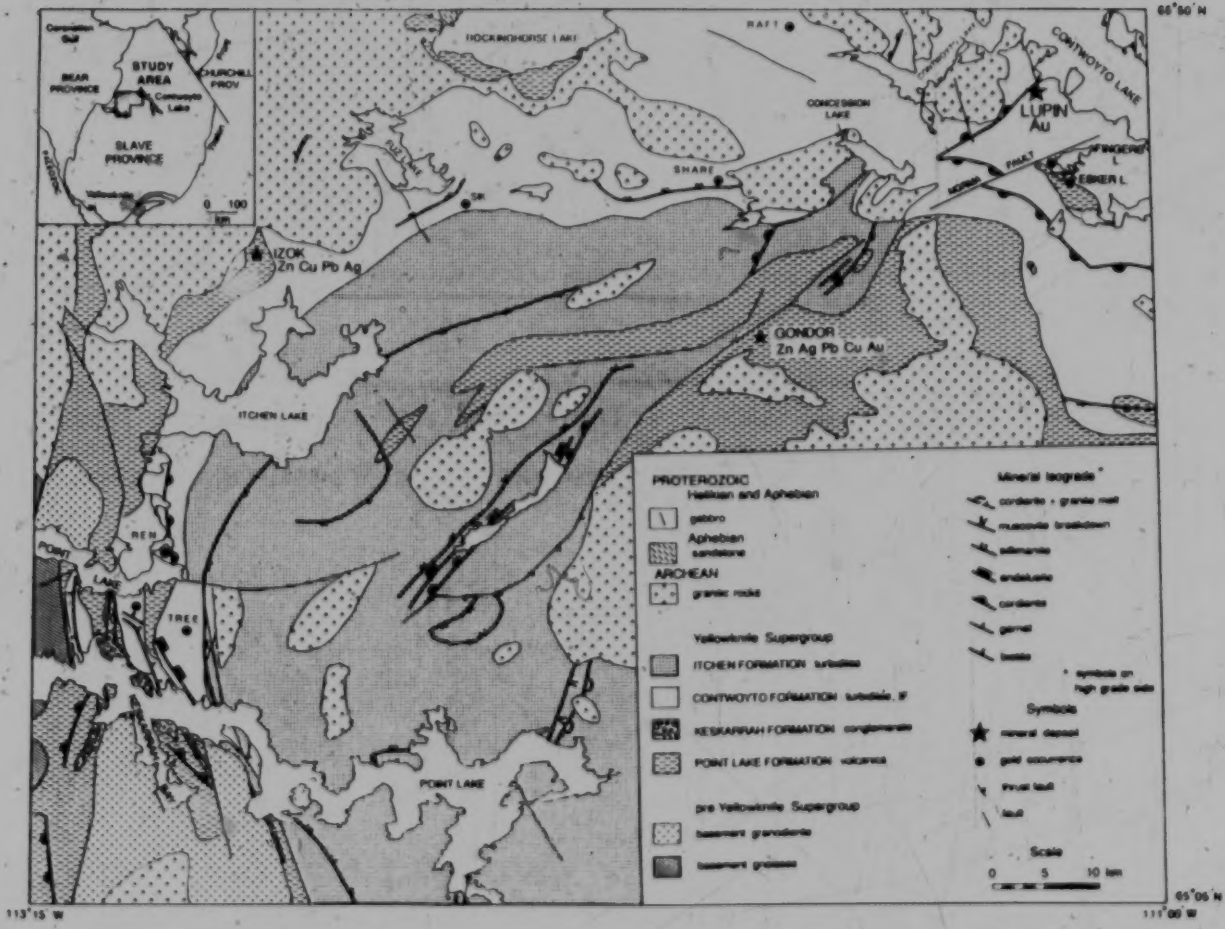

Fig. 5.1. Geology of the Contwoyto Lake-Point Lake region. Modified after Bostock (1980) and others.

gneissic (Fig. 5.1) and although the contacts with the less deformed supracrustals are faulted or mylonitized, there are several lines of field evidence that suggest the gneisses are older than the supracrustals (Easton *et al.* 1981).

Yellowknife Supergroup

The term Yellowknife Supergroup was defined by Henderson (1970) to include all of the supracrustal rocks in the Slave Province. Bostock (1980) subdivided the supergroup into four formations in the Contwoyto Lake-Point Lake region as follows: the Point Lake Formation which comprises mafic to felsic volcanic rocks; the Keskarrah Formation which comprises conglomerates and lithic sandstones; the Contwoyto Formation which comprises greywacke and mudstone beds with lenses and beds of iron formation; and the Itchen Formation which comprises greywacke and mudstone beds lacking iron formation (Fig. 5.1). The iron formations of the Contwoyto Formation are the subject of this study.

Age relationships between these formations are equivocal due in part to faulting of the contacts and intense folding in the sedimentary formations. Bostock (1980) considers the Keskarrah Formation to be a facies equivalent to the upper part of the Point Lake Formation. He believes the Contwoyto Formation is a facies equivalent to a late phase of Point Lake volcanism and that the Itchen Formation is younger than the other three formations. On the basis of detailed mapping at Point Lake, Henderson and Easton (1977b) concluded that all four formations are essentially contemporaneous.

Archean plutonic rocks

Bostock (1980) separated the Archean plutonic rocks in the area into three age groups based on field relationships as follows: an older group of

plutons possibly representing basement to the supracrustals; Early Kenoran (Archean) plutons that are essentially coeval with the Point Lake Formation; and Late Kenoran (Archean) plutons that are intrusive into all of the supracrustal formations. The first group consists of the granitic rocks at Keskarrah Bay and is in fact pre-Yellowknife Supergroup as was described above. Recent work by King *et al.* (1988) in the area south and east from Rockinghorse Lake to Contwoyto Lake (Fig. 5.1) has subdivided Bostock's (1980) second and third groups into six groups. These six groups are defined by their compositions and interpreted timing of emplacement. The first four groups of plutons (King *et al.* 1988) have all been affected by the major Archean deformations and metamorphism. The fifth and sixth groups are later and are only affected by minor Archean deformation. The fifth group is apparently coincident with peak metamorphism and the sixth group slightly postdates peak metamorphic conditions. Petrologically, the plutons evolved with time from early hornblende-diorite and tonalite through to biotite tonalite and granodiorite to monzogranite and syenogranite (King *et al.* 1988).

Proterozoic rocks

Aphebian sedimentary rocks including sandstone, argillite and minor dolomite are exposed at Rockinghorse Lake, and northeast of Contwoyto Lake (Fig. 5.1). These rocks are subhorizontally dipping, gently folded and are apparently unmetamorphosed, or metamorphosed to very low grades (Tremblay 1976; Bostock 1980).

Both the Aphebian sedimentary rocks and the Archean rocks are intruded by Proterozoic gabbro and diabase dykes and sills of several ages (Bostock 1980).

Metamorphism and deformation

Archean rocks have been deformed and metamorphosed by Archean tectonic events. Archean structures comprise complexly interfering isoclinal folds with associated penetrative fabrics (King *et al.* 1988). Metamorphic isograds are defined in the pelitic sediments by the first appearance of the characteristic minerals biotite, garnet, cordierite, andalusite, sillimanite, and the breakdown of muscovite + quartz to form K-feldspar + sillimanite + H_2O (Fig. 5.1). The distribution of the isograds generally suggests that the thermal highs are spatially associated with the fifth group of granitic plutons of King *et al.* (1988). Isograds cut across some of the folds indicating that peak metamorphism postdated at least some of the early deformation. Aphebian and later geological events have had little or no visible effect on Archean mineral assemblages except immediately adjacent to Proterozoic gabbro dykes.

C. Gold mineralization in iron formation

At present, relatively little is known about the gold-bearing iron formations in the region of interest. The only detailed published work is that of Gardiner (1986). Other publications are less detailed or of a more regional nature (Lhotka and Nesbitt 1987a,b; Kerswill 1986, 1985a,b, 1984; Padgham 1984; Gibbins 1981; Franklin and Thorpe 1982; and Bostock 1980).

On the basis of detailed fieldwork and petrographic studies (Chapter 2) iron formation has been subdivided into unmineralized iron formation, containing trace or no visible iron sulphide minerals, and mineralized iron formation, containing abundant iron sulphide and/or arsenide minerals. Enhanced gold values are associated only with the sulphide mineralized iron

formation. The following geological descriptions are summarized from Chapter 2.

Unmineralized iron formation in most of the region is comprised largely of grunerite + quartz ± magnetite with minor amounts of hornblende. This rock type, comprised largely of chemical sediment, is interbedded with a rock of mixed parentage that is referred to as pelitic iron formation. Pelitic iron formation is a mixture of chemical and fine grained detrital sediment which, following metamorphism, comprises chlorite, quartz, ilmenite ± almandine garnet ± grunerite ± hornblende. Unmineralized iron formation and interbedded pelitic iron formation generally contain ≤0.03 ppm Au.

All of the known gold occurrences in iron formation, except Lupin, are small-scale gold occurrences, many of which contain ore grade gold values within volumes of mineralized rock too small to be economic. At the small-scale occurrences, gold is associated with increased concentrations of sulphides, which are in turn spatially associated with quartz veins (Kerswill 1985a; Lhotka and Nesbitt 1987a,b; Chapter 2) Pelitic iron formation is interbedded with the mineralized iron formation but does not contain more than trace amounts of sulphide or enhanced gold values.

At the small-scale gold occurrences, the distribution of mineralized iron formation is clearly controlled by late quartz veins (Fig. 5.2). Mineralized iron formation is comprised of iron sulphides ± arsenides (arsenopyrite and loellingite) in iron formation that is predominantly comprised of hornblende with little or no grunerite. In the sub-garnet metamorphic zone the iron sulphide is pyrite, whereas at higher metamorphic grades it is pyrrhotite. If present, arsenides always occur immediately adjacent to the vein and are enveloped by a larger haloe of iron sulphides. Gold values of mineralized iron formation are generally between about 5 and 30 ppm. Mineralized iron formation grades into

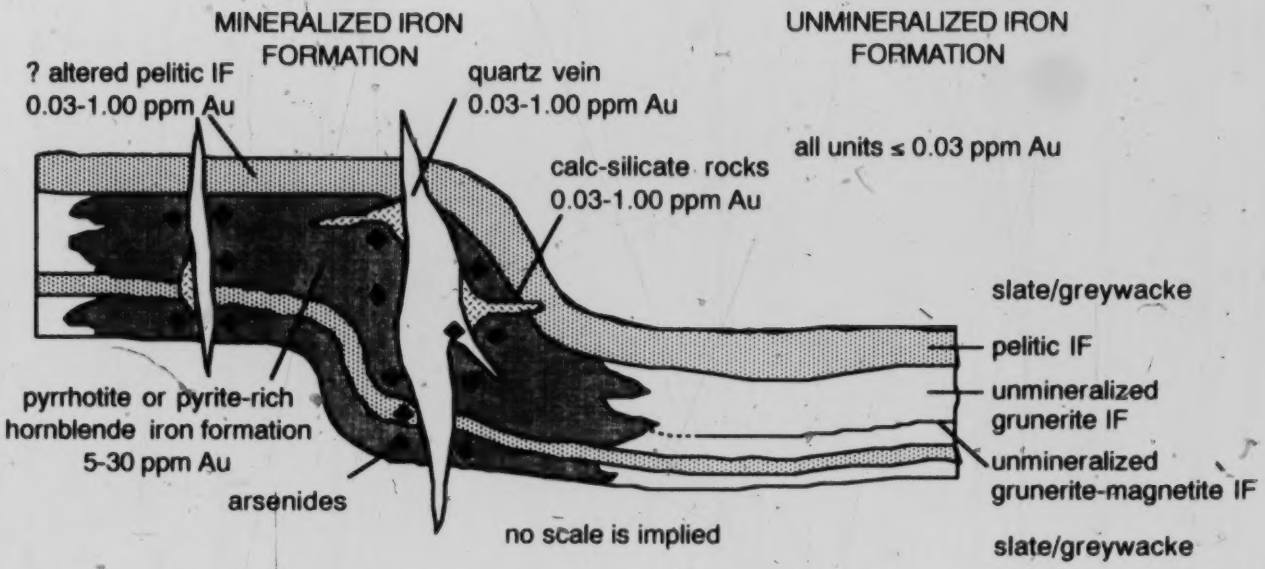

Fig. 5.2. Schematic summary diagram of the relationships between quartz veining and gold mineralization in iron formation in the Contwoyto Lake-Point Lake region. The mineralogy and typical gold values of iron formation and associated units are shown. A scale is not indicated because the relationships occur at scales ranging from a hand specimen to an ore zone.

unmineralized grunerite iron formation along strike. Textural evidence suggests that those minerals that predominate in mineralized iron formation replace those minerals that predominate in unmineralized iron formation: thus, hornblende replaces grunerite and iron sulphides replace amphiboles and magnetite (Chapter 2). Samples of mineralized iron formation at the small-scale occurrences analysed in this study are from the Esker Lake, Fingers Lake and Sik occurrences (Fig.5.1). These occurrences are described individually in greater detail in Chapters 2 and 3. Unmineralized iron formation samples were collected in the vicinity of these occurrences, and along strike from the Lupin mine, away from areas of known mineralization.

Lupin is the only known economic gold deposit. It differs from the small-scale occurrences in its much larger size and continuity of the mineralized zones, and the fact that unmineralized grunerite iron formation is rare within the deposit. The geology of the Lupin mine has previously been described by Kerswill (1984, 1985a,b, 1986), Lhotka and Nesbitt (1987a,b) and Gardiner (1986). The following description is summarized from Chapter 2. The Lupin iron formation unit can be subdivided into unmineralized and mineralized iron formation, pelitic iron formation, and minor amounts of mudstone and fine grained greywacke.

Mineralized iron formation constitutes the principal gold-bearing lithology in the mine. This rock type comprises abundant fine grained disseminated grains of pyrrhotite which, together with quartz and amphibole, commonly form bands in the iron formation. Hornblende is the predominant amphibole and is much more abundant than grunerite, which never predominates where pyrrhotite is abundant. In well mineralized samples grunerite is often absent. Where grunerite is present it forms the core to grains of hornblende. Coarse grained hedenbergite is often present, and may be locally abundant. Actinolite

replaces hedenbergite along fractures and sometimes rims hornblende. Other minor or trace phases include epidote, chalcopyrite, ilmenite, pyrite and graphite.

Adjacent to late quartz veins, 1 cm diameter porphyroblasts of arsenopyrite, containing cores of loellingite, overgrow pyrrhotite in sulphide-rich iron formation. The veins comprise strained quartz with sutured grain boundaries. Trace amounts of hedenbergite, hornblende, actinolite, pyrrhotite, pyrite, arsenopyrite, loellingite, scheelite, and rarely, visible gold generally comprise <2 % of the vein material. These veins clearly control the distribution of arsenides, which are present only where pyrrhotite-rich, iron formation is intersected by the vein.

Unmineralized iron formation is rarely present within ore grade portions of the Lupin mine, but is more common in relatively gold-poor parts of the mine. This rock type comprises well banded grunerite and quartz. In thin section, grunerite is the predominant amphibole. Hornblende forms rims to grains of grunerite and varies from a minor proportion of the total amphibole up to about 50 %. Minor amounts of ilmenite, graphite and pyrrhotite are also present, but arsenides are absent. In the northern part of the East Zone, near the edge of the orebody on the 130 m level, gold- and sulphide-poor, grunerite iron formation can be traced into gold- and pyrrhotite-rich, hornblende iron formation, and finally into gold- and arsenide-rich, hornblende iron formation. This transition occurs along the strike of the banding, as a late quartz vein is approached over a distance of 2.5 m. Beyond the end of the East Zone unmineralized grunerite-rich iron formation is the predominant type of iron formation and mineralized iron formation is absent or present only as narrow zones adjacent to quartz veins.

Pelitic iron formation forms thin, generally <1 m wide, lenses or beds within the Lupin iron formation unit. Almandine-rich garnet, grunerite, chlorite and quartz comprise the pelitic iron formation. Hornblende and biotite are sometimes present, as are trace amounts of ilmenite, graphite, allanite, zircon, and rarely, pyrrhotite and arsenopyrite.

Sulphide-poor, calc-silicate rocks form a volumetrically minor, but important, part of the Lupin orebody. Calc-silicate rocks comprise hedenbergite and quartz as the major phases. Epidote is commonly present as a minor component; however, in some samples intergrown epidote and grossular-rich garnet are abundant. Minor phases present include scheelite, calcite, sphene, apatite, ilmenite and graphite. The calc-silicate rocks are spatially associated with the quartz veins and are interpreted to represent alteration zones within the iron formation.

These observations suggest that sulphidation and wallrock alteration of iron formation, which produces pyrrhotite- and hornblende-rich iron formation, are important processes in the gold mineralization at the small-scale occurrences and probably at Lupin as well. The field observations and petrographic data for the small-scale occurrences and Lupin have been summarized into a scaleless schematic diagram to show the critical features of the gold-bearing zones (Fig. 5.2). The evidence supports an epigenetic model of gold mineralization.

D. Previous geochronology

The majority of the geochronological studies completed in the region are on the plutonic and volcanic rocks and comprise K-Ar determinations, on biotite or muscovite, or Rb-Sr whole rock isochrons. Most of the ages obtained are too

young to represent Archean crystallization ages and probably represent final cooling after peak metamorphism (King 1982; Easton 1984). In addition, there may be partial resetting of Archean isotopic systems by events in the adjacent, younger Bear Province to the west (Easton 1983).

U-Pb geochronology on zircons from the granitic basement rocks at Keskarrah Bay by Krogh and Gibbins (1978) gave an age of 3155 Ma which was later confirmed by Henderson *et al.* (1982). Additional U-Pb geochronology was done on single detrital zircon grains from greywacke of the Contwoyto Formation on the north shore of the north arm of Point Lake (Fig. 5.1) by Schärer and Allègre (1982). Their work indicated that the zircons were derived from rocks with a wide range of ages that includes the 3155 Ma basement found by Krogh and Gibbins (1978) as well as from felsic volcanic and/or granitic rocks of about 2660 to 2690 Ma.

A discordant $^{207}Pb/^{206}Pb$ minimum age of 2643 ± 15 Ma on a zircon, and a nearly concordant $^{207}Pb/^{206}Pb$ minimum age of 2638 ±15 Ma on a sphene, are reported from a granodiorite south of Keskarrah Bay (Wanless personal communication in Bostock 1980, and in Stockwell 1982). The field relationships of this granodiorite to the Point Lake Formation are uncertain.

The Point Lake Formation has not yet been accurately dated in the region of interest. A whole rock Rb-Sr isochron age of 2440 ± 48 Ma with an initial $^{87}Sr/^{86}Sr$ ratio of 0.7025, which was interpreted to represent resetting during high grade metamorphism, was found for amphibolite grade, felsic tuffaceous rocks of the Point Lake Formation (Wanless and Loveridge 1978).

A whole rock Rb-Sr errorchron for the Yamba Batholith of 2527 Ma with an initial $^{87}Sr/^{86}Sr$ ratio of 0.7032, reported by Wanless and Loveridge (1978), is here interpreted as a minimum age that may approximate the time of intrusion. K-Ar ages on biotite from plutonic rocks range widely (Stockwell

1982) and are as young as 1815 Ma for plutons which, from field evidence, are undoubtedly Archean.

Elsewhere in the Slave Province, U-Pb geochronology on zircons from volcanic rocks, which are thought to correlate with the Point Lake Formation, indicate the volcanics were erupted at about 2670 Ma (Frith and Loveridge 1982). Frith and Loveridge's assertion is based on data from Lambert and Henderson (1980) who report a $^{207}Pb/^{206}Pb$ minimum age of 2667 ±7 Ma for zircons from rhyolites of the Back River complex; on recalculated data from Green (1968) and Lambert and Henderson (1980) for zircons from felsic volcanics and greywackes from the Yellowknife area; and on their own new concordia intercept of $2666^{+20}/_{-28}$ Ma for zircons from a granodiorite coeval with the volcanics. All of these zircons plotted together define a chord that intersects the concordia at $2669^{+16}/_{-14}$ Ma which is interpreted by Frith and Loveridge (1982) as the age of the volcanics, coeval intrusions and greywackes. New data on zircons from the Townsite Formation at Yellowknife Bay area give an age of 2665 (Bowring and Padgham 1987), which is consistent with Frith and Loveridge's (1982) model.

Reliable U-Pb ages of zircons from granitic plutons that cut volcanic rocks of the Yellowknife Supergroup range widely from about 2670 Ma for coeval intrusions to as young as 2588 ± 8 Ma for late plutons such as the Uist Lake pluton (Frith and Loveridge 1982) or even younger. Many of the plutons have been dated only by the Rb-Sr whole rock isocron technique. This method often results in ages which are too young. For example, the Uist Lake pluton has an Rb-Sr isochron age of 2350 ±37 Ma with an initial $^{87}Sr/^{86}Sr$ ratio of 0.7035 ± 0.0006, an age that is 238 Ma younger than its U-Pb zircon age (Frith and Loveridge 1982).

In summary, although the data are far from complete the geochronology can be summarized as follows:

1) Basement rocks of circa 3150 Ma unconformably underlie the Yellowknife Supergroup at Point Lake. Definitive field evidence for more extensive sialic basement to the Yellowknife Supergroup is lacking within the present field area.

2) The Point Lake, Contwoyto, and Itchen Formations are probably of a similar age to equivalent formations elsewhere in the Slave Province which are about 2670 Ma old.

3) Granitic rocks intrusive into the supracrustal formations range in age from 2670 Ma to about 2550 Ma or possibly somewhat younger.

4) Rb-Sr mineral and whole rock isotopic systems are commonly disturbed and give ages that are up to 240 Ma younger than U-Pb ages on zircons from the same rocks. The Rb-Sr systems may have been disturbed during Archean metamorphism and/or by younger events related to orogeny in the adjacent Bear Province to the west. An awareness of this regional disruption in the Rb-Sr system is important in interpreting the new Rb-Sr data presented here.

E. Analytical techniques

The 28 whole rock and 11 mineral separates analysed in this study are all from the Contwoyto Formation. Samples for analysis were chosen from a larger group of samples for which petrographic, electron microprobe and whole rock geochemical data were available. This larger database enabled efficient selection of representative samples for isotopic analysis. Representative whole rock samples of about 2 kg were jaw crushed to less than 1 cm diameter. The

whole sample was then ground in a disc mill fitted with alumina plates. At this point, the entire sample was rolled on paper and split by coning and quartering until about 150 g of sample were isolated. This subsample was then ground in a motorized, agate mortar and pestle. Aliquots of the whole rock subsample of about 0.5 to 1.0 g were digested for analysis. From the portion of the sample that was disc milled, but not ground by mortar and pestle, mineral separates were prepared by a combination of heavy liquid and magnetic separation followed by hand picking. Aliquots of 0.1 to 1.0 g were digested for analysis.

The purity and composition of the mineral separates was confirmed by powder X-ray diffraction analysis. Sulphide separates contained less than 1 % nonsulphide minerals. Arsenopyrite (FeAsS) and loellingite ($FeAs_2$) could not be separated and were analysed together. Separates of pyrrhotite contained from 0 to at most 3 % arsenides, and arsenide separates contained less than 1 % pyrrhotite or pyrite. The scheelite separate was > 99 % pure and the epidote separate contained about 1 % graphite.

Whole rock, scheelite and epidote samples were decomposed in a mixture of vapour distilled HNO_3-HF and dissolved for analysis of Rb, Sr, Pb and U. Separate aliquots of the resultant sample solution were used for determination of isotopic ratios and concentrations. Sulphide and arsenide minerals were decomposed in vapour distilled HNO_3. In two cases separate aliquots of sample powder were analysed for determination of Pb concentration and isotopic ratios. Later, because of concern for the homogeneity of the sulphide samples, a single aliquot of the mineral separate was decomposed and dissolved. The resulting sample solution was then split into aliquots for determination of isotopic ratios and concentrations.

Pb and Sr were separated by coprecipitation with $Ba(NO_3)_2$, followed by chloride anion exchange separation of the Pb, and chloride cation exchange of

the Sr, following the methods of Cavell and Baadsgaard (1986) and Baadsgaard *et al.* (1986). U was separated from the supernatant solution of the $Ba(NO_3)_2$ precipitation by nitrate anion exchange. Rb was recovered from a split of the spiked portion of the sample solution by conversion to sulphate by heating. The soluble Rb-sulphate was then separated from the insoluble oxide residue using vapour distilled H_2O.

Pb was loaded onto a single Re-filament, or the centre filament of a double filament, as a silica gel-phosphoric acid mixture; U was loaded onto the side filament of a double Re-filament as a nitrate; Sr was loaded onto the side filament of a double Re-filament as a chloride; and Rb was loaded as perchlorate onto the side filament of a double Re-filament. All isotopic ratios were measured on a VG MM 30 mass spectrometer. Pb isotopic ratios were corrected to the NBS 981 standard using mass fractionation corrections of Cavell and Baadsgaard (1986). Total blanks were determined as follows: 5 ng of ^{208}Pb; 0.2 ng of ^{238}U; 3 ng of ^{88}Sr; and 4 ng of ^{87}Rb. Uncertainties for Sr are quoted at 2σ. Uncertainties for Pb were calculated as per mil errors for $^{206}Pb/^{204}Pb$ (0.24), $^{207}Pb/^{204}Pb$ (0.32), and $^{208}Pb/^{204}Pb$ (0.35) from repeat analyses of NBS 981 (personal communication P. Wagner 1987). Where the 2σ precision of an individual analysis exceeds these values the larger value was substituted. All of the subsequent calculations were made using the recommended decay constants of Steiger and Jäger (1977) and data from older literature quoted here were recalculated to these constants where necessary.

F. Lead isotope data

Unmineralized whole rock samples

Data for unmineralized whole rock samples are given in Table 5.1. When the data for unmineralized iron formation, pelitic iron formation, and metapelites

Table 5.1 Lead isotope data for rocks and minerals from Contwoyto Lake. The corrected lead isotopic ratios are estimated initial ratios at the indicated assumed age. See text for method of calculation.

WHOLE ROCKS	rock type or mineral	$^{206}Pb/^{204}Pb$	$^{207}Pb/^{204}Pb$	$^{208}Pb/^{204}Pb$	Pb ppm	U ppb	$^{206}Pb/^{204}Pb$ corrected to 2670 Ma	$^{207}Pb/^{204}Pb$ corrected to 2670 Ma	$^{206}Pb/^{204}Pb$ corrected to 2550 Ma	$^{207}Pb/^{204}Pb$ corrected to 2550 Ma
Lupin										
4A031	calc-silicate	14.585 ± 0.017	14.998 ± 0.018	34.327 ± 0.044	22.6	41.0	13.795	14.822	13.810	14.834
5A041	calc-silicate	16.156 ± 0.004	15.355 ± 0.005	36.047 ± 0.013			13.961	14.956	14.001	14.988
5A056	calc-silicate	17.230 ± 0.004	15.497 ± 0.005	36.987 ± 0.013			13.874	14.886	13.938	14.937
5A080	calc-silicate	15.840 ± 0.013	15.223 ± 0.013	35.556 ± 0.184			13.840	14.859	13.878	14.898
5A017	min. IF	16.104 ± 0.032	15.253 ± 0.030	36.982 ± 0.073			13.812	14.836	13.855	14.871
5A020	min. IF	16.544 ± 0.004	15.337 ± 0.005	36.218 ± 0.013			13.818	14.841	13.870	14.883
5A082	min. IF	15.585 ± 0.004	15.174 ± 0.005	35.556 ± 0.012			13.837	14.856	13.870	14.883
5A105	pelitic IF	20.582 ± 0.012	15.971 ± 0.010	39.679 ± 0.024			13.656	14.711	13.787	14.816
5A114	pelitic IF	22.623 ± 0.007	16.127 ± 0.006	40.242 ± 0.014			13.310	14.432	13.486	14.574
5A122	unmin.IF	17.478 ± 0.019	15.406 ± 0.017	36.926 ± 0.040			13.656	14.711	13.728	14.768
Fingers Lake										
4B017	unmin.IF	19.420 ± 0.005	15.847 ± 0.005	38.825 ± 0.014			13.797	14.824	13.903	14.909
5B004	unmin.IF	26.971 ± 0.011	16.871 ± 0.007	41.831 ± 0.017			12.912	14.112	13.179	14.327
5B091	unmin.IF	19.875 ± 0.005	15.709 ± 0.005	38.841 ± 0.014			13.442	14.538	13.563	14.636
5B095	unmin.IF	19.034 ± 0.028	15.641 ± 0.023	38.777 ± 0.062			13.579	14.649	13.681	14.731
4B022	pelite	17.551 ± 0.005	15.438 ± 0.005	37.337 ± 0.013			13.686	14.735	13.758	14.793
4B024	pelite	18.304 ± 0.004	15.764 ± 0.005	37.632 ± 0.013			13.990	14.979	14.070	15.044
5B088	pelite	18.394 ± 0.009	15.420 ± 0.074	37.758 ± 0.018			13.410	14.513	13.505	14.589
Esker Lake										
5C015b	unmin.IF	21.456 ± 0.020	16.114 ± 0.015	40.848 ± 0.038			13.830	14.890	13.777	14.808
Sik										
4E025	unmin.IF	16.953 ± 0.008	15.356 ± 0.008	36.477 ± 0.013			13.730	14.770	13.790	14.818
4E025dp	unmin.IF	16.975 ± 0.006	15.362 ± 0.005	36.507 ± 0.013			13.733	14.773	13.793	14.821
4E029	unmin. IF	17.811 ± 0.004	15.478 ± 0.005	36.672 ± 0.013			13.570	14.722	13.749	14.785
4E029dp	unmin.IF	18.503 ± 0.018	15.654 ± 0.017	37.588 ± 0.044			13.754	14.789	13.843	14.861
5E003	unmin.IF	23.959 ± 0.012	16.397 ± 0.008	41.397 ± 0.021			13.352	14.486	13.554	14.628
5E006	unmin.IF	16.728 ± 0.004	15.279 ± 0.005	35.552 ± 0.012			13.672	14.723	13.728	14.768
5E019	unmin.IF	16.706 ± 0.004	15.283 ± 0.005	35.281 ± 0.012			13.685	14.734	13.741	14.779
5E048	unmin.IF	16.579 ± 0.004	15.348 ± 0.005	36.186 ± 0.013			13.826	14.847	13.878	14.889
4E026	pelitic IF	26.512 ± 0.016	16.901 ± 0.010	41.874 ± 0.026			13.416	14.517	13.664	14.717
4E022b	pelite	16.841 ± 0.004	15.336 ± 0.005	36.617 ± 0.013			13.730	14.770	13.788	14.817
5E037	pelite	21.357 ± 0.005	16.125 ± 0.005	41.993 ± 0.015			13.677	14.727	13.821	14.843
5E039	pelite	18.420 ± 0.004	15.599 ± 0.005	39.564 ± 0.014			13.691	14.739	13.780	14.810
MINERALS										
Lupin										
4A031	scheelite	16.734 ± 0.012	15.562 ± 0.013	36.406 ± 0.029	28.0	3.8	14.123	15.086	14.173	15.127
4A031	epidote	14.189 ± 0.017	14.935 ± 0.018	33.978 ± 0.041	45.0		13.861	14.876	13.867	14.880
5A017	arsenides	14.741 ± 0.004	15.036 ± 0.005	34.721 ± 0.012			13.861	14.876	13.878	14.889
5A020	arsenides	16.416 ± 0.008	15.415 ± 0.005	36.296 ± 0.013	8.07*		13.980	14.971	14.026	15.008
5A020	arsenides dp	16.439 ± 0.004	15.378 ± 0.005	36.196 ± 0.013	7.8	41.0	13.914	14.918	13.962	14.957
5A020	hex. po	17.841 ± 0.043	15.597 ± 0.006	37.802 ± 0.013	8.3*		13.857	14.872	13.932	14.933
5A020	hex. po dp	17.238 ± 0.004	15.549 ± 0.005	37.154 ± 0.013	35.8	54.9	13.956	14.952	14.018	15.002
5A017	hex. po	17.582 ± 0.004	15.574 ± 0.005	37.874 ± 0.013			13.895	14.903	13.965	14.959
Fingers Lake										
5B073	arsenides	16.165 ± 0.009	15.287 ± 0.008	35.976 ± 0.019			13.848	14.865	13.892	14.900
Esker Lake										
4C008	arsenides	19.561 ± 0.005	16.002 ± 0.005	40.128 ± 0.014			14.004	14.991	14.110	15.076
4C008	mono. po	21.275 ± 0.007	16.294 ± 0.006	41.996 ± 0.015			13.972	14.965	14.110	15.076
4C008	mono. po dp	21.541 ± 0.005	16.322 ± 0.005	42.245 ± 0.015		42.1	13.940	14.939	14.083	15.054
Sik										
4E033	mono. po	21.431 ± 0.008	16.300 ± 0.006	42.163 ± 0.016			13.937	14.937	14.078	15.050
4E033	arsenides	18.815 ± 0.005	15.952 ± 0.005	39.040 ± 0.014			14.142	15.102	14.230	15.172

Abbreviations: calc-silicate= calc-silicate rocks; IF= iron formation; min.= mineralized; unmin.= unmineralized; dp= duplicate; hex. po= hexagonal pyrrhotite; mono. po= monoclinic pyrrhotite.)

* denotes IR/ID from separate aliquots of sample from the same vial.

NBS 981 corrected values

are examined it can be seen that there is considerable scatter in the data points on a standard plot of $^{206}Pb/^{204}Pb$ versus $^{207}Pb/^{204}Pb$ (Fig. 5.3). Since the age of these samples is thought to be similar to the probable age of the Point Lake Formation, which is 2670 Ma, a reference line with a slope age of 2670 Ma has been drawn for comparison. Visual inspection indicates that the points generally have a slope similar to that of the reference line except for the most radiogenic sample, which suggests a shallower slope, and therefore younger age.

When the data for unmineralized iron formation, pelitic iron formation and metapelite samples are examined as separate groups or, are grouped geographically or by metamorphic grade, the points still scatter (Table 5.1, Fig. 5.3). The degree of scatter precludes calculation of a $^{207}Pb/^{206}Pb$ slope age for these rocks. The scatter is probably attributable to one or both of the following reasons:

1) The sediments were from diverse sources which had different lead isotopic ratios and were not homogenized during sedimentation. This resulted in heterogeneous sedimentary units of the same age with different lead isotopic compositions and different μ ($^{238}U/^{204}Pb$) values.

2) The sedimentary rocks were homogeneous in their initial lead isotopic ratios but were variably affected by one or more events subsequent to sedimentation.

Data on galenas (Franklin and Thorpe 1982; Thorpe 1982; and Thorpe personal communication 1987) from the Izok, Gondor and other syngenetic, volcanogenic massive sulphide deposits of the Slave Province place constraints on the cause of the scatter and suggest that the first reason is predominant (Table 5.2). Although these deposits are hosted by volcanic rocks that are thought to be about 2670 Ma old, the galenas define a steep, short

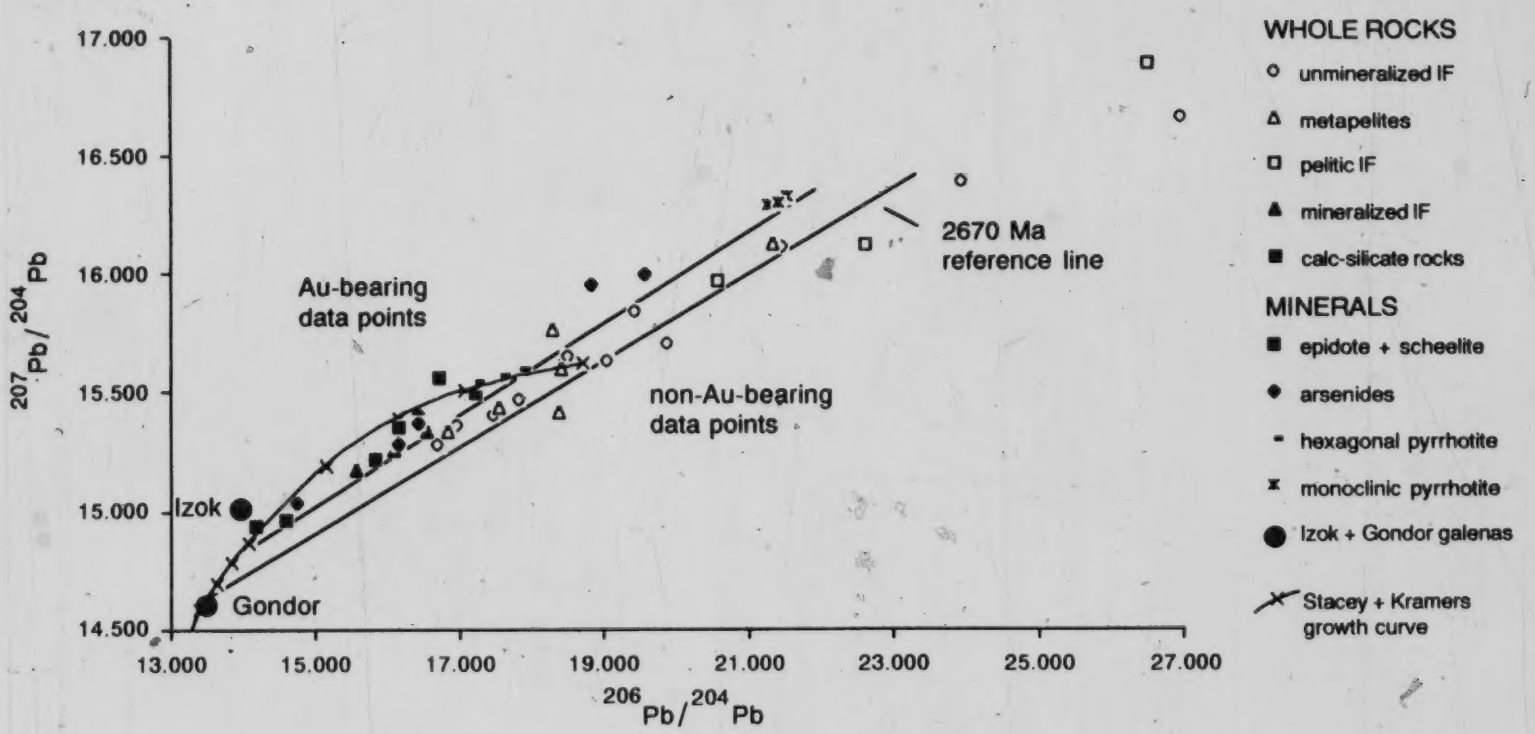

Fig. 5.3. A $^{206}Pb/^{204}Pb$ versus $^{207}Pb/^{204}Pb$ plot of data for whole rocks and minerals from Contwoyto Lake.

Table 5.2 Lead isotopic ratios for galenas from volcanogenic massive sulphide deposits of the Slave Province. Data from R. Thorpe personal communication 1987.

Location	sample	$^{206}Pb/^{204}Pb$	$^{207}Pb/^{204}Pb$	$^{208}Pb/^{204}Pb$
Indian Mountain Lake	TQ72-38	13.621	14.680	33.400
Indian Mountain Lake	SP-1497	13.653	14.692	33.421
No. 41 deposit	SP-2323	13.968	14.994	33.771
Homer Lake	TQ71-238	14.091	15.064	33.960
Homer Lake	TQ71-238dp	14.097	15.069	33.960
Homer Lake	TQ71-309	14.106	15.076	33.990
Homer Lake	TQ71-309dp	14.101	15.073	33.977
Victory Lake	TQ71-308	14.677	15.239	34.403
Victory Lake	TQ71-308	14.681	15.244	34.425
Ross Lake	TQ72-13	14.288	15.189	34.043
Ross Lake	TQ72-13dp	14.286	15.189	34.028
Turnback Lake	RF78-112	14.207	15.146	33.937
Turnback Lake	RF78-112dp	14.204	15.138	33.937
Turnback Lake	TQ71-267	14.194	15.136	33.917
Turnback Lake	TQ71-267dp	14.196	15.138	33.931
Yava	RF79-427237	13.454	14.537	33.272
Yava	RF79-427290	13.451	14.538	33.276
Yava	RF79-427345	13.450	14.535	33.270
Yava	RF79-427B300.5	13.456	14.549	33.296
Yava	RF79-427B253	13.453	14.546	33.289
Musk	RF79-452	13.477	14.560	33.358
Musk	RF79-456	13.472	14.557	33.342
Izok Lake	TQ84-163	13.991	15.008	33.801
Izok Lake	TQ84-163dp	13.991	15.001	33.778
Izok Lake	TQ84-162	13.998	15.009	33.803
Izok Lake	TQ84-162dp	13.994	15.011	33.791
Gondor	TQ83-48	13.521	14.608	33.366
Gondor	TQ83-49	13.520	14.604	33.358

Abbreviations: dp= duplicate.

Note: linear regression of all data, except the two Victory Lake samples, gives a slope of 0.8047 ± 0.0019 with a mean squared weighted deviate of 27.78 and an intercept of 3.7218.

period line on a conventional $^{206}Pb/^{204}Pb$ versus $^{207}Pb/^{204}Pb$ plot instead of plotting as a tight group on or near the Stacey-Kramers (1975) growth curve at about 2670 Ma. These galenas would be expected to have "conformable" lead and plot on the growth curve at the age of formation of the deposits. Duplicate analyses of samples and analyses of multiple samples from individual deposits indicate that while the individual deposits have homogeneous lead isotopic ratios, large variations exist regionally between deposits within the area encompassed by the present study. The Izok and Gondor deposits (Fig. 5.1) have significantly different galena lead isotopic ratios despite their geographic proximity and probable similarity in age (Fig. 5.3 and Table 5.2). Since syngenetic volcanogenic deposits leach lead from their footwall rocks the deposits have lead isotopic ratios that reflect the isotopic composition of the footwall rocks at the time the deposit formed. This has been shown by analyses of sulphides and whole rocks both from actively forming volcanogenic massive sulphide deposits (Brevart *et al.* 1981; and Chen 1987) and from ancient deposits by Aggarwal and Nesbitt (1984) and many other workers. Thus the galena data indicate that the initial lead isotopic ratios of the predominantly volcanic rocks underlying the massive sulphides, and probably of the sedimentary rocks, were inhomogeneous at the time of deposition within the region of interest. This is probably the major cause of the scatter in the whole rock samples of unmineralized iron formation, pelitic iron formation and metapelites (Fig. 5.3).

In interpreting the steep slope of the galenas from the massive sulphide deposits, Franklin and Thorpe (1982) assume that they are two-stage deposits that formed at 2670 Ma. Their calculations indicate that the lead in these deposits was variably contaminated by a crustal lead component with an age of 4017± 60 Ma. Calculations based on the newer data from Thorpe (personal

communication 1987) in Table 5.2, excluding the two samples from Victory Lake which lie considerably off the main trend, give a slightly older age assuming the deposits formed at 2670 Ma. These very old ages are difficult to explain within the context of the known geology and geochronology of the Slave Province.

Mineralized whole rock samples

Three whole rock samples of mineralized iron formation and four samples of calc-silicate rock from the mineralized zones at Lupin were analysed (Table 5.1). These samples also scatter on the conventional $^{206}Pb/^{204}Pb$ versus $^{207}Pb/^{204}Pb$ plot (Fig. 5.3), but as a group tend to lie towards higher $^{207}Pb/^{204}Pb$ ratios than samples of unmineralized iron formation with similar $^{206}Pb/^{204}Pb$ ratios.

Unlike many types of ore deposits the mineralized iron formations are lead poor. X-ray fluorescence (XRF) analyses of fifteen samples of mineralized iron formation average 10 ppm Pb in comparison to seven samples of unmineralized iron formation, which average 6 ppm Pb (Chapter 4). Thus even in the very sulphide-rich, whole rock samples the lead isotopic ratio represents, like most whole rocks, the sum composition of the common and radiogenic components of the lead at the time of analysis.

One important observation is that when the mineralized iron formation samples from Lupin are compared to the unmineralized and pelitic iron formation samples from Lupin and other areas, the mineralized samples have relatively higher $^{207}Pb/^{204}Pb$ ratios. These samples fall to the left of a line subparallel to the 2670 Ma reference line while the unmineralized samples fall to the right (Fig. 5.3). This line effectively separates all but one sample of the group of non-gold-bearing samples from the group of gold-bearing samples.

Even samples from within the Lupin mine and samples along strike 220 m to the north on the same iron formation unit conform to this pattern. The one sample that does not fit the pattern is a sample of metapelite from Fingers Lake.

Mineral separates

The lead isotopic composition of arsenide and sulphide minerals from samples of mineralized iron formation from Lupin, Sik, Esker Lake and Fingers Lake, as well as epidote and scheelite from a calc-silicate rock from Lupin, are given in Table 5.1 and plotted in Fig. 5.3. Data points for these minerals plot in a similar position to the data points for whole rock samples of mineralized iron formation and calc-silicate rocks from Lupin, but extend to more and less radiogenic compositions (Fig. 5.3). Several important observations can be made about the distribution of the mineral data:

1) The lead isotopic ratios of the minerals plot to the left of the line separating the gold-bearing whole rock samples from the non-gold-bearing samples.

2) The similarity in the isotopic compositions of the minerals and the mineralized whole rocks and calc-silicate rocks suggests that the sulphide and arsenide minerals are not common lead minerals and instead they contain both common and radiogenic lead.

3) Analyses of duplicate samples from the same vial of mineral separate (Table 5.1) show that both the lead concentration and isotopic ratios vary implying that the lead is inhomogeneous on a very small scale. (Duplicate samples of unmineralized whole rocks in Table 5.1 have values within or near the analytical precision).

4) Uranium and lead concentrations of selected mineral separates (Table 5.1) show that the lead isotope ratios are not supported by sufficient uranium to

produce the observed radiogenic composition of the lead in the available time frame.

5) There is no significant difference in isotopic composition of the lead in minerals from Lupin and the other small-scale gold occurrences. All plot in a similar range along the same trend (Table 5. 1 and Fig. 5.3).

6) There is no obvious difference in the distribution of the data for the arsenides to that of the pyrrhotites even though the arsenides are more closely spatially associated with the quartz veining in iron formation than the pyrrhotites, which are more broadly distributed (Fig.5.2).

7) The epidote from Lupin contains the highest lead concentration and has the least radiogenic composition. It approaches the isotopic composition of the galena from the Izok deposit (Fig. 5.3).

The observation that the sulphides contain unsupported radiogenic lead may indicate that the sulphides have recently lost uranium or that the sulphides are a recent sink for radiogenic lead. Neither explanation is attractive, however, this phenomena is not uncommon and is not easily explained. In any case, it seems that the sulphides are best interpreted in the same manner as whole rock samples instead of as common lead minerals. This conclusion is borne out by the similarity in the isotopic ratios of lead in sulphides and the whole rocks from which they were separated, and by the similarity in the abundance of lead in the sulphides and whole rocks.

Interpretation of lead isotopes

By far the most important observation is that the lead isotope ratios of whole rock and mineral samples from the gold-bearing zones are distinctly different to those of whole rock samples from the non-gold-bearing zones. This fundamental difference indicates that the more radiogenic $^{207}Pb/^{204}Pb$ ratios of

samples from the gold-bearing zones are related to the mineralization process. In order to further examine these differences the data for all whole rock and mineral samples were corrected to their initial lead isotopic composition by assuming that all the samples have an age of 2670 Ma (Table 5.1). This was accomplished by finding the intersection of the 2670 Ma "isochrons" for each data point with the regression line defined by the galenas from the syngenetic, volcanogenic massive sulphide deposits. This galena line apparently reflects the composition of the lead in the region of each of these massive sulphide deposits at the time they formed which is also thought to be 2670 Ma. The resulting data are shown in Fig. 5.4. Although the calculations were done numerically, Fig. 5.4 can be thought of as a graphical projection of the data points in Fig 5.3 along a series of lines parallel to the 2670 Ma reference line, to the intersection with a line through the points for Izok and Gondor.

The excellent separation of the gold-bearing samples from the non-gold-bearing samples (Fig. 5.4 and Table 5.1) emphasizes the fundamental difference in the lead isotopic composition of these two groups of samples. As stated earlier, the Izok and Gondor galena data points indicate the lead isotopic composition of the immediately adjacent source rocks in the area of these deposits at the time they formed. Similarly, the recalculated non-gold-bearing sample data are thought to reflect the isotopic compositions of the unmineralized iron formation, pelitic iron formation and metapelite samples at the time they were deposited. Apparently, the non-gold-bearing rocks had a similar, initial lead isotopic composition to the host rocks at Gondor. The distinctly more radiogenic character of rocks and minerals from the gold-bearing zones is not compatible with a syngenetic model of gold mineralization in which heated evolved seawater leached lead from the underlying and adjacent rock units and deposited the lead, as well as gold and other components of the

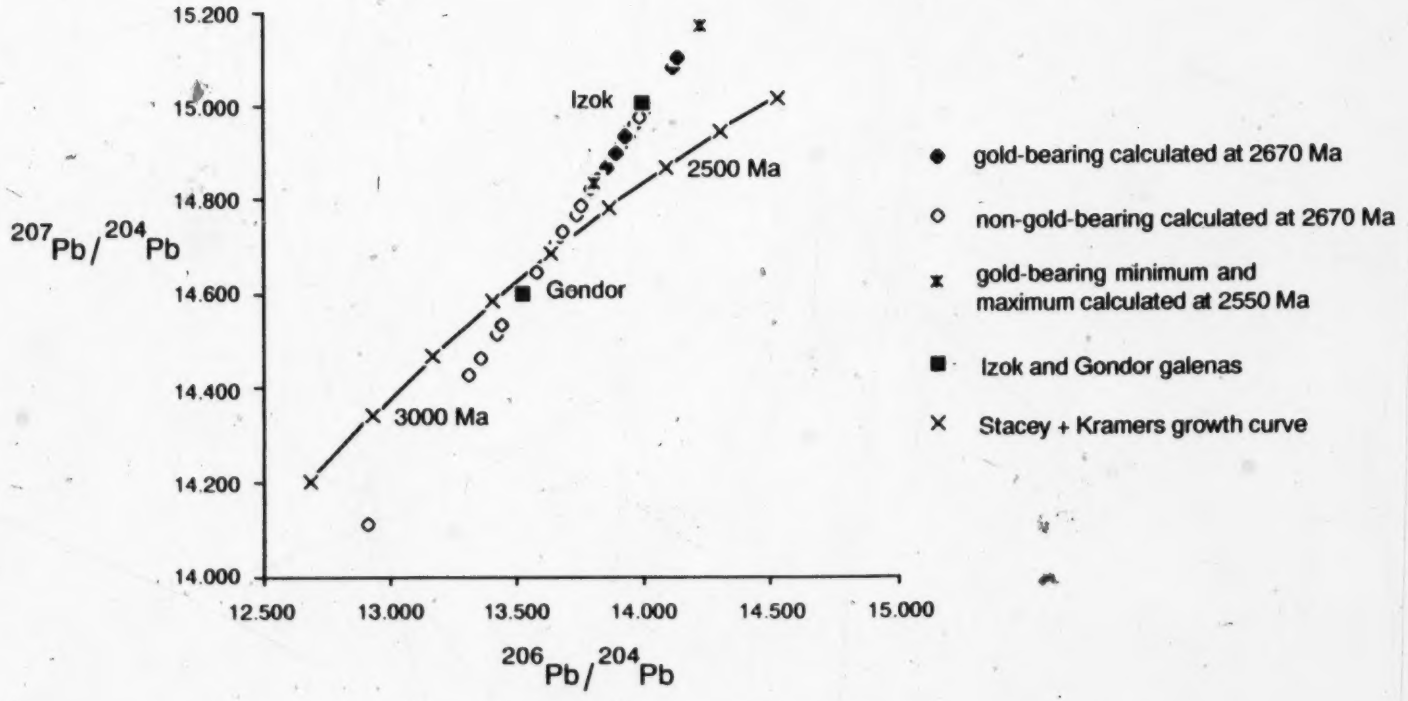

Fig. 5.4. A $^{206}Pb/^{204}Pb$ versus $^{207}Pb/^{204}Pb$ plot of calculated initial lead isotopic compositions of whole rocks and minerals at 2670 Ma. See text for method of calculation.

mineralization, upon venting on the seafloor. This type of model has been proposed by Fripp (1976) and Ridler (1970) for gold deposits in iron formation. This possibility can be excluded because if this were the case then the initial lead isotopic ratio of the sulphides and mineralized iron formation should be the same as the immediately adjacent rock units: in this case the non-gold-bearing unmineralized iron formation, pelitic iron formation, and metapelites.

Similarly, the differences in the lead isotopic ratios of mineralized iron formation and unmineralized iron formation along strike within a single stratigraphic unit cannot be explained by a syngenetic model in which the lead in the mineralized iron formation is largely from a chemical source and the lead in the unmineralized iron formation is largely from a detrital source. Theoretically these different sources could have had different lead isotopic ratios. However, analyses of Ti and Zr, which are very good indicators of the proportions of chemical and detrital sediment (Chapter 4), have virtually identical abundances in both mineralized and unmineralized iron formation. Data in Chapter 4 show that seven samples of unmineralized iron formation average 0.11 % TiO_2 and 30 ppm Zr while eight samples of arsenide-rich mineralized iron formation average 0.09 % TiO_2 and 27 ppm Zr. These data eliminate a syngenetic mixing model for the lead isotopic ratios in which the lead isotopic ratios vary due to the proportions of chemical and detrital sediment in the iron formation.

Instead, the data indicate that the more radiogenic lead isotopic ratios of the gold-bearing samples are the result of the addition of radiogenic lead to the unmineralized iron formation by an Archean epigenetic process. This is compatible with XRF whole rock data that show that the average mineralized iron formation contains 10 ppm Pb and the average unmineralized iron formation contains 6 ppm Pb (Chapter 4). Apparently the small amount of lead

that was added had an isotopic composition similar to, or more radiogenic than, the Izok deposit. Since the lead addition occurred after 2670 Ma the data for the gold-bearing group of samples should be recalculated by using an age younger than 2670 Ma. Geological evidence (Chapters 2 and 3) suggests that a more appropriate age for the lead and gold mineralization may be about 2550 Ma: an age that would be coincident with the peak metamorphism which is late in the deformational history. Data for both the gold-bearing and non-gold-bearing sample groups were recalculated using an age of 2550 Ma (Table 5.1). The most and least radiogenic points of the gold-bearing sample group recalculated to 2550 Ma are shown for comparison with all of the data calculated to 2670 Ma (Fig. 5.4). It can be seen from these two points and the data in Table 5.1 that the age to which the samples are recalculated is not the critical parameter in determining their position. The critical parameter is the addition of a more radiogenic lead during an epigenetic event. This addition of radiogenic lead is probably part of an epigenetic event that also deposited gold.

G. Strontium isotope data

Unmineralized whole rocks

Data for strontium and rubidium isotopes from unmineralized samples from the Lupin and Sik areas are given in Table 5.3 and are plotted in Fig. 5.5 on standard plots of $^{87}Rb/^{86}Sr$ atomic ratio versus $^{87}Sr/^{86}Sr$. Unmineralized iron formation samples have Sr concentrations of about 50 to 180 ppm and Rb concentrations of about 2 to 5 ppm, while samples of pelitic iron formation have Sr concentrations of 30 to 160 ppm and Rb concentrations of about 11 to 210 ppm. These values are similar to a larger set of XRF analyses (Chapter 4) that showed that seven samples of unmineralized iron formation average 83 ppm Sr and 5 ppm Rb, and eight samples of pelitic iron formation average 49 ppm Sr

Table 5.3 Strontium and rubidium data for rocks and minerals from Contwoyto Lake.

WHOLE ROCKS	rock type or mineral	^{86}Sr ppm	Sr ppm	^{87}Rb ppm	Rb ppm	$^{87}Sr/^{86}Sr$ measured	$^{87}Rb/^{86}Sr$ atomic ratio	$^{87}Sr/^{86}Sr$ corrected 2670 Ma	$^{87}Sr/^{86}Sr$ corrected 2550 Ma
Lupin									
4A031	calc-silicate	212.4	2152	0.1234	0.4433	0.70215 ± 3	0.0006	0.70213	0.70213
5A041	calc-silicate	57.13	578.8	0.1127	0.4049	0.70210 ± 3	0.0019	0.70202	0.70203
5A056	calc-silicate	145.2	1471	0.0760	0.2730	0.70218 ± 3	0.0005	0.70216	0.70216
5A060	calc-silicate	343.4	3479	0.0490	0.1760	0.70197 ± 2	0.0001	0.70196	0.70196
5A017	min. IF	39.76	402.9	0.2324	0.8349	0.70227 ± 4	0.0058	0.70205	0.70206
5A020	min. IF	21.13	214.1	0.3614	1.298	0.70255 ± 3	0.0169	0.70190	0.70193
5A062	min. IF	37.03	375.1	0.1546	0.5554	0.70217 ± 5	0.0041	0.70201	0.70202
5A105	pelitic IF	3.213	32.55	21.77	78.21	0.94753 ± 7	6.6974	0.68873	0.70057
5A114	pelitic IF	3.445	34.90	3.203	11.51	0.73041 ± 4	0.9191	0.69490	0.69652
5A122	unmin.IF	5.151	52.19	0.6105	2.193	0.70585 ± 2	0.1172	0.70132	0.70153
Sik									
4E025	unmin.IF	11.93	120.9	0.5447	1.957	0.70396 ± 3	0.0451	0.70222	0.70230
4E029	unmin. IF	17.58	178.1	1.454	5.223	0.70515 ± 7	0.0817	0.70199	0.70214
4E026	pelitic IF	15.81	160.1	57.71	207.3	0.86202 ±15	3.6089	0.72256	0.72895
MINERALS									
Lupin									
4A031	scheelite	102.7	1041	0.2288	0.8220	0.70202 ± 3	0.0022	0.70193	0.70194
4A031	epidote	612.3	6203	0.0675	0.2425	0.70206 ± 3	0.0001	0.70206	0.70206

Abbreviations: calc-silicate= calc-silicate rocks; IF= iron formation; min.= mineralized; unmin.= unmineralized

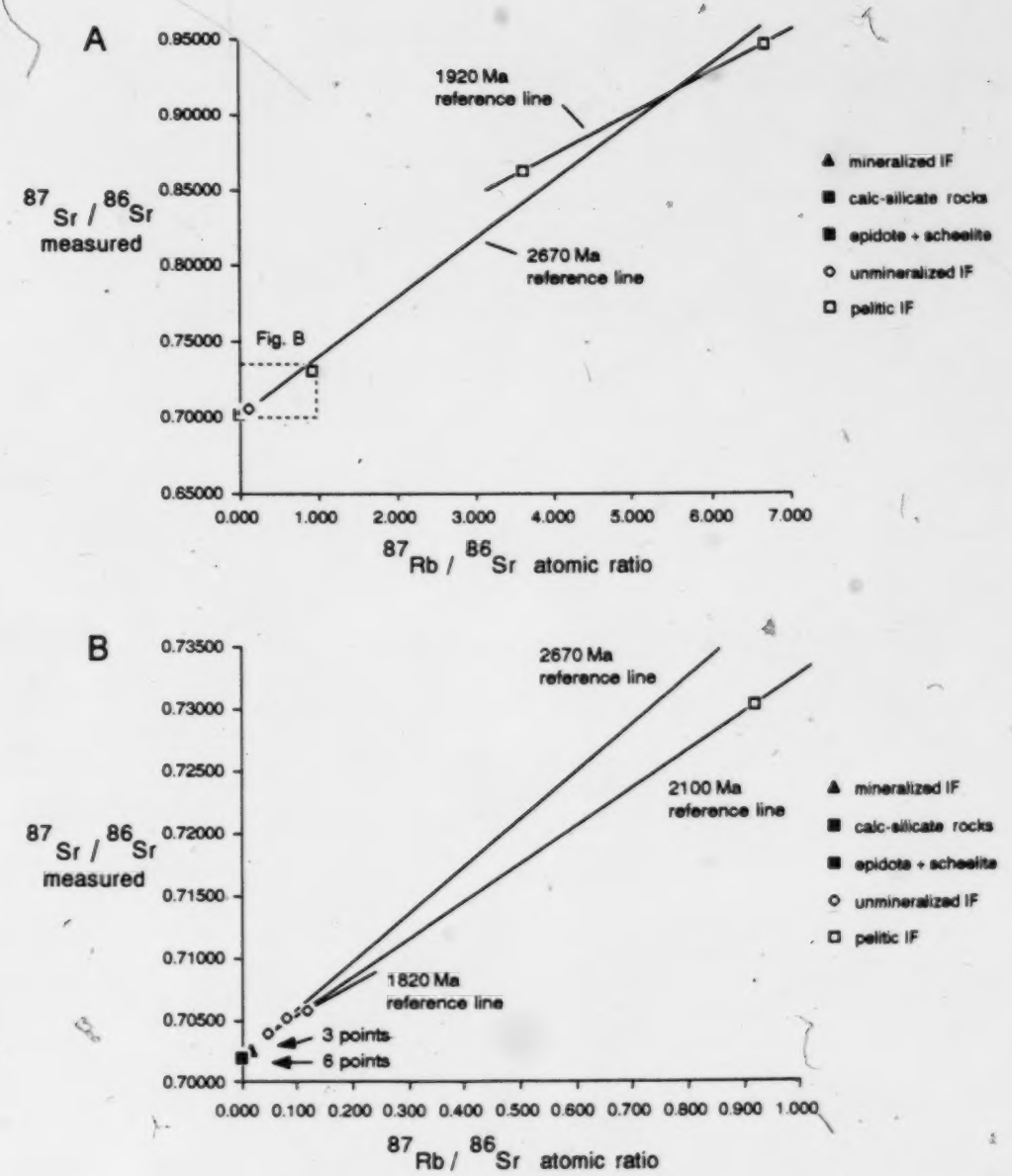

Fig. 5.5. Plots of $^{87}Rb/^{86}Sr$ atomic ratio versus $^{87}Sr/^{86}Sr$ (measured) for whole rocks and minerals. *A.* All data. *B.* Selected data plotted at an expanded scale.

and 56 ppm Rb. Typical unmineralized iron formation therefore has low Rb/Sr ratios and moderate Sr concentrations as would be expected for dominantly chemical sedimentary rocks. Pelitic iron formation tends to have higher Rb/Sr ratios, higher Rb concentrations and similar Sr concentrations compared to unmineralized iron formation.

The scatter present in the isochron plot (Fig. 5.5*A*) is typical of Rb-Sr isotopic data in the Slave Province in that the points are not isochronous (Stockwell 1982). A 2670 Ma reference line, plotted for comparison, roughly bisects the data. Two samples of pelitic iron formation, which are biotite-rich, have very high Rb/Sr ratios in comparison to the rest of the more typical unmineralized iron formation and pelitic iron formation samples (Fig. 5.5*A*). These two samples probably have had their Rb-Sr isotopic systems disturbed. Together they suggest a slope age of about 1920 Ma. In the expanded Rb-Sr plot (Fig. 5.5*B*) the less radiogenic unmineralized iron formation samples and a sample of pelitic iron formation suggest slope ages of about 1820 Ma and 2100 Ma. These ages are not purported to represent well defined events, but they probably reflect disruptions of the Archean isotopic systems due to thermal and tectonic events in the adjacent Proterozoic Bear Province. Without further work definitive conclusions cannot be made on the basis of the present data. However, Easton (1983) and Stockwell (1982) have concluded that such disturbances are common in the Slave Province and Wanless and Loveridge (1978) have found evidence of these disturbances in the present study area.

Mineralized whole rocks and minerals

Samples from Lupin of mineralized iron formation, calc-silicate rocks, and scheelite and epidote from a calc-silicate rock were analysed for strontium and rubidium (Table 5.3). These samples characteristically have extremely low

Rb/Sr ratios and high to very high concentrations of strontium. None of the samples contain more than 1 ppm Rb and Sr concentrations range from 214 to 6200 ppm. These data are similar to XRF data on seven samples of calc-silicate rocks from the Contwoyto Lake area that average 1307 ppm Sr and 3 ppm Rb, while fifteen samples of mineralized iron formation average 174 ppm Sr and 3 ppm Rb (Chapter 4). Data in Chapter 4 indicate that the high concentrations of Sr in the mineralized iron formation result from addition of Sr during an epigenetic mineralizing event that deposited Sr along with Au, S, As, Ca and other components in previously unmineralized iron formation.

Isotopic data (Table 5.3) for the nine whole rock and mineral samples from the mineralized zones at Lupin have very homogeneous $^{87}Sr/^{86}Sr$ ratios and extremely low Rb/Sr ratios and therefore plot virtually as a point on Fig. 5.5*B*. Measured $^{87}Sr/^{86}Sr$ ratios range from 0.70197 ± 2 to 0.70255 ± 3. The lack of significant variation precludes any attempt at dating the mineralized zones. However, the similarity of the measured $^{87}Sr/^{86}Sr$ ratios and the evidence that strontium was added to the iron formation during mineralization indicates that the strontium added must have been very homogeneous.

Interpretation

In order to further examine this model of strontium addition during Archean mineralization the measured strontium isotopic ratios must first be corrected for decay of ^{87}Rb to ^{87}Sr. In the mineralized samples the corrections will be nonexistent or very small but in the unmineralized samples the corrections are significant because of the higher Rb/Sr ratios. All of the $^{87}Sr/^{86}Sr$ data have been corrected to an age of 2670 Ma (the probable depositional age of the unmineralized samples) and to an age of 2550 Ma (the estimated age of mineralization). Results for both calculations are given in Table 5.3. Two of the

pelitic iron formation samples have age corrected initial ratios at 2670 Ma of less than BABI (0.69899), the interpreted initial $^{87}Sr/^{86}Sr$ ratio of the solar nebula (Faure 1977). Since ratios lower than BABI are not possible, the Rb-Sr systems of these samples could not have remained closed since the time of sedimentation, unless the estimated age of the sediments is grossly overestimated, a highly unlikely possibility. The remaining pelitic iron formation sample has a very radiogenic calculated initial ratio at 2670 Ma of 0.72256. These data indicate that the pelitic iron formation samples must have been open Rb-Sr systems. It is also probable that the unmineralized iron formation samples were open Rb-Sr systems as well.

A plot of $^{87}Sr/^{86}Sr$ ratios corrected to 2550 Ma versus strontium concentration shows the markedly different strontium isotopic ratios of two samples of pelitic iron formation (one very high, the other very low) at the inferred time of gold mineralization and strontium addition (Fig. 5.6*A*). The remaining data fall in a narrow range of $^{87}Sr/^{86}Sr$ and are plotted at an expanded scale in Fig. 5.6*B* . The expanded plot clearly shows that the nine samples of mineralized iron formation, calc-silicate rocks, epidote and scheelite have high concentrations of strontium, extremely low Rb/Sr ratios (Table 5.3), and very homogeneous $^{87}Sr/^{86}Sr$ ratios of 0.70193 to 0.70216 with an average of 0.70203 $\pm$0.00008 (1σ). Since strontium isotopes are not fractionated during deposition from fluids (Faure 1977), this value must reflect the mean $^{87}Sr/^{86}Sr$ of the strontium in the hydrothermal fluid that was added during mineralization at Lupin. The unusually high Sr concentrations and low Rb/Sr ratios of these samples have thus locked in the $^{87}Sr/^{86}Sr$ ratio of the fluid and preserved it unchanged to the present.

Samples of unmineralized iron formation have age-corrected $^{87}Sr/^{86}Sr$ ratios at 2550 Ma of about 0.7015 to 0.7023 and lower concentrations of

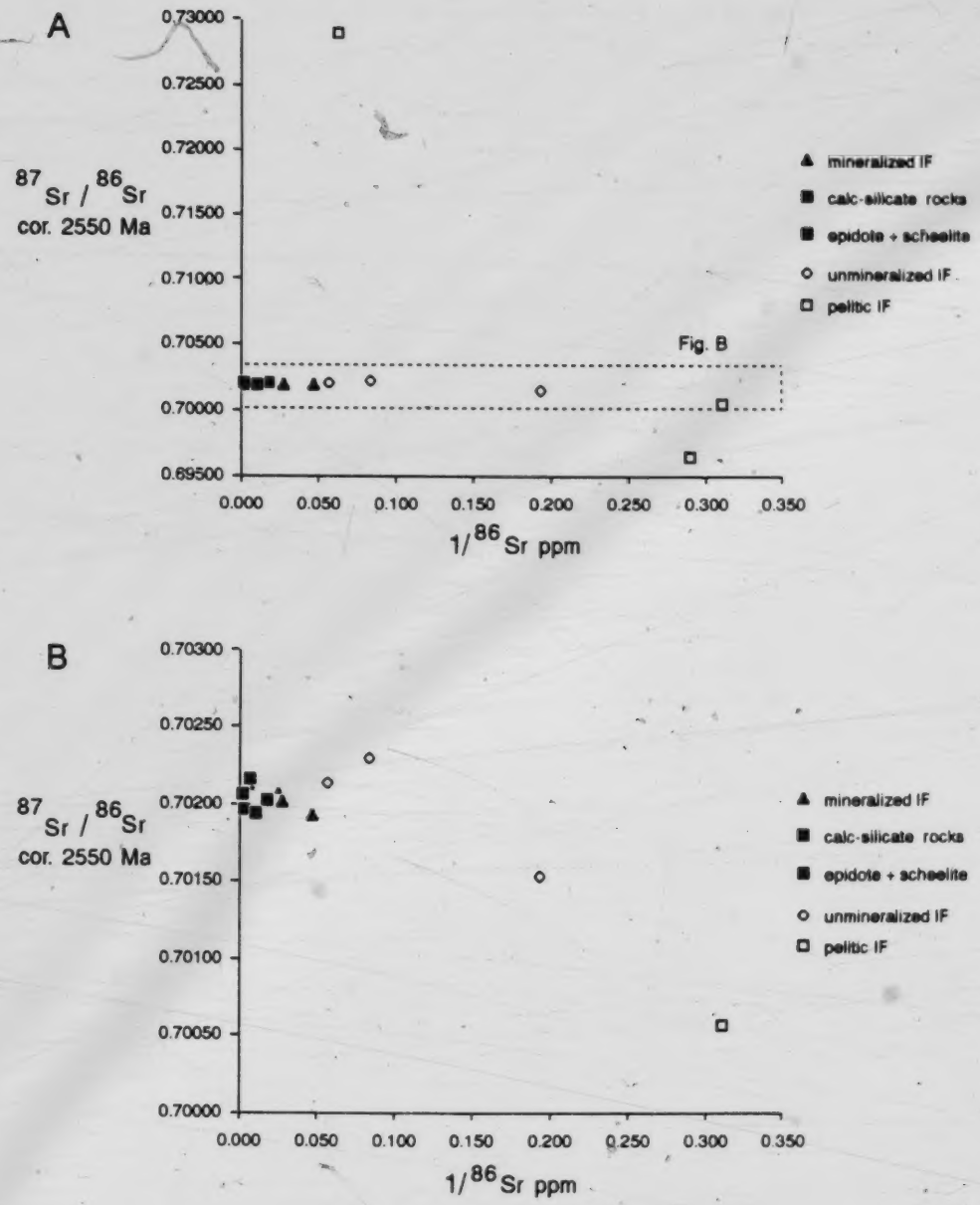

Fig. 5.6. Plots of $1/^{86}Sr$ ppm versus $^{87}Sr/^{86}Sr$ (corrected to 2550 Ma) for whole rocks and minerals. *A.* All data. *B.* Selected data plotted at an expanded scale.

strontium (Fig. 5.6*B*). These ratios are similar to, but more variable than, the $^{87}Sr/^{86}Sr$ ratios of the mineralized rocks. This suggests that the unmineralized iron formation samples may have been affected by the same strontium metasomatic event. However, caution must be used in this comparison because of the possibility that the unmineralized iron formation samples have had open Rb-Sr systems in Proterozoic times like the pelitic iron formation samples. If the unmineralized iron formation samples were also affected in the Proterozoic then the comparison of the $^{87}Sr/^{86}Sr$ ratios corrected to 2550 Ma is meaningless. Since the $^{87}Sr/^{86}Sr$ ratios of the unmineralized and pelitic iron formation samples were likely disturbed by Proterozoic events, the $^{87}Sr/^{86}Sr$ ratios of the mineralized zones will instead be compared to estimated bulk Earth $^{87}Sr/^{86}Sr$ ratios.

Bulk Earth estimates are probably a reasonable estimate of the initial $^{87}Sr/^{86}Sr$ ratios of the unmineralized rocks at the time of deposition because these same samples have lead isotopic ratios that fall on or near the growth curve of Stacey-Kramers (1975) in Fig. 5.3 and Fig. 5.4. Estimates of the bulk Earth $^{87}Sr/^{86}Sr$ ratio at 2670 Ma, based on the parameters of DePaulo and Wasserburg (1976) and Zindler *et al.* (1982), range from 0.7014 to 0.7018 because of differences in the assumptions of present day bulk Earth $^{87}Sr/^{86}Sr$ ratios of 0.7045 and 0.7052 in the respective models. When these estimates are compared to the average $^{87}Sr/^{86}Sr$ ratio of the mineralization (0.70203), it is clear that the $^{87}Sr/^{86}Sr$ ratio of the mineralized iron formation is significantly more radiogenic than the bulk Earth estimate. This observation suggests that the unmineralized samples of iron formation and pelitic iron formation could not have been the reservoir for the strontium if a syngenetic model was assumed for the mineralization at 2670 Ma. Rather, it suggests that the strontium, like the lead, came from a more radiogenic source.

H. Discussion

Possible source regions

From the present work it is difficult to place specific constraints on the lead and strontium isotopic source areas of the mineralization. This is because of uncertainty of the extent, age, and isotopic character of basement units like those at Point Lake, the general lack of modern geochronological data in the area, and in the case of strontium, the disruption of the Rb-Sr isotopic systems of the unmineralized rock units by late Archean or Proterozoic events. Nevertheless, some general constraints can be made. The lead isotopic analyses of unmineralized sedimentary rocks have μ values that on average approximate the Stacey-Kramers (1975) growth curve. Thus in Fig. 5.7*A* it can be seen that growth of lead of this average composition on the growth curve at 2670 Ma would parallel the growth curve and at 2550 Ma would still lie on the growth curve. Clearly, addition of this type of lead to the mineralized zones at 2550 Ma cannot account for the radiogenic composition of the lead in the mineralized samples. Instead the radiogenic lead must have sourced from an area of higher μ. This lead may have come directly from volcanic rocks with a μ equal to or higher than the volcanics in the Izok area. Alternatively, the lead may have come directly from the radiogenic source, presumably older granitic basement that produced the inferred higher μ values in the Izok volcanics. At present, there is no other direct or indirect evidence for either Izok type volcanics or granitic basement in the immediate vicinity of the Lupin mine (Fig. 5.1). This suggests that the circulation systems involved in the mineralization are of large scale.

Samples of calc-silicate rocks, mineralized iron formation, epidote and scheelite have homogeneous age-corrected $^{87}Sr/^{86}Sr$ ratios of 0.70203 ±

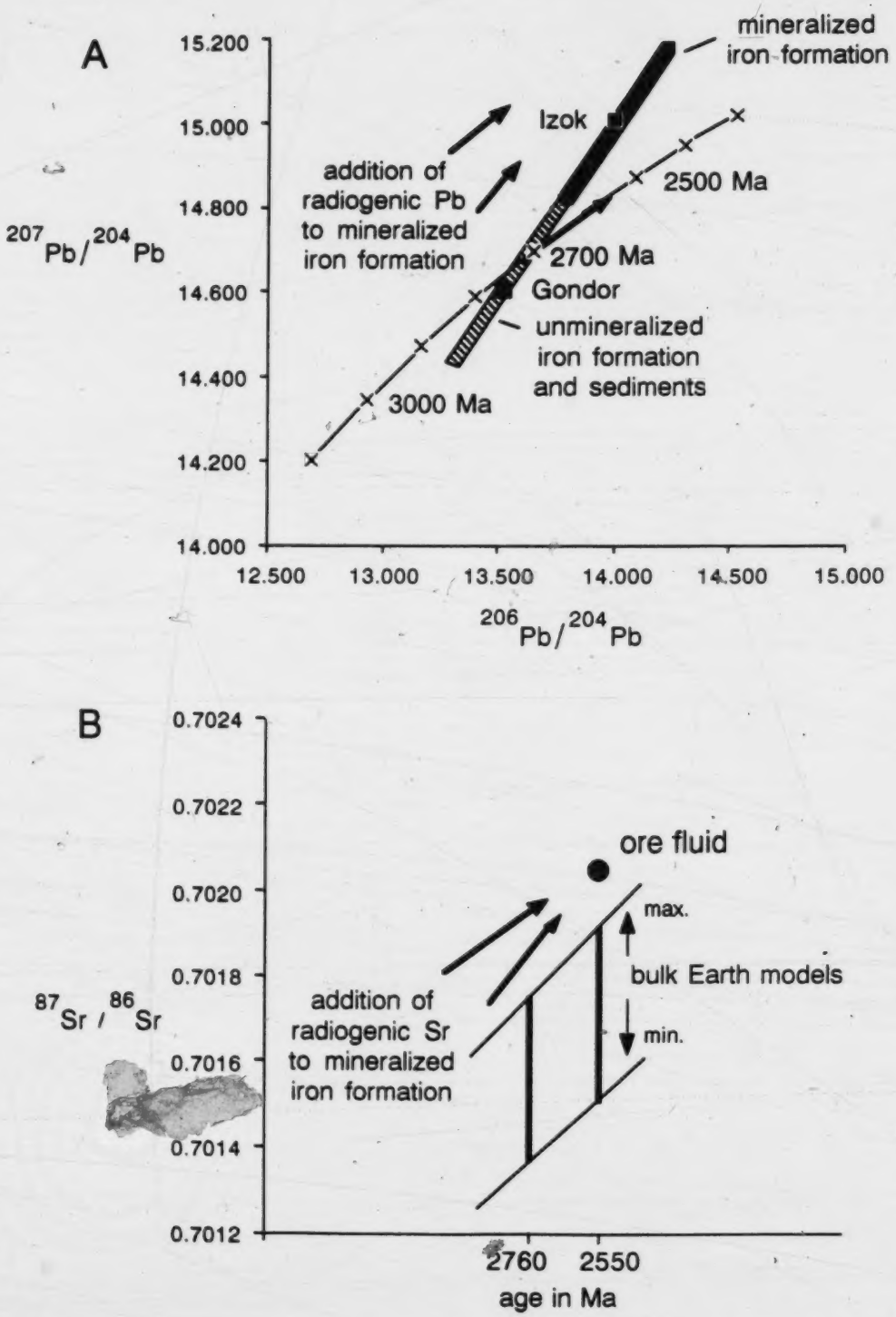

Fig. 5.7. Possible source regions of lead and strontium in mineralized iron formation. *A.* Lead isotopes. *B.* Strontium isotopes.

0.00008 (1σ) that represent the $^{87}Sr/^{86}Sr$ of the ore fluid. Unmineralized iron formation samples have similar but more variable calculated $^{87}Sr/^{86}Sr$ ratios at 2550 Ma. The variability in these ratios may be due to Proterozoic resetting or partial resetting of these samples. In addition, these samples may have been affected by the Archean event which caused gold mineralization because this event obviously mobilized strontium on a large scale. In fact, since the gold mineralization event is regional in scale with numerous gold occurrences spread over a large area, the gold mineralizing event may be at least partially responsible for the widespread Rb-Sr open system behavior noted by other workers (Stockwell 1982; Easton 1983). If the bulk Earth models are reasonable estimates of the initial $^{87}Sr/^{86}Sr$ ratios of the unmineralized iron formation and pelitic iron formation at the time of deposition and mineralization, then it is clear that the ore fluid must have been more radiogenic than the host iron formation. Thus the strontium data, like the lead data, are consistent with the strontium being derived either directly or indirectly from an older crustal source region with a higher Rb/Sr ratio. The very homogeneous composition of the strontium in the mineralized samples also indicates a large scale hydrothermal system.

Comparisons to other Archean gold deposits

A previous study of lead isotopes in iron formation by Rye *et al.* (1974) on the Homestake South Dakota area is difficult to compare to the present study because it comprises analyses for galenas from mineralization in the Homestake Mine and does not include whole rock lead data on unmineralized rocks or galena from undoubtedly syngenetic deposits. Data of Robertson (1973) and Kramers and Foster (1984) on the gold deposits of Zimbabwe are also difficult to compare to the present study for the same reason, although their

data clearly show that the lead in many of the deposits must have been derived in part from a long lived crustal source.

The recent lead isotopic work of Browning *et al.* (1987) on Australian sulphide deposits is more easily compared to the present study. They have shown that in the Norseman-Wiluna belt of the Yilgarn block of Australia galenas in epigenetic gold deposits, hosted by volcanic rocks, are more radiogenic than galenas from syngenetic base metal deposits. This was interpreted as evidence of contamination of the lead by old crustal (basement) material during gold mineralization. The gold mineralization is interpreted to have formed at about 2.7 Ga during regional metamorphism shortly after greenstone belt formation. Additional work by these authors on the Murchison and Southern Cross Provinces of the Yilgarn block has shown that galenas, some of which are from gold mineralization in iron formation, are more radiogenic than galenas from syngenetic base metal deposits from the same areas. The Murchison and Southern Cross data are interpreted as remobilization of the 3.0 Ga greenstone belt lead during regional metamorphism at 2.87 to 2.75 Ga. Browning *et al.*'s (1987) conclusion that the lead isotopic data on the gold deposits of the Yilgarn block are consistent with an epigenetic model is supported by the present study.

I. Conclusions

Several conclusions can be made from the lead and strontium isotopic data:

1) The lead-poor sulphide and arsenide minerals are not common lead minerals. They contain radiogenic lead that is not supported by the present day uranium concentrations.

2) Samples of sulphides and arsenides from Lupin and small-scale gold occurrences have similar lead isotopic ratios which overlap with the lead isotopic ratios of whole rock samples of mineralized iron formation from Lupin.

3) Age corrected lead isotopic ratios of the unmineralized samples show scatter due to the inhomogeneous isotopic nature of the lead at the time of sedimentation. Age corrected lead isotopic ratios of minerals and whole rocks from the gold-bearing zones are more radiogenic than the unmineralized samples due to the addition of lead from a more radiogenic, older crustal source.

4) Intense strontium metasomatism associated with gold mineralization at Lupin added strontium with an $^{87}Sr/^{86}Sr$ ratio of 0.70203 ± 0.00008 (1 σ).

5) Bulk Earth models of strontium isotope ratios are interpreted to approximate the initial ratios of the unmineralized iron formation at the time of sedimentation and also at mineralization. The higher $^{87}Sr/^{86}Sr$ ratios of the mineralization reflect the addition of strontium from a source with higher Rb/Sr ratios, possibly older crustal rocks.

6) Together the lead and strontium isotopic data support an epigenetic model of gold mineralization and are not compatible with syngenetic or syngenetic/remobilization models in which the mineralization was derived from unmineralized iron formation.

7) This study has also shown that analyses of unmineralized samples may provide additional constraints on genetic models for ore deposits that would be missed by studying only mineralized samples.

J. References

Aggarwal, P. K., and Nesbitt, B. E. 1984. Geology and geochemistry of the Chu Chua massive sulfide deposit, British Columbia. Economic Geology, **79**: 815-825.

Baadsgaard, H., Chaplin, C., and Griffin, W. L. 1986. Geochronology of the Gloserheia Pegmatite, Froland, Southern Norway. Norsk. Geologisk. Tidsskift, **64**: 111-119.

Bau, A. F. S. 1979a. Geological map of 86H/9 District of Mackenzie: Department of Indian Affairs and Northern Development, Geology Division, Preliminary Geological Map EGS-1979-2A.

Bau, A. F. S. 1979b. Geological map of 86H/10 District of Mackenzie: Department of Indian Affairs and Northern Development, Geology Division, Preliminary Geological Map EGS-1979-2B.

Bau, A. F. S. 1979c. Geological map of 86H/11 District of Mackenzie: Department of Indian Affairs and Northern Development, Geology Division, Preliminary Geological Map EGS-1979-2C.

Bau, A. F. S. 1979d. Geological map of 86H/14 District of Mackenzie: Department of Indian Affairs and Northern Development, Geology Division, Preliminary Geological Map EGS-1979-4A.

Bau, A. F. S. 1979e. Geological map of 86H/15 District of Mackenzie: Department of Indian Affairs and Northern Development, Geology Division, Preliminary Geological Map EGS-1979-4B.

Bau, A. F. S. 1979f. Geological map of 86H/16 District of Mackenzie: Department of Indian Affairs and Northern Development, Geology Division, Preliminary Geological Map EGS-1979-4C.

Bostock, H. H. 1980. Geology of the Itchen Lake area, District of Mackenzie. Geological Survey of Canada, Memoir 391.

Bowring, S. A., and Padgham, W. A. 1987. New U/Pb zircon dates from the Yellowknife Volcanic Belt: Stratigraphic gold deposit model implications. Geological Association of Canada, Summer Field Meeting, Yellowknife, N.W.T., Program with Abstracts.

Brevart, O., Dupre, B., and Allègre, C. J. 1981. Metallogenesis at spreading centers: Lead isotope systematics for sulfides, manganese-rich crusts, basalts, and sediments from the Cyamex and Alvin areas (East Pacific Rise). Economic Geology, **76**: 1205-1210.

Browning, P., Groves, D. I., Blockley, J. G., and Rosman, K. J. R. 1987. Lead isotope constraints on the age and source of gold mineralization in the Archean Yilgarn Block, Western Australia. Economic Geology, **82**: 971-986.

Cavell, P. A., and Baadsgaard, H. 1986. Geochronology of the Big Spruce Lake alkaline intrusion. Canadian Journal of Earth Sciences, **23**: 1-10.

Chen, J. H. 1987. U, Th, and Pb isotopes in hot springs on the Juan de Fuca Ridge. Journal of Geophysical Research, **92**: 11,411-11,415.

DePaulo, D. J., and Wasserburg, G. J. 1976. Inferences about magma sources and mantle structure from variations of $^{143}Nd/^{144}Nd$. Geophysical Research Letters, **3**: 743-746.

Easton, R. M. 1985. The nature and significance of pre-Yellowknife Supergroup rocks in the Point Lake area, Slave Structural Province, Canada. *In* Evolution of Archean Supracrustal Sequences. *Edited by* L. D. Ayres, P. C. Thurston, K. D. Card, and W. Weber, Geological Association of Canada, Special Paper 28, pp. 153-167.

Easton, R. M. 1984. Compilation of geochronologic data for the Yellowknife greenstone belt (85 J/8, 85 J/9) and vicinity, District of Mackenzie, N.W.T. Contributions to geology of the Northwest Territories, **1**: 1-20.

Easton, R. M. 1983. Regional resetting of Rb-Sr and K-Ar isotopic systems at ca. 1770 Ma in the Bear and Western Slave Provinces, N.W.T. Geological Association of Canada, Program with Abstracts, **8**: A19.

Easton, R. M., Boodle, R. L., Zalusky, L., Eiche, G., and McKinnon, D. 1981. Geology of 86H/3, H/4, H/5 and H/6, District of Mackenzie: Department of Indian Affairs and Northern Development, Geology Division, Preliminary Geological Map EGS-1981-5.

Faure, G. 1977. Principles of isotope geology. John Wiley & Sons, New York, New York.

Franklin, J. M., and Thorpe, R. I. 1982. Comparative metallogeny of the Superior, Slave and Churchill Provinces. *In* Precambrian sulphide deposits. *Edited by* R. W. Hutchinson, C. D. Spence, and J. M. Franklin. Geological Association of Canada, Special Paper 25, pp. 3-90.

Fripp, R. E. P. 1976. Stratabound gold deposits in Archean banded iron formation, Rhodesia. Economic Geology, **71**: 58-75.

Frith, R. A., and Loveridge, W. D. 1982. Ages of Yellowknife Supergroup volcanic rocks, granitoid intrusive rocks and regional metamorphism in the northern Slave Structural Province. *In* Current research, part A. Geological Survey of Canada, paper 82-1A, pp. 225-237.

Gardiner, J. J. 1986. Structural geology of the Lupin gold mine, Northwest Territories. M.Sc. thesis, Acadia University, Wolfville, Nova Scotia.

Gibbins, W. 1981. Gold and Precambrian iron formation in the Northwest Territories. *In* Proceedings of the Gold Workshop, Yellowknife, 1979. *Edited by* R. D. Morton, Yellowknife Gold Workshop Committee, pp. 258-287.

Green, D. C. 1968. Precambrian geology and geochronology of the Yellowknife area, N. W. T. Ph. D. thesis, University of Alberta, Edmonton, Alberta.

Groves, D. I., Phillips, G. N., Falconer, L. J., Houstoun, S. M., Ho, S. E., Browning, P., Dahl, N., and McNaughton, N. J. 1987. Evidence for an epigenetic origin for BIF-hosted gold deposits in the greenstone belts of the Yilgarn Block, Western Australia. *In* recent advances in understanding Precambrian gold depsoits. *Edited by* S. E. Ho and D. I. Groves, Geology Department & University Extension, University of Western Australia, Publication II, pp. 167-179.

Henderson, J. B. 1970. Stratigraphy of the Yellowknife Supergroup, Yellowknife Bay; Prosperous Lake area, District of Mackenzie. Geological Survey of Canada, paper 70-26.

Henderson, J. B., and Easton, R. M. 1977a. Archean supracrustal-basement rock relationships in the Keskarrah Bay map-area, Slave Structural Province, District of Mackenzie. Geological Survey of Canada, Open File 447.

Henderson, J. B., and Easton, R. M. 1977b. Archean supracrustal-basement rock relationships in the Keskarrah Bay map-area, Slave Structural Province, District of Mackenzie. *In* Current research, part A. Geological Survey of Canada, paper 77-1A, pp. 217-221.

Henderson, J. B., Loveridge, W. D., and Sullivan, R. W. 1982. A U-Pb study of zircon from granitic basement beneath Yellowknife Supergroup, Point Lake, District of Mackenzie. *In* Current research, part C. Geological Survey of Canada, paper 82-1C, pp. 173-178.

Jackson, V. A. 1982. Preliminary geological map of the Keskarrah Bay area, Slave Structural Province, District of Mackenzie, N.W.T., (86 H/2w, 6e and 7w). Department of Indian Affairs and Northern Development, Geology Division, preliminary geological map, EGS 1982-4.

Kerswill, J. A. 1986. Gold deposits hosted by iron formation in the Contwoyto Lake area, Northwest Territories. *In* Gold'86 Poster Paper Abstracts. *Edited by* A. M. Chater, Geological Association of Canada, Mineral Deposits Division, pp. 82-85.

Kerswill, J. A. 1985a. Gold, Sulphur, and Arsenic in metamorphosed iron formation of the Contwoyto Lake area, Northwest Territories, Canada.

Geological Society of America, Abstracts with Program, Annual Meeting, Orlando, Florida, pp. 627.

Kerswill, J. A. 1985b. Gold metallogeny of Archean iron formation in the Contwoyto Lake area, N.W.T. Geological Association of Canada, Program with Abstracts, **10**: A31.

Kerswill, J. A. 1984. The Lupin gold deposit, Contwoyto Lake area, N.W.T; Styles of gold distribution and possible genetic models. Geological Association of Canada, Program with Abstracts, **9**: 78.

King, J. E. 1982. Low pressure regional metamorphism and progressive deformation in the eastern Point Lake area, Slave Province, N.W.T. M.Sc. thesis, Queen's University, Kingston, Ontario.

King, J. E., Boodle, R. L., and St-Onge, M. R. 1980. Geological map of 86 H/1, H/8, H/2 E1/2 and H/7 E1/2, District of Mackenzie: Department of Indian Affairs and Northern Development, Geology Division, Preliminary Geological Map, EGS-1980-10.

King, J. E., Davis, W. J., Relf, C., and Avery, R. W. 1988. Deformation and plutonism in the western Contwoyto Lake map area, central Slave Province, District of Mackenzie, N.W.T. *In* Current research part C. Geological Survey of Canada, paper 88-1C, pp. 161-176.

Kramers, J. D., and Foster, R. P. 1984. A reappraisal of lead isotope investigations of gold deposits in Zimbabwe. *In* Gold'82: The geology, geochemistry and genesis of gold deposits. *Edited by* R. P. Foster, Geological Survey of Zimbabwe, special publication no. 1., pp.569-582.

Krogh, T. E., and Gibbins, W. 1978. U-Pb isotopic ages of basement and supracrustal rocks in the Point Lake area of the Slave Structural Province, Canada. Joint meeting of the Geological Association of Canada, Mineralogical Association of Canada and Geological Association of America, program with abstracts, pp. 438.

Lambert, M. B., and Henderson, J. B. 1980. A uranium-lead age of zircons from volcanics and sediments of the Back River volcanic complex, eastern Slave Province, District of Mackenzie. *In* Current research, part C. Geological Survey of Canada, paper 80-1C, pp. 239-242.

Lhotka, P. G., and Nesbitt, B. E. 1987a. An epigenetic origin for gold in iron formation in and around the Lupin mine, N.W.T. Geological Association of Canada, Annual General Meeting, Saskatoon, Saskatchewan, Program with Abstracts, **12**: p.67.

Lhotka, P. G., and Nesbitt, B. E. 1987b. Epigenetic gold hosted by iron formation at the Lupin mine, Contwoyto Lake, N.W.T. Geological Association of Canada, Summer Field Meeting, Yellowknife, N.W.T., Program with Abstracts.

Macdonald, A. J. 1983. The iron formation-gold association evidence from the Geraldton area. *In* The geology of gold in Ontario. *Edited by* A. C. Colvine, Ontario Geological Survey, Miscellaneous Paper 110, pp. 75-83.

Padgham, W. A. 1984. Gold deposits of N. W. T. ; Classes, styles, genesis, exploration methods and success probabilities. Contributions to the geology of the Northwest Territories, **1**: 121-129.

Phillips, G. N., Groves, D. I., and Martyn, J. E. 1984. An epigenetic origin for Archean banded-iron-formation-hosted gold deposits. Economic Geology, **79**: 162-171.

Ridler, R. H. 1970. Relationships of mineralization to volcanic stratigraphy in the Kirkland-Larder Lakes area, Ontario. Geological Association of Canada Proceedings, **21**: 33-42.

Robertson, D. K. 1973. A model discussing the early history of the Earth based on a study of lead isotope ratios from veins in some Archean cratons of Africa. Geochemica et Cosmochemica Acta, **37**: 2099-2124.

Rye, D. M., and Rye, R. O. 1974. Homestake Gold Mine, South Dakota: I. Stable isotope studies. Economic Geology, **69**: 293-317.

Rye, D. M., Doe, B. R., and Deleveaux, M. H. 1974. Homestake Gold Mine, South Dakota: II. Lead isotopes, mineralization ages, and source of lead in ores of the Northern Black Hills. Economic Geology, **69**: 814-822.

Sawkins, F. J., and Rye, D. M. 1974. Relationship of Homestake type gold deposits to iron-rich Precambrian sedimentary rock. Institute of Mining and Metallurgy, Transactions, Section B, **84**: pp. B37-B38.

Schärer, U., and Allègre, C. J. 1982. Investigation of the Archaean crust by single grain dating of detrital zircon: greywackes of the Slave Province, Canada. Canadian Journal of Earth Sciences, **19**: 1910-1918.

Stacey, J. S., and Kramers, J. D. 1975. Approximation of terrestrial lead isotope evolution by a two-stage model. Earth and Planetary Science Letters, **26**: 207-221.

Steiger, R. H., and Jäger, E. 1977. Subcommission on Geochronology: convention on the use of decay constants in geo- and cosmochronology. Earth and Planetary Science Letters, **36**: 359-362.

Stockwell, C. H. 1982. Proposals for time classification and correlation of Precambrian rocks and events in Canada and adjacent areas of the Canadian Shield. Part A . Geological Survey of Canada, paper 80-19.

Stockwell, C. H. 1933. Great Slave Lake-Coppermine River area, Northwest Territories. Geological Survey of Canada, Summary Report 1932, Part C, pp.37-63.

Thorpe, R. I. 1982. Lead isotope evidence regarding Archean and Proterozoic metallogeny in Canada. Revista Brazileira de Geosciencias, **12**: 510-521.

Tremblay, L. P. 1976. Geology of northern Contwoyto Lake area, District of Mackenzie. Geological Survey of Canada, Memoir 381.

Wanless, R. K., and Loveridge, W. D. 1978. Rubidium-strontium isotopic age studies, Report 2 (Canadian Shield). Geological Survey of Canada paper 77-14.

Zindler, A., Jagoutz, E., and Goldstein, S. 1982. Nd, Sr, Pb, isotopic systematics in a three component mantle: a new perspective. Nature, **298**: 519-523.

6. SUMMARY

The central objective of this thesis was to determine the process or processes that led to gold mineralization in iron formation, and the timing of that event, in the Contwoyto Lake-Point Lake region.

Fieldwork and petrographic studies on small-scale gold occurrences and the Lupin mine suggested that the gold occurrences in iron formation are epigenetic deposits. Subsequent geochemical studies on the iron formations including the chemistry of silicate minerals, whole rock major, minor and trace element geochemistry, as well as isotopic studies of lead and strontium, are consistent with an epigenetic model for gold mineralization. The geochemical data are not consistent with syngenetic or syngenetic-remobilization models. The major conclusions of the previous four chapters are summarized here.

A. Fieldwork and petrography

Fieldwork and petrographic studies showed that at small-scale gold occurrences gold is spatially associated with a late set of quartz veins that cut iron formation. Where these veins traverse iron formation, the iron formation wallrock is mineralized with sulphides and gold. Where the veins traverse pelitic iron formation, mudstone and greywacke, there is no mineralization in the wallrock. Adjacent to the veins the mineralized iron formation is hornblende-rich. Arsenides are abundant near the quartz veins in mineralized iron formation but rapidly decrease in abundance further from the veins. Iron sulphides (either pyrrhotite or pyrite) are present as more extensive haloes enveloping the veins. Further from the veins the mineralized iron formation passes laterally into unmineralized iron formation, which has low concentrations of sulphides and

gold. The unmineralized iron formation is grunerite-rich. Textures in the transition zone between mineralized iron formation and unmineralized iron formation indicate that hornblende replaces grunerite in the mineralized zones. Textures also indicate that pyrrhotite and pyrite replace amphiboles and magnetite in mineralized iron formation. Calc-silicate rocks, which represent alteration of iron formation, are sometimes present adjacent to quartz veins at small-scale occurrences.

The close association between gold mineralization and quartz veining at small-scale gold occurrences suggests that the gold and sulphides were introduced by hydrothermal fluids which formed the quartz veins. This epigenetic model of gold mineralization can be applied to Lupin because the spatial and mineralogical patterns used to develop the model are present at Lupin as well as at the small-scale occurrences. The major differences between Lupin and the small-scale occurrences are the greater size and continuity of the mineralized zones, and the greater abundance of calc-silicate alteration zones at Lupin.

Work by Gardiner (1986) and King *et al.* (1988) indicates that the set of quartz veins associated with gold mineralization were emplaced during regional deformation in the late Archean. This deformation was coincident or nearly coincident with near peak metamorphic conditions.

B. Mineral chemistry

Analyses were done on silicate minerals in unmineralized and mineralized iron formation and pelitic iron formation from Lupin and small-scale gold occurrences. The resulting data show that at both types of gold occurrence the X_{Fe} values of amphiboles in mineralized iron formation are lower than the

X_{Fe} values of amphiboles in unmineralized iron formation. Amphiboles in pelitic iron formation have the lowest X_{Fe} values. Data from the Lupin mine and the Esker Lake occurrence show that the decrease in X_{Fe} values of amphiboles in mineralized iron formation occurs near quartz veins as the abundance of gold and sulphides increases.

These data indicate that the addition of sulphur and arsenic to the iron formation adjacent to veins caused precipitation of sulphides and arsenides, which in turn lowered the X_{Fe} values of amphiboles. Deposition of sulphur caused deposition of gold because gold was transported in solution as a gold-sulphide complex. This reaction explains the close association between gold and sulphide mineralization. The lower limit of amphibole X_{Fe} values in mineralized iron formation (about 0.81) probably represents the equilibrium value between the hydrothermal fluid and mineralized iron formation.

These data are very similar to an earlier study on the Homestake deposit by Chinn (1969). He also interpreted that the lower X_{Fe} values in mineralized iron formation were due to sulphidation of iron formation.

Pelitic iron formation is not sulphidized adjacent to the late quartz veins. The lack of sulphidation is due to the lower bulk X_{Fe} values of pelitic iron formation, which is reflected in the lower X_{Fe} values of amphiboles in this rock type. These data indicate that the X_{Fe} values of amphiboles in pelitic iron formation are below the X_{Fe} values of amphiboles in equilibrium with the hydrothermal fluid. The lower X_{Fe} values of these amphiboles does not permit deposition of sulphides, and therefore gold, in pelitic iron formation.

The silicate minerals present in mineralized iron formation and calc-silicate rocks are Ca- and Al-rich. This suggests that Ca and Al were added to iron formation during mineralization along with S, As and Au.

C. Whole rock geochemistry

Analyses of major, minor and trace element abundances in iron formation and associated rock types were completed on samples from Lupin and small-scale gold occurrences. These data confirm that pelitic iron formation represents a mixture of detrital and chemical sedimentary components. Binary plots of the abundances of the commonly immobile elements, Al, Ti, Zr, Y and Sc, indicate that only Ti and Zr are truly immobile during the alteration of unmineralized iron formation to mineralized iron formation. The abundances of Ti and Zr suggest that calc-silicate rocks formed by alteration of iron formation and not by alteration of pelitic iron formation. Increasing Al/Ti ratios of iron formation from unmineralized iron formation to mineralized iron formation and finally calc-silicate rocks show that Al has been added to the mineralized iron formation.

Patterns of elemental gains and losses were calculated independently for samples of the different types of mineralized iron formation at Lupin and the small-scale occurrences. The patterns for the samples from Lupin are very similar to the patterns for the samples from small-scale occurrences. The calculations indicate that both the number of elements showing large gains or losses, as well as the degree of enrichment or depletion of individual elements, increases from weakly mineralized iron formation to pyrrhotite or pyrite mineralized iron formation to arsenide mineralized iron formation to calc-silicate rocks. These data, and the increase in the mobility of the commonly immobile elements Al, Sc and Y towards the veins, suggest that the zonation in chemistry and mineralogy enveloping the veins is due to increasing water/rock ratios near the veins. Elements added from an external source to the iron formation system during alteration include Al, Ca, P, Au, As, Bi, Ce, Cr, Pb, S, Sr, W and Y.

Addition of Al and Ca to iron formation is consistent with the observed mineralogical change in the predominant amphibole, from grunerite in unmineralized iron formation, to hornblende in mineralized iron formation. It is also consistent with the development of the calc-silicate rocks by alteration of unmineralized iron formation.

The very high gold/base metal ratios of the Contwoyto Lake gold mineralization and the suite of elements enriched during mineralization, are similar to other epigenetic Archean gold deposits (Kerrich and Hodder 1982). The gold/base metal ratios are distinctly different to gold/base metal ratios of syngenetic, volcanogenic massive sulphide deposits (Kerrich and Hodder 1982). This suggests that the Contwoyto Lake gold mineralization formed from hydrothermal systems similar to other epigenetic Archean gold deposits and not from hydrothermal systems like those which formed syngenetic, massive sulphide deposits.

D. Lead and strontium isotope geochemistry

Analyses of lead and strontium isotopic ratios were done on whole rocks and mineral separates of unmineralized and mineralized iron formation, pelitic iron formation, calc-silicate rocks and metapelites from the Lupin mine and small-scale gold occurrences.

The lead isotope data show that rocks and minerals from the gold-bearing zones are characterized by radiogenic lead with a higher $^{207}Pb/^{204}Pb$ ratio than unmineralized iron formation and metapelites. When all of the lead isotopic ratios are age corrected to 2670 Ma (the estimated age of the unmineralized host rocks), the more radiogenic nature of the lead in samples associated with the gold-bearing zones is obvious. The pattern of more

radiogenic lead in the gold-bearing zones is not compatible with a syngenetic or syngenetic-remobilization model for the mineralization. Instead, the radiogenic composition of the lead indicates that lead in the mineralized iron formation was added during the gold mineralization event from an external, older crustal source.

The increase in the abundance of strontium in mineralized iron formation shows that strontium was added to the iron formation during mineralization. The homogeneous $^{87}Sr/^{86}Sr$ ratio of the strontium in the mineralized zones and the calc-silicate rocks indicates that the strontium added was isotopically homogeneous. Age corrected $^{87}Sr/^{86}Sr$ ratios at the time of mineralization averaged 0.70203 ± 0.00008 (1σ).

Both the lead and strontium isotopes indicate that these elements were added to the mineralized iron formation from an older crustal source. This implies that gold itself was also added to the iron formation from an external source.

The lead isotope data are similar to a recent study by Browning *et al.* (1987) on Australian sulphide deposits, which shows that galenas in epigenetic gold deposits hosted by volcanic rocks, are more radiogenic than galenas from syngenetic base metal deposits. They interpret this as evidence of contamination of the lead by old crustal material (basement) during gold mineralization.

E. Major conclusions

This study has shown that the gold mineralization in iron formation in the Contwoyto Lake region is epigenetic. An epigenetic model of gold mineralization by selective replacement and sulphidation of iron formation is

consistent with the available field, petrographic and geochemical data. Lead isotope data are incompatible with syngenetic or syngenetic-remobilization models for the gold mineralization.

This study has also shown that the close association between gold mineralization and iron formation is a predictable consequence of the epigenetic sulphidation model and is not proof of syngenetic gold deposition. Similarly, the banding of the sulphides in mineralized iron formation is not proof of syngenetic sulphide deposition. This is because textural evidence indicates that sulphides replace preexisting iron-rich minerals which defined the banding in iron formation. Geochemical data indicate that the high bulk X_{Fe} values of the unmineralized iron formation provided an excellent chemical trap for deposition of the sulphides and gold from the hydrothermal fluid. Sulphides and gold were not deposited in rock types with lower bulk X_{Fe} values.

F. References

Browning, P., Groves, D. I., Blockley, J. G., and Rosman, K. J. R. 1987. Lead isotope constraints on the age and source of gold mineralization in the Archean Yilgarn Block, Western Australia. Economic Geology, **82**: 971-986.

Chinn, W. 1969. Structural and mineralogical studies at the Homestake Mine, Lead, South Dakota. Ph.D. thesis, University of California, Berkeley, California. Available from University Microfilms International, Ann Arbour, Michigan.

Gardiner, J. J. 1986. Structural geology of the Lupin gold mine, Northwest Territories. M.Sc. thesis, Acadia University, Wolfville, Nova Scotia.

Kerrich, R., and Hodder, R. W. 1982. Archean lode gold and base metal deposits: Evidence for metal separation into independant hydrothermal systems. *In* Geology of Canadian gold deposits. *Edited by* R. W. Hodder and W. Petruk. Canadian Institute of Mining and Metallurgy, Special Volume 24, pp. 144-160.

King, J. E., Davis, W. J., Relf, C., and Avery, R. W. 1988. Deformation and plutonism in the western Contwoyto Lake map area, central Slave Province, District of Mackenzie, N.W.T. *In* Current research part C. Geological Survey of Canada, paper 88-1C, pp. 161-176.

APPENDICES

APPENDIX 1

SAMPLE SECTION FROM ROCK
TYPE WORK TYPE
act ain alm and ath apt aug bio crb cal dol eld cat chl crd epi fay gre gro gru hed hbl kap mon mus pkg qtz-v qtz-m sil tph stl trm tre zir asp cpy gos gld grb hem ilm kno mag py po sch

SAMPLE	SECTION TYPE	PROBE WORK	ROCK TYPE	act	ala	alm	and	ath	apt	aug	bio	crb	cal	dol	ald	cal	chl	crd	epi	fay	gra	gre	grs	hed	hbl	hyp	mus	mus	plg	qtz-v	qtz-m	sil	sph	stl	tra	tre	zir	asp	cpy	gee	gld	grb	hem	ilm	lim	mag	py	po	sch
4PLD006	TS		calc-silicate						X															X							X																	
4PLD007	TS		weakly min. IF																			X									X					X											
4PLD011	TS		weakly min. IF						X													X	X								X					X									X		
Silk area																																																
4PLE001	TS		weakly min. IF			X			X															X							X	X					X										
4PLE002	TS		contact meta IF																																													
4PLE0015	PTS		As-rich min. IF			X																		X							X								X	X		X	X		X			X	
4PLE016	TS		pelitic IF			X											R							X							X					R											
4PLE019	PTS	Y	a) calc-silicate																					R	X						X												X			X	
	PTS	Y	b) As-poor min. IF																												X																X	
	PTS	Y	c) As-poor min. IF																					X							X																X	
4PLE016d	PTS		d) weakly min. IF		X																			X							X																X	
4PLE022a	TS		greywacke			X			X		X						X											X	X		X						X										
4PLE022b	TS		mudstone			X					X							X										X	X		X						X										
4PLE024	TS		a) quartz vein																											X																	
	TS		b) weakly min. IF																				X												R										
	TS		c) weakly min. IF																				X								X						X									
	TS		d) unmin. IF																				X								X															
	TS		e) unmin. IF			X																	X								X															
4PLE025	TS		unmin. IF			X																	X								X															X	
4PLE026	TS		pelitic IF			X					X						R						X								X					X		X								
4PLE027	TS		pelitic IF			X					X						R						X								X															
4PLE029	TS		unmin. IF			X			X		X												X								X												X		X		X	
4PLE029	PTS		unmin. IF	same as above																																												
4PLE033	PTS		As-poor min. IF			X																	X								X								X	X		X	X		X			X	
4PLE038	TS		unmin. IF		X	X															X		X																						X			
4PLE039	TS		unmin. IF		X	X																	X																						X		X	
4PLE040	TS		weakly min. IF																		X		X																						X		X	
4PLE041	TS		quartz vein			X																		X						X																X	
4PLE048	TS		mudstone						X		X							X										X	X		X						X										
5PLE003	PTS		unmin. IF			X																	X								X								X				X			X	
5PLE015	PTS		unmin. IF																				X								X												X		X		X	
Raft																																																	
4PLF004	TS		pelitic IF			X			X		X							X										X	X		X						X										
4PLF006	TS		pelitic IF			X					X												X					X			X						X										
4PLF011	PTS	Y	As-rich min. IF			X					XX							X					X						X		X				R			X	X		X	X				X	
4PLF012	PTS	Y	weakly min. IF															X					X	X					X		X				R			X								X	
4PLF016	TS		weakly min. IF	R														X					X								X				R											X	
4PLF024	PTS		a) calc-silicate															X					X	X																							X	
	PTS		b) As-poor min. IF																				X													R											X	
	PTS		c) weakly min. IF																		X		X													R											X	
Hollow L.																																																
4PLG004	TS		greywacke								X													X	X					X						X		X									
4PLG006	TS		greywacke								X													X	X					X						X											
Rush																																															
4PLH013	PTS		pelitic IF			X	X				X						X	X							X					X						X		X						X		X	
4PLH014	PTS		pelitic IF			X	X	X			X						X	X							X					X						X		X						X		X	
4PLH015	PTS		pelitic IF								X	R					X	X							X					X						X		X						X			
Flow L.																																															
4PLI006	TS		metatuff								X		X						X						X					X	X	X														
4PLI012	TS		pelitic IF ?			X					X								X					X	X					X																
4PLI024	TS		calc-silicate gneiss	X									X												X					X		X														
Hilltop oxide																																															
4PLJ004	PTS	Y	unmin. IF								X	X			X									X																					X	X		
4PLJ005	TS		unmin. IF									X			X		X							X																					X			
4PLJ006	TS		pelitic IF									X			X		X							X																					X			
4PLJ007	TS		a) carb. band									X	X											X																								
	TS		b) pelitic-carb. IF								X	X			X									X																								
4PLJ009	TS		carb. IF									X			X									X	X					X																	

SAMPLE	SECTION TYPE	PROBE WORK	ROCK TYPE	act	ah	alm	and	ath	apt	aug	bio	crb	cal	dol	sid	cel	chl	crd	epi	fay	grs	gre	gru	hed	hbl	ksp	mon	mus	plg	qtz-v	qtz-m	sil	sph	stl	tra	tre	zir	asp	cpy	goe	gld	grh	hem	ilm	loe	mag	py	po	sch
4PLJ011	TS		unmin. IF									X			X		X														X																		
4PLJ012	TS		calcitic marble									X	X															X			X															X				
4PLJ013	TS		mudstone														X											X	X		X																		
4PLJ014	TS		greywacke									X					X											X	X		X				X														
4PLJ019	TS		carb. IF								X				X														X		X																		
4PLJ022	TS		unmin. IF									X			X													X			X																		
4PLJ023	TS		quartz vein												X													X		X																		
4PLJ024	TS		weakly min. IF									X			X		X														X																		
4PLJ027	TS		mudstone														X											X	X		X															X			
4PLJ030	TS		pelitic IF								X						X												X		X																		
4PLJ031	TS		pelitic IF								X	X			X		X												X		X																X		
4PLJ032	TS		pelitic IF									X			X		X												X		X																X		
64-2 area																																																		
4PLO003	TS		calcitic marble									X																X			X																		
4PLO004	TS		greywacke									X					X											X	X		X							X									X	X
4PLO007	TS		unmin. IF									X											X		X						X																	
4PLO009	TS		unmin. IF		X							X											X		X						X						X										
4PLO013	TS		unmin. IF																				X		X						X																	
4PLO014	TS		pelitic IF									X					X														X																	
4PLO020	TS		greywacke									X					X												X		X																	
Faber Fault																																																	
4PLP006	TS		pyritic mudstone														X											X			X																		
4PLP009	TS		pyritic mudstone														X											X			X																		
Shere																																																	
4PLQ001	TS		metadiabase							X							X												X		X																		
4PLQ003	TS		mudstone						X		X																	X	X		X				R	X		X							X			
4PLQ007	TS		unmin. IF																				X		X												X										
4PLQ010	TS		As-poor min. IF						X														X	X	X						X															X		X
4PLQ011	TS		weakly min. IF						X														X	X	X						X																	
4PLQ014	TS		weakly min. IF		X																										X																		
4PLQ020	TS		pelitic IF		X				X		X						X						X	X	X						X																X	

SYMBOLS
X- PRESENT
PTS- POLISHED THIN SECTION

R- RETROGRADE PHASE
TS- THIN SECTION

MINERAL ABBREVIATIONS

act- actinolite
ah- alkalite
alm- almandine garnet
and- andalusite
ath- anthophyllite
apt- apatite

aug- augite
bio- biotite
crb- carbonate
cal- calcite
dol- dolomite
sid- siderite

cel- celcian
chl- chlorite
crd- cordierite
epi- epidote
fay- fayalite
gre- grossular garnet

gre- greenalite ?
gru- grunerite
hed- hedenbergite
hbl- hornblende
ksp- k-feldspar
mon- monazite

mus- muscovite
plg- plagioclase
qtz-v- quartz vein
qtz-m- quartz matrix
sil- sillimanite
sph- sphene

sil- sillimanite/andalusite
tra- tourmaline
tre- tremolite
zir- zircon
asp- arsenopyrite
cpy- chalcopyrite

goe- goethite
gld- gold
grh- graphite
hem- hematite
loe- loellingite

mag- magnetite
py- pyrite
po- pyrrhotite
sch- scheelite

ROCK TYPE ABBREVIATIONS

IF- iron formation
min - mineralized
altered ?- possibly altered

calc-silicate- calc-silicate rocks
unmin - unmineralized

APPENDIX 2

	pyrope std (oxide %)		
	this study		accepted
	average	std.dev.	values
	n= 39	1 sigma	
MgO	18.548	0.324	18.507
Al2O3	23.690	0.283	23.732
SiO2	41.507	0.295	41.458
K2O	0.0	0.0	-
CaO	5.026	0.081	5.170
TiO2	0.410	0.049	0.470
V2O5	0.0	0.0	-
Cr2O3	0.085	0.067	-
MnO	0.302	0.041	0.280
FeO*	10.528	0.171	10.681
TOTAL	100.091	0.663	100.298

* all Fe as FeO

cations based on 12 oxygens	average	std.dev.	
Mg	1.978	0.027	1.972
Al	1.998	0.021	2.000
Si	2.970	0.015	2.963
K	0.0	0.0	-
Ca	0.385	0.006	0.396
Ti	0.022	0.003	0.025
V	0.0	0.0	-
Cr	0.005	0.004	-
Mn	0.018	0.003	0.017
Fe	0.630	0.011	0.639
SUM	8.007	0.013	8.012

APPENDIX 3

	A	B	C	D	E	F	G	H	I	J	K	L	M	N	O	P
1	date	13-Nov-85	13-Nov-85	12-Dec-85	12-Dec-85	12-Dec-85	19-Dec-85	9-Apr-86	9-Apr-86	9-Apr-86	9-Apr-86	9-Apr-86	9-Apr-86	9-Apr-86	14-Mar-86	14-Mar-86
2	method	wda/eda	wda/eda	wda/eda	wda/eda	wda/eda	eda	eda	eda	eda	eda	eda	eda	eda	eda	eda
3	rock type	4	4	9	9	9	9	9	9	9	9	9	9	9	9	9
4	mineral	grun	hbl	act	act	act	hbl	act	act	hbl	act	hbl	act	act	act	hbl
5	study area	a	a	a	a	a	a	a	a	a	a	a	a	a	a	a
6					"hbl 1"											"act 1"
7	sample	4PLA018	4PLA019	4PLA031	4PLA031	4PLA031	4PLA031	5PLA041	5PLA041	5PLA041	5PLA041	5PLA041	5PLA041	5PLA041	5PLA056	5PLA056
8	PTS area	circ 1	circ 1	circ 2	circ 3	circ 3	circ 3	circ 1	circ 2	circ 2	circ 2	circ 2	circ 3	circ 4	circ 1	circ 2
9	analysis	grun 1	hbl 1	act 1	act 1	act 1	hbl 2	act 1	act 1	hbl 1	act 2	hbl 2	act 1	act 1	act 1	hbl 1
10																
11	SiO2	50.813	41.442	50.084	47.308	48.491	38.950	48.715	48.777	42.973	48.682	44.566	47.103	47.926	48.067	48.268
12	Al2O3	0.519	15.529	0.179	3.214	1.201	16.858	0.587	0.747	7.890	0.781	5.922	2.451	1.831	2.873	5.037
13	Cr2O3	0.000	0.000	0.000	0.000	0.000	0.000	0.000	0.000	0.000	0.000	0.000	0.000	0.000	0.103	0.000
14	TiO2	0.000	0.146	0.000	0.000	0.000	0.000	0.000	0.000	0.107	0.000	0.104	0.000	0.000	0.000	0.000
15	MgO	7.157	3.075	1.244	0.925	0.814	1.240	1.107	1.043	0.843	1.278	0.903	0.757	0.997	2.588	1.306
16	FeO	38.986	25.593	34.897	35.057	35.282	28.072	34.626	34.467	32.167	34.306	32.930	34.693	34.899	32.206	33.424
17	MnO	0.000	0.000	0.075	0.000	0.000	0.000	0.000	0.000	0.000	0.000	0.000	0.000	0.000	0.086	0.000
18	CaO	0.264	10.595	11.505	11.357	11.320	11.372	11.422	11.344	11.267	11.386	11.317	11.190	11.285	11.476	11.296
19	Na2O	0.000	0.944	0.000	0.000	0.000	0.943	0.000	0.000	0.289	0.000	0.179	0.000	0.000	0.218	0.284
20	K2O	0.000	0.453	0.000	0.146	0.000	0.358	0.000	0.000	0.287	0.088	0.202	0.000	0.078	0.140	0.205
21	Cl	0.000	0.000	0.066	0.259	0.123	0.000	0.079	0.000	0.000	0.000	0.000	0.000	0.000	0.145	0.162
22	TOTAL	97.740	97.780	98.036	98.276	98.240	98.790	96.540	96.400	95.820	96.530	96.040	96.190	97.010	98.690	98.000
23	O based on anhyrous O+Cl=23															
24		23.0000	23.0000	22.9911	22.9846	22.9833	23.0000	22.8591	23.0000	23.0000	23.0000	23.0000	23.0000	23.0000	22.9897	22.9781
25	cations based on 23O															
26	Si	7.9992	6.3927	8.0063	7.6088	7.9124	6.1935	7.9323	7.9324	7.0070	7.9088	7.2610	7.7013	7.7679	7.7134	7.4058
27	Al iv	0.0008	1.6073	0.0000	0.3832	0.0876	1.8065	0.0677	0.0676	0.9930	0.0931	0.7390	0.2987	0.2321	0.2866	0.5942
28	Al vi	0.0955	1.2158	0.0337	0.2158	0.1388	1.2738	0.0450	0.0756	0.5460	0.0565	0.4003	0.1736	0.1177	0.2088	0.3556
29	Cr	0.0000	0.0000	0.0000	0.0000	0.0000	0.0000	0.0000	0.0000	0.0000	0.0000	0.0000	0.0000	0.0000	0.0127	0.0000
30	Ti	0.0000	0.0169	0.0000	0.0000	0.0000	0.0000	0.0000	0.0000	0.0132	0.0000	0.0128	0.0000	0.0000	0.0000	0.0000
31	Mg	1.6784	0.7069	0.2985	0.2257	0.1939	0.2868	0.2687	0.2529	0.2054	0.3098	0.2196	0.1846	0.2408	0.5685	0.3114
32	Fe 2+	5.1328	3.3016	4.6872	4.7141	4.7173	3.6398	4.7151	4.6903	4.3956	4.6586	4.4850	4.7436	4.7305	4.2338	4.4723
33	Mn	0.0000	0.0000	0.0102	0.0000	0.0000	0.0000	0.0000	0.0000	0.0000	0.0000	0.0000	0.0000	0.0000	0.0088	0.0000
34	Ca	0.0446	1.7511	1.9712	1.9566	1.9405	1.8889	1.9926	1.9766	1.9730	1.9892	1.9792	1.9803	1.9566	1.9333	1.9364
35	Na	0.0000	0.2825	0.0000	0.0000	0.0000	0.2835	0.0000	0.0000	0.0916	0.0000	0.0565	0.0000	0.0000	0.0887	0.0862
36	K	0.0000	0.0892	0.0000	0.0303	0.0000	0.0705	0.0000	0.0000	0.0588	0.0181	0.0420	0.0000	0.0158	0.0280	0.0419
37	SUM	14.9520	15.3640	14.9850	15.1390	14.9910	15.4430	15.0220	14.9950	15.2860	15.0270	15.2050	15.0620	15.0650	15.0990	15.2060
38	Cl	0.0000	0.0000	0.0179	0.0705	0.0334	0.0000	0.0218	0.0000	0.0000	0.0000	0.0000	0.0000	0.0000	0.0386	0.0439
39																
40	Fe/(Fe+Mg)	0.7535	0.8238	0.9403	0.9551	0.9605	0.9270	0.9461	0.9488	0.9554	0.9377	0.9534	0.9625	0.9516	0.8747	0.9349
41	AFM															
42	Al2O3	0.0070	0.2804	0.0034	0.0581	0.0225	0.2818	0.0112	0.0143	0.1433	0.0148	0.1078	0.0457	0.0340	0.0487	0.0903
43	FeO	0.7482	0.6081	0.9371	0.9996	0.9360	0.8658	0.9355	0.9353	0.8185	0.9236	0.8506	0.9185	0.9192	0.8321	0.8505
44	MgO	0.2448	0.1304	0.0595	0.0423	0.0368	0.0524	0.0533	0.0504	0.0382	0.0614	0.0416	0.0357	0.0468	0.1192	0.0592
45	CFM															
46	CaO	0.0065	0.3040	0.2842	0.2839	0.2832	0.3248	0.2856	0.2856	0.3001	0.2852	0.2957	0.2846	0.2828	0.2854	0.2882
47	FeO	0.7486	0.5732	0.6730	0.6840	0.6885	0.6259	0.6758	0.6776	0.6887	0.6702	0.6715	0.6886	0.6825	0.6250	0.6655
48	MgO	0.2448	0.1227	0.0426	0.0322	0.0283	0.0493	0.0385	0.0365	0.0312	0.0445	0.0328	0.0258	0.0347	0.0895	0.0463
49	ACF															
50	Al2O3	0.0070	0.1968	0.0024	0.0423	0.0163	0.2094	0.0080	0.0102	0.1048	0.0106	0.0784	0.0331	0.0246	0.0353	0.0666
51	CaO	0.0065	0.2442	0.2838	0.2719	0.2788	0.2588	0.2834	0.2827	0.2886	0.2822	0.2725	0.2751	0.2756	0.2753	0.2691
52	FeO+MgO	0.9866	0.5590	0.7140	0.6956	0.7051	0.5338	0.7086	0.7070	0.6266	0.7072	0.6491	0.6917	0.6896	0.6884	0.6646
53																

	Q	R	S	T	U	V	W	X	Y	Z	AA	AB	AC	AD	AE	AF
1	date	26-Mar-86	26-Mar-86	26-Mar-86	26-Mar-86	24-Mar-86	24-Mar-86	26-Mar-86	26-Mar-86	26-Mar-86	26-Mar-86	26-Mar-86	26-Mar-86	13-May-86	13-May-86	13-May-86
2	method	edx	edx	edx	edx	edx	edx	edx	edx	edx	edx	edx	edx	edx	edx	edx
3	rock type	6	6	6	6	6	6	6	6	6	6	6	6	9	9	9
4	mineral	grun	hbl	grun	hbl	grun	hbl	grun	hbl	grun	hbl	grun	hbl	act	act	hbl
5	study area	a	a	a	a	a	a	a	a	a	a	a	a	a	a	a
6																
7	sample	SPLA057	SPLA057	SPLA057	SPLA057	SPLA057	SPLA057	SPLA057	SPLA057	SPLA057	SPLA057	SPLA057	SPLA057	SPLA060	SPLA060	SPLA060
8	PTS area	circ 1	circ 1	circ 1	circ 1	circ 2	circ 2	circ 2	circ 2	circ 3	circ 3	circ 3	circ 3	circ 1	circ 1	circ 2
9	analysis	grun 1	hbl 1	grun 2	hbl 2	grun 1	hbl 1	grun 2	hbl 2	grun 1	hbl 1	grun 2	hbl 2	act 1	act 2	hbl 1
10																
11	SiO2	48.236	40.133	48.672	39.350	48.232	39.053	48.316	39.796	47.935	39.035	48.084	39.456	49.281	47.577	43.977
12	Al2O3	0.529	15.919	0.415	17.248	0.514	16.215	0.519	16.624	0.547	17.784	0.588	16.956	2.036	4.245	9.658
13	Cr2O3	0.000	0.000	0.000	0.000	0.000	0.000	0.000	0.000	0.000	0.000	0.000	0.000	0.000	0.000	0.000
14	TiO2	0.000	0.217	0.000	0.000	0.000	0.000	0.000	0.161	0.000	0.097	0.006	0.142	0.000	0.000	0.197
15	MgO	2.352	1.154	2.314	1.015	2.029	0.896	1.957	1.010	1.381	0.807	1.447	0.777	3.058	2.719	1.902
16	FeO	45.623	29.315	46.280	27.550	45.419	26.651	46.367	28.009	46.737	27.822	47.184	28.012	31.771	31.511	29.602
17	MnO	0.000	0.000	0.000	0.000	0.000	0.000	0.000	0.000	0.000	0.000	0.000	0.000	0.000	0.000	0.000
18	CaO	0.513	11.051	0.500	10.980	0.486	10.831	0.478	10.949	0.529	10.848	0.478	10.921	11.745	11.442	11.354
19	Na2O	0.000	0.591	0.000	0.505	0.000	0.531	0.000	0.481	0.000	0.693	0.000	0.573	0.000	0.183	0.313
20	K2O	0.000	0.365	0.000	0.343	0.000	0.332	0.000	0.352	0.000	0.369	0.000	0.343	0.000	0.090	0.209
21	Cl	0.000	0.000	0.000	0.000	0.000	0.000	0.000	0.000	0.000	0.000	0.000	0.000	0.000	0.000	0.000
22	TOTAL	97.260	97.750	98.180	97.000	96.780	96.510	97.640	97.380	97.140	97.460	97.770	97.180	97.890	97.770	97.110
23	O based on anhydrous O+Cl=23															
24		23.0000	23.0000	23.0000	23.0000	23.0000	23.0000	23.0000	23.0000	23.0000	23.0000	23.0000	23.0000	23.0000	23.0000	23.0000
25	cations based on 23O															
26	Si	7.9462	6.2686	7.9533	6.1902	7.9778	6.1410	7.9514	6.2455	7.9586	6.1217	7.9396	6.2089	7.7698	7.5175	6.9445
27	Al iv	0.0538	1.7114	0.0467	1.8098	0.0221	1.8590	0.0486	1.7545	0.0434	1.8783	0.0604	1.7911	0.2301	0.4825	1.0555
28	Al vi	0.0489	1.2284	0.0333	1.3874	0.0781	1.5168	0.0521	1.3202	0.0536	1.4088	0.0500	1.3534	0.1483	0.3081	0.7461
29	Cr	0.0000	0.0000	0.0000	0.0000	0.0000	0.0000	0.0000	0.0000	0.0000	0.0000	0.0000	0.0000	0.0000	0.0000	0.0000
30	Ti	0.0000	0.0255	0.0000	0.0000	0.0122	0.0000	0.0000	0.0190	0.0000	0.0114	0.0000	0.0167	0.0000	0.0000	0.0234
31	Mg	0.5774	0.2695	0.5636	0.2378	0.5003	0.2101	0.4801	0.2362	0.3440	0.1887	0.3561	0.1821	0.7187	0.6405	0.4486
32	Fe 2+	6.2851	3.7104	6.3216	3.6237	6.2827	3.5047	6.3811	3.6758	6.4677	3.6489	6.5143	3.6662	4.1891	4.1639	3.9181
33	Mn	0.0000	0.0000	0.0000	0.0000	0.0000	0.0000	0.0000	0.0000	0.0000	0.0000	0.0000	0.0000	0.0000	0.0000	0.0000
34	Ca	0.0805	1.8553	0.0878	1.8503	0.0861	1.8248	0.0845	1.8410	0.0941	1.8228	0.0842	1.8412	1.9841	1.9371	1.9254
35	Na	0.0000	0.1795	0.0000	0.1541	0.0000	0.1618	0.0000	0.1402	0.0000	0.2106	0.0000	0.1749	0.0000	0.0561	0.0959
36	K	0.0000	0.0729	0.0000	0.0688	0.0000	0.0665	0.0000	0.0704	0.0000	0.0739	0.0000	0.0689	0.0000	0.0181	0.0423
37	SUM	15.0020	15.3420	15.0060	15.3220	14.9580	15.2650	14.9980	15.3030	14.9880	15.3650	15.0050	15.3230	15.0400	15.1240	15.2000
38	Cl	0.0000	0.0000	0.0000	0.0000	0.0000	0.0000	0.0000	0.0000	0.0000	0.0000	0.0000	0.0000	0.0000	0.0000	0.0000
39																
40	Fe/(Fe+Mg)	0.9159	0.9323	0.9181	0.9384	0.9262	0.9434	0.9300	0.9396	0.9496	0.9508	0.9482	0.9529	0.8536	0.8667	0.8973
41	AFM															
42	Al2O3	0.0074	0.2697	0.0058	0.2928	0.0073	0.3124	0.0073	0.2821	0.0078	0.2899	0.0080	0.2890	0.0371	0.0780	0.1710
43	FeO	0.9091	0.6808	0.9126	0.6637	0.9195	0.6487	0.9233	0.8745	0.9423	0.6857	0.9406	0.6775	0.8219	0.8008	0.7438
44	MgO	0.0835	0.0495	0.0814	0.0438	0.0732	0.0389	0.0695	0.0433	0.0500	0.0344	0.0514	0.0335	0.1410	0.1232	0.0852
45	CFM															
46	CaO	0.0130	0.3179	0.0126	0.3239	0.0125	0.3294	0.0122	0.3200	0.0136	0.3220	0.0121	0.3225	0.2679	0.2873	0.3060
47	FeO	0.9039	0.6359	0.9086	0.6344	0.9146	0.6327	0.9187	0.8388	0.9367	0.6448	0.9367	0.6456	0.8078	0.8177	0.6227
48	MgO	0.0830	0.0462	0.0808	0.0418	0.0728	0.0379	0.0691	0.0411	0.0497	0.0333	0.0512	0.0319	0.1043	0.0950	0.0713
49	ACF															
50	Al2O3	0.0073	0.2012	0.0057	0.2187	0.0072	0.2335	0.0072	0.2109	0.0077	0.2250	0.0079	0.2159	0.0267	0.0554	0.1252
51	CaO	0.0129	0.2540	0.0125	0.2531	0.0124	0.2525	0.0121	0.2525	0.0135	0.2498	0.0120	0.2529	0.2802	0.2714	0.2677
52	FeO+MgO	0.9797	0.5448	0.9818	0.5282	0.9803	0.5140	0.9807	0.5386	0.9789	0.5254	0.9801	0.5312	0.6931	0.6732	0.6071
53																

	AG	AH	AI	AJ	AK	AL	AM	AN	AO	AP	AQ	AR	AS	AT	AU	AV
1	date	26-Mar-86	26-Mar-86	9-Apr-86	9-Apr-86	9-Apr-86	9-Apr-86	24-Mar-86	24-Mar-86	26-Mar-86	26-Mar-86	26-Mar-86	26-Mar-86	26-Mar-86	26-Mar-86	26-Mar-86	17-Mar-86
2	method	eda	eda	eda	eda	eda	eda	eda	eda	eda	eda	eda	eda	eda	eda	eda	eda
3	rock type	7	7	9	9	9	9	8	8	8	8	8	8	8	8	8	4
4	mineral	hbl	hbl	act	hbl	act	hbl	act	hbl	act	hbl	act	hbl	act	hbl	act	grun
5	study area	a	a	a	a	a	a	a	a	a	a	a	a	a	a	a	a
6																	
7	sample	5PLA062	5PLA062	5PLA062	5PLA062	5PLA062	5PLA062	5PLA064	5PLA064	5PLA064	5PLA064	5PLA064	5PLA064	5PLA064	5PLA064	5PLA064	5PLA065
8	PTS area	circ 1	circ 1	circ 2	circ 2	circ 2	circ 2	circ 1	circ 1	circ 1	circ 1	circ 2	circ 2	circ 2	circ 2	circ 2	circ 1
9	analysis	hbl 1	hbl 2	act 1	hbl 1	act 2	hbl 2	act 1	hbl 1	act 2	hbl 2	act 1	hbl 1	act 2	hbl 2	grun 1	
10																	
11	SiO2	43.774	40.753	48.942	43.439	48.771	43.971	49.808	45.543	49.461	46.575	50.138	45.084	50.226	40.872	50.457	
12	Al2O3	10.107	15.372	0.471	7.832	0.565	7.374	0.379	7.067	0.794	6.184	0.567	7.056	0.404	14.755	0.866	
13	Cr2O3	0.000	0.000	0.000	0.000	0.000	0.000	0.000	0.000	0.000	0.000	0.000	0.000	0.000	0.105	0.081	
14	TiO2	0.187	0.000	0.000	0.993	0.000	0.000	0.000	0.120	0.000	0.135	0.000	0.208	0.000	0.139	0.000	
15	MgO	2.206	1.634	0.645	0.644	0.854	0.930	2.119	3.310	2.014	3.480	1.870	1.442	1.797	1.057	7.153	
16	FeO	29.885	27.787	35.343	31.910	35.255	32.117	33.835	29.880	34.438	30.414	34.934	32.431	34.579	28.996	30.744	
17	MnO	0.000	0.000	0.000	0.000	0.000	0.000	0.000	0.000	0.000	0.000	0.000	0.000	0.000	0.000	0.000	
18	CaO	11.248	11.353	11.436	11.142	11.370	11.195	11.082	11.002	11.158	11.142	11.077	11.092	11.097	11.339	0.373	
19	Na2O	0.485	0.562	0.000	0.330	0.000	0.336	0.000	0.231	0.000	0.310	0.000	0.376	0.000	0.569	0.000	
20	K2O	0.217	0.299	0.068	0.211	0.000	0.174	0.000	0.146	0.000	0.091	0.000	0.118	0.000	0.333	0.000	
21	Cl	0.000	0.000	0.181	0.000	0.114	0.000	0.000	0.000	0.000	0.000	0.058	0.000	0.000	0.000	0.000	
22	TOTAL	98.190	97.760	97.090	95.800	96.930	96.100	97.220	97.300	97.870	98.340	98.580	97.700	98.100	97.970	98.670	
23	O based on anhyrous O+Cl=23																
24		23.0000	23.0000	22.9750	23.0000	22.9843	23.0000	23.0000	23.0000	23.0000	23.0000	22.9922	23.0000	23.0000	23.0000	23.0000	
25	cations based on 23O																
26	SI	6.6632	6.3651	7.9619	7.0755	7.9338	7.1392	7.9787	7.1848	7.8853	7.2761	7.9530	7.1722	7.9858	6.3853	7.9030	
27	Al iv	1.1368	1.6349	0.0381	0.9245	0.0662	0.8608	0.0233	0.8152	0.1047	0.7239	0.0470	0.8278	0.0142	1.6147	0.0970	
28	Al vi	0.7308	1.1948	0.0523	0.5701	0.0422	0.5553	0.0482	0.4988	0.0446	0.4185	0.0478	0.4856	0.0616	1.1153	0.0829	
29	Cr	0.0000	0.0000	0.0000	0.0000	0.0000	0.0050	0.0000	0.0000	0.0000	0.0000	0.0000	0.0000	0.0000	0.0130	0.0100	
30	Ti	0.0187	0.0000	0.0000	0.0114	0.0000	0.0000	0.0000	0.0142	0.0000	0.0159	0.0000	0.0248	0.0000	0.0164	0.0000	
31	Mg	0.5136	0.3803	0.1503	0.2050	0.2071	0.2250	0.5057	0.7784	0.4782	0.8104	0.4421	0.3420	0.4258	0.2474	1.6699	
32	Fe 2+	3.9317	3.6298	4.8084	4.3468	4.7963	4.3810	4.5316	3.9422	4.5973	3.9738	4.6342	4.3166	4.5979	3.8070	5.2059	
33	Mn	0.0000	0.0000	0.0000	0.0000	0.0000	0.0000	0.0000	0.0000	0.0000	0.0000	0.0000	0.0000	0.0000	0.0000	0.0000	
34	Ca	1.8885	1.8999	1.9033	1.9445	1.9817	1.9475	1.9015	1.8597	1.9063	1.8649	1.8826	1.8914	1.8903	1.9073	0.0626	
35	Na	0.1478	0.1703	0.0000	0.1041	0.0000	0.1057	0.0000	0.0706	0.0000	0.0938	0.0000	0.1160	0.0000	0.1732	0.0000	
36	K	0.0434	0.0595	0.0143	0.0436	0.0000	0.0586	0.0000	0.0295	0.0000	0.0181	0.0000	0.0239	0.0000	0.0588	0.0000	
37	SUM	15.2780	15.3340	15.0250	15.2350	15.0270	15.2260	14.9870	15.1940	15.0280	15.1930	15.0070	15.2100	14.9760	15.3460	15.0110	
38	Cl	0.0000	0.0000	0.0500	0.0000	0.0315	0.0000	0.0000	0.0000	0.0000	0.0000	0.0157	0.0000	0.0000	0.0000	0.0000	
39																	
40	Fe/(Fe+Mg)	0.8841	0.9052	0.9885	0.9550	0.9586	0.9509	0.8996	0.8351	0.9056	0.8306	0.9129	0.9266	0.9152	0.9390	0.7571	
41	AFM																
42	Al2O3	0.1735	0.2608	0.0080	0.1418	0.0107	0.1333	0.0070	0.1222	0.0145	0.1065	0.0093	0.1244	0.0075	0.2518	0.0115	
43	FeO	0.7308	0.6691	0.8598	0.8100	0.9483	0.8241	0.8933	0.7331	0.8925	0.7421	0.9045	0.8113	0.9084	0.7025	0.7484	
44	MgO	0.0958	0.0701	0.0312	0.0367	0.0409	0.0425	0.0997	0.1447	0.0930	0.1514	0.0863	0.0643	0.0841	0.0457	0.2401	
45	CFM																
46	CaO	0.2982	0.3215	0.2865	0.2993	0.2637	0.2881	0.2740	0.2826	0.2732	0.2805	0.2705	0.2888	0.2734	0.3199	0.0090	
47	FeO	0.6205	0.6142	0.6911	0.6808	0.6875	0.6531	0.5891	0.6582	0.5976	0.6590	0.6650	0.6590	0.6650	0.6586	0.7503	
48	MgO	0.0814	0.0644	0.0225	0.0316	0.0296	0.0344	0.0729	0.1183	0.0686	0.1219	0.0635	0.0522	0.0618	0.0415	0.2407	
49	ACF																
50	Al2O3	0.1264	0.1932	0.0065	0.1037	0.0077	0.0975	0.0051	0.0808	0.0106	0.0780	0.0060	0.0818	0.0055	0.1863	0.0114	
51	CaO	0.2599	0.2594	0.2846	0.2683	0.2815	0.2690	0.2726	0.2570	0.2703	0.2583	0.2687	0.2623	0.2719	0.2693	0.0089	
52	FeO+MgO	0.6117	0.5475	0.7069	0.6260	0.7108	0.6335	0.7222	0.6523	0.7191	0.6627	0.7245	0.6468	0.7229	0.5534	0.9797	
53																	

	AW	AX	AY	AZ	BA	BB	BC	BD	BE	BF	BG	BH	BI	BJ	BK	BL
1	date	17-Mar-86	17-Mar-86	17-Mar-86	17-Mar-86	17-Mar-86	6-Mar-86	17-Mar-86	24-Mar-86	24-Mar-86	24-Mar-86	24-Mar-86	24-Mar-86	24-Mar-86	24-Mar-86	24-Mar-86
2	method	eds	eds	eds	eds	eds	eds	eds	eds	eds	eds	eds	eds	eds	eds	eds
3	rock type	4	4	4	4	4	3	3	5	5	5	5	5	5	5	5
4	mineral	hbl	grun	hbl	grun	grun	hbl	hbl	grun	hbl	grun	hbl	grun	hbl	grun	hbl
5	study area	a	a	a	a	a	a	a	a	a	a	a	a	a	a	a
6																
7	sample	SPLA085	SPLA085	SPLA085	SPLA088	SPLA088	SPLA105	SPLA105	SPLA120	SPLA120	SPLA120	SPLA120	SPLA120	SPLA120	SPLA120	SPLA120
8	PTB area	circ 1	circ 2	circ 2	circ 1	circ 1	circ 1	circ 2	circ 1	circ 1	circ 1	circ 1	circ 2	circ 2	circ 2	circ 2
9	analysis	hbl 1	grun 1	hbl 1	grun 1	grun 2	hbl 1	hbl 1	grun 1	hbl 1	grun 2	hbl 2	grun 1	hbl 1	grun 2	hbl 2
10																
11	SiO2	40.150	50.480	40.570	51.051	50.870	40.253	40.168	48.388	43.704	48.217	42.207	48.346	42.347	48.484	40.061
12	Al2O3	16.747	0.650	16.991	0.353	0.922	19.343	19.325	0.403	7.160	0.384	9.072	0.472	9.127	0.441	12.510
13	Cr2O3	0.000	0.078	0.000	0.000	0.000	0.089	0.000	0.000	0.000	0.000	0.000	0.000	0.000	0.000	0.000
14	TiO2	0.000	0.000	0.000	0.394	0.093	0.115	0.000	0.000	0.000	0.146	0.000	0.161	0.000	0.000	0.000
15	MgO	2.576	7.006	2.578	7.561	8.419	3.575	3.498	1.534	1.269	1.642	1.138	2.162	1.562	2.233	1.216
16	FeO	24.450	30.758	24.555	30.067	37.838	21.937	22.383	46.191	33.688	46.266	32.604	45.258	32.214	45.406	30.821
17	MnO	0.000	0.000	0.000	0.000	0.000	0.000	0.000	0.000	0.000	0.000	0.000	0.000	0.000	0.000	0.000
18	CaO	10.647	0.617	10.586	0.632	0.315	11.019	11.081	0.883	10.515	0.702	10.780	0.675	10.598	0.899	10.835
19	Na2O	0.700	0.000	0.792	0.000	0.000	1.071	0.893	0.000	0.492	0.000	0.516	0.000	0.422	0.000	0.773
20	K2O	0.323	0.000	0.266	0.000	0.000	0.419	0.407	0.000	0.265	0.000	0.422	0.000	0.350	0.000	0.563
21	Cl	0.000	0.000	0.000	0.000	0.000	0.000	0.000	0.000	0.000	0.000	0.000	0.000	0.000	0.000	0.000
22	TOTAL	97.600	98.590	97.930	99.060	98.450	97.820	97.765	97.200	97.240	97.220	96.880	96.930	96.820	97.260	96.780
23	O based on anhyrous O+Cl=23															
24		23.0000	23.0000	23.0000	23.0000	23.0000	23.0000	23.0000	23.0000	23.0000	23.0000	23.0000	23.0000	23.0000	23.0000	23.0000
25	cations based on 23O															
26	Si	6.1560	7.9206	6.1945	7.9368	7.9031	6.1001	6.1008	7.8987	7.0656	7.9765	6.8383	7.9794	6.8547	7.9765	6.4636
27	Al iv	1.8440	0.0792	1.8055	0.0632	0.0969	1.8999	1.8992	0.0013	0.9344	0.0232	1.1617	0.0206	1.1453	0.0235	1.5362
28	Al vi	1.5429	0.0427	1.5384	0.0015	0.0720	1.5549	1.5600	0.0773	0.4299	0.0536	0.5706	0.0712	0.5959	0.0820	0.8427
29	Cr	0.0000	0.0094	0.0000	0.0000	0.0000	0.0106	0.0000	0.0000	0.0000	0.0000	0.0000	0.0000	0.0000	0.0000	0.0000
30	Ti	0.0000	0.0000	0.0000	0.0461	0.0109	0.0131	0.0000	0.0000	0.0177	0.0000	0.0186	0.0000	0.0000	0.0000	0.0000
31	Mg	0.5886	1.6389	0.5886	1.7520	1.9494	0.8075	0.7919	0.3779	0.3057	0.4050	0.2749	0.5367	0.3770	0.5477	0.2925
32	Fe 2+	3.1344	5.2182	3.1348	5.0784	4.9163	2.7802	2.8430	6.3853	4.5547	6.4012	4.4177	6.2488	4.3608	6.2473	4.1589
33	Mn	0.0000	0.0000	0.0000	0.0000	0.0000	0.0000	0.0000	0.0000	0.0000	0.0000	0.0000	0.0000	0.0000	0.0000	0.0000
34	Ca	1.7486	0.1038	1.7285	0.1052	0.0524	1.7892	1.8032	0.1210	1.8214	0.1244	1.8679	0.1193	1.8380	0.1232	1.8732
35	Na	0.2080	0.0000	0.2345	0.0000	0.0000	0.3147	0.2630	0.0000	0.1542	0.0000	0.1622	0.0000	0.1325	0.0000	0.2416
36	K	0.0632	0.0000	0.0519	0.0000	0.0000	0.0810	0.0789	0.0000	0.0547	0.0000	0.0873	0.0000	0.0722	0.0000	0.1160
37	SUM	15.2860	15.0130	15.2760	14.9840	15.0010	15.3510	15.3400	14.9820	15.3380	14.9840	15.4000	14.9740	15.3760	14.9800	15.5250
38	Cl	0.0000	0.0000	0.0000	0.0000	0.0000	0.0000	0.0000	0.0000	0.0000	0.0000	0.0000	0.0000	0.0000	0.0000	0.0000
39																
40	Fe/(Fe+Mg)	0.8419	0.7610	0.8424	0.7435	0.7161	0.7749	0.7821	0.9441	0.9371	0.9405	0.9414	0.9209	0.9204	0.9194	0.9343
41	AFM															
42	Al2O3	0.3126	0.0086	0.3191	0.0047	0.0122	0.3250	0.3224	0.0058	0.1231	0.0056	0.1558	0.0067	0.1552	0.0083	0.2109
43	FeO	0.5787	0.7543	0.5812	0.7400	0.7074	0.5231	0.5300	0.9387	0.8218	0.9352	0.7947	0.9147	0.7775	0.9138	0.7373
44	MgO	0.1087	0.2369	0.1088	0.2553	0.2805	0.1519	0.1476	0.0556	0.0552	0.0592	0.0485	0.0786	0.0672	0.0801	0.0519
45	CFM															
46	CaO	0.3196	0.0149	0.3172	0.0152	0.0076	0.3328	0.3316	0.0176	0.2726	0.0179	0.2847	0.0173	0.2795	0.0178	0.2962
47	FeO	0.5728	0.7486	0.5752	0.7323	0.7106	0.5171	0.5228	0.9275	0.8117	0.9236	0.8734	0.9050	0.8632	0.9030	0.6576
48	MgO	0.1076	0.2354	0.1076	0.2526	0.2818	0.1502	0.1456	0.0549	0.0458	0.0584	0.0419	0.0777	0.0573	0.0792	0.0462
49	ACF															
50	Al2O3	0.2363	0.0087	0.2348	0.0048	0.0121	0.2431	0.2413	0.0057	0.0926	0.0055	0.1186	0.0068	0.1169	0.0081	0.1583
51	CaO	0.2440	0.0148	0.2427	0.0151	0.0075	0.2518	0.2516	0.0175	0.2473	0.0179	0.2515	0.0172	0.2466	0.0177	0.2493
52	FeO+MgO	0.5196	0.9765	0.5225	0.9803	0.9805	0.5050	0.5071	0.9766	0.8600	0.9766	0.8319	0.9762	0.8363	0.9762	0.5924
53																

	BM	BN	BO	BP	BQ	BR	BS	BT	BU	BV	BW	BX	BY	BZ	CA	CB
1	date	17-Mar-86	24-Mar-86	24-Mar-86	24-Mar-86	24-Mar-86	24-Mar-86	24-Mar-86	24-Mar-86	24-Mar-86	11-Jan-88	11-Jan-88	11-Jan-88	11-Jan-88	11-Jan-88	11-Jan-88
2	method	eds	eds	eds	eds	eds	eds	eds	eds	eds	wds	wds	wds	wds	wds	wds
3	rock type	5	5	5	5	5	5	5	5	5	7	7	7	7	8	8
4	mineral	grun	hbl	hbl	act	grun	grun	hbl	grun	hbl	hbl	hbl	hbl	hbl	hbl	hbl
5	study area	a	a	a	a	a	a	a	a	a	a	a	a	a	a	a
6																
7	sample	5PLA122	5PLA122	5PLA122	5PLA122	5PLA122	5PLA122	5PLA122	5PLA122	5PLA122	5PLA062	5PLA062	5PLA062	5PLA062	5PLA010	5PLA010
8	PTS area	circ 1	circ 1	circ 1	circ 1	circ 1	circ 2	circ 2	circ 2	circ 2	aver.		aver.	aver.	aver.	aver.
9	analysis	grun 1	hbl 1	hbl 2	act 1	grun 2	grun 1	hbl 1	grun 2	hbl 2	hbl 1	hbl 1.2	hbl 2	hbl 2.1	hbl 1	hbl 2
10																
11	SiO2	48.796	42.084	40.323	50.765	49.301	48.721	40.510	48.578	40.271	41.869	44.889	39.686	43.264	40.845	40.160
12	Al2O3	0.484	12.036	15.590	0.163	0.445	0.546	14.580	0.518	14.738	11.872	7.399	16.771	12.896	13.724	15.854
13	Cr2O3	0.000	0.000	0.000	0.000	0.000	0.085	0.000	0.000	0.000	n.a.	n.a.	n.a.	n.a.	n.a.	n.a.
14	TiO2	0.000	0.282	0.134	0.000	0.000	0.144	0.246	0.000	0.245	0.117	0.147	0.067	0.115	0.070	0.089
15	MgO	4.741	2.652	2.173	3.841	4.745	3.295	1.555	3.215	1.544	1.736	2.291	1.233	1.377	0.617	0.580
16	FeO	42.676	27.936	26.985	31.620	42.227	43.904	27.776	43.889	28.133	30.432	31.937	28.551	29.146	31.186	29.809
17	MnO	0.067	0.000	0.000	0.000	0.100	0.100	0.000	0.068	0.000	n.a.	n.a.	n.a.	n.a.	n.a.	n.a.
18	CaO	0.524	11.068	11.116	11.268	0.615	0.481	10.734	0.491	10.765	11.913	11.739	11.791	11.627	11.950	12.089
19	Na2O	0.000	0.486	0.587	0.000	0.000	0.000	0.583	0.000	0.496	0.425	0.239	0.486	0.427	0.512	0.456
20	K2O	0.000	0.350	0.451	0.000	0.000	0.000	0.367	0.000	0.384	0.253	0.144	0.309	0.291	0.381	0.400
21	Cl	0.000	0.000	0.000	0.000	0.000	0.000	0.000	0.000	0.000	n.a.	n.a.	n.a.	n.a.	n.a.	n.a.
22	TOTAL	96.490	97.485	97.360	97.660	97.430	97.370	96.330	96.760	96.580	96.619	96.785	98.674	99.145	99.045	99.417
23	O based on anhyrous O+Cl=23															
24		23.0000	23.0000	23.0000	23.0000	23.0000	23.0000	23.0000	23.0000	23.0000	23.0000	23.0000	23.0000	23.0000	23.0000	23.0000
25	cations based on 23O															
26	Si	7.0539	6.5919	6.3097	7.0937	7.0580	7.0505	6.4266	7.0718	6.3653	6.5631	6.9865	6.1597	6.6765	6.3650	6.2450
27	Al iv	0.0461	1.4081	1.6903	0.0063	0.0440	0.0495	1.5734	0.0282	1.6147	1.4169	1.0135	1.8403	1.3215	1.5850	1.7550
28	Al vi	0.0450	0.9260	1.1849	0.0240	0.0406	0.0554	1.1489	0.0721	1.1394	0.7033	0.4393	1.2297	1.0253	0.9402	1.1510
29	Cr	0.0000	0.0000	0.0000	0.0000	0.0000	0.0123	0.0000	0.0000	0.0000	0.0000	0.0000	0.0000	0.0000	0.0000	0.0000
30	Ti	0.0000	0.0332	0.0158	0.0000	0.0000	0.0177	0.0293	0.0000	0.0293	0.0137	0.0175	0.0079	0.0134	0.0085	0.0103
31	Mg	1.1287	0.6196	0.5067	0.8014	1.1414	0.8014	0.3677	0.7864	0.3648	0.4072	0.5373	0.2855	0.3172	0.1447	0.1346
32	Fe 2+	5.7274	3.6812	3.5313	4.1640	5.6990	5.9916	3.6851	6.0233	3.7305	4.0014	4.2048	3.7083	3.7032	4.1014	3.8766
33	Mn	0.0090	0.0000	0.0000	0.0000	0.0137	0.0134	0.0000	0.0094	0.0000	0.0000	0.0000	0.0000	0.0000	0.0000	0.0000
34	Ca	0.0897	1.8584	1.8637	1.9010	0.1064	0.0805	1.8246	0.0864	1.8267	2.0068	1.9796	1.9624	1.9229	2.0148	2.0108
35	Na	0.0000	0.1476	0.1781	0.0000	0.0000	0.0000	0.1793	0.0000	0.1526	0.1304	0.0738	0.1456	0.1260	0.1569	0.1383
36	K	0.0000	0.0701	0.0901	0.0000	0.0000	0.0000	0.0743	0.0000	0.0778	0.0510	0.0284	0.0610	0.0575	0.0718	0.0705
37	SUM	15.0000	15.3186	15.3710	14.9900	15.0010	14.9720	15.3090	14.9780	15.3230	15.3938	15.2607	15.4010	15.2275	15.4384	15.4003
38	Cl	0.0000	0.0000	0.0000	0.0000	0.0000	0.0000	0.0000	0.0000	0.0000	0.0000	0.0000	0.0000	0.0000	0.0000	0.0000
39																
40	Fe/(Fe+Mg)	0.8354	0.8553	0.8745	0.8229	0.8331	0.8820	0.9093	0.8845	0.9109	0.9076	0.8867	0.9265	0.9223	0.9659	0.9664
41	AFM															
42	Al2O3	0.0096	0.2142	0.2825	0.0030	0.0081	0.0077	0.2514	0.0073	0.2516	0.1997	0.1264	0.2776	0.2233	0.2306	0.2650
43	FeO	0.8299	0.6720	0.6448	0.8196	0.8260	0.8753	0.6907	0.8781	0.6817	0.7264	0.7746	0.6707	0.7163	0.7432	0.7095
44	MgO	0.1635	0.1137	0.0925	0.1774	0.1658	0.1171	0.0878	0.1146	0.0867	0.0739	0.0990	0.0516	0.0604	0.0262	0.0246
45	CFM															
46	CaO	0.0129	0.3027	0.3156	0.2729	0.0153	0.0117	0.3104	0.0125	0.3087	0.3128	0.2945	0.3295	0.3293	0.3218	0.3339
47	FeO	0.8246	0.5864	0.5877	0.8204	0.8717	0.8270	0.8734	0.8297	0.8255	0.8226	0.8269	0.8269	0.8551	0.8438
48	MgO	0.1625	0.1009	0.0859	0.1294	0.1643	0.1198	0.0826	0.1148	0.0818	0.0835	0.0789	0.0479	0.0526	0.0231	0.0224
49	ACF															
50	Al2O3	0.0085	0.1597	0.1859	0.0022	0.0081	0.0076	0.1880	0.0072	0.1886	0.1464	0.0927	0.2048	0.1635	0.1869	0.1944
51	CaO	0.0120	0.2544	0.2539	0.2723	0.0152	0.0118	0.2521	0.0124	0.2585	0.2670	0.2672	0.2629	0.2679	0.2674	0.2690
52	FeO+MgO	0.9807	0.5836	0.5502	0.7255	0.9787	0.9668	0.5599	0.9803	0.5409	0.5866	0.6401	0.5331	0.5866	0.5638	0.5366
53																

	CC	CD	CE	CF	CG	CH	CI	CJ	CK	CL	CM	CN	CO	CP	CQ	CR
1	date	11-Jan-88	11-Jan-88	11-Jan-88	11-Jan-88	11-Jan-88	11-Jan-88	11-Jan-88	11-Jan-88	11-Jan-88	11-Jan-88	11-Jan-88	11-Jan-88	11-Jan-88	11-Jan-88	11-Jan-88	11-Jan-88
2	method	wds	wds	wds	wds	wds	wds	wds	wds	wds	wds	wds	wds	wds	wds	wds	wds
3	rock type	8	8	8	8	8	8	8	7	7	7	7	7	7	7	7	7
4	mineral	act	act	act	hbl	hbl	act	hbl	hbl	hbl	hbl	hbl	hbl	hbl	hbl	hbl	hbl
5	study area	a	a	a	a	a	a	a	a	a	a	a	a	a	a	a	a
6		"hbl 3"	"hbl 4"	"hbl 5"			"hbl 6"										
7	sample	SPLA010	SPLA010	SPLA010	SPLA010	SPLA010	SPLA010	SPLA010	SPLA017	SPLA017	SPLA017	SPLA017	SPLA017	SPLA017	SPLA017	SPLA017	SPLA017
8	PTS area	aver.	aver.	aver.	aver.	aver.	aver.		aver.	aver.	aver.	aver.		aver.	aver.	aver.	aver.
9	analysis	act 3	act 4	act 5	hbl 6	hbl 7	act 8	hbl 6.1	hbl 1	hbl 2	hbl 2.1	hbl 3	hbl 3.1	hbl 4	hbl 5	hbl 6	
10																	
11	SiO2	48.250	47.580	48.424	48.739	47.202	48.665	48.347	40.354	41.084	43.299	41.178	41.715	42.885	41.253	42.233	
12	Al2O3	3.056	2.611	1.287	3.660	3.435	0.891	3.697	17.963	16.265	11.449	16.634	11.382	13.941	15.637	13.065	
13	Cr2O3	n.a.	n.a.	n.a.	n.a.	n.a.	n.a.	n.a.	n.a.	n.a.	n.a.	n.a.	n.a.	n.a.	n.a.	n.a.	
14	TiO2	0.070	0.087	0.033	0.152	0.104	0.021	0.097	0.101	0.184	0.231	0.142	0.236	0.206	0.206	0.192	
15	MgO	1.334	0.941	0.913	0.860	0.921	0.673	0.877	2.586	2.900	3.524	2.669	2.170	3.414	3.315	3.666	
16	FeO	35.191	36.248	36.880	36.154	36.042	37.211	36.396	25.292	25.686	27.434	25.140	29.716	26.143	25.843	26.421	
17	MnO	n.a.	n.a.	n.a.	n.a.	n.a.	n.a.	n.a.	n.a.	n.a.	n.a.	n.a.	n.a.	n.a.	n.a.	n.a.	
18	CaO	11.460	11.335	11.428	11.177	11.286	11.425	11.206	11.921	11.837	11.618	11.864	11.634	11.736	11.796	11.639	
19	Na2O	0.153	0.111	0.024	0.210	0.120	0.000	0.222	0.566	0.579	0.464	0.631	0.587	0.552	0.561	0.515	
20	K2O	0.030	0.026	0.007	0.052	0.040	0.000	0.040	0.220	0.290	0.271	0.258	0.828	0.240	0.250	0.224	
21	Cl	n.a.	n.a.	n.a.	n.a.	n.a.	n.a.	n.a.	n.a.	n.a.	n.a.	n.a.	n.a.	n.a.	n.a.	n.a.	
22	TOTAL	99.544	98.939	99.986	99.004	99.152	98.886	98.882	98.705	98.797	98.290	98.537	98.280	98.899	98.663	98.097	
23	O based on anhydrous O+Cl=23																
24		23.0000	23.0000	23.0000	23.0000	23.0000	23.0000	23.0000	23.0000	23.0000	23.0000	23.0000	23.0000	23.0000	23.0000	23.0000	
25	cations based on 23O																
26	Si	7.6071	7.6052	7.7531	7.4686	7.5193	7.6108	7.4350	6.1564	6.2605	6.7060	6.2827	6.5901	6.5197	6.3170	6.5315	
27	Al iv	0.3929	0.3948	0.2431	0.5302	0.4807	0.1885	0.5650	1.8436	1.7195	1.2920	1.7073	1.4089	1.4803	1.6830	1.4685	
28	Al vi	0.1749	0.0970	0.0000	0.1593	0.1645	0.0000	0.1342	1.3864	1.2130	0.7988	1.2868	0.7115	1.0309	1.1385	0.9024	
29	Cr	0.0000	0.0000	0.0000	0.0000	0.0000	0.0000	0.0000	0.0000	0.0000	0.0000	0.0000	0.0000	0.0000	0.0000	0.0000	
30	Ti	0.0085	0.0106	0.0038	0.0182	0.0124	0.0024	0.0118	0.0115	0.0188	0.0270	0.0165	0.0285	0.0239	0.0238	0.0223	
31	Mg	0.3136	0.2236	0.2174	0.2046	0.2183	0.1611	0.2101	0.5878	0.6606	0.8137	0.6125	0.5107	0.7778	0.7564	0.8512	
32	Fe 2+	4.6404	4.8457	4.9385	4.6326	4.8016	4.9950	4.8834	3.2268	3.2875	3.5544	3.2132	3.9263	3.3416	3.2841	3.4170	
33	Mn	0.0000	0.0000	0.0000	0.0000	0.0000	0.0000	0.0000	0.0000	0.0000	0.0000	0.0000	0.0000	0.0000	0.0000	0.0000	
34	Ca	1.9365	1.9412	1.9606	1.9140	1.9270	1.9646	1.9260	1.8995	1.9402	1.9269	1.9431	1.9696	1.9219	1.9351	1.9263	
35	Na	0.0474	0.0346	0.0077	0.0653	0.0384	0.0000	0.0694	0.1687	0.1709	0.1396	0.1873	0.1804	0.1635	0.1875	0.1543	
36	K	0.0057	0.0058	0.0019	0.0115	0.0077	0.0000	0.0077	0.0422	0.0570	0.0540	0.0496	0.1671	0.0459	0.0497	0.0446	
37	SUM	15.1270	15.1587	15.1263	15.2055	15.1679	15.1024	15.2424	15.3228	15.3482	15.3165	15.3110	15.4843	15.3055	15.3562	15.3601	
38	Cl	0.0000	0.0000	0.0000	0.0000	0.0000	0.0000	0.0000	0.0000	0.0000	0.0000	0.0000	0.0000	0.0000	0.0000	0.0000	
39																	
40	Fe/(Fe+Mg)	0.9367	0.9559	0.9578	0.9594	0.9565	0.9666	0.9586	0.8488	0.8326	0.8137	0.8399	0.8849	0.8112	0.8128	0.7931	
41	AFM																
42	Al2O3	0.0542	0.0463	0.0230	0.0641	0.0604	0.0161	0.0642	0.2974	0.2706	0.1931	0.2814	0.1929	0.2336	0.2588	0.2158	
43	FeO	0.8858	0.9116	0.9358	0.8979	0.8986	0.9532	0.8972	0.5843	0.6072	0.6566	0.6036	0.7142	0.6217	0.6024	0.6220	
44	MgO	0.0599	0.0421	0.0412	0.0380	0.0409	0.0307	0.0386	0.1082	0.1220	0.1503	0.1151	0.0929	0.1447	0.1387	0.1622	
45	CFM																
46	CaO	0.2810	0.2769	0.2755	0.2753	0.2774	0.2759	0.2744	0.3324	0.3285	0.3063	0.3368	0.3075	0.3181	0.3238	0.3092	
47	FeO	0.6734	0.6912	0.6938	0.6852	0.6912	0.7015	0.6957	0.5647	0.5583	0.5645	0.5570	0.6126	0.5531	0.5486	0.5478	
48	MgO	0.0455	0.0319	0.0305	0.0294	0.0314	0.0226	0.0299	0.1028	0.1122	0.1292	0.1062	0.0797	0.1287	0.1266	0.1429	
49	ACF																
50	Al2O3	0.0386	0.0339	0.0166	0.0475	0.0444	0.0117	0.0474	0.2204	0.1994	0.1424	0.2081	0.1420	0.1721	0.1910	0.1597	
51	CaO	0.2689	0.2675	0.2709	0.2623	0.2651	0.2727	0.2614	0.2592	0.2636	0.2627	0.2674	0.2636	0.2634	0.2626	0.2598	
52	FeO+MgO	0.6905	0.6986	0.7123	0.6904	0.6905	0.7156	0.6912	0.5205	0.5368	0.5949	0.5265	0.5942	0.5845	0.5470	0.5805	
53																	

	CS	CT	CU	CV	CW	CX	CY	CZ	DA	DB	DC	DD	DE	DF	DG	DH
1	date	11-Jan-88	11-Jan-88	11-Jan-88	11-Jan-88	11-Jan-88	11-Jan-88	11-Jan-88	11-Jan-88	11-Jan-88	11-Jan-88	11-Jan-88	11-Jan-88	11-Jan-88	11-Jan-88	11-Jan-88
2	method	wds	wds	wds	wds	wds	wds	wds	wds	wds	wds	wds	wds	wds	wds	wds
3	rock type	7	8	8	8	8	8	8	8	8	8	8	7	7	7	7
4	mineral	hbl	hbl	hbl	hbl	hbl	hbl	hbl	hbl	hbl	hbl	hbl	hbl	hbl	hbl	hbl
5	study area	a	a	a	a	a	a	a	a	a	a	a	a	a	a	a
6																
7	sample	5PLA017	5PLA020	5PLA020	5PLA020	5PLA020	5PLA020	5PLA020	5PLA020	5PLA020	5PLA020	5PLA020	5PLA024	5PLA024	5PLA024	5PLA024
8	PTS area	aver.	aver.	aver.	aver.		aver.	aver.	aver.	aver.	aver.	aver.		aver.	aver.	aver.
9	analysis	hbl 7	hbl 1	hbl 2	hbl 3	hbl 3.1	hbl 4	hbl 5	hbl 6	hbl 7	hbl 8	hbl 9	hbl 1.1	hbl 1	hbl 2	hbl 3
10																
11	SiO2	41.650	41.744	41.272	41.955	42.718	41.553	42.550	40.511	39.685	41.029	42.999	42.107	45.583	41.012	42.077
12	Al2O3	15.466	14.874	15.014	14.638	12.436	14.960	13.261	16.061	17.671	15.102	13.365	12.588	7.389	15.773	14.465
13	Cr2O3	n.a	n.a	n.a	n.a	n.a	n.a	n.a	n.a	n.a	n.a	n.a	n.a	n.a	n.a	n.a
14	TiO2	0.174	0.109	0.163	0.185	0.158	0.155	0.156	0.085	0.082	0.149	0.197	0.107	0.150	0.164	0.173
15	MgO	3.324	2.898	2.853	2.561	2.789	2.696	3.089	2.032	1.885	2.673	2.766	2.567	3.577	2.354	2.571
16	FeO	26.126	26.462	26.991	26.777	26.399	26.578	27.962	27.197	26.139	26.890	26.031	26.399	29.710	26.917	27.189
17	MnO	n.a	n.a	n.a	n.a	n.a	n.a	n.a	n.a	n.a	n.a	n.a	n.a	n.a	n.a	n.a
18	CaO	11.356	11.621	11.506	11.663	11.199	11.638	11.287	11.764	11.881	11.781	11.276	12.087	11.940	12.035	12.050
19	Na2O	0.545	0.528	0.560	0.588	0.471	0.563	0.521	0.589	0.522	0.539	0.478	0.510	0.341	0.535	0.525
20	K2O	0.231	0.246	0.185	0.200	0.256	0.253	0.244	0.141	0.439	0.202	0.259	0.247	0.123	0.259	0.261
21	Cl	n.a	n.a	n.a	n.a	n.a	n.a	n.a	n.a	n.a	n.a	n.a	n.a	n.a	n.a	n.a
22	TOTAL	98.874	98.704	98.544	98.847	98.426	98.596	99.070	98.360	98.504	98.965	99.372	98.632	98.813	99.049	99.321
23	O based on anhyrous O+Cl=23															
24		23.0000	23.0000	23.0000	23.0000	23.0000	23.0000	23.0000	23.0000	23.0000	23.0000	23.0000	23.0000	23.0000	23.0000	23.0000
25	cations based on 23O															
26	Si	6.3627	6.4115	6.3641	6.4443	6.6266	6.3855	6.5446	6.2714	6.1143	6.3860	6.5846	6.5507	7.0818	6.2989	6.4449
27	Al iv	1.6373	1.5885	1.6359	1.5557	1.3704	1.6045	1.4554	1.7286	1.8857	1.6140	1.4152	1.4493	0.9182	1.7011	1.5551
28	Al vi	1.1477	1.1040	1.0931	1.0845	0.9051	1.1097	0.9526	1.2024	1.3505	1.1169	0.9868	0.8581	0.4467	1.1544	1.0569
29	Cr	0.0000	0.0000	0.0000	0.0000	0.0000	0.0000	0.0000	0.0000	0.0000	0.0000	0.0000	0.0000	0.0000	0.0000	0.0000
30	Ti	0.0202	0.0125	0.0190	0.0212	0.0187	0.0180	0.0180	0.0098	0.0097	0.0171	0.0225	0.0126	0.0178	0.0189	0.0198
31	Mg	0.7564	0.6636	0.6580	0.5861	0.6453	0.6187	0.7034	0.4689	0.4333	0.6111	0.6312	0.6001	0.8292	0.5380	0.5872
32	Fe 2+	3.3378	3.4019	3.4811	3.4400	3.6864	3.4211	3.5972	3.5211	3.3680	3.4502	3.5896	3.6853	3.8656	3.4573	3.4845
33	Mn	0.0000	0.0000	0.0000	0.0000	0.0000	0.0000	0.0000	0.0000	0.0000	0.0000	0.0000	0.0000	0.0000	0.0000	0.0000
34	Ca	1.8588	1.9455	1.9013	1.9521	1.8623	1.9524	1.8605	1.9517	1.9617	1.9366	1.8509	2.0145	1.9903	1.9806	1.9779
35	Na	0.1610	0.1568	0.1666	0.1754	0.1418	0.1683	0.1553	0.1712	0.1555	0.1604	0.1417	0.1533	0.1028	0.1567	0.1565
36	K	0.0459	0.0480	0.0371	0.0554	0.0504	0.0499	0.0481	0.0279	0.0870	0.0397	0.0497	0.0486	0.0243	0.0496	0.0515
37	SUM	15.3282	15.3324	15.3544	15.3247	15.3100	15.3381	15.3351	15.3530	15.3747	15.3310	15.2821	15.3635	15.2787	15.3587	15.3337
38	Cl	0.0000	0.0000	0.0000	0.0000	0.0000	0.0000	0.0000	0.0000	0.0000	0.0000	0.0000	0.0000	0.0000	0.0000	0.0000
39																
40	Fe/(Fe+Mg)	0.8152	0.8368	0.8414	0.8544	0.8510	0.8468	0.8364	0.8825	0.8860	0.8495	0.8505	0.8603	0.8234	0.8651	0.8558
41	AFM															
42	Al2O3	0.2538	0.2488	0.2480	0.2476	0.2080	0.2515	0.2187	0.2668	0.2882	0.2516	0.2222	0.2118	0.1261	0.2632	0.2428
43	FeO	0.6063	0.6286	0.6327	0.6428	0.6740	0.6339	0.6535	0.6454	0.6210	0.6358	0.6615	0.6781	0.7195	0.6374	0.6480
44	MgO	0.1379	0.1226	0.1192	0.1095	0.1180	0.1146	0.1278	0.0858	0.0799	0.1126	0.1183	0.1101	0.1543	0.0994	0.1092
45	CFM															
46	CaO	0.3123	0.3237	0.3148	0.3265	0.3007	0.3256	0.3020	0.3265	0.3404	0.3229	0.3048	0.3193	0.2977	0.3314	0.3260
47	FeO	0.5607	0.5650	0.5765	0.5754	0.5852	0.5709	0.5839	0.5826	0.5844	0.5752	0.5812	0.5856	0.5782	0.5784	0.5766
48	MgO	0.1271	0.1104	0.1086	0.0980	0.1042	0.1033	0.1142	0.0788	0.0752	0.1018	0.1048	0.0951	0.1240	0.0902	0.0971
49	ACF															
50	Al2O3	0.1696	0.1630	0.1643	0.1614	0.1552	0.1647	0.1635	0.1978	0.2187	0.1854	0.1657	0.1548	0.0920	0.1928	0.1775
51	CaO	0.2531	0.2644	0.2586	0.2673	0.2540	0.2657	0.2526	0.2635	0.2656	0.2630	0.2543	0.2699	0.2703	0.2675	0.2680
52	FeO+MgO	0.5574	0.5526	0.5586	0.5513	0.5906	0.5497	0.5839	0.5387	0.5147	0.5516	0.5800	0.5755	0.6377	0.5387	0.5536
53																

	DI	DJ	DK	DL	DM	DN	DO	DP	DQ	DR	DS	DT	DU	DV	DW	DX
1	date	11-Jan-88	11-Jan-88	11-Jan-88	11-Jan-88	11-Jan-88	1-Mar-88	1-Mar-88	1-Mar-88	1-Mar-88	1-Mar-88	1-Mar-88	1-Mar-88	1-Mar-88	1-Mar-88	30-Oct-88	30-Oct-88
2	method	wds	wds	wds	wds	wds	eds	eds	eds	eds	eds	eds	eds	eds	eds	eds	eds
3	rock type	7	7	7	7	7	7	7	7	7	7	7	7	7	7	7	7
4	mineral	hbl	hbl	hbl	hbl	hbl	grun	hbl	grun	hbl	grun	hbl	grun	hbl	grun	hbl	hbl
5	study area	a	a	a	a	a	b	b	b	b	b	b	b	b	b	b	b
6															rerun	rerun	
7	sample	5PLA024	5PLA024	5PLA024	5PLA024	5PLA024	4PLB026c	4PLB026c	4PLB026c	4PLB026c	4PLB026c	4PLB026c	4PLB026c	4PLB026c	4PLB026c	4PLB033	4PLB033
8	PTS area	aver.	aver.	aver.	aver.	aver.	area 2	area 2	area 2	area 2	circ 1	circ 1	circ 1	circ 1	circ 1	circ 2	circ 2
9	analysis	hbl 4	hbl 5	hbl 6	hbl 7	hbl 8	grun 1	hbl 1	grun 2	hbl 2	grun 2	hbl 2	grun 3	hbl 3	grun 2	hbl 1	
10																	
11	SiO2	41.995	40.562	41.617	41.187	41.010	46.779	41.450	46.662	41.779	46.836	40.208	46.706	41.074	46.745	41.244	
12	Al2O3	14.697	15.444	15.093	15.237	14.875	9.436	11.271	9.585	10.648	9.406	12.947	9.331	11.575	9.246	11.064	
13	Cr2O3	n.a.	n.a.	n.a.	n.a.	n.a.	0.108	0.000	0.000	0.000	0.000	0.000	0.000	0.000	0.000	0.000	
14	TiO2	0.157	0.143	0.161	0.189	0.201	0.104	0.000	0.000	0.000	0.099	0.000	0.000	0.000	0.000	0.000	
15	MgO	2.614	2.659	2.725	2.647	2.984	2.325	1.473	2.489	1.550	2.381	1.245	2.395	1.421	2.573	1.511	
16	FeO	27.075	27.447	27.350	26.794	26.943	46.187	31.322	45.520	31.851	45.748	31.021	45.692	31.486	45.859	32.884	
17	MnO	n.a.	n.a.	n.a.	n.a.	n.a.	0.190	0.000	0.173	0.000	0.262	0.000	0.192	0.000	0.214	0.000	
18	CaO	11.985	11.521	11.587	11.929	11.728	9.458	10.570	9.575	10.105	9.492	10.763	9.404	10.453	9.386	9.281	
19	Na2O	0.526	0.516	0.531	0.536	0.536	0.000	0.915	0.000	0.912	0.000	1.025	0.000	1.015	0.000	0.662	
20	K2O	0.237	0.252	0.248	0.259	0.234	0.000	0.329	0.000	0.365	0.000	0.448	0.000	0.350	0.000	0.466	
21	Cl	n.a.	n.a.	n.a.	n.a.	n.a.	0.000	0.000	0.000	0.000	0.000	0.000	0.000	0.000	0.000	0.000	
22	TOTAL	99.288	98.564	99.322	98.895	98.613	98.590	97.330	98.000	97.210	98.220	97.660	97.720	97.370	98.840	98.930	
23	O based on anhyrous O+Cl=23																
24		23.0000	23.0000	23.0000	23.0000	23.0000	23.0000	23.0000	23.0000	23.0000	23.0000	23.0000	23.0000	23.0000	23.0000	23.0000	
25	cations based on 23O																
26	Si	6.4284	6.2810	6.3730	6.3300	6.3299	7.9366	6.6370	7.9433	6.7087	7.9805	6.4249	7.9602	6.5847	8.0258	6.6552	
27	Al iv	1.5706	1.7190	1.6270	1.6700	1.6701	0.0634	1.3630	0.0567	1.2933	0.0395	1.5751	0.0398	1.4153	0.0000	1.3448	
28	Al vi	1.0815	1.0984	1.0973	1.0902	1.0542	0.0202	0.7849	0.0558	0.7211	0.0363	0.8631	0.0441	0.7716	0.0468	0.7592	
29	Cr	0.0000	0.0000	0.0000	0.0000	0.0000	0.0139	0.0000	0.0000	0.0000	0.0000	0.0000	0.0000	0.0000	0.0000	0.0000	
30	Ti	0.0179	0.0167	0.0184	0.0231	0.0232	0.0127	0.0000	0.0000	0.0000	0.0121	0.0000	0.0000	0.0000	0.0000	0.0000	
31	Mg	0.5962	0.6129	0.6220	0.6520	0.6863	0.5638	0.3517	0.6055	0.3710	0.5785	0.2964	0.5848	0.3395	0.6187	0.3634	
32	Fe 2+	3.4666	3.5528	3.5030	3.4326	3.4780	6.2846	4.1943	6.2140	4.2780	6.2365	4.1455	6.2609	4.2213	6.1607	4.4105	
33	Mn	0.0000	0.0000	0.0000	0.0000	0.0000	0.0262	0.0000	0.0240	0.0000	0.0361	0.0000	0.0266	0.0000	0.0292	0.0000	
34	Ca	1.9633	1.9103	1.9029	1.9644	1.9393	0.0798	1.6123	0.1008	1.7380	0.0860	1.8461	0.0710	1.7955	0.0687	1.6046	
35	Na	0.1564	0.1544	0.1563	0.1589	0.1614	0.0000	0.2840	0.0000	0.2840	0.0000	0.3178	0.0000	0.3135	0.0000	0.2134	
36	K	0.0460	0.0502	0.0478	0.0499	0.0464	0.0000	0.0671	0.0000	0.0747	0.0000	0.0913	0.0000	0.0716	0.0000	0.0958	
37	SUM	15.3279	15.3957	15.3497	15.3713	15.3868	15.0010	15.4740	15.0000	15.4650	14.8880	15.5800	14.9870	15.5150	14.9500	15.4470	
38	Cl	0.0000	0.0000	0.0000	0.0000	0.0000	0.0000	0.0000	0.0000	0.0000	0.0000	0.0000	0.0000	0.0000	0.0000	0.0000	
39																	
40	Fe/(Fe+Mg)	0.8533	0.8529	0.8492	0.8404	0.8352	0.9177	0.9226	0.9112	0.9202	0.9151	0.9333	0.9148	0.9256	0.9087	0.9239	
41	AFM																
42	Al2O3	0.2481	0.2527	0.2482	0.2525	0.2465											
43	FeO	0.6433	0.6373	0.6384	0.6282	0.6293	0.0061	0.1896	0.0082	0.1781	0.0057	0.2154	0.0046	0.1934	0.0034	0.1806	
44	MgO	0.1106	0.1099	0.1134	0.1193	0.1242	0.9121	0.7477	0.9036	0.7563	0.9099	0.7323	0.9103	0.7466	0.9056	0.7571	
45	CFM						0.0818	0.0627	0.0881	0.0656	0.0844	0.0524	0.0850	0.0600	0.0909	0.0624	
46	CaO	0.3258	0.3144	0.3197	0.3247	0.3177											
47	FeO	0.5753	0.5847	0.5811	0.5675	0.5688	0.0115	0.2851	0.0145	0.2722	0.0125	0.2936	0.0103	0.2825	0.0100	0.2516	
48	MgO	0.0989	0.1009	0.1032	0.1078	0.1124	0.9071	0.6596	0.8980	0.6697	0.9037	0.6593	0.9052	0.6641	0.8896	0.6915	
49	ACF						0.0814	0.0553	0.0675	0.0581	0.0638	0.0471	0.0645	0.0534	0.0803	0.0570	
50	Al2O3	0.1604	0.1662	0.1643	0.1658	0.1625											
51	CaO	0.2670	0.2552	0.2575	0.2644	0.2596	0.0060	0.1433	0.0081	0.1363	0.0056	0.1624	0.0046	0.1468	0.0034	0.1416	
52	FeO+MgO	0.5526	0.5566	0.5582	0.5498	0.5578	0.0114	0.2443	0.0144	0.2351	0.0124	0.2459	0.0102	0.2410	0.0100	0.2158	
53							0.9826	0.8124	0.9775	0.8286	0.9820	0.9917	0.9852	0.8122	0.9866	0.8425	

	DY	DZ	EA	EB	EC	ED	EE	EF	EG	EH	EI	EJ	EK	EL	EM	EN
1	date	30-Oct-86	30-Oct-86	12-Feb-86	12-Feb-86	12-Feb-86	12-Feb-86	12-Feb-86	12-Feb-86	12-Feb-86	12-Feb-86	12-Feb-86	12-Feb-86	12-Feb-86	12-Feb-86	12-Feb-86
2	method	eds	eds	eds	eds	eds	eds	eds	eds	eds	eds	eds	eds	eds	eds	eds
3	rock type	7	7	5	5	5	5	5	5	5	5	6	6	6	6	3
4	mineral	grun	grun	grun	hbl	grun	hbl	grun	hbl	grun	hbl	grun	hbl	grun	hbl	grun
5	study area	b	b	b	b	b	b	b	b	b	b	b	b	b	b	b
6		rerun	rerun													
7	sample	4PLB033	4PLB033	5PLB004	5PLB004	5PLB004	5PLB004	5PLB004	5PLB004	5PLB004	5PLB004	5PLB005	5PLB005	5PLB005	5PLB005	5PLB006
8	PTS area	circ 1	circ 1	circ 1	circ 1	circ 1	circ 1	circ 3	circ 3	circ 3	circ 3	circ 1	circ 1	circ 1	circ 1	circ 1
9	analysis	grun 1	grun 2	grun 1	hbl 1	grun 2	hbl 2	grun 1	hbl 1	grun 2	hbl 2	grun 1	hbl 1	grun 2	hbl 2	grun 1
10																
11	SiO2	48 927	48 945	48 851	39 182	48 055	39 446	48 145	39 876	48 884	40 074	48 215	40 211	48 233	40 334	48 233
12	Al2O3	0 133	0 153	0 375	15 178	0 325	14 446	0 406	14 922	0 357	13 857	0 252	11 496	0 366	11 883	0 456
13	Cr2O3	0 000	0 000	0 000	0 000	0 000	0 000	0 000	0 000	0 000	0 000	0 000	0 000	0 000	0 000	0 000
14	TiO2	0 000	0 000	0 000	0 129	0 000	0 088	0 000	0 145	0 000	0 131	0 000	0 000	0 000	0 000	0 000
15	MgO	2 511	2 581	2 852	1 306	2 955	1 320	3 025	1 353	3 045	1 448	1 010	0 632	1 044	0 765	3 981
16	FeO	46 581	46 421	45 766	28 788	45 646	28 945	46 031	29 196	45 510	29 458	46 423	32 730	46 132	32 618	44 757
17	MnO	0 158	0 225	0 000	0 000	0 000	0 000	0 000	0 000	0 000	0 000	0 000	0 000	0 000	0 000	0 000
18	CaO	0 378	0 372	0 382	11 002	0 361	10 862	0 375	10 866	0 386	10 803	0 488	10 862	0 801	11 070	0 387
19	Na2O	0 000	0 000	0 000	0 937	0 000	1 001	0 000	1 007	0 000	1 102	0 000	0 859	0 000	0 943	0 000
20	K2O	0 000	0 000	0 000	0 436	0 000	0 448	0 000	0 437	0 000	0 447	0 000	0 398	0 000	0 441	0 000
21	Cl	0 000	0 000	0 000	0 000	0 000	0 000	0 000	0 000	0 000	0 000	0 000	0 000	0 000	0 000	0 000
22	TOTAL	99 700	99 719	98 230	96 980	97 840	96 680	98 980	97 810	97 980	97 420	98 390	97 310	96 380	97 860	98 830
23	O based on anhyrous O+Cl=23															
24		23 0000	23 0000	23 0000	23 0000	23 0000	23 0000	23 0000	23 0000	23 0000	23 0000	23 0000	23 0000	23 0000	23 0000	23 0000
25	cations based on 23O															
26	Si	8 0112	8 0088	7 9516	6 2415	7 8448	6 3101	7 9366	6 2909	7 9410	6 3708	7 9549	6 5186	7 9465	6 4903	7 9142
27	Al iv	0 0000	0 0000	0 0484	1 7585	0 0551	1 6899	0 0634	1 7091	0 0590	1 6292	0 0451	1 4831	0 0515	1 5037	0 0858
28	Al vi	0 0252	0 0288	0 0238	1 0806	0 0074	1 0337	0 0143	1 0652	0 0097	0 0671	0 0038	0 7128	0 0186	0 7141	0 0000
29	Cr	0 0000	0 0000	0 0000	0 0000	0 0000	0 0000	0 0000	0 0000	0 0000	0 0000	0 0000	0 0000	0 0000	0 0000	0 0000
30	Ti	0 0000	0 0000	0 0000	0 0154	0 0000	0 0118	0 0000	0 0172	0 0000	0 0156	0 0000	0 0000	0 0000	0 0000	0 0000
31	Mg	0 0006	0 0182	0 0810	0 3100	0 7192	0 3148	0 7261	0 3182	0 7402	0 3434	0 2483	0 1527	0 2564	0 1837	0 9563
32	Fe 2+	6 2521	6 2251	6 2290	3 8351	6 2335	3 8723	6 2168	3 8521	6 2068	3 9186	6 8814	4 4381	6 8334	4 3837	6 0168
33	Mn	0 0216	0 0305	0 0000	0 0000	0 0000	0 0000	0 0000	0 0000	0 0000	0 0000	0 0000	0 0000	0 0000	0 0000	0 0000
34	Ca	0 0650	0 0639	0 0666	1 8777	0 0632	1 8822	0 0650	1 8535	0 0675	1 8572	0 8603	1 8068	0 1000	1 9102	0 0983
35	Na	0 0000	0 0000	0 0000	0 2895	0 0000	0 3106	0 0000	0 3080	0 0000	0 3398	0 0000	0 2899	0 0000	0 2946	0 0000
36	K	0 0000	0 0000	0 0000	0 0885	0 0000	0 0914	0 0000	0 0879	0 0000	0 0906	0 0000	0 0823	0 0000	0 0905	0 0000
37	SUM	14 9780	14 9760	15 0120	15 5070	15 0230	15 5170	15 0240	15 5020	15 0240	15 5300	15 0200	15 5610	15 0150	15 5670	15 0420
38	Cl	0 0000	0 0000	0 0000	0 0000	0 0000	0 0000	0 0000	0 0000	0 0000	0 0000	0 0000	0 0000	0 0000	0 0000	0 0000
39																
40	Fe/(Fe+Mg	0 9124	0 9085	0 8000	0 9252	0 8866	0 9248	0 8952	0 9237	0 8835	0 9184	0 9642	0 9667	0 9626	0 9599	0 8629
41	AFM															
42	Al2O3															
43	FeO	0 9018	0 9021	0 9052	0 2556	0 9045	0 2454	0 9056	0 2496	0 9049	0 2336	0 9035	0 1931	0 9051	0 1950	0 9062
44	MgO	0 9107	0 9078	0 8854	0 8886	0 8825	0 8978	0 8902	0 8931	0 8801	0 7047	0 9608	0 7801	0 9576	0 7727	0 8575
45	CFM	0 0875	0 0903	0 0894	0 0557	0 1030	0 0587	0 1043	0 0573	0 1060	0 0618	0 0357	0 0268	0 0370	0 0323	0 1363
46	CaO															
47	FeO	0 9094	0 9092	0 9095	0 3118	0 9080	0 3101	0 9083	0 3077	0 9096	0 3036	0 9123	0 2936	0 9152	0 2944	0 9097
48	MgO	0 9038	0 9011	0 8815	0 8388	0 8885	0 8380	0 8869	0 8395	0 8840	0 8403	0 9523	0 8629	0 9462	0 8772	0 8545
49	ACF	0 0868	0 0896	0 0890	0 0515	0 1025	0 0519	0 1039	0 0528	0 1055	0 0561	0 0354	0 0235	0 0367	0 0283	0 1358
50	Al2O3															
51	CaO	0 0018	0 0021	0 0051	0 1813	0 0044	0 1833	0 0055	0 1672	0 0046	0 1751	0 0035	0 1446	0 0051	0 1460	0 0061
52	FeO+MgO	0 9094	0 9092	0 9095	0 2521	0 9090	0 2533	0 9082	0 2501	0 9096	0 2505	0 9123	0 2911	0 9151	0 2515	0 9096
53		0 9946	0 9887	0 9854	0 5566	0 9666	0 5635	0 9853	0 5627	0 9856	0 5745	0 9643	0 6043	0 9799	0 6026	0 9643

	EO	EP	EQ	ER	ES	ET	EU	EV	EW	EX	EY	EZ	FA	FB	FC	FD
1	date	12-Feb-86	12-Feb-86	12-Feb-86	6-Mar-86	6-Mar-86	6-Mar-86	6-Mar-86	6-Mar-86	6-Mar-86	6-Mar-86	6-Mar-86	6-Mar-86	6-Mar-86	6-Mar-86	10-Feb-86	3-Mar-86
2	method	ede	ede	ede	ede	ede	ede	ede	ede	ede	ede	ede	ede	ede	ede	ede	ede
3	rock type	3	3	3	6	6	6	6	5	5	5	5	5	5	5	3	3
4	mineral	hbl	grun	hbl	grun	hbl	grun	hbl	grun	hbl	grun	hbl	grun	hbl	hbl	hbl	grun
5	study area	b	b	b	b	b	b	b	b	b	b	b	b	b	b	b	b
6																	
7	sample	SPLB008	SPLB008	SPLB008	SPLB038	SPLB038	SPLB038	SPLB038	SPLB038	SPLB038	SPLB038	SPLB038	SPLB038	SPLB038	SPLB038	SPLB038	SPLB038
8	PTS area	circ 1	circ 2	circ 2	circ 1	circ 1	circ 1	circ 1	circ 2	circ 2	circ 2	circ 2	circ 3	circ 3	circ 1	circ 1	
9	analysis	hbl 1	grun 1	hbl 1	grun 1	hbl 1	grun 2	hbl 2	grun 1	hbl 1	grun 2	hbl 2	grun 1	hbl 1	hbl 1	grun 1	
10																	
11	SiO2	41.821	40.306	40.174	40.978	40.983	40.646	40.409	40.575	40.320	40.275	40.871	40.479	40.674	43.436	40.938	
12	Al2O3	11.460	0.456	14.355	0.462	13.540	0.378	12.816	0.454	13.226	0.306	11.924	0.377	12.424	10.440	0.437	
13	Cr2O3	0.000	0.000	0.000	0.000	0.000	0.037	0.000	0.000	0.000	0.000	0.000	0.082	0.000	0.000	0.000	
14	TiO2	0.102	0.000	0.128	0.000	0.000	0.000	0.000	0.000	0.000	0.000	0.060	0.000	0.148	0.177	0.000	
15	MgO	2.274	4.044	1.886	2.137	1.114	2.082	1.179	1.055	0.748	1.125	0.732	1.057	0.712	3.366	5.153	
16	FeO	29.905	44.279	28.036	46.700	30.789	46.764	31.348	48.275	31.881	48.316	32.988	48.104	32.476	28.315	42.980	
17	MnO	0.000	0.000	0.000	0.000	0.000	0.000	0.000	0.000	0.000	0.000	0.000	0.070	0.000	0.000	0.154	
18	CaO	10.582	0.416	10.431	0.527	11.055	0.457	10.977	0.448	10.870	0.404	10.838	0.460	10.602	10.913	0.531	
19	Na2O	0.756	0.000	0.977	0.000	0.816	0.000	0.818	0.000	0.940	0.000	0.748	0.000	0.854	0.753	0.000	
20	K2O	0.366	0.000	0.487	0.000	0.431	0.000	0.415	0.000	0.428	0.000	0.402	0.000	0.411	0.306	0.000	
21	Cl	0.000	0.000	0.000	0.000	0.000	0.000	0.000	0.000	0.000	0.000	0.000	0.000	0.000	0.000	0.000	
22	TOTAL	97.070	98.500	97.260	98.880	98.410	98.580	97.960	98.810	98.410	98.490	98.480	98.620	98.300	97.710	99.190	
23	O based on anhynus O+Cl=23																
24		23.0000	23.0000	23.0000	23.0000	23.0000	23.0000	23.0000	23.0000	23.0000	23.0000	23.0000	23.0000	23.0000	23.0000	23.0000	
25	cations based on 23O																
26	Si	6.6398	7.0342	6.3601	7.0527	6.4261	7.0807	6.4421	7.0585	6.4119	7.0471	6.5244	7.0594	6.4671	6.6001	7.0226	
27	Al iv	1.3602	0.0658	1.6399	0.0473	1.5738	0.0393	1.5579	0.0415	1.5881	0.0529	1.4756	0.0406	1.5129	1.1999	0.0774	
28	Al vi	0.7826	0.0207	1.0364	0.0411	0.9466	0.0335	0.8501	0.0462	0.8906	0.0181	0.7878	0.0323	0.8225	0.7264	0.0044	
29	Cr	0.0000	0.0000	0.0000	0.0000	0.0000	0.0048	0.0000	0.0000	0.0000	0.0000	0.0000	0.0106	0.0000	0.0000	0.0000	
30	Ti	0.0123	0.0000	0.0152	0.0000	0.0000	0.0000	0.0000	0.0000	0.0000	0.0000	0.0000	0.0000	0.0178	0.0206	0.0000	
31	Mg	0.5400	0.8750	0.4450	0.5172	0.2623	0.5082	0.2801	0.2577	0.1773	0.2758	0.1741	0.2567	0.1693	0.7854	1.2185	
32	Fe 2+	3.9844	5.9586	3.8181	6.3523	4.0648	6.3736	4.1784	6.6146	4.2389	6.6517	4.4013	6.6061	4.3316	3.7073	5.7023	
33	Mn	0.0000	0.0000	0.0000	0.0000	0.0000	0.0000	0.0000	0.0000	0.0000	0.0000	0.0000	0.0097	0.0000	0.0000	0.0207	
34	Ca	1.8079	0.0717	1.7693	0.0918	1.8709	0.0798	1.8749	0.0786	1.8520	0.0712	1.8537	0.0808	1.8118	1.8305	0.0902	
35	Na	0.2336	0.0000	0.2998	0.0000	0.2500	0.0000	0.2529	0.0000	0.2899	0.0000	0.2309	0.0000	0.2640	0.2285	0.0000	
36	K	0.0731	0.0000	0.0864	0.0000	0.0859	0.0000	0.0845	0.0000	0.0870	0.0000	0.0819	0.0000	0.0838	0.0615	0.0000	
37	SUM	15.4340	15.0220	15.4840	15.0020	15.4820	15.0000	15.5220	14.9970	15.5370	15.0170	15.5100	14.9980	15.5010	15.3600	15.0360	
38	Cl	0.0000	0.0000	0.0000	0.0000	0.0000	0.0000	0.0000	0.0000	0.0000	0.0000	0.0000	0.0000	0.0000	0.0000	0.0000	
39																	
40	Fe/(Fe+Mg)	0.8806	0.8800	0.8956	0.9247	0.9394	0.9262	0.9372	0.9625	0.9599	0.9602	0.9619	0.9623	0.9624	0.8252	0.8239	
41	AFM																
42	Al2O3																
43	FeO	0.1921	0.0062	0.2390	0.0064	0.2256	0.0053	0.2126	0.0063	0.2181	0.0051	0.1969	0.0053	0.2060	0.1765	0.0059	
44	MgO	0.7115	0.8547	0.6815	0.9188	0.7275	0.9213	0.7360	0.9584	0.7496	0.9553	0.7726	0.9572	0.7641	0.6795	0.8191	
45	CFM	0.0964	0.1391	0.0794	0.0748	0.0469	0.0735	0.0495	0.0373	0.0313	0.0396	0.0306	0.0375	0.0299	0.1440	0.1750	
46	CaO																
47	FeO	0.2855	0.0102	0.2933	0.0132	0.3018	0.0115	0.2960	0.0113	0.2954	0.0102	0.2883	0.0116	0.2870	0.2895	0.0129	
48	MgO	0.6292	0.8512	0.6329	0.9125	0.6558	0.9155	0.6598	0.9516	0.6783	0.9504	0.6846	0.9511	0.6662	0.5863	0.8133	
49	ACF	0.0853	0.1385	0.0736	0.0743	0.0423	0.0730	0.0442	0.0371	0.0283	0.0394	0.0271	0.0372	0.0268	0.1242	0.1736	
50	Al2O3																
51	CaO	0.1452	0.0081	0.1817	0.0083	0.1690	0.0052	0.1597	0.0063	0.1651	0.0050	0.1488	0.0052	0.1561	0.1322	0.0058	
52	FeO+MgO	0.2440	0.0102	0.2400	0.0131	0.2509	0.0114	0.2487	0.0112	0.2487	0.0101	0.2455	0.0116	0.2422	0.2512	0.0128	
53		0.6107	0.9837	0.5763	0.9808	0.5802	0.9834	0.5916	0.9825	0.5883	0.9846	0.6059	0.9832	0.9017	0.6166	0.9814	

	FE	FF	FG	FH	FI	FJ	FK	FL	FM	FN	FO	FP	FQ	FR	FS	FT
1	date	3-Mar-86	3-Mar-86	3-Mar-86	3-Mar-86	3-Mar-86	3-Mar-86	13-Feb-86	13-Feb-86	13-Feb-86	13-Feb-86	13-Feb-86	13-Feb-86	13-Feb-86	13-Feb-86	16-Feb-86
2	method	eds	eds	eds	eds	eds	eds	eds	eds	eds	eds	eds	eds	eds	eds	eds
3	rock type	3	3	3	3	3	3	5	5	5	5	5	5	5	5	7
4	mineral	hbl	grun	grun	hbl	grun	hbl	grun	hbl	grun	hbl	grun	hbl	grun	hbl	grun
5	study area	b	b	b	b	b	b	b	b	b	b	b	b	b	b	b
6																
7	sample	5PLB030	5PLB030	5PLB030	5PLB030	5PLB030	5PLB030	5PLB045	5PLB045	5PLB045	5PLB045	5PLB045	5PLB045	5PLB045	5PLB045	5PLB046
8	PTS area	circ 1	circ 1	circ 2	circ 2	circ 2	circ 2	circ 1	circ 1	circ 1	circ 1	circ 3	circ 3	circ 3	circ 3	circ 1
9	analysis	hbl 2	grun 2	grun 1	hbl 1	grun 2	hbl 2	grun 1	hbl 1	grun 2	hbl 2	grun 1	hbl 1	grun 2	hbl 2	grun 1
10																
11	SiO2	40.460	49.884	50.017	41.619	49.864	41.414	48.801	41.350	48.864	40.787	48.693	40.780	48.626	40.862	48.593
12	Al2O3	15.249	0.530	0.540	14.305	0.530	14.082	0.284	10.542	0.486	11.987	0.268	11.498	0.293	11.740	0.299
13	Cr2O3	0.000	0.088	0.000	0.000	0.000	0.000	0.000	0.000	0.000	0.000	0.000	0.000	0.000	0.000	0.000
14	TiO2	0.182	0.094	0.000	0.133	0.117	0.118	0.000	0.000	0.000	0.000	0.000	0.000	0.000	0.000	0.000
15	MgO	2.146	5.315	5.152	2.502	5.214	2.558	0.997	0.649	1.097	0.733	1.276	0.816	1.229	0.778	1.386
16	FeO	27.591	42.502	42.416	27.756	42.106	27.906	47.892	32.825	47.153	31.759	47.301	32.455	47.685	32.452	47.523
17	MnO	0.000	0.148	0.102	0.000	0.138	0.000	0.000	0.000	0.000	0.000	0.000	0.000	0.068	0.000	0.000
18	CaO	10.580	0.393	0.466	10.461	0.446	10.540	0.535	10.957	0.881	11.106	0.479	11.071	0.548	10.928	0.454
19	Na2O	0.000	0.000	0.000	0.838	0.000	0.759	0.000	0.810	0.000	0.916	0.000	0.868	0.000	0.883	0.000
20	K2O	0.427	0.000	0.000	0.384	0.000	0.351	0.000	0.363	0.000	0.359	0.000	0.384	0.000	0.376	0.000
21	Cl	0.000	0.000	0.000	0.000	0.000	0.000	0.000	0.000	0.000	0.000	0.000	0.000	0.000	0.000	0.000
22	TOTAL	97.450	98.960	98.700	98.000	98.520	97.650	98.310	97.500	98.280	97.630	98.020	97.850	98.450	98.000	98.260
23	O based on anhyrous O+Cl=23															
24		23.0000	23.0000	23.0000	23.0000	23.0000	23.0000	23.0000	23.0000	23.0000	23.0000	23.0000	23.0000	23.0000	23.0000	23.0000
25	cations based on 23O															
26	Si	6.3208	7.9150	7.9485	6.4706	7.9458	6.4727	7.9948	6.6733	7.9850	6.5417	8.0080	6.5486	7.9813	6.5465	7.9824
27	Al iv	1.6792	0.0850	0.0515	1.5294	0.0541	1.5273	0.0052	1.3267	0.0170	1.4583	0.0000	1.4514	0.0187	1.4535	0.0176
28	Al vi	1.1284	0.0141	0.0496	1.0818	0.0453	1.0519	0.0489	0.6785	0.0773	0.6039	0.0519	0.7258	0.0360	0.7632	0.0403
29	Cr	0.0000	0.0110	0.0000	0.0000	0.0000	0.0000	0.0000	0.0000	0.0000	0.0000	0.0000	0.0000	0.0000	0.0000	0.0000
30	Ti	0.0214	0.0112	0.0000	0.0155	0.0140	0.0138	0.0000	0.0000	0.0000	0.0000	0.0000	0.0000	0.0000	0.0000	0.0000
31	Mg	0.5627	1.2567	1.2202	0.5797	1.2358	0.5958	0.2445	0.1561	0.2681	0.1751	0.3128	0.1954	0.3006	0.1654	0.3393
32	Fe 2+	3.6047	5.6365	5.6371	3.6089	5.6002	3.6474	6.5884	4.4302	6.4690	4.2599	6.5063	4.3607	6.5456	4.3480	6.5287
33	Mn	0.0000	0.0199	0.0137	0.0000	0.0186	0.0000	0.0000	0.0000	0.0000	0.0000	0.0000	0.0000	0.0091	0.0000	0.0000
34	Ca	1.7725	0.0667	0.0796	1.7426	0.0760	1.7648	0.0943	1.8948	0.1548	1.9085	0.0845	1.9058	0.0964	1.8756	0.0800
35	Na	0.2422	0.0000	0.0000	0.2525	0.0000	0.2289	0.0000	0.2535	0.0000	0.2648	0.0000	0.2704	0.0000	0.2686	0.0000
36	K	0.0850	0.0000	0.0000	0.0761	0.0000	0.0699	0.0000	0.0748	0.0000	0.0735	0.0000	0.0788	0.0000	0.0768	0.0000
37	SUM	15.4170	15.0180	15.0000	15.3870	14.9900	15.3730	14.9770	15.4880	14.9850	15.5060	14.9650	15.5370	14.9900	15.5170	14.9880
38	Cl	0.0000	0.0000	0.0000	0.0000	0.0000	0.0000	0.0000	0.0000	0.0000	0.0000	0.0000	0.0000	0.0000	0.0000	0.0000
39																
40	Fe/(Fe+Mg)	0.8650	0.8177	0.8221	0.8616	0.8192	0.8596	0.9642	0.9660	0.9602	0.9605	0.9541	0.9571	0.9561	0.9591	0.9506
41	AFM															
42	Al2O3															
43	FeO	0.2520	0.0071	0.0073	0.2363	0.0072	0.2331	0.0040	0.1784	0.0069	0.2032	0.0038	0.1929	0.0041	0.1965	0.0042
44	MgO	0.6470	0.8118	0.8160	0.6563	0.8133	0.6582	0.9603	0.7927	0.9535	0.7653	0.9505	0.7725	0.9521	0.7797	0.9466
45	CFM	0.1010	0.1810	0.1766	0.1054	0.1795	0.1077	0.0358	0.0278	0.0385	0.0315	0.0457	0.0346	0.0437	0.0329	0.0492
46	CaO															
47	FeO	0.2984	0.0096	0.0115	0.2936	0.0110	0.2936	0.0136	0.2923	0.0225	0.3009	0.0122	0.2948	0.0139	0.2927	0.0115
48	MgO	0.6069	0.8089	0.8126	0.6065	0.8102	0.6071	0.9511	0.6636	0.9386	0.6715	0.9425	0.6748	0.9426	0.6784	0.9387
49	ACF	0.0947	0.1805	0.1758	0.0977	0.1788	0.0992	0.0353	0.0241	0.0389	0.0276	0.0453	0.0302	0.0433	0.0289	0.0498
50	Al2O3															
51	CaO	0.1012	0.0071	0.0072	0.1010	0.0071	0.1767	0.0040	0.1340	0.0068	0.1513	0.0037	0.1442	0.0041	0.1474	0.0041
52	FeO+MgO	0.2414	0.0095	0.0114	0.2406	0.0108	0.2418	0.0136	0.2532	0.0223	0.2553	0.0122	0.2524	0.0138	0.2495	0.0115
53		0.5575	0.9834	0.9814	0.5784	0.9819	0.5814	0.9825	0.8128	0.9708	0.9033	0.9841	0.9034	0.9821	0.9031	0.9844

	FU	FV	FW	FX	FY	FZ	GA	GB	GC	GD	GE	GF	GG	GH	GI	GJ
1	date	18-Feb-86	18-Feb-86	18-Feb-86	18-Feb-86	18-Feb-86	18-Feb-86	18-Feb-86	18-Feb-86	18-Feb-86	18-Feb-86	1-Mar-86	1-Mar-86	1-Mar-86	1-Mar-86	18-Apr-86
2	method	eds	eds	eds	eds	eds	eds	eds	eds	eds	eds	eds	eds	eds	eds	eds/wds(Cl)
3	rock type	7	7	7	7	7	7	7	4	4	4	8	8	8	8	8
4	mineral	hbl	grun	hbl	grun	hbl	grun	hbl	hbl	hbl	hbl	grun	hbl	grun	hbl	grun
5	study area	b	b	b	b	b	b	b	b	b	b	b	b	b	b	b
6																rerun
7	sample	5PLB046	5PLB046	5PLB046	5PLB046	5PLB046	5PLB046	5PLB046	5PLB071	5PLB071	5PLB071	5PLB073	5PLB073	5PLB073	5PLB073	5PLB073
8	PTS area	circ 1	circ 1	circ 1	circ 2	circ 2	circ 2	circ 2	circ 1	circ 2	circ 2	circ 1	circ 1	circ 1	circ 1	circ 1
9	analysis	hbl 1	grun 2	hbl 2	grun 1	hbl 1	grun 2	hbl 2	hbl 1	hbl 1	hbl 2	grun 1	hbl 1	grun 2	hbl 2	grun 1
10																
11	SiO2	46.492	46.459	46.880	45.275	46.266	46.065	46.303	46.404	46.804	46.197	48.581	47.637	48.613	46.042	46.066
12	Al2O3	12.601	9.266	12.384	9.256	13.695	9.313	13.677	14.616	15.044	15.987	9.325	11.022	9.484	13.851	9.251
13	Cr2O3	0.000	0.000	0.000	0.000	0.000	0.000	0.000	0.000	0.000	0.000	0.000	0.000	0.075	0.000	0.000
14	TiO2	0.000	0.000	0.000	0.000	0.000	0.000	0.000	0.000	0.000	0.000	0.000	0.140	0.000	0.170	0.000
15	MgO	0.797	1.315	0.776	2.851	1.386	2.768	1.343	2.862	3.054	2.934	2.790	1.677	2.843	1.485	2.910
16	FeO	31.132	47.231	31.161	45.525	29.696	45.536	29.884	27.152	25.798	25.616	44.823	31.558	45.358	29.970	46.076
17	MnO	0.000	0.087	0.000	0.000	0.000	0.000	0.000	0.000	0.075	0.000	0.123	0.000	0.145	0.000	0.070
18	CaO	11.100	9.439	10.979	9.422	10.986	9.437	11.080	11.062	11.271	11.357	9.438	9.881	9.457	10.586	9.393
19	Na2O	0.807	0.000	0.784	0.000	0.928	0.000	0.815	0.975	1.078	0.891	0.000	0.737	0.000	0.882	0.000
20	K2O	0.351	0.000	0.357	0.000	0.424	0.000	0.425	0.391	0.388	0.447	0.000	0.278	0.000	0.418	0.000
21	Cl	0.000	0.000	0.000	0.000	0.000	0.000	0.000	0.000	0.000	0.000	0.000	0.000	0.000	0.000	0.000
22	TOTAL	97.280	97.780	97.100	98.280	97.400	96.160	97.530	97.260	97.510	97.430	97.080	96.930	97.970	97.180	98.770
23	O based on anhyrous O+Cl=23															
24		23.0000	23.0000	23.0000	23.0000	23.0000	23.0000	23.0000	23.0000	23.0000	23.0000	23.0000	23.0000	23.0000	23.0000	23.0000
25	cations based on 23O															
26	Si	6.4951	7.9984	6.5336	7.9920	6.4066	7.9823	6.4055	6.3489	6.3513	6.2564	7.9835	6.8808	7.8323	6.3873	7.9512
27	Al iv	1.5049	0.0036	1.4664	0.0080	1.5934	0.0177	1.5945	1.6511	1.6487	1.7436	0.0165	1.3192	0.0677	1.6127	0.0481
28	Al vi	0.8784	0.0486	0.8778	0.0398	0.9734	0.0422	0.9675	1.0556	1.1111	1.1890	0.0465	0.7651	0.0254	0.9536	0.0000
29	Cr	0.0000	0.0000	0.0000	0.0000	0.0000	0.0000	0.0000	0.0000	0.0000	0.0000	0.0000	0.0000	0.0097	0.0000	0.0000
30	Ti	0.0000	0.0000	0.0000	0.0000	0.0000	0.0000	0.0000	0.0000	0.0000	0.0000	0.0000	0.0189	0.0000	0.0204	0.0000
31	Mg	0.1906	0.3234	0.1858	0.6898	0.3286	0.6759	0.3182	0.6234	0.7085	0.6807	0.6834	0.4010	0.6914	0.3484	0.7029
32	Fe 2+	4.1782	6.5179	4.1854	6.1805	3.9494	6.1928	3.9720	3.5881	3.3579	3.3343	6.1602	4.2347	6.1894	3.9981	6.2444
33	Mn	0.0000	0.0083	0.0000	0.0000	0.0000	0.0000	0.0000	0.0000	0.0099	0.0000	0.0171	0.0000	0.0200	0.0000	0.0095
34	Ca	1.9077	0.0776	1.8893	0.0735	1.8722	0.0762	1.8667	1.8623	1.8796	1.8938	0.0771	1.6987	0.0798	1.8093	0.0682
35	Na	0.2511	0.0000	0.2378	0.0000	0.2862	0.0000	0.2510	0.2971	0.3255	0.2688	0.0000	0.2292	0.0000	0.2728	0.0000
36	K	0.0719	0.0000	0.0732	0.0000	0.0859	0.0000	0.0862	0.0784	0.0771	0.0887	0.0000	0.0570	0.0000	0.0847	0.0000
37	SUM	15.4760	14.9770	15.4490	14.9840	15.4960	14.9870	15.4820	15.4850	15.4700	15.4550	14.9840	15.4030	15.0160	15.4870	15.0240
38	Cl	0.0000	0.0000	0.0000	0.0000	0.0000	0.0000	0.0000	0.0000	0.0000	0.0000	0.0000	0.0000	0.0000	0.0000	0.0000
39																
40	Fe/(Fe+Mg)	0.9564	0.9527	0.9575	0.8996	0.9232	0.9016	0.9258	0.8513	0.8258	0.8305	0.9081	0.9135	0.8995	0.9199	0.8988
41	AFM															
42	Al2O3															
43	FeO	0.2144	0.0038	0.2114	0.0035	0.2308	0.0043	0.2299	0.2441	0.2534	0.2675	0.0046	0.1835	0.0067	0.2279	0.0034
44	MgO	0.7513	0.9491	0.7550	0.8965	0.7101	0.8977	0.7130	0.6435	0.6165	0.6083	0.8960	0.7456	0.8935	0.7102	0.8957
45	CFM	0.0343	0.0471	0.0335	0.1001	0.0591	0.0980	0.0571	0.1124	0.1301	0.1242	0.0994	0.0706	0.0998	0.0619	0.1008
46	CaO															
47	FeO	0.3040	0.0112	0.3018	0.0106	0.3044	0.0110	0.3054	0.3078	0.3161	0.3205	0.0111	0.2682	0.0115	0.2939	0.0097
48	MgO	0.6656	0.9420	0.6685	0.8901	0.6422	0.8917	0.6430	0.5894	0.5647	0.5643	0.8901	0.6685	0.8892	0.6495	0.8901
49	ACF	0.0304	0.0467	0.0297	0.0993	0.0534	0.0973	0.0515	0.1030	0.1192	0.1152	0.0987	0.0633	0.0993	0.0566	0.1002
50	Al2O3															
51	CaO	0.1596	0.0038	0.1577	0.0034	0.1726	0.0043	0.1718	0.1827	0.1884	0.1988	0.0045	0.1413	0.0066	0.1725	0.0034
52	FeO+MgO	0.2555	0.0112	0.2542	0.0105	0.2519	0.0109	0.2530	0.2514	0.2566	0.2568	0.0111	0.2303	0.0114	0.2432	0.0097
53		0.5849	0.9851	0.5881	0.9860	0.5755	0.9848	0.5753	0.5659	0.5551	0.5444	0.9844	0.6284	0.9820	0.5843	0.9869

	GK	GL	GM	GN	GO	GP	GQ	GR	GS	GT	GU	GV	GW	GX	GY	GZ
1	date	3-Mar-86	3-Mar-86	3-Mar-86	3-Mar-86	16-Apr-86	3-Mar-86	3-Mar-86	3-Mar-86	3-Mar-86	30-Oct-86	30-Oct-86	17-Dec-85	17-Dec-85	17-Dec-85	14-Jan-86
2	method	eda	eda	eda	eda	eda/wda(Cl)	eda	eda	eda	eda	eda	eda	wda/eda	wda/eda	wda/eda	eda
3	rock type	8	8	8	8	8	8	8	8	8	8	8	7	7	7	7
4	mineral	grun	hbl	grun	hbl	grun	grun	hbl	grun	hbl	grun	grun	grun	hbl	act	grun
5	study area	b	b	b	b	b	c	c	c	c	c	c	c	c	c	c
6						rerun	rerun	rerun			rerun	rerun				"act" 2
7	sample	5PLB073	5PLB073	5PLB073	5PLB073	5PLB073	4PLC006	4PLC006	4PLC006	4PLC006	4PLC006	4PLC006	4PLC007	4PLC007	4PLC007	4PLC007
8	PTS area	circ 2	circ 2	circ 2	circ 2	circ 2	circ 1	circ 1	circ 1	circ 1	circ 1	circ 1	circ 1	circ 1	circ 1	circ 1
9	analysis	grun 1	hbl 1	grun 2	hbl 2	grun 1	grun 2	hbl 2	grun 3	hbl 3	grun 1	grun 2	grun 1	hbl 1	act 1	grun 2
10							49.251	40.476	49.346	40.849	50.327	50.084	49.278	45.670	49.018	49.412
11	SiO2	49.056	40.530	49.079	41.253	49.437	0.625	15.843	0.549	15.272	0.317	0.391	0.155	6.147	1.012	1.002
12	Al2O3	0.387	13.536	0.430	12.299	0.372	0.000	0.000	0.000	0.000	0.000	0.000	0.000	0.000	0.000	0.000
13	Cr2O3	0.000	0.000	0.000	0.000	0.000	0.000	0.000	0.000	0.000	0.000	0.000	0.000	0.151	0.000	0.000
14	TiO2	0.000	0.160	0.000	0.116	0.000	4.365	2.033	4.315	2.058	4.253	4.297	2.921	2.417	3.187	2.917
15	MgO	2.850	1.457	2.879	1.588	2.912	42.918	27.531	43.215	27.380	43.694	43.467	44.815	32.166	32.981	41.563
16	FeO	45.585	30.148	46.195	35.807	46.595	0.112	0.000	0.144	0.000	0.134	0.108	0.154	0.000	0.000	0.079
17	MnO	0.106	0.000	0.126	0.000	0.000	0.590	10.853	0.497	10.926	0.449	0.560	1.053	10.986	10.756	4.361
18	CaO	0.439	10.826	0.436	10.586	0.379	0.000	0.772	0.000	0.884	0.000	0.000	0.000	0.321	0.000	0.000
19	Na2O	0.000	0.844	0.000	0.823	0.000	0.000	0.403	0.000	0.348	0.000	0.000	0.000	0.159	0.000	0.000
20	K2O	0.000	0.421	0.000	0.350	0.000	0.000	0.000	0.000	0.000	0.000	0.000	0.000	0.000	0.000	0.000
21	Cl	0.000	0.000	0.000	0.000	0.060	97.850	97.910	98.070	97.720	99.170	98.880	98.380	98.020	97.850	99.330
22	TOTAL	98.420	97.820	98.150	97.820	99.780										
23	O based on anhyrous O+Cl=23						23.0000	23.0000	23.0000	23.0000	23.0000	23.0000	23.0000	23.0000	23.0000	23.0000
24		23.0000	23.0000	23.0000	23.0000	22.9819										
25	cations based on 23O						7.9362	6.3050	7.9427	6.3719	7.9999	7.9815	7.9859	7.2380	7.8916	7.8679
26	Si	7.9807	6.4155	7.9728	6.5472	7.9404	0.0638	1.6950	0.0573	1.6281	0.0001	0.0185	0.0141	0.7620	0.1084	0.1321
27	Al iv	0.0393	1.5845	0.0272	1.4528	0.0596	0.0549	1.2135	0.0469	1.1795	0.0593	0.0549	0.0155	0.3882	0.0802	0.0559
28	Al vi	0.0348	0.9467	0.0552	0.8477	0.0108	0.0000	0.0000	0.0000	0.0000	0.0000	0.0000	0.0000	0.0000	0.0000	0.0000
29	Cr	0.0000	0.0000	0.0000	0.0000	0.0000	0.0000	0.0000	0.0000	0.0000	0.0000	0.0000	0.0000	0.0180	0.0000	0.0000
30	Ti	0.0000	0.0190	0.0000	0.0138	0.0000	1.0484	0.4721	1.0352	0.4781	1.0076	1.0211	0.7056	0.5710	0.7508	0.8924
31	Mg	0.6893	0.3437	0.6971	0.3756	0.6970	5.7836	3.5865	5.8171	3.5717	5.8084	5.7952	6.0737	4.2633	4.3605	5.5347
32	Fe 2+	6.1865	3.9900	6.1399	4.0869	6.2588	0.0153	0.0000	0.0197	0.0000	0.0138	0.0143	0.0211	0.0000	0.0000	0.0106
33	Mn	0.0146	0.0000	0.0174	0.0000	0.0000	0.1018	1.8114	0.0857	1.8260	0.0765	0.0957	0.1828	1.8654	1.8220	0.7439
34	Ca	0.0764	1.8360	0.0758	1.8001	0.0652	0.0000	0.2332	0.0000	0.2675	0.0000	0.0000	0.0000	0.0887	0.0000	0.0000
35	Na	0.0000	0.2588	0.0000	0.2532	0.0000	0.0000	0.0800	0.0000	0.0682	0.0000	0.0000	0.0000	0.0322	0.0000	0.0000
36	K	0.0000	0.0850	0.0000	0.0708	0.0000	15.0040	15.3970	15.0050	15.3920	14.9700	14.9810	14.9990	15.2350	15.0140	15.0380
37	SUM	15.0020	15.4740	14.9860	15.4500	15.0320	0.0000	0.0000	0.0000	0.0000	0.0000	0.0000	0.0000	0.0000	0.0000	0.0000
38	Cl	0.0000	0.0000	0.0000	0.0000	0.0163										
39							0.8485	0.8837	0.8489	0.8819	0.8522	0.8502	0.8858	0.8819	0.8531	0.8886
40	Fe/(Fe+Mg)	0.8997	0.9207	0.8980	0.9150	0.8998										
41	AFM															
42	Al2O3						0.0086	0.2638	0.0075	0.2574	0.0043	0.0054	0.0022	0.1061	0.0181	0.0148
43	FeO	0.0054	0.2256	0.0060	0.2049	0.0050	0.8393	0.6506	0.8425	0.6549	0.8485	0.8456	0.8940	0.7883	0.8376	0.8756
44	MgO	0.8948	0.7130	0.8927	0.7282	0.8953	0.1521	0.0856	0.1498	0.0877	0.1472	0.1490	0.1029	0.1058	0.1442	0.1095
45	CFM	0.0997	0.0614	0.1013	0.0669	0.0997										
46	CaO						0.0147	0.3086	0.0124	0.3108	0.0111	0.0138	0.0263	0.2784	0.2628	0.1067
47	FeO	0.0110	0.2975	0.0110	0.2673	0.0093	0.8341	0.6110	0.8384	0.6078	0.8427	0.8384	0.8724	0.6363	0.8288	0.7940
48	MgO	0.8890	0.6466	0.8882	0.6527	0.8914	0.1512	0.0804	0.1492	0.0814	0.1462	0.1477	0.1013	0.0852	0.1083	0.0993
49	ACF	0.0991	0.0557	0.1006	0.0600	0.0993										
50	Al2O3						0.0085	0.1886	0.0075	0.1928	0.0043	0.0053	0.0021	0.0788	0.0134	0.0133
51	CaO	0.0053	0.1090	0.0050	0.1551	0.0050	0.0146	0.2473	0.0123	0.2586	0.0111	0.0136	0.0262	0.2565	0.2583	0.1053
52	FeO+MgO	0.9109	0.2470	0.9109	0.2428	0.9092	0.9770	0.5541	0.9803	0.5563	0.9847	0.9809	0.9717	0.6046	0.7273	0.8814
53		0.9838	0.5831	0.9832	0.6021	0.9858										

	HA	HB	HC	HD	HE	HF	HG	HH	HI	HJ	HK	HL	HM	HN	HO	HP
1	date	14-Jan-86	14-Jan-86	13-Nov-85	13-Nov-85	13-Nov-85	13-Nov-85	19-Dec-85	19-Dec-85	19-Dec-85	19-Dec-85	19-Dec-85	19-Dec-85	19-Dec-85	19-Dec-85	23-Jan-86
2	method	eds	eds	wds/eds	wds/eds	wds/eds	wds/eds	eds	eds	eds	eds	eds	eds	eds	eds	eds
3	rock type	7	7	6	6	6	6	6	6	6	6	6	6	6	6	7
4	mineral	hbl	hbl	grun	hbl	grun	hbl	grun	hbl	grun	hbl	grun	hbl	grun	hbl	grun
5	study area	c	c	c	c	c	c	c	c	c	c	c	c	c	c	c
6																
7	sample	4PLC007	4PLC007	4PLC008	4PLC008	4PLC008	4PLC008	4PLC011	4PLC011	4PLC011	4PLC011	4PLC011	4PLC011	4PLC011	4PLC011	4PLC012
8	PTS area	circ 1	circ 1	circ 1	circ 1	circ 2	circ 2	circ 1	circ 1	circ 1	circ 1	circ 2	circ 2	circ 3	circ 3	circ 1
9	analysis	hbl 2	hbl 3	grun 1	hbl 1	grun 1	hbl 1	grun 1	hbl 1	grun 2	hbl 2	grun 1	hbl 1	grun 1	hbl 1	grun 1
10		47.172	41.988	48.431	43.133	49.062	43.818	48.855	44.544	48.554	43.103	48.776	42.803	48.775	41.917	49.263
11	SiO2	5.139	11.819	0.142	8.458	0.221	8.556	0.253	7.199	0.201	8.791	0.268	9.166	0.313	10.201	0.277
12	Al2O3	0.000	0.000	0.000	0.000	0.000	0.000	0.000	0.000	0.000	0.000	0.000	0.000	0.000	0.000	0.000
13	Cr2O3	0.000	0.126	0.000	0.150	0.000	0.123	0.000	0.000	0.000	0.000	0.000	0.000	0.000	0.256	0.000
14	TiO2	2.464	1.650	1.745	1.118	1.662	0.970	0.706	0.625	0.736	0.907	0.665	0.570	0.693	0.651	2.453
15	MgO	32.312	30.497	46.552	32.262	47.364	32.711	49.090	35.957	48.956	34.866	49.876	34.836	49.924	34.414	45.778
16	FeO	0.000	0.000	0.155	0.000	0.115	0.000	0.000	0.000	0.000	0.000	0.000	0.000	0.000	0.000	0.162
17	MnO	10.991	11.196	0.536	11.132	0.677	11.076	0.563	10.536	0.856	10.887	0.602	10.687	0.526	10.873	0.473
18	CaO	0.283	0.606	0.000	0.927	0.000	0.795	0.000	0.635	0.000	0.887	0.000	0.907	0.000	1.199	0.000
19	Na2O	0.096	0.376	0.000	0.309	0.000	0.284	0.000	0.188	0.000	0.265	0.000	0.241	0.000	0.375	0.000
20	K2O	0.000	0.000	0.000	0.000	0.000	0.000	0.000	0.000	0.000	0.000	0.000	0.000	0.000	0.000	0.000
21	Cl	98.460	98.250	98.560	97.490	99.040	98.340	100.470	99.660	99.120	99.420	100.180	99.210	100.340	99.860	98.430
22	TOTAL															
23	O based on a	23.0000	23.0000	23.0000	23.0000	23.0000	23.0000	23.0000	23.0000	23.0000	23.0000	23.0000	23.0000	23.0000	23.0000	23.0000
24																
25	cations based	7.4190	6.6216	8.0429	6.9318	7.9838	6.9702	7.9391	7.0737	7.9843	6.8596	7.9352	6.8232	7.9213	6.6465	8.0028
26	Si	0.5810	1.3784	0.0000	1.0682	0.0161	1.0298	0.0484	0.9263	0.0357	1.1402	0.0513	1.1768	0.0600	1.3535	0.0000
27	Al iv	0.3715	0.6167	0.0273	0.5337	0.0263	0.5747	0.0000	0.4212	0.0031	0.5087	0.0000	0.5453	0.0000	0.5529	0.0530
28	Al vi	0.0000	0.0000	0.0000	0.0000	0.0000	0.0000	0.0000	0.0000	0.0000	0.0000	0.0000	0.0000	0.0000	0.0000	0.0000
29	Cr	0.0000	0.0152	0.0000	0.0181	0.0000	0.0147	0.0000	0.0000	0.0000	0.0000	0.0000	0.0000	0.0000	0.0307	0.0000
30	Ti	0.5777	0.3901	0.4231	0.2679	0.3885	0.2322	0.1711	0.1480	0.1800	0.1439	0.1613	0.1355	0.1644	0.1540	0.5938
31	Mg	4.2500	4.0206	6.3345	4.3360	6.4456	4.3516	6.7786	4.7754	6.7170	4.6406	6.7858	4.6445	6.7806	4.5635	6.2165
32	Fe 2+	0.0000	0.0000	0.0214	0.0000	0.0158	0.0000	0.0000	0.0000	0.0000	0.0000	0.0000	0.0000	0.0000	0.0000	0.0223
33	Mn	1.8520	1.8818	0.0836	1.9167	0.1181	1.8877	0.0877	1.7926	0.1158	1.8582	0.1048	1.8253	0.0918	1.8471	0.0822
34	Ca	0.0862	0.1854	0.0000	0.2888	0.0000	0.2453	0.0000	0.1955	0.0000	0.2736	0.0000	0.2802	0.0000	0.3658	0.0000
35	Na	0.0188	0.0758	0.0000	0.0633	0.0000	0.0576	0.0000	0.0338	0.0000	0.0538	0.0000	0.0490	0.0000	0.0758	0.0000
36	K	15.1570	15.3960	14.9430	15.4250	14.9950	15.3840	15.0360	15.3670	15.0180	15.4790	15.0380	15.4800	15.0480	15.5900	14.9700
37	SUM	0.0000	0.0000	0.0000	0.0000	0.0000	0.0000	0.0000	0.0000	0.0000	0.0000	0.0000	0.0000	0.0000	0.0000	0.0000
38	Cl															
39		0.6803	0.9116	0.9374	0.9418	0.9432	0.9493	0.9754	0.9699	0.9738	0.9689	0.9766	0.9717	0.9721	0.9674	0.9128
40	Fe/(Fe+Mg)															
41	AFM															
42	Al2O3	0.0898	0.1992	0.0020	0.1482	0.0031	0.1489	0.0035	0.1204	0.0028	0.1470	0.0037	0.1526	0.0043	0.1881	0.0038
43	FeO	0.8013	0.7298	0.9355	0.8022	0.9402	0.8079	0.9720	0.8532	0.9712	0.8274	0.9732	0.8233	0.9680	0.8046	0.9093
44	MgO	0.1988	0.0706	0.0625	0.0496	0.0587	0.0431	0.0245	0.0264	0.0260	0.0257	0.0231	0.0240	0.0276	0.0272	0.0869
45	CFM															
46	CaO	0.2773	0.3002	0.0137	0.2938	0.0170	0.2817	0.0139	0.2668	0.0165	0.2797	0.0149	0.2763	0.0130	0.2814	0.0119
47	FeO	0.6363	0.6378	0.9246	0.6650	0.9271	0.6724	0.9819	0.7110	0.9578	0.6986	0.9823	0.7031	0.9585	0.6852	0.9019
48	MgO	0.0865	0.0619	0.0618	0.0411	0.0558	0.0359	0.0243	0.0220	0.0257	0.0217	0.0228	0.0205	0.0275	0.0235	0.0862
49	ACF															
50	Al2O3	0.0866	0.1483	0.0020	0.1094	0.0030	0.1103	0.0034	0.0912	0.0028	0.1104	0.0036	0.1153	0.0042	0.1266	0.0036
51	CaO	0.2588	0.2556	0.0137	0.2616	0.0169	0.2505	0.0138	0.2426	0.0165	0.2486	0.0148	0.2445	0.0129	0.2457	0.0118
52	FeO+MgO	0.9746	0.9980	0.9843	0.9288	0.9800	0.9302	0.9828	0.9682	0.9808	0.9407	0.9816	0.9402	0.9828	0.9275	0.9843
53																

	HQ	HR	HS	HT	HU	HV	HW	HX	HY	HZ	IA	IB	IC	ID	IE	IF
1	date	23-Jan-86	23-Jan-86	23-Jan-86	19-Dec-85	14-Jan-86	14-Jan-86	16-Jan-86	16-Jan-86	16-Jan-86	16-Jan-86	16-Jan-86	30-Jan-86	30-Jan-86	30-Jan-86	30-Jan-86
2	method	eds	eds	eds	eds	eds	eds	eds	eds	eds	eds	eds	eds	eds	eds	eds
3	rock type	7	7	7	3	3	3	4	4	4	4	4	4	4	4	4
4	mineral	hbl	grun	hbl	grun	grun	hbl	grun	grun	hbl	grun	hbl	grun	grun	hbl	grun
5	study area	c	c	c	c	c	c	c	c	c	c	c	c	c	c	c
6									in hbl 1		in hbl 1					
7	sample	4PLC012	4PLC012	4PLC012	4PLC017	4PLC017	4PLC017	4PLC018	4PLC018	4PLC018	4PLC018	4PLC018	4PLC019	4PLC019	4PLC019	4PLC019
8	PTS area	circ 1	circ 1	circ 1	circ 1	circ 2	circ 2	circ 1	circ 1	circ 1	circ 2	circ 2	circ 1	circ 1	circ 1	circ 2
9	analysis	hbl 1	grun 2	hbl 2	grun 1	grun 1	hbl 1	grun	grun 1	hbl 1	grun 1	hbl 1	grun 1	grun	hbl 1	grun
10		40.116	49.312	40.812	51.084	51.019	41.871	50.515	50.737	41.614	50.074	40.117	51.052	50.713	41.229	51.519
11	SiO2	10.505	0.261	15.553	0.702	0.394	15.518	0.734	0.392	15.166	0.485	17.720	0.581	0.730	17.233	0.762
12	Al2O3	0.000	0.000	0.000	0.000	0.000	0.000	0.000	0.000	0.000	0.000	0.000	0.000	0.000	0.000	0.000
13	Cr2O3	0.000	0.000	0.000	0.000	0.000	0.135	0.000	0.000	0.000	0.000	0.106	0.000	0.000	0.090	0.000
14	TiO2	1.440	0.465	1.574	0.359	0.411	3.604	0.635	0.380	3.305	0.910	1.951	0.395	0.921	3.560	0.284
15	MgO	27.089	45.960	27.478	38.844	39.773	25.795	40.667	40.627	25.542	42.724	25.773	37.239	41.882	23.641	38.731
16	FeO	0.000	0.168	0.000	0.000	0.000	0.000	0.000	0.000	0.000	0.000	0.000	0.000	0.000	0.000	0.000
17	MnO	11.092	0.417	10.843	0.381	0.474	9.961	0.413	0.546	10.896	0.459	10.844	0.530	0.300	10.296	0.287
18	CaO	0.460	0.000	0.431	0.000	0.000	0.671	0.000	0.000	1.655	0.000	1.781	0.000	0.000	1.920	0.000
19	Na2O	0.360	0.000	0.333	0.000	0.000	0.420	0.000	0.000	0.464	0.000	0.383	0.000	0.000	0.355	0.000
20	K2O	0.000	0.000	0.000	0.000	0.000	0.000	0.000	0.000	0.000	0.000	0.000	0.000	0.000	0.000	0.000
21	Cl	97.080	98.580	97.020	99.360	99.070	96.080	98.980	98.680	98.830	98.650	98.670	97.797	99.530	98.320	99.580
22	TOTAL															
23	O based on a	23.0000	23.0000	23.0000	23.0000	23.0000	23.0000	23.0000	23.0000	23.0000	23.0000	23.0000	23.0000	23.0000	23.0000	23.0000
24																
25	cations based	6.2664	7.0091	6.3987	7.0998	7.0526	6.4306	7.0214	7.0812	6.3726	7.0675	6.1606	7.0883	7.0414	6.2692	7.0312
26	Si	1.7136	0.0009	1.8013	0.1002	0.0474	1.5894	0.0786	0.0188	1.6272	0.0325	1.8394	0.0317	0.0586	1.7308	0.0668
27	Al iv	1.3346	0.0490	1.2727	0.0277	0.0250	1.2327	0.0570	0.0539	1.1100	0.0585	1.3677	0.0752	0.0761	1.3576	0.0684
28	Al vi	0.0000	0.0000	0.0000	0.0000	0.0000	0.0000	0.0000	0.0000	0.0000	0.0000	0.0000	0.0000	0.0000	0.0000	0.0000
29	Cr	0.0000	0.0000	0.0000	0.0000	0.0000	0.0156	0.0000	0.0000	0.0219	0.0000	0.0122	0.0000	0.0000	0.0102	0.0000
30	Ti	0.3382	0.5960	0.3678	1.9254	1.7218	0.8230	1.5507	1.4913	0.7544	1.1845	0.4465	1.9531	1.3820	0.8078	1.8981
31	Mg	3.5501	6.2348	3.6029	5.0227	5.1847	3.8052	5.3331	5.3447	3.2712	5.6851	3.3100	4.8606	5.4822	3.0063	4.9863
32	Fe 2+	0.0000	0.0231	0.0000	0.0000	0.0000	0.0000	0.0000	0.0000	0.0000	0.0000	0.0000	0.0000	0.0000	0.0000	0.0000
33	Mn	1.8623	0.0726	1.8215	0.0599	0.0781	1.6352	0.0684	0.0920	1.7876	0.0783	1.7843	0.0887	0.0504	1.6774	0.0473
34	Ca	0.1386	0.0000	0.1311	0.0000	0.0000	0.1993	0.0000	0.0000	0.4813	0.0000	0.5333	0.0000	0.0000	0.5666	0.0000
35	Na	0.0719	0.0000	0.0868	0.0000	0.0000	0.0820	0.0000	0.0000	0.0907	0.0000	0.0712	0.0000	0.0000	0.0668	0.0000
36	K	15.2850	14.8760	15.2830	15.0360	15.0110	15.2930	15.0100	14.9820	15.5270	14.8880	15.5250	14.8780	14.9910	15.4930	14.9900
37	SUM	0.0000	0.0000	0.0000	0.0000	0.0000	0.0000	0.0000	0.0000	0.0000	0.0000	0.0000	0.0000	0.0000	0.0000	0.0000
38	Cl															
39		0.8135	0.8127	0.8074	0.7229	0.7507	0.8008	0.7747	0.7818	0.8126	0.8390	0.8811	0.7134	0.7987	0.7884	0.7245
40	Fe/(Fe+Mg)															
41	AFM															
42	Al2O3	0.2617	0.0036	0.2657	0.0081	0.0052	0.2534	0.0088	0.0053	0.2537	0.0064	0.2982	0.0076	0.0097	0.2882	0.0099
43	FeO	0.6562	0.8094	0.6663	0.7163	0.7466	0.5876	0.7672	0.7777	0.6064	0.8245	0.6175	0.7078	0.7909	0.5811	0.7173
44	MgO	0.0821	0.0869	0.0680	0.2746	0.2480	0.1488	0.2231	0.2170	0.1389	0.1888	0.0833	0.2844	0.1994	0.1506	0.2728
45	CFM															
46	CaO	0.3240	0.0105	0.3145	0.0085	0.0113	0.2837	0.0100	0.0133	0.3075	0.0113	0.3229	0.0129	0.0075	0.3055	0.0086
47	FeO	0.8176	0.8031	0.8229	0.7167	0.7422	0.5735	0.7670	0.7715	0.5827	0.8206	0.5874	0.7042	0.7926	0.5475	0.7196
48	MgO	0.0585	0.0863	0.0635	0.2747	0.2485	0.1428	0.2230	0.2153	0.1288	0.1881	0.0806	0.2830	0.1999	0.1470	0.2736
49	ACF															
50	Al2O3	0.2080	0.0036	0.1988	0.0090	0.0052	0.1856	0.0087	0.0052	0.1806	0.0065	0.2245	0.0077	0.0096	0.2195	0.0099
51	CaO	0.2581	0.0105	0.2520	0.0085	0.0113	0.2282	0.0099	0.0132	0.2489	0.0112	0.2497	0.0128	0.0072	0.2364	0.0086
52	FeO+MgO	0.5344	0.8858	0.5483	0.9625	0.9636	0.5792	0.9805	0.9818	0.5805	0.9822	0.5258	0.9796	0.9831	0.5421	0.9834
53																

	10	1H	1I	1J	1K	1L
1	date	30-Jan-86	30-Jan-86	23-Jan-86	23-Jan-86	23-Jan-86
2	method	eds	eds	eds	eds	eds
3	rock type	4	4	3	3	3
4	mineral	grun	hbl	grun	grun	hbl
5	study area	c	c	c	c	c
6					(in hbl 1)	
7	sample	4PLC018	4PLC018	4PLC020	4PLC020	4PLC020
8	PTS area	circ 2	circ 2	circ 1	circ 1	circ 1
9	analysis	grun 1	hbl 1	grun	grun 1	hbl 1
10		51.281	41.852	50.701	51.021	40.756
11	SiO2	0.597	16.194	0.945	0.521	16.982
12	Al2O3	0.000	0.000	0.000	0.000	0.000
13	Cr2O3	0.000	0.196	0.000	0.000	0.114
14	TiO2	8.486	3.951	7.805	8.093	3.372
15	MgO	37.737	24.479	38.552	38.378	24.123
16	FeO	0.000	0.000	0.000	0.000	0.000
17	MnO	0.461	10.244	0.277	0.364	10.775
18	CaO	0.153	1.886	0.000	0.000	0.484
19	Na2O	0.000	0.380	0.000	0.000	0.380
20	K2O	0.000	0.000	0.000	0.000	0.000
21	Cl	98.740	99.190	98.280	98.400	96.950
22	TOTAL					
23	O based on a	23.0000	23.0000	23.0000	23.0000	23.0000
24						
25	cations based	7.9428	6.3317	7.9195	7.9538	6.2863
26	Si	0.0572	1.6683	0.0805	0.0462	1.7137
27	Al iv	0.0516	1.2192	0.0934	0.0485	1.3807
28	Al vi	0.0000	0.0000	0.0000	0.0000	0.0000
29	Cr	0.0000	0.0222	0.0000	0.0000	0.0132
30	Ti	1.9506	0.8910	1.8171	1.8506	0.7751
31	Mg	4.8881	3.8971	5.0360	5.0035	3.1117
32	Fe 2+	0.0000	0.0000	0.0000	0.0000	0.0000
33	Mn	0.0796	1.6604	0.0464	0.0642	1.7806
34	Ca	0.0458	0.5541	0.0000	0.0000	0.1448
35	Na	0.0000	0.0895	0.0000	0.0000	0.0709
36	K	15.0250	15.5140	14.9930	14.9980	15.2660
37	SUM	0.0000	0.0000	0.0000	0.0000	0.0000
38	Cl					
39		0.7136	0.7766	0.7348	0.7268	0.8006
40	Fe/(Fe+Mg)					
41	AFM					
42	Al2O3	0.0079	0.2658	0.0125	0.0068	0.2840
43	FeO	0.7082	0.5702	0.7256	0.7218	0.5732
44	MgO	0.2839	0.1640	0.2618	0.2713	0.1428
45	CFM					
46	CaO	0.0115	0.2940	0.0087	0.0092	0.3142
47	FeO	0.7056	0.5483	0.7299	0.7201	0.5491
48	MgO	0.2829	0.1577	0.2634	0.2707	0.1368
49	ACF					
50	Al2O3	0.0078	0.2036	0.0124	0.0068	0.2139
51	CaO	0.0114	0.2341	0.0086	0.0092	0.2470
52	FeO+MgO	0.9808	0.5623	0.9809	0.9840	0.5392
53						

	A	B	C	D	E	F	G	H	I	J	K	L	M	N	O	P
1	date	23-Jan-86	23-Jan-86	23-Jan-86	16-Jan-86	16-Jan-86	14-Jan-86	14-Jan-86	27-Jan-86	27-Jan-86	30-Jan-86	30-Jan-86	30-Jan-86	30-Jan-86	30-Jan-86	30-Jan-86
2	method	eda	eda	eda	eda	eda	eda	eda	eda	eda	eda	eda	eda	eda	eda	eda
3	rock type	3	3	3	0	0	3	3	3	3	3	3	3	3	3	3
4	mineral	grun	grun	hbl	hbl	hbl	grun	grun	grun	grun	grun	hbl	grun	act	grun	grun
5	study area	c	c	c	c	c	c	c	c	c	c	c	c	c	c	c
6			(in hbl 1)													
7	sample	4PLC020	4PLC020	4PLC020	5PLC008	5PLC008	5PLC012	5PLC012	5PLC015	5PLC015	5PLC015	5PLC015	5PLC015	5PLC015	5PLC015	5PLC015
8	PTS area	circ 2	circ 2	circ 2	circ 1	circ 1	circ 1	circ 1	circ 1	circ 1	circ 2	circ 2	circ 2	circ 2	circ 3	circ 3
9	analysis	grun	grun 1	hbl 1	hbl 1	hbl 2	grun	grun 1	grun 1	grun 2	grun 1	hbl 1	grun 2	hbl 2	grun 1	grun 2
10	SiO2	50.359	50.646	41.310	42.912	41.550	50.883	50.518	49.869	50.127	50.224	47.500	50.172	47.721	50.381	50.462
11	Al2O3	0.821	0.650	16.011	12.990	15.032	0.550	0.872	0.883	0.667	0.849	5.262	0.834	5.141	0.478	0.352
12	Cr2O3	0.000	0.000	0.000	0.000	0.000	0.000	0.000	0.000	0.000	0.000	0.000	0.000	0.000	0.000	0.000
13	TiO2	0.000	0.154	0.113	0.172	0.087	0.000	0.000	0.101	0.000	0.000	0.000	0.000	0.000	0.000	0.000
14	MgO	7.743	8.268	3.758	2.881	2.408	7.091	6.763	5.392	5.874	5.936	3.978	6.004	3.997	5.851	5.784
15	FeO	38.454	37.837	24.609	28.160	25.858	40.865	40.513	42.041	41.469	41.025	30.266	41.319	30.227	42.003	41.844
16	MnO	0.000	0.000	0.000	0.000	0.000	0.000	0.000	0.000	0.000	0.000	0.000	0.000	0.000	0.000	0.000
17	CaO	0.320	0.453	10.123	11.572	11.668	0.269	0.200	0.383	0.470	0.294	11.068	0.451	11.280	0.327	0.379
18	Na2O	0.000	0.000	0.492	0.988	1.123	0.000	0.000	0.000	0.000	0.174	0.623	0.000	0.884	0.000	0.000
19	K2O	0.000	0.000	0.397	0.261	0.274	0.000	0.000	0.000	0.000	0.000	0.118	0.000	0.131	0.000	0.000
20	Cl	0.000	0.000	0.000	0.000	0.000	0.000	0.000	0.000	0.000	0.000	0.000	0.000	0.000	0.000	0.000
21	TOTAL	97.700	98.010	96.810	97.856	98.000	99.400	98.870	98.870	98.410	98.500	98.810	98.870	99.190	99.040	98.820
22	O based on anhyrous O+Cl=23															
23		23.0000	23.0000	23.0000	23.0000	23.0000	23.0000	23.0000	23.0000	23.0000	23.0000	23.0000	23.0000	23.0000	23.0000	23.0000
24	cations based on 23O															
25	SI	7.9217	7.9174	6.3826	6.6348	6.4229	7.9313	7.9172	7.9068	7.9468	7.9341	7.3776	7.9068	7.8550	7.9474	7.9730
26	Al iv	0.0783	0.0826	1.6172	1.3651	1.5771	0.0687	0.0828	0.0931	0.0531	0.0659	0.6224	0.0932	0.1450	0.0526	0.0270
27	Al vi	0.0738	0.0371	1.2984	1.0019	1.1615	0.0323	0.0783	0.0719	0.0716	0.0922	0.3409	0.0616	0.7928	0.0360	0.0385
28	Cr	0.0000	0.0000	0.0000	0.0000	0.0000	0.0000	0.0000	0.0000	0.0000	0.0000	0.0000	0.0000	0.0000	0.0000	0.0000
29	TI	0.0000	0.0181	0.0132	0.0200	0.0101	0.0000	0.0000	0.0121	0.0000	0.0000	0.0000	0.0107	0.0000	0.0000	0.0000
30	Mg	1.8154	1.9264	0.8656	0.6640	0.5548	1.6474	1.5799	1.2742	1.3407	1.3978	0.9209	1.4104	0.9220	1.3758	1.3621
31	Fe 2+	5.0587	4.9467	3.1799	3.3828	3.3427	5.2830	5.3098	5.5746	5.4580	5.4200	3.9313	5.4455	3.9123	5.5411	5.5290
32	Mn	0.0000	0.0000	0.0000	0.0000	0.0000	0.0000	0.0000	0.0000	0.0000	0.0000	0.0000	0.0000	0.0000	0.0000	0.0000
33	Ca	0.0539	0.0758	1.6758	1.9170	1.9324	0.0449	0.0338	0.0651	0.0796	0.0496	1.8419	0.0762	1.8704	0.0552	0.0641
34	Na	0.0000	0.0000	0.1473	0.2893	0.3367	0.0000	0.0000	0.0000	0.0000	0.0534	0.1877	0.0000	0.2884	0.0000	0.0000
35	K	0.0000	0.0000	0.0782	0.0515	0.0541	0.0000	0.0000	0.0000	0.0000	0.0000	0.0231	0.0000	0.0259	0.0000	0.0000
36	SUM	15.0020	15.0040	15.2590	15.3380	15.3920	15.0180	15.0020	14.9980	14.9800	15.0130	15.2480	15.0040	15.7320	15.0080	14.9940
37	CI	0.0000	0.0000	0.0000	0.0000	0.0000	0.0000	0.0000	0.0000	0.0000	0.0000	0.0000	0.0000	0.0000	0.0000	0.0000
38																
39	Fe/(Fe+Mg)	0.7358	0.7197	0.7860	0.8358	0.8578	0.7628	0.7707	0.8140	0.8040	0.7950	0.8102	0.7943	0.8093	0.8011	0.8023
40																
41	AFM															
42	Al2O3	0.0108	0.0086	0.2849	0.2263	0.2690	0.0072	0.0119	0.0119	0.0090	0.0115	0.0903	0.0112	0.0884	0.0064	0.0047
43	FeO	0.7279	0.7135	0.5778	0.6466	0.6347	0.7571	0.7618	0.8043	0.7967	0.7858	0.7370	0.7854	0.7377	0.7986	0.7985
44	MgO	0.2612	0.2779	0.1573	0.1270	0.1054	0.2358	0.2287	0.1838	0.1943	0.2026	0.1727	0.2034	0.1738	0.1976	0.1967
45	CFM															
46	CaO	0.0078	0.0109	0.2829	0.3215	0.3315	0.0064	0.0048	0.0054	0.0115	0.0073	0.2752	0.0110	0.2790	0.0078	0.0092
47	FeO	0.7302	0.7119	0.5556	0.5872	0.5734	0.7577	0.7668	0.8083	0.7947	0.7892	0.5073	0.7855	0.5835	0.7948	0.7949
48	MgO	0.2620	0.2772	0.1513	0.1113	0.0952	0.2358	0.2282	0.1843	0.1938	0.2035	0.1378	0.2035	0.1375	0.1973	0.1958
49	ACF															
50	Al2O3	0.0100	0.0085	0.2031	0.1654	0.1952	0.0072	0.0115	0.0118	0.0089	0.0114	0.0671	0.0110	0.0654	0.0063	0.0047
51	CaO	0.0077	0.0108	0.2334	0.2682	0.2684	0.0064	0.0048	0.0053	0.0114	0.0072	0.2567	0.0109	0.2607	0.0079	0.0092
52	FeO+MgO	0.9914	0.9906	0.7335	0.7582	0.7414	0.9934	0.9937	0.9726	0.9796	0.9915	0.6762	0.9781	0.7738	0.9858	0.9941

	A	B	C	D	E	F	G	H	I	J	K	L	M	N
1	date	30-Oct-86	12-Dec-85	12-Dec-85	20-Nov-86	20-Nov-86	12-Dec-85	12-Dec-85	17-Dec-85	17-Dec-85	25-Nov-86	20-Nov-86	20-Nov-86	20-Nov-86
2	method	edx	wda/eda	wda/eda	edx	edx	wda/eda	wda/eda	wda/eda	wda/eda	edx	edx	edx	edx
3	rock type	6	7	7	7	7	6	6	7	7	6	6	7	7
4	mineral	grun	hbl	grun	grun	hbl	act	hbl	grun	hbl	grun	hbl	grun	hbl
5	study area	e	f	f	f	f	f	f	f	f	f	f	f	f
6		reren												
7	sample	4PLE019	4PLF011	4PLF011	4PLF011	4PLF011	4PLF012	4PLF012	4PLF012	4PLF012	4PLF024	4PLF024	4PLF024	4PLF024
8	PTS area	circ 3	circ 1	circ 1	circ 1	circ 1	circ 1	circ 2	circ 3	circ 3	circ 1	circ 1	circ 2	circ 2
9	analysis	grun 1	hbl 1	grun 1	grun 1	hbl 1	act 1	hbl 1	grun 1	hbl 1	grun 1	hbl 1	grun 1	hbl 1
10	SiO2	49.282	41.182	50.184	50.223	40.950	49.106	44.582	48.785	42.903	49.661	40.885	49.938	42.871
11	Al2O3	0.306	12.927	0.540	0.583	13.350	2.083	7.362	0.[illegible]	7.629	0.267	5.370	0.201	6.025
12	Cr2O3	0.000	0.000	0.000	0.000	0.000	0.000	0.000	0.000	0.000	0.000	0.000	0.000	0.000
13	TiO2	0.000	0.291	0.000	0.000	0.268	0.000	0.112	0.000	0.182	0.000	0.332	0.000	0.227
14	MgO	2.181	2.751	5.345	5.530	2.882	2.366	1.896	3.493	2.269	3.441	2.115	3.022	2.414
15	FeO	46.750	28.531	41.979	42.050	27.869	33.313	32.504	44.614	32.018	44.501	31.625	43.843	31.837
16	MnO	0.066	0.000	0.065	0.000	0.000	0.000	0.000	0.075	0.000	0.006	0.000	0.096	0.000
17	CaO	0.988	10.520	0.615	0.615	10.766	10.669	10.896	0.821	10.567	0.494	10.032	0.854	10.496
18	Na2O	0.000	1.758	0.000	0.000	1.858	0.258	0.885	0.000	0.655	0.000	1.494	0.000	1.586
19	K2O	0.000	0.651	0.000	0.000	0.679	0.086	0.544	0.000	0.494	0.000	0.887	0.000	0.635
20	Cl	0.000	0.000	0.000	0.000	0.000	0.000	0.000	0.000	0.000	0.000	0.000	0.000	0.000
21	TOTAL	98.64	98.59	98.73	99.01	98.86	98.00	98.59	98.00	98.70	98.78	95.84	97.05	98.09
22	O based on anhyrous O+Cl=23													
23		23.0000	23.0000	23.0000	23.0000	23.0000	23.0000	23.0000	23.0000	23.0000	23.0000	23.0000	23.0000	23.0000
24	cations based on 23O													
25	Si	7.9918	6.4415	7.9540	7.9356	6.3854	7.7768	7.0708	7.9345	6.9507	7.9871	6.7571	8.0121	6.8823
26	Al iv	0.0082	1.5585	0.0460	0.0644	1.6146	0.2234	0.9292	0.4150	1.0493	0.0129	1.2429	0.0000	1.1377
27	Al vi	0.0617	0.8258	0.0548	0.0458	0.8405	0.1653	0.4467	0.0000	0.4072	0.0378	0.3835	0.0388	0.3782
28	Cr	0.0000	0.0000	0.0000	0.0000	0.0000	0.0000	0.0000	0.0000	0.0000	0.0000	0.0000	0.0000	0.0000
29	Ti	0.0000	0.0343	0.0000	0.0000	0.0316	0.0000	0.0134	0.0000	0.0197	0.0000	0.0412	0.0000	0.0274
30	Mg	0.5271	0.6418	1.2628	1.3023	0.6698	0.5589	0.4482	0.8468	0.5478	0.8250	0.5197	0.7375	0.5758
31	Fe 2+	6.2033	3.7340	5.5842	5.5564	3.6499	4.4117	4.3103	6.0682	4.3380	6.0382	4.3884	6.0185	4.2618
32	Mn	0.0091	0.0000	0.0088	0.0000	0.0000	0.0000	0.0000	0.0103	0.0000	0.0000	0.0000	0.0133	0.0000
33	Ca	0.1716	1.7939	0.1045	0.1041	1.7992	1.8442	1.8175	0.1430	1.8342	0.0851	1.7721	0.1497	1.8005
34	Na	0.0000	0.5334	0.0000	0.0000	0.5923	0.0784	0.2722	0.0000	0.2057	0.0000	0.4777	0.0000	0.4823
35	K	0.0000	0.1300	0.0000	0.0000	0.1352	0.0174	0.1101	0.0000	0.1020	0.0000	0.1445	0.0000	0.1296
36	SUM	14.973	15.663	14.995	15.009	15.710	15.077	15.418	15.416	15.455	14.987	15.888	14.968	15.664
37	Cl	0.0000	0.0000	0.0000	0.0000	0.0000	0.0000	0.0000	0.0000	0.0000	0.0000	0.0000	0.0000	0.0000
38														
39	Fe/(Fe+Mg)	0.9217	0.8533	0.8150	0.8101	0.8449	0.8876	0.9058	0.8775	0.8879	0.8798	0.8935	0.8908	0.8810
40														
41	AFM													
42	Al2O3	0.0052	0.2141	0.0073	0.0080	0.2213	0.0376	0.1263	0.0030	0.1297	0.0037	0.1428	0.0029	0.1353
43	FeO	0.9169	0.6706	0.8090	0.8037	0.8580	0.8542	0.7914	0.8749	0.7727	0.8766	0.7659	0.8883	0.7618
44	MgO	0.0779	0.1153	0.1836	0.1884	0.1207	0.1082	0.0823	0.1221	0.0976	0.1197	0.0813	0.1089	0.1029
45	CFM													
46	CaO	0.0249	0.2873	0.0151	0.0150	0.2940	0.2786	0.2784	0.0203	0.2729	0.0122	0.2664	0.0217	0.2712
47	FeO	0.8988	0.6082	0.8027	0.7980	0.5965	0.6474	0.6555	0.8598	0.6455	0.8590	0.6555	0.8715	0.6420
48	MgO	0.0764	0.1045	0.1822	0.1870	0.1095	0.0820	0.0682	0.1200	0.0815	0.1167	0.0781	0.1088	0.0867
49	ACF													
50	Al2O3	0.0050	0.1626	0.0072	0.0079	0.1671	0.0277	0.0947	0.0029	0.0978	0.0036	0.1089	0.0028	0.1024
51	CaO	0.0247	0.2406	0.0150	0.0148	0.2448	0.2631	0.2502	0.0202	0.2463	0.0122	0.2374	0.0216	0.2435
52	FeO+MgO	0.9702	0.5988	0.9776	0.9773	0.5880	0.7092	0.6551	0.9769	0.6560	0.9842	0.6537	0.9756	0.6542

	A	B	C	D	E	F	G	H	I	J	K	L	M	N	O
1	date	13-Nov-85	17-Mar-86	17-Mar-86	17-Mar-86	17-Mar-86	6-Mar-86	6-Mar-86	17-Mar-86	17-Mar-86	1-Mar-86	1-Mar-86	1-Mar-86	12-Feb-86	12 Feb-86
2	method	wds-eds	eds	eds	eds	eds	eds	eds	eds	eds	eds	eds	eds	eds	eds
3	rock type	4	4	4	4	4	3	3	3	3	7	7	7	5	5
4	mineral	chlor	chlor	chlor	chlor	chlor	bio	chlor	bio	chlor	stilp	stilp	stilp	stilp	stilp
5	study area	a	a	a	a	a	a	a	a	a	b	b	b	b	b
6															
7	sample	4PLA010	5PLA085	5PLA085	5PLA069	5PLA069	5PLA105	5PLA105	5PLA105	5PLA105	4PLB028c	4PLB028c	4PLB028c	5PLB004	5PLB004
8	PTS area	circ 1	circ 1	circ 2	circ 1	circ 1	circ 1	circ 1	circ 2	circ 2	area 2	circ 1	circ 1	circ 1	circ 3
9	analysis	chlor 1	chlor 1	chlor 1	chlor 1	chlor 1	bio 1	chlor 1	bio 1	chlor 1	stilp 2	stilp 3	stilp 4	stilp	stilp 1
10															
11	SiO2	23.685	23.335	23.947	24.036	22.995	34.280	24.206	34.666	23.040	45.075	45.095	44.483	44.585	44.103
12	Al2O3	20.159	20.396	19.572	19.743	21.003	18.060	21.292	17.700	21.689	6.004	6.422	6.321	6.393	6.474
13	TiO2	0.000	0.093	0.149	0.193	0.117	2.076	0.218	2.104	0.000	0.000	0.000	0.000	0.000	0.000
14	Cr2O3	0.000	0.085	0.084	0.134	0.107	0.000	0.106	0.000	0.082	0.000	0.000	0.000	0.000	0.000
15	MgO	6.547	6.184	6.310	6.562	6.181	6.629	9.687	6.606	9.216	1.376	1.317	1.186	1.737	1.679
16	FeO*	37.902	38.800	38.071	38.778	38.911	24.854	33.294	25.120	33.697	37.429	37.211	37.026	36.479	35.978
17	MnO	0.000	0.000	0.000	0.000	0.000	0.000	0.000	0.000	0.000	0.000	0.085	0.000	0.000	0.000
18	CaO	0.000	0.000	0.162	0.120	0.000	0.000	0.102	0.000	0.000	0.166	0.174	0.143	0.171	0.189
19	Na2O	0.204	0.207	0.000	0.117	0.251	0.134	0.265	0.317	0.254	0.000	0.000	0.000	0.000	0.172
20	K2O	0.000	0.000	0.000	0.000	0.000	8.555	0.080	8.966	0.000	1.863	2.111	2.141	1.563	1.817
21	Cl	0.000	0.000	0.000	0.000	0.000	0.000	0.000	0.000	0.000	0.286	0.274	0.286	0.192	0.179
22	TOTAL	88.477	89.110	88.295	89.665	89.565	94.610	89.250	95.481	88.566	92.148	92.606	91.470	91.056	90.551
23	H2O (diff)	11.523	10.890	10.705	10.315	10.435	5.380	10.750	4.519	11.434	7.854	7.394	8.529	8.944	9.449
24															
25	cations based on 22 oxygens (bio,stilp) , 28 oxygens (chlor)														
26	Si	5.3188	5.2333	5.3809	5.3487	5.1335	5.3805	5.2455	5.4215	5.1770	7.3328	7.2956	7.2988	7.2868	7.2814
27	Al iv	2.6832	2.7667	2.6391	2.6533	2.8665	2.6095	2.7545	2.5785	2.8221	0.6672	0.7044	0.7011	0.7132	0.7386
28	Al vi	2.6549	2.6241	2.5248	2.5222	2.6596	0.7413	2.6835	0.8838	2.7703	0.4840	0.5201	0.5213	0.5188	0.5176
29	Ti	0.0000	0.0157	0.0250	0.0323	0.0197	0.2457	0.0355	0.2474	0.0000	0.0000	0.0000	0.0000	0.0000	0.0000
30	Cr	0.0000	0.0151	0.0148	0.0236	0.0189	0.0000	0.0181	0.0000	0.0142	0.0000	0.0000	0.0000	0.0000	0.0000
31	Mg	2.1924	2.0705	2.1057	2.1755	2.0566	1.5537	3.1268	1.5402	3.0086	0.3336	0.3175	0.2777	0.4233	0.4120
32	Fe2+	7.1215	7.2770	7.3149	7.2132	7.2645	3.2685	6.0337	3.2654	6.1710	5.0921	5.0348	5.0809	4.9882	4.9538
33	Mn	0.0000	0.0000	0.0000	0.0000	0.0000	0.0000	0.0000	0.0000	0.0000	0.0000	0.0000	0.0000	0.0000	0.0000
34	Ca	0.0000	0.0000	0.0388	0.0286	0.0000	0.0000	0.0237	0.0000	0.0000	0.0283	0.0301	0.0251	0.0299	0.0333
35	Na	0.0888	0.0899	0.0000	0.0505	0.1085	0.0410	0.1114	0.0963	0.1079	0.0000	0.0000	0.0000	0.0000	0.0550
36	K	0.0000	0.0000	0.0000	0.0000	0.0000	1.7162	0.0221	1.7888	0.0000	0.3888	0.4357	0.4481	0.3260	0.3810
37	SUM	20.0576	20.0923	20.0241	20.0458	20.1280	15.5664	20.0588	15.6420	20.0720	14.3258	14.3488	14.3531	14.2862	14.3533
38	Cl	0.0000	0.0000	0.0000	0.0000	0.0000	0.0000	0.0000	0.0000	0.0000	0.0823	0.0750	0.0784	0.0531	0.0501
39															
40	Fe2+/(Mg+Fe2+)	0.7646	0.7785	0.7765	0.7683	0.7793	0.6778	0.6585	0.6806	0.6723	0.9385	0.9407	0.9462	0.9216	0.9232
41	AFM														
42	Al2O3	0.2227	0.2238	0.2151	0.2161	0.2288	0.2578	0.2288	0.2526	0.2335	0.0958	0.1027	0.1024	0.1022	0.1048
43	FeO	0.5845	0.6043	0.6084	0.6023	0.6011	0.5030	0.5078	0.5068	0.5153	0.8485	0.8441	0.8511	0.8276	0.8265
44	MgO	0.1830	0.1719	0.1754	0.1816	0.1702	0.2391	0.2633	0.2385	0.2512	0.0536	0.0532	0.0465	0.0702	0.0667
45	CFM														
46	CaO	0.0000	0.0000	0.0041	0.0030	0.0000	0.0000	0.0020	0.0000	0.0000	0.0054	0.0058	0.0047	0.0055	0.0062
47	FeO	0.7648	0.7785	0.7733	0.7660	0.7793	0.6778	0.6568	0.6800	0.6725	0.9335	0.9354	0.9438	0.9167	0.9175
48	MgO	0.2354	0.2215	0.2226	0.2310	0.2207	0.3222	0.3408	0.3182	0.3277	0.0612	0.0590	0.0516	0.0778	0.0763
49	ACF														
50	Al2O3	0.2227	0.2238	0.2144	0.2156	0.2288	0.2578	0.2284	0.2526	0.2335	0.0954	0.1021	0.1026	0.1017	0.1042
51	CaO	0.0000	0.0000	0.0032	0.0024	0.0000	0.0000	0.0020	0.0000	0.0000	0.0040	0.0050	0.0042	0.0049	0.0055
52	FeO+MgO	0.7773	0.7762	0.7824	0.7821	0.7714	0.7422	0.7688	0.7474	0.7665	0.9397	0.9328	0.9336	0.9334	0.9303

	P	Q	R	S	T	U	V	W	X	Y	Z	AA	AB	AC	AD
1	date	12-Feb-86	12-Feb-86	3-Mar-86	3-Mar-86	3-Mar-86	3-Mar-86	16-Feb-86	16-Feb-86	16-Feb-86	19-Dec-85	14-Jan-86	30-Jan-86	23-Jan-86	23-Jan-86
2	method	edx	edx	edx	edx	edx	edx	edx	edx	edx	edx	edx	edx	edx	edx
3	rock type	3	3	3	3	3	3	4	4	4	3	3	4	3	3
4	mineral	chlor	chlor	chlor	chlor	chlor	chlor	chlor	chlor	chlor	chlor	chlor	chlor	chlor	chlor
5	study area	b	b	b	b	b	b	b	b	b	c	c	c	c	c
6															
7	sample	5PLB006	5PLB006	5PLB030	5PLB030	5PLB030	5PLB030	5PLB071	5PLB071	5PLB071	4PLC017	4PLC017	4PLC018	4PLC020	4PLC020
8	PTS area	circ 1	circ 2	circ 1	circ 1	circ 2	circ 2	circ 1	circ 2	circ 2	circ 1	circ 2	circ 1	circ 1	circ 2
9	analysis	chlor 1	chlor 1	chlor 1	chlor 2	chlor 2	chlor 2	chlor 1	chlor 1	chlor 2	chlor 1	chlor 1	chlor 1	chlor 1	chlor 1
10															
11	SiO2	22.363	22.306	23.357	23.298	23.467	23.262	23.686	23.653	23.729	23.884	23.458	23.473	23.248	23.794
12	Al2O3	19.176	19.270	19.302	18.573	19.691	19.283	19.180	19.083	18.978	21.888	22.141	21.932	20.378	20.568
13	TiO2	0.090	0.097	0.118	0.137	0.127	0.115	0.115	0.090	0.094	0.000	0.088	0.000	0.097	0.094
14	Cr2O3	0.000	0.000	0.000	0.000	0.101	0.000	0.000	0.000	0.000	0.000	0.000	0.000	0.091	0.000
15	MgO	3.877	3.586	4.763	4.606	4.600	4.517	5.803	5.297	5.306	7.573	6.752	6.922	6.478	7.701
16	FeO*	42.976	42.760	41.725	41.415	41.428	41.432	39.436	39.742	39.669	37.383	36.182	37.752	37.926	36.187
17	MnO	0.000	0.000	0.000	0.000	0.000	0.000	0.134	0.000	0.101	0.000	0.000	0.000	0.000	0.000
18	CaO	0.000	0.000	0.000	0.000	0.127	0.092	0.000	0.074	0.140	0.000	0.000	0.000	0.000	0.000
19	Na2O	0.170	0.000	0.000	0.000	0.000	0.000	0.154	0.000	0.156	0.196	0.204	0.390	0.000	0.000
20	K2O	0.000	0.000	0.000	0.000	0.000	0.000	0.000	0.000	0.000	0.000	0.000	0.000	0.000	0.000
21	Cl	0.000	0.000	0.000	0.000	0.000	0.000	0.000	0.000	0.000	0.000	0.000	0.000	0.000	0.000
22	TOTAL	88.362	88.109	89.277	88.231	89.541	88.701	88.508	87.929	88.185	90.529	90.805	89.569	88.222	88.255
23	H2O (diff)	11.638	11.891	10.723	10.769	10.459	11.299	11.492	12.171	11.805	9.474	9.195	10.431	11.778	11.745
24															
25	cations based on 22 oxygens (bio,ottg) , 28 oxygens (chlor)														
26	Si	5.2067	5.2033	5.3156	5.2945	5.3120	5.3271	5.3768	5.4189	5.4175	5.1624	5.1166	5.1986	5.2430	5.2819
27	Al iv	2.7913	2.7967	2.6842	2.7055	2.6880	2.6729	2.6232	2.5811	2.5825	2.8376	2.8834	2.8002	2.7570	2.7181
28	Al vi	2.4727	2.5011	2.4931	2.5370	2.5652	2.5313	2.5061	2.5659	2.5238	2.7340	2.8064	2.8009	2.6596	2.6837
29	Ti	0.0000	0.0170	0.0169	0.0234	0.0217	0.0196	0.0196	0.0000	0.0160	0.0000	0.0145	0.0000	0.0165	0.0156
30	Cr	0.0000	0.0000	0.0000	0.0000	0.0180	0.0000	0.0000	0.0000	0.0000	0.0000	0.0000	0.0000	0.0162	0.0000
31	Mg	1.2766	1.2504	1.6224	1.6287	1.5519	1.5419	1.9634	1.8056	1.8056	2.4606	2.1951	2.2855	2.1778	2.5578
32	Fe2+	8.3711	8.3416	7.9416	7.8711	7.8423	7.9347	7.4866	7.6141	7.5781	6.8147	6.6612	6.9938	7.1535	6.7433
33	Mn	0.0000	0.0000	0.0000	0.0000	0.0000	0.0000	0.0257	0.0000	0.0195	0.0000	0.0000	0.0000	0.0000	0.0000
34	Ca	0.0000	0.0200	0.0000	0.0000	0.0306	0.0226	0.0000	0.0182	0.0344	0.0000	0.0000	0.0000	0.0000	0.0000
35	Na	0.0787	0.0000	0.0000	0.0000	0.0000	0.0000	0.0678	0.0000	0.0701	0.0837	0.0884	0.1674	0.0000	0.0000
36	K	0.0000	0.0000	0.0000	0.0000	0.0000	0.0000	0.0000	0.0000	0.0000	0.0000	0.0000	0.0000	0.0000	0.0000
37	SUM	20.1971	20.1301	20.0760	20.0802	20.0298	20.0503	20.0712	20.0070	20.0476	20.0830	20.0856	20.1376	20.0236	20.0006
38	Cl	0.0000	0.0000	0.0000	0.0000	0.0000	0.0000	0.0000	0.0000	0.0000	0.0000	0.0000	0.0000	0.0000	0.0000
39															
40	Fe2+/(Mg+Fe2+	0.8677	0.8696	0.8304	0.8286	0.8348	0.8373	0.7922	0.8080	0.8076	0.7347	0.7603	0.7537	0.7866	0.7250
41	AFM														
42	Al2O3	0.2143	0.2164	0.2130	0.2163	0.2165	0.2154	0.2135	0.2145	0.2139	0.2310	0.2371	0.2283	0.2249	0.2250
43	FeO	0.6817	0.6815	0.6535	0.6494	0.6524	0.6569	0.6231	0.6347	0.6348	0.5650	0.5800	0.5816	0.5942	0.5818
44	MgO	0.1040	0.1021	0.1335	0.1344	0.1291	0.1277	0.1634	0.1508	0.1513	0.2040	0.1829	0.1901	0.1809	0.2131
45	CFM														
46	CaO	0.0000	0.0021	0.0000	0.0000	0.0033	0.0024	0.0000	0.0019	0.0037	0.0000	0.0000	0.0000	0.0000	0.0000
47	FeO	0.8677	0.8676	0.8304	0.8286	0.8321	0.8353	0.7922	0.8065	0.8046	0.7347	0.7603	0.7537	0.7866	0.7250
48	MgO	0.1323	0.1301	0.1696	0.1714	0.1647	0.1623	0.2078	0.1916	0.1917	0.2653	0.2397	0.2463	0.2334	0.2750
49	ACF														
50	Al2O3	0.2143	0.2160	0.2130	0.2163	0.2170	0.2150	0.2135	0.2142	0.2133	0.2310	0.2371	0.2283	0.2249	0.2250
51	CaO	0.0000	0.0016	0.0000	0.0000	0.0026	0.0018	0.0000	0.0015	0.0029	0.0000	0.0000	0.0000	0.0000	0.0000
52	FeO+MgO	0.7857	0.7823	0.7870	0.7837	0.7795	0.7831	0.7865	0.7843	0.7836	0.7690	0.7629	0.7717	0.7751	0.7750

	AE	AF	AG	AH	AI	AJ	AK	AL	AM	AN	AO	AP	AQ
1	date	23-Jan-86	27-Jan-86	27-Jan-86	27-Jan-86	14-Jan-86	14-Jan-86	14-Jan-86	12-Dec-85	20-Nov-85	12-Dec-85	20-Nov-85	17-Dec-85
2	method	eds	eds	eds	eds	eds	eds	eds	wds-eds	eds	wds-eds	eds	wds-eds
3	rock type	2	2	2	2	3	3	3	8	8	8	8	8
4	mineral	bio	bio	chlor	chlor	chlor	chlor	chlor	bio	bio	stilp	stilp	stilp
5	study area	c	c	c	c	c	c	c	f	f	f	f	f
6						in grun	matrix	matrix					
7	sample	4PLC023	4PLC023	4PLC023	4PLC023	5PLC012	5PLC012	5PLC012	4PLF011	4PLFQ11	4PLF011	4PLF011	4PLF012
8	PTS area	circ 1	circ 1	circ 1	circ 1	circ 1	circ 1	circ 2	circ 1	circ 1	circ 1	circ 1	circ 3
9	analysis	bio 1	bio 2	chlor 1	chlor 2	chlor 1	chlor 1	chlor 1	bio 1	bio 1	stilp 1	stilp 1	stilp 1
10													
11	SiO2	34.378	34.989	23.580	24.145	23.747	23.828	23.542	30.132	29.384	45.818	45.178	43.922
12	Al2O3	17.616	18.503	21.777	21.552	20.380	21.447	21.586	14.970	15.780	6.663	6.543	6.225
13	TiO2	2.024	2.123	0.000	0.107	0.000	0.000	0.000	1.698	1.657	0.000	0.000	0.000
14	Cr2O3	0.000	0.000	0.074	0.121	0.000	0.000	0.074	0.000	0.000	0.000	0.000	0.000
15	MgO	6.823	6.551	8.760	8.724	5.854	6.852	6.778	3.345	3.679	1.929	2.273	1.031
16	FeO*	25.496	24.472	33.106	33.424	35.780	37.233	38.154	38.382	37.121	36.061	35.464	36.599
17	MnO	0.000	0.000	0.000	0.086	0.000	0.000	0.000	0.000	0.000	0.000	0.000	0.000
18	CaO	0.000	0.000	0.000	0.078	0.000	0.000	0.000	0.081	0.000	0.000	0.000	0.216
19	Na2O	0.000	0.164	0.358	0.172	0.000	0.000	0.000	0.000	0.194	0.000	0.215	0.000
20	K2O	9.878	9.058	0.000	0.103	0.000	0.000	0.000	5.425	4.854	2.403	2.324	2.591
21	Cl	0.000	0.000	0.000	0.000	0.000	0.000	0.000	0.000	0.000	0.000	0.000	0.000
22	TOTAL	95.013	95.840	87.725	88.513	89.761	89.360	90.145	92.743	92.629	92.875	91.989	90.564
23	H2O (diff)	4.987	4.160	12.275	11.487	10.238	10.640	9.855	7.757	7.371	7.125	8.011	9.436
24													
25	cations based on 22 oxygens (bio,stilp) ; 28 oxygens (chlor)												
26	Si	5.4097	5.4173	5.1985	5.2799	5.2973	5.2588	5.1754	5.1586	5.0051	7.3051	7.2723	7.2710
27	Al iv	2.5903	2.5827	2.8005	2.7201	2.7027	2.7434	2.8246	2.8434	2.8949	0.6949	0.7277	0.7282
28	Al vi	0.6768	0.7955	2.8630	2.8345	2.8554	2.8327	2.7709	0.176	0.171	0.5572	0.5138	0.4865
29	Ti	0.2396	0.2474	0.0000	0.0176	0.0000	0.0000	0.0000	0.2443	0.2380	0.0000	0.0000	0.0000
30	Cr	0.0000	0.0000	0.0130	0.0209	0.0000	0.0000	0.0128	0.0000	0.0000	0.0000	0.0000	0.0000
31	Mg	1.5536	1.5125	2.8815	2.8434	1.9465	2.2531	2.2213	0.8532	0.8347	0.4585	0.5454	0.2544
32	Fe2+	3.3555	3.1705	6.1267	6.1125	7.4211	6.8689	7.0146	5.2084	5.2915	4.8082	4.7748	5.0674
33	Mn	0.0000	0.0000	0.0000	0.0158	0.0000	0.0000	0.0000	0.0000	0.0000	0.0000	0.0000	0.0000
34	Ca	0.0000	0.0000	0.0000	0.0186	0.0000	0.0000	0.0000	0.0148	0.0000	0.0000	0.0000	0.0383
35	Na	0.0000	0.0493	0.1531	0.0728	0.0000	0.0000	0.0000	0.0000	0.0543	0.0000	0.0672	0.0000
36	K	1.7823	1.7901	0.0000	0.0288	0.0000	0.0000	0.0000	1.1843	1.0118	0.4886	0.4774	0.5473
37	SUM	15.8078	15.5653	20.0361	19.9650	20.0230	19.8547	20.0180	15.681	15.7114	14.3127	14.3788	14.3838
38	Cl	0.0000	0.0000	0.0000	0.0000	0.0000	0.0000	0.0000	0.0000	0.0000	0.0000	0.0000	0.0000
39													
40	Fe2+/(Mg+Fe2+	0.6835	0.6770	0.6801	0.6825	0.7922	0.7530	0.7595	0.8582	0.8480	0.9129	0.8978	0.9522
41	AFM												
42	Al2O3	0.2487	0.2651	0.2392	0.2367	0.2224	0.2341	0.2325	0.1984	0.2027	0.1082	0.1045	0.1024
43	FeO	0.5128	0.4876	0.5174	0.5210	0.6160	0.5767	0.5829	0.6879	0.6776	0.6160	0.6037	0.6547
44	MgO	0.2375	0.2374	0.2434	0.2423	0.1616	0.1892	0.1846	0.1127	0.1197	0.0778	0.0918	0.0429
45	CFM												
46	CaO	0.0000	0.0000	0.0000	0.0021	0.0000	0.0000	0.0000	0.0024	0.0000	0.0000	0.0000	0.0071
47	FeO	0.6835	0.6770	0.6801	0.6811	0.7922	0.7530	0.7595	0.8572	0.8480	0.9129	0.8978	0.9464
48	MgO	0.3165	0.3230	0.3199	0.3166	0.2078	0.2470	0.2405	0.1404	0.1501	0.0871	0.1025	0.0475
49	ACF												
50	Al2O3	0.2487	0.2651	0.2392	0.2363	0.2224	0.2341	0.2325	0.1990	0.2027	0.1082	0.1045	0.1018
51	CaO	0.0000	0.0000	0.0000	0.0010	0.0000	0.0000	0.0000	0.0020	0.0000	0.0000	0.0000	0.0064
52	FeO+MgO	0.7503	0.7348	0.7606	0.7621	0.8776	0.7650	0.7675	0.7990	0.7973	0.8938	0.8955	0.8918

	A	B	C	D	E	F	G	H	I	J	K	L	M	N	O
1	date	3-Apr-86	3-Apr-86	3-Apr-86	13-Mar-86	13-Mar-86	13-Mar-86	13-Mar-86	13-Mar-86	13-May-86	13-May-86	13-May-86	13-May-86	3-Apr-86	3-Apr-86
2	method	sem	sem	sem	sem	sem	sem	sem	sem	sem	sem	sem	sem	sem	sem
3	rock type														
4	mineral	epi-low z	epi-high z	epi-low z	epi core low z	epi core high z	epi 1 rim	epi low z	epi high z	epi low z	epi high z	epi low z	epi high z	epi low z	epi high z
5	study area	a	a	a	a	a	a	a	a	a	a	a	a	a	a
6	"z" denotes average atomic number														
7	sample	SPLA041	SPLA041	SPLA041	SPLA056	SPLA056	SPLA056	SPLA056	SPLA056	SPLA060	SPLA060	SPLA060	SPLA060	SPLA062	SPLA062
8	PTS area	circ 1	circ 1	circ 1	circ 1	circ 1	circ 1	circ 2	circ 2	circ 1	circ 1	circ 2	circ 2	circ 2	circ 2
9	analysis	epi 1	epi 1	epi 2	epi	epi	epi 1	epi	epi	epi 1	epi 1	epi 1	epi 1	epi 1	epi 1
10															
11	SiO2	38.975	41.070	39.566	39.834	40.382	39.814	39.222	39.286	39.927	40.166	39.166	39.817	39.644	40.741
12	Al2O3	25.351	24.479	25.204	25.442	25.030	25.435	25.883	25.200	25.629	25.334	25.456	26.017	24.906	23.886
13	TiO2	0.000	0.000	0.000	0.000	0.000	0.000	0.000	0.000	0.000	0.000	0.000	0.000	0.000	0.000
14	Cr2O3	0.062	0.000	0.000	n.a.	n.a.	n.a.	n.a.	n.a.	0.000	0.000	0.000	0.000	0.000	0.000
15	Fe2O3*	7.934	6.829	6.984	8.016	7.491	7.834	9.913	9.673	7.156	7.378	9.467	7.650	9.427	7.847
16	FeO*	2.476	4.718	1.490	2.346	3.506	2.700	0.000	1.138	2.441	2.655	0.266	1.816	1.358	4.126
17	MgO	0.419	0.457	0.450	0.488	0.487	0.520	0.464	0.482	0.306	0.335	0.332	0.374	0.489	0.472
18	MnO	0.000	0.000	0.000	0.000	0.000	0.000	0.000	0.000	0.000	0.000	0.000	0.000	0.000	0.000
19	CaO	21.259	19.500	21.997	21.323	20.401	20.957	24.064	22.267	21.453	21.079	23.079	21.938	22.046	19.721
20	K2O	0.000	0.000	0.000	0.000	0.000	0.000	0.000	0.000	0.000	0.000	0.000	0.000	0.000	0.000
21	Na2O	n.a.	n.a.	n.a.	0.000	0.000	0.000	0.000	0.000	n.a.	n.a.	n.a.	n.a.	n.a.	n.a.
22	TOTAL	97.256	97.058	97.703	97.432	97.277	97.259	98.546	98.057	97.106	97.146	97.806	97.811	97.873	96.585
23															
24	cations normalized to 8														
25	Si	3.1671	3.2798	3.1217	3.1500	3.2058	3.1551	2.9785	3.0810	3.1616	3.1675	3.0796	3.1332	3.1257	3.2757
26	Al	2.3671	2.3036	2.3435	2.3713	2.3430	2.3756	2.3771	2.3360	2.4036	2.3665	2.4128	2.3143	2.2444	
27	Ti	0.0000	0.0000	0.0000	0.0000	0.0000	0.0000	0.0000	0.0000	0.0000	0.0000	0.0000	0.0000	0.0000	0.0000
28	Cr	0.0052	0.0000	0.0000	0.0000	0.0000	0.0000	0.0000	0.0000	0.0000	0.0000	0.0000	0.0000	0.0000	0.0000
29	Fe3+	0.4521	0.4014	0.5295	0.4716	0.4405	0.4614	0.5833	0.5699	0.4215	0.4344	0.5592	0.4487	0.5547	0.4651
30	Fe2+	0.1458	0.2773	0.0978	0.1382	0.2062	0.1590	0.0000	0.0669	0.1437	0.1561	0.0156	0.1065	0.0800	0.2447
31	Mg	0.0485	0.0544	0.0528	0.0553	0.0577	0.0615	0.0539	0.0566	0.0361	0.0396	0.0389	0.0438	0.0575	0.0566
32	Mn	0.0000	0.0000	0.0000	0.0000	0.0000	0.0000	0.0000	0.0000	0.0000	0.0000	0.0000	0.0000	0.0000	0.0000
33	Ca	1.8047	1.6883	1.8594	1.8065	1.7361	1.7795	2.0081	1.8765	1.8202	1.7823	1.9442	1.8496	1.8625	1.6986
34	O	12.5723	12.6172	12.5531	12.5645	12.5868	12.5658	12.4606	12.5395	12.5705	12.5809	12.5364	12.5566	12.5550	12.6156
35															
36	Fe3+/(Fe3+Fe2+)	0.2435	0.4086	0.1422	0.2286	0.3188	0.2583	0.0000	0.1052	0.2543	0.2790	0.0283	0.1918	0.1260	0.3447
37	AFM														
38	Al2O3+Fe2O3	0.9352	0.8006	0.9533	0.9363	0.9134	0.9278	0.9821	0.9592	0.9403	0.9310	0.9812	0.9501	0.9543	0.9000
39	FeO	0.0464	0.0913	0.0291	0.0455	0.0677	0.0520	0.0000	0.0221	0.0477	0.0558	0.0057	0.0354	0.0266	0.0813
40	MgO	0.0164	0.0179	0.0175	0.0192	0.0189	0.0201	0.0179	0.0187	0.0120	0.0131	0.0131	0.0148	0.0191	0.0188
41	CFM														
42	CaO	0.9023	0.8341	0.9297	0.9033	0.8681	0.8896	0.9730	0.9382	0.9101	0.8962	0.9721	0.9248	0.9313	0.8494
43	FeO	0.0729	0.1387	0.0439	0.0681	0.1031	0.0795	0.0000	0.0335	0.0719	0.0841	0.0084	0.0533	0.0400	0.1223
44	MgO	0.0248	0.0272	0.0264	0.0277	0.0288	0.0307	0.0261	0.0283	0.0181	0.0198	0.0195	0.0220	0.0287	0.0283
45	ACF														
46	Al2O3+Fe2O3	0.5651	0.5748	0.5896	0.5870	0.5818	0.5865	0.5893	0.5923	0.5890	0.5837	0.5933	0.5886	0.5692	0.5753
47	CaO	0.3744	0.3546	0.3818	0.3730	0.3629	0.3678	0.4000	0.3626	0.3768	0.3731	0.3953	0.3805	0.3625	0.3607
48	FeO+MgO	0.0405	0.0705	0.0286	0.0400	0.0552	0.0456	0.0107	0.0252	0.0372	0.0432	0.0113	0.0309	0.0282	0.0640
49															
50	n.a. denotes not analyzed														
51	*ferrous/ferric based on stoichiometry														

	P	Q	R	S	T
1	date	3-Apr-86	3-Apr-86	13-May-86	13-May-86
2	method	eds	eds	eds	eds
3	rock type				
4	mineral	epi low z	epi high z	epi core	epi rim
5	study area	a	a	c	c
6					
7	sample	SPLA062	SPLA062	SPLC000	SPLC000
8	PTS area	circ 2	circ 2	circ 2	circ 2
9	analysis	epi 2	epi 2	epi	epi
10					
11	SiO2	39.354	40.213	38.376	38.238
12	Al2O3	25.462	24.347	26.436	26.422
13	TiO2	0.000	0.000	0.000	0.000
14	Cr2O3	0.000	0.000	0.000	0.000
15	Fe2O3*	9.284	8.506	9.613	9.344
16	FeO*	0.854	3.055	0.000	0.000
17	MgO	0.385	0.455	0.337	0.239
18	MnO	0.000	0.000	0.000	0.000
19	CaO	22.611	20.694	24.301	24.216
20	K2O	0.000	0.000	0.000	0.000
21	Na2O	n.a.	n.a.	n.a.	n.a.
22	TOTAL	97.950	97.270	99.063	98.459
23					
24	cations normalized to 8				
25	Si	3.0922	3.2024	2.9718	2.9762
26	Al	2.3578	2.2651	2.4127	2.4254
27	Ti	0.0000	0.0000	0.0000	0.0000
28	Cr	0.0000	0.0000	0.0000	0.0000
29	Fe3+	0.5464	0.5021	0.5622	0.5492
30	Fe2+	0.0502	0.1803	0.0000	0.0000
31	Mg	0.0483	0.0540	0.0388	0.0278
32	Mn	0.0000	0.0000	0.0000	0.0000
33	Ca	1.9036	1.7657	2.0163	2.0206
34	O	12.5410	12.5855	12.4811	12.4871
35					
36	Fe3+/(Fe2+Fe3+)	0.0841	0.2642	0.0000	0.0000
37	AFM				
38	Al2O3+Fe2O3	0.9678	0.9224	0.9871	0.9907
39	FeO	0.0187	0.0587	0.0000	0.0000
40	MgO	0.0134	0.0178	0.0129	0.0093
41	CFM				
42	CaO	0.9518	0.9826	0.9811	0.9864
43	FeO	0.0251	0.0902	0.0000	0.0000
44	MgO	0.0231	0.0270	0.0189	0.0136
45	ACF				
46	Al2O3+Fe2O3	0.5922	0.5822	0.5814	0.5922
47	CaO	0.3891	0.3686	0.4008	0.4023
48	FeO+MgO	0.0197	0.0480	0.0077	0.0055
49					
50	n.a. denotes not analyzed				
51	*ferrous/ferric based on stoichiometry				

	A	B	C	D	E	F	G	H	I	J	K	L	M	N	O	P	Q
1	date	13-Nov-86	12-Dec-86	12-Dec-86	13-Mar-86	13-Mar-86	13-Mar-86	13-Mar-86	10-Mar-86	13-Mar-86	13-Mar-86	13-Mar-86	10-Mar-86	10-Mar-86	10-Mar-86	10-Mar-86	10-Mar-86
2	method	wds/eds	wds-eds	wds-eds	eds	eds	eds	eds	eds	eds	eds	eds	eds	eds	eds	eds	eds
3	rock type	4	4	4	4	4	4	4	4	4	4	4	4	4	4	4	4
4	mineral	gar	gar	gar	gar	gar	gar	gar	gar	gar	gar	gar	gar	gar	gar	gar	gar
5	study area	a	a	a	a	a	a	a	a	a	a	a	a	a	a	a	a
6																	
7	sample	4PLA019	4PLA031	4PLA031	5PLA056	5PLA056	5PLA056	5PLA056	5PLA065	5PLA065	5PLA065	5PLA065	5PLA069	5PLA069	5PLA069	5PLA069	5PLA069
8	PTS area	circ 1	circ 2	circ 2	circ 1	circ 1	circ 2	circ 2	circ 1	circ 1	circ 2	circ 2	circ 1	circ 1	circ 1	circ 1	circ 2
9	analysis	gar 1	gar	gar	gar 1	gar 2	gar 1	gar 2	gar 1	gar 1	gar 2	gar 2	gar 1	gar 1	gar 1	gar 1	gar 2
10			core	rim					core 1	rim 1	core 1	rim 1	core 1	core 2	rim 1	rim 2	core 1
11	SiO2	36 550	36 676	36 602	36 644	36 566	36 547	36 614	36 367	36 629	36 661	36 676	36 367	36 583	36 466	36 463	36 566
12	Al2O3	21 472	19 466	19 267	19 652	19 596	19 396	19 652	21 226	20 554	20 767	20 732	21 277	21 206	21 214	21 291	21 007
13	TiO2	0 000	0 000	0 000	0 000	0 000	0 000	0 000	0 000	0 000	0 000	0 000	0 000	0 081	0 000	0 000	0 113
14	Cr2O3	0 000	0 000	0 000	0 000	0 000	0 000	0 089	0 078	0 068	0 114	0 000	0 000	0 000	0 000	0 084	0 000
15	V2O5	n a	n a	n a	0 000	0 000	0 000	0 000	0 000	0 000	0 000	0 000	0 000	0 000	0 000	0 000	0 000
16	FeOt	0 268	4 173	4 347	4 663	4 772	5 216	5 211	1 223	1 000	1 068	1 264	0 949	0 949	0 917	0 642	1 068
17	FeO	36 941	4 907	4 256	1 670	1 684	1 692	1 639	36 899	36 957	36 868	36 551	36 636	36 699	36 964	37 309	36 192
18	MgO	0 630	0 127	0 063	0 360	0 379	0 191	0 306	1 421	1 376	1 334	1 357	1 634	1 687	1 674	1 627	1 128
19	MnO	0 499	0 139	0 107	0 000	0 000	0 000	0 000	0 188	0 128	0 098	0 098	0 000	0 000	0 000	0 000	0 566
20	CaO	4 379	32 086	32 641	34 615	34 593	35 001	34 966	4 036	3 747	3 940	4 269	3 778	3 779	3 630	3 672	4 329
21	K2O	0 000	0 000	0 000	0 000	0 000	0 000	0 000	n a	0 000	0 000	0 000	n a	n a	n a	n a	n a
22	Na2O	0 000	na	n a	n a	n a	n a	n a	n a	n a	n a	n a	n a	n a	n a	n a	n a
23	TOTAL	100 906	99 616	99 306	99 804	99 901	100 046	100 679	101 534	100 583	100 980	100 967	100 831	101 206	100 868	100 886	100 320
24																	
25	cations normalized to 8																
26	Si	2 9461	2 9972	2 9887	2 9563	2 9585	2 9500	2 9356	2 9121	2 9637	2 9590	2 9542	2 9250	2 9336	2 9336	2 9124	2 9189
27	Al	2 0386	1 7703	1 7561	1 7730	1 7569	1 7494	1 7609	2 0032	1 9590	1 9724	1 9681	2 0174	2 0037	2 0112	1 9958	2 0081
28	Ti	0 0000	0 0000	0 0000	0 0000	0 0000	0 0000	0 0000	0 0058	0 0000	0 0000	0 0000	0 0000	0 0055	0 0000	0 0000	0 0069
29	Cr	0 0000	0 0000	0 0000	0 0000	0 0000	0 0000	0 0053	0 0050	0 0054	0 0073	0 0000	0 0000	0 0000	0 0000	0 0054	0 0000
30	V	0 0000	0 0000	0 0000	0 0000	0 0000	0 0000	0 0000	0 0000	0 0000	0 0000	0 0000	0 0000	0 0000	0 0000	0 0000	0 0000
31	Fe3+	0 0174	0 2425	0 2532	0 2697	0 2746	0 3006	0 2953	0 0739	0 0611	0 0643	0 0777	0 0576	0 0572	0 0552	0 0384	0 0651
32	Fe2+	2 4687	0 3200	0 2756	0 1196	0 1213	0 1081	0 1167	2 4710	2 5010	2 4926	2 4823	2 4763	2 4736	2 4869	2 4923	2 4490
33	Mg	0 0996	0 0146	0 0098	0 0411	0 0432	0 0218	0 0349	0 1696	0 1658	0 1603	0 1629	0 1958	0 2016	0 2007	0 1937	0 1364
34	Mn	0 0340	0 0091	0 0070	0 0000	0 0000	0 0000	0 0000	0 0127	0 0087	0 0067	0 0067	0 0000	0 0000	0 0000	0 0000	0 0388
35	Ca	0 3790	2 8566	2 7077	2 8392	2 8366	2 8699	2 8481	0 3464	0 3248	0 3402	0 3684	0 3256	0 3246	0 3128	0 3142	0 3762
36	SUM	8 0000	8 0000	8 0000	8 0000	8 0000	8 0000	8 0000	8 0000	8 0000	8 0000	8 0000	8 0000	8 0000	8 0000	8 0000	8 0000
37	O	11 9720	11 9940	11 9940	11 9790	11 9800	11 9750	11 9680	11 9590	11 9820	11 9760	11 9770	11 9820	11 9790	11 9870	11 9660	11 9630
38																	
39	Fe2+/(Mg+Fe2+)	0 9615	0 9566	0 9664	0 7442	0 7374	0 8322	0 7686	0 9358	0 9378	0 9396	0 9378	0 9267	0 9246	0 9253	0 9279	0 9472
40	AFM																
41	Al2O3+Fe2O3	0 2643	0 7500	0 7789	0 8640	0 8612	0 8875	0 8717	0 2823	0 2757	0 2774	0 2804	0 2706	0 2781	0 2777	0 2747	0 2663
42	FeO	0 6662	0 2391	0 2136	0 1012	0 1023	0 0936	0 0986	0 6719	0 6792	0 6790	0 6750	0 6677	0 6675	0 6664	0 6730	0 6761
43	MgO	0 0275	0 0109	0 0074	0 0348	0 0364	0 0186	0 0295	0 0461	0 0451	0 0437	0 0447	0 0526	0 0544	0 0539	0 0523	0 0377
44	CFM																
45	CaO	0 1274	0 8679	0 9046	0 9464	0 9452	0 9567	0 9485	0 1160	0 1066	0 1137	0 1231	0 1086	0 1082	0 1043	0 1047	0 1270
46	FeO	0 0380	0 1073	0 0921	0 0389	0 0404	0 0360	0 0389	0 6273	0 6360	0 6329	0 6225	0 6262	0 6246	0 6289	0 6307	0 6269
47	MgO	0 0336	0 0048	0 0032	0 0137	0 0144	0 0073	0 0116	0 0568	0 0556	0 0536	0 0544	0 0653	0 0672	0 0669	0 0646	0 0461
48	ACF																
49	Al2O3+Fe2O3	0 2674	0 2518	0 2515	0 2539	0 2539	0 2547	0 2555	0 2560	0 2534	0 2539	0 2547	0 2570	0 2557	0 2561	0 2532	0 2684
50	CaO	0 0946	0 8643	0 8771	0 7061	0 7052	0 7131	0 7069	0 0861	0 0811	0 0848	0 0917	0 0806	0 0805	0 0775	0 0782	0 0941
51	FeO+MgO	0 648	0 0939	0 0714	0 04	0 0408	0 0323	0 0378	0 658	0 6656	0 6613	0 6536	0 6624	0 6638	0 6683	0 6666	0 6466
52																	
53	CaO	0 1303	0 8695	0 9054	0 9596	0 9590	0 9637	0 9606	0 1224	0 1146	0 1196	0 1296	0 1161	0 1160	0 1117	0 1120	0 1314
54	FeO	0 6560	0 1076	0 0922	0 0404	0 0410	0 0363	0 0394	0 6731	0 6823	0 6778	0 6678	0 6839	0 6840	0 6883	0 6860	0 6551
55	MnO	0 0117	0 0030	0 0023	0 0000	0 0000	0 0000	0 0000	0 0045	0 0031	0 0024	0 0024	0 0000	0 0000	0 0000	0 0000	0 0135
56	n.a. denotes not analyzed																

	R	S	T	U	V	W	X	Y	Z	AA	AB	AC	AD	AE	AF	AG	AH
1	date	10-Mar-86	10-Mar-86	10-Mar-86	10-Mar-86	10-Mar-86	10-Mar-86	6-Mar-86	6-Mar-86	6-Mar-86	6-Mar-86	19-Dec-85	19-Dec-85	14-Jan-86	14-Jan-86	9-Jan-86	9-Jan-86
2	method	ede	ede	ede	ede	ede	ede	ede	ede	ede	ede	ede	ede	ede	ede	ede	ede
3	rock type	4	4	4	4	4	4	3	3	3	3	3	3	3	3	3	3
4	mineral	gar	gar	gar	gar	gar	gar	gar	gar	gar	gar	gar	gar	gar	gar	gar	gar
5	study area	a	a	a	a	a	a	a	a	a	a	c	c	c	c	c	c
6														rerun	rerun	rerun	rerun 2
7	sample	5PLA089	5PLA089	5PLA089	5PLA089	5PLA089	5PLA089	5PLA105	5PLA105	5PLA105	5PLA105	4PLC017	4PLC017	4PLC017	4PLC017	4PLC017	4PLC017
8	PTS area	circ 2	circ 2	circ 2	circ 2	circ 2	circ 2	circ 1	circ 1	circ 2	circ 2	circ 1	circ 1	circ 1	circ 1	circ 1	circ 1
9	chalysis	gar 2	gar 2	gar 2	gar 2	gar 2	gar 2	gar	gar	gar	gar	gar	gar	gar	gar	gar	gar
10		core 2	inner rim 1	inner rim 2	inclus zone	outer rim 1	outer rim 2	core	rim	core	rim	rim	core	rim	core	rim	rim
11	SiO2	36.282	36.311	36.225	36.326	36.266	36.396	36.637	36.733	36.963	36.737	37.006	36.924	37.419	37.337	37.031	37.106
12	Al2O3	21.087	21.151	21.178	21.186	21.150	21.413	21.524	21.474	21.493	21.486	21.540	21.619	21.934	21.713	21.726	21.643
13	TiO2	0.089	0.000	0.000	0.000	0.116	0.136	0.000	0.090	0.108	0.000	0.000	0.000	0.000	0.000	0.000	0.000
14	Cr2O3	0.000	0.065	0.000	0.078	0.000	0.110	0.000	0.102	0.101	0.062	0.000	0.000	0.000	0.000	0.000	0.000
15	V2O5	0.000	0.000	0.000	0.000	0.000	0.000	n.a.	n.a.	n.a.	n.a.	n.a.	n.a.	n.a.	n.a.	n.a.	n.a.
16	Fe2O3	1.126	0.974	0.968	0.920	1.038	0.914	0.494	0.529	0.776	0.704	0.858	0.978	0.476	0.829	0.861	0.899
17	FeO	36.145	36.715	37.100	36.974	36.864	37.294	36.534	36.529	36.586	36.499	37.579	37.636	37.842	37.962	37.446	37.333
18	MgO	1.136	1.165	1.164	1.210	1.393	1.741	1.552	1.758	1.741	1.711	1.326	1.255	1.343	1.236	1.374	1.349
19	MnO	0.597	0.179	0.083	0.000	0.000	0.000	1.346	0.386	0.730	0.339	0.000	0.000	0.000	0.000	0.000	0.000
20	CaO	4.463	4.294	4.043	4.442	4.063	3.431	3.971	3.782	3.746	3.956	4.144	4.193	4.159	4.245	4.299	4.340
21	K2O	n.a.	n.a.	n.a.	n.a.	n.a.	n.a.	0.000	0.000	0.000	0.000	0.000	0.000	0.000	0.000	0.000	0.000
22	Na2O	n.a.	n.a.	n.a.	n.a.	n.a.	n.a.	n.a.	n.a.	n.a.	n.a.	n.a.	n.a.	n.a.	n.a.	n.a.	n.a.
23	TOTAL	100.943	100.894	100.762	100.641	100.902	101.336	101.058	101.374	102.244	101.528	102.492	102.604	103.074	103.311	102.736	102.470
24	cations normalized to 8																
25																	
26	Si	2.9236	2.9265	2.9255	2.9272	2.9226	2.9148	2.9369	2.9347	2.9317	2.9312	2.9336	2.9276	2.9459	2.9376	2.9258	2.9384
27	Al	2.0026	2.0090	2.0159	2.0122	2.0076	2.0211	2.0336	2.0220	2.0091	2.0216	2.0127	2.0292	2.0259	2.0134	2.0230	2.0199
28	Ti	0.0054	0.0000	0.0000	0.0000	0.0070	0.0083	0.0000	0.0054	0.0065	0.0000	0.0000	0.0000	0.0000	0.0000	0.0000	0.0000
29	Cr	0.0000	0.0055	0.0000	0.0050	0.0000	0.0070	0.0000	0.0065	0.0063	0.0052	0.0000	0.0000	0.0000	0.0000	0.0000	0.0000
30	V	0.0000	0.0000	0.0000	0.0000	0.0000	0.0000	0.0000	0.0000	0.0000	0.0000	0.0000	0.0000	0.0000	0.0000	0.0000	0.0000
31	Fe3+	0.0684	0.0590	0.0586	0.0556	0.0628	0.0488	0.0298	0.0314	0.0464	0.0420	0.0536	0.0623	0.0282	0.0491	0.0512	0.0417
32	Fe2+	2.4356	2.4747	2.5059	2.4715	2.4824	2.4961	2.3625	2.4406	2.4266	2.4357	2.4915	2.4956	2.4915	2.4972	2.4743	2.4726
33	Mg	0.1363	0.1424	0.1389	0.1453	0.1672	0.2079	0.1854	0.2094	0.2059	0.2036	0.1565	0.1483	0.1577	0.1449	0.1619	0.1593
34	Mn	0.0406	0.0122	0.0057	0.0000	0.0000	0.0000	0.0914	0.0261	0.0491	0.0229	0.0000	0.0000	0.0000	0.0000	0.0000	0.0000
35	Ca	0.3870	0.3707	0.3499	0.3835	0.3506	0.2945	0.3411	0.3237	0.3183	0.3383	0.3819	0.3561	0.3588	0.3679	0.3739	0.3662
36	SUM	8.0000	8.0000	8.0000	8.0000	8.0000	8.0000	8.0000	8.0000	8.0000	8.0000	8.0000	8.0000	8.0000	8.0000	8.0000	8.0000
37	O	11.9640	11.9630	11.9630	11.9640	11.9660	11.9620	11.9690	11.9700	11.9690	11.9660	11.9669	11.9636	11.9730	11.9669	11.9629	11.9662
38																	
39	Fe2+/(Mg+Fe2+)	0.9470	0.9456	0.9475	0.9445	0.9369	0.9232	0.9278	0.9210	0.9218	0.9229	0.9409	0.9439	0.9405	0.9451	0.9384	0.9395
40	AFM																
41	Al2O3+Fe2O3	0.2870	0.2832	0.2817	0.2832	0.2800	0.2767	0.2666	0.2792	0.2606	0.2611	0.2666	0.2816	0.2794	0.2807	0.2823	0.2814
42	FeO	0.6752	0.6776	0.6806	0.6770	0.6737	0.6678	0.6619	0.6636	0.6630	0.6636	0.6766	0.6761	0.6777	0.6788	0.6736	0.6751
43	MgO	0.0378	0.0390	0.0377	0.0398	0.0454	0.0565	0.0515	0.0570	0.0563	0.0554	0.0425	0.0403	0.0429	0.0396	0.0441	0.0436
44	CFM																
45	CaO	0.1306	0.1241	0.1168	0.1278	0.1169	0.0982	0.1173	0.1089	0.1079	0.1136	0.1173	0.1187	0.1168	0.1193	0.1213	0.1227
46	FeO	0.8231	0.8283	0.8366	0.8238	0.8274	0.8326	0.8190	0.8207	0.8224	0.8180	0.8306	0.8318	0.8306	0.8324	0.8248	0.8242
47	MgO	0.0461	0.0477	0.0464	0.0484	0.0557	0.0693	0.0637	0.0704	0.0696	0.0683	0.0522	0.0494	0.0529	0.0483	0.0540	0.0531
48	AOF																
49	Al2O3+Fe2O3	0.2592	0.2571	0.2573	0.2563	0.2565	0.2546	0.2619	0.2586	0.2583	0.2574	0.2562	0.2567	0.2560	0.2556	0.2560	0.2567
50	CaO	0.0988	0.0922	0.0868	0.0951	0.0869	0.073	0.0866	0.0809	0.08	0.0844	0.0873	0.0882	0.0871	0.0888	0.0901	0.0914
51	FeO+MgO	0.8630	0.8507	0.858	0.8487	0.8500	0.8705	0.8517	0.8624	0.8617	0.8583	0.8688	0.8550	0.8579	0.8564	0.8530	0.8529
52																	
53	CaO	0.1352	0.1297	0.1223	0.1343	0.1238	0.1069	0.1212	0.1160	0.1139	0.1210	0.1238	0.1249	0.1234	0.1253	0.1282	0.1298
54	FeO	0.8506	0.8660	0.8757	0.8657	0.8762	0.8945	0.8464	0.8746	0.8685	0.8708	0.8762	0.8751	0.8766	0.8747	0.8718	0.8704
55	MnO	0.0142	0.0043	0.0020	0.0000	0.0000	0.0000	0.0326	0.0094	0.0176	0.0082	0.0000	0.0000	0.0000	0.0000	0.0000	0.0000
56	n.a. denotes not analyzed																

	A1	AJ	AK	AL	AM	AN	AO	AP	AQ	AR	AS	AT	AU	AV	AW	AX	AY
1	date	9-Jan-96	9-Jan-96	9-Jan-96	30-Jan-96	30-Jan-96	30-Jan-96	30-Jan-96	23-Jan-96	23-Jan-96	23-Jan-96	23-Jan-96	9-Jan-96	9-Jan-96	9-Jan-96	9-Jan-96	27-Jan-96
2	method	ede	ede	ede	ede	ede	ede	ede	ede	ede	ede	ede	ede	ede	ede	ede	ede
3	rock type	3	4	4	4	4	4	4	3	3	3	3	3	3	3	3	3
4	mineral	gar	gar	gar	gar	gar	gar	gar	gar	gar	gar	gar	gar	gar	gar	gar	gar
5	study area	c	c	c	c	c	c	c	c	c	c	c	c	c	c	c	c
6		rorea															
7	sample	4PLC017	4PLC018	4PLC018	4PLC018	4PLC018	4PLC018	4PLC018	4PLC020	4PLC020	4PLC020	4PLC020	5PLC012	5PLC012	5PLC012	5PLC012	5PLC018
8	PTS area	circ 1	circ 1	circ 1	circ 1	circ 1	circ 2	circ 2	circ 1	circ 1	circ 2	circ 2	circ 1	circ 1	circ 2	circ 2	circ 1
9	analysis	gar	gar	gar	gar	gar	gar	gar	gar	gar	gar	gar	gar	gar	gar	gar	gar 1
10		core	rim	core	rim	core	rim	core	rim	core	rim	core	core	rim	core	rim	
11	SiO2	37.018	37.143	36.990	37.244	37.343	37.380	37.147	37.533	37.288	37.526	37.453	36.936	36.645	36.943	36.690	37.621
12	Al2O3	21.756	21.454	21.296	21.664	21.460	21.656	21.550	21.714	21.691	21.609	21.599	21.463	21.455	21.589	21.529	21.612
13	TiO2	0.000	0.000	0.000	0.000	0.000	0.000	0.000	0.000	0.000	0.000	0.000	0.000	0.000	0.000	0.000	0.091
14	Cr2O3	0.000	0.000	0.000	0.000	0.000	0.000	0.000	0.000	0.000	0.000	0.000	0.000	0.000	0.000	0.000	0.000
15	V2O6	n.a.	n.a.	n.a.	n.a.	n.a.	n.a.	n.a.	n.a.	n.a.	n.a.	n.a.	n.a.	n.a.	n.a.	n.a.	n.a.
16	Fe2O3	0.849	0.587	1.154	0.312	0.344	0.000	0.347	0.072	0.014	0.033	0.150	0.741	0.706	0.681	0.857	0.097
17	FeO	37.650	35.941	36.488	36.592	37.402	36.902	37.630	37.411	37.507	37.787	37.747	37.464	40.182	38.655	38.867	37.010
18	MgO	1.291	1.039	1.146	1.320	0.977	1.284	0.960	1.309	1.123	1.233	1.260	1.079	1.302	1.061	1.288	1.033
19	MnO	0.000	0.000	0.000	0.000	0.492	0.000	0.471	0.000	0.226	0.000	0.000	1.008	0.000	0.893	0.000	0.083
20	CaO	4.264	5.706	5.162	4.882	4.276	4.294	4.170	4.357	4.167	4.061	4.076	3.637	1.917	2.957	2.203	5.021
21	K2O	0.000	0.000	0.000	0.000	0.000	0.000	0.000	0.000	0.000	0.000	0.000	0.000	0.000	0.000	0.000	0.000
22	Na2O	n.a.	n.a.	n.a.	n.a.	n.a.	n.a.	n.a.	n.a.	n.a.	n.a.	n.a.	n.a.	n.a.	n.a.	n.a.	n.a.
23	TOTAL	102.828	101.873	102.256	102.004	102.296	101.518	102.176	102.396	102.037	102.298	102.285	102.348	102.409	102.659	102.436	102.566
24																	
25	cations normalized to 8																
26	Si	2.9241	2.9539	2.9377	2.9559	2.9667	2.9620	2.9573	2.9704	2.9658	2.9773	2.9714	2.9401	2.9389	2.9377	2.9254	2.9748
27	Al	2.0254	2.0109	1.9934	2.0254	2.0107	2.0363	2.0219	2.0253	2.0333	2.0207	2.0197	2.0155	2.0176	2.0215	2.0232	2.0141
28	Ti	0.0000	0.0000	0.0000	0.0000	0.0000	0.0000	0.0000	0.0000	0.0000	0.0000	0.0000	0.0000	0.0000	0.0000	0.0000	0.0054
29	Cr	0.0000	0.0000	0.0000	0.0000	0.0000	0.0000	0.0000	0.0000	0.0000	0.0000	0.0000	0.0000	0.0000	0.0000	0.0000	0.0000
30	V	0.0000	0.0000	0.0000	0.0000	0.0000	0.0000	0.0000	0.0000	0.0000	0.0000	0.0000	0.0000	0.0000	0.0000	0.0000	0.0000
31	Fe3+	0.0504	0.0352	0.0690	0.0187	0.0206	0.0000	0.0208	0.0043	0.0008	0.0020	0.0089	0.0444	0.0426	0.0408	0.0514	0.0057
32	Fe2+	2.4872	2.3901	2.4234	2.4287	2.4866	2.4620	2.4987	2.4762	2.4948	2.5073	2.5046	2.4940	2.6813	2.5706	2.5585	2.4474
33	Mg	0.1520	0.1232	0.1357	0.1562	0.1159	0.1526	0.1139	0.1544	0.1331	0.1458	0.1490	0.1279	0.1548	0.1258	0.1533	0.1217
34	Mn	0.0000	0.0000	0.0000	0.0000	0.0331	0.0000	0.0317	0.0000	0.0153	0.0000	0.0000	0.0679	0.0000	0.0601	0.0000	0.0056
35	Ca	0.3606	0.4864	0.4410	0.4151	0.3644	0.3670	0.3557	0.3694	0.3566	0.3470	0.3466	0.3102	0.1639	0.2435	0.1882	0.4254
36	SUM	8.0000	8.0000	8.0000	8.0000	8.0000	8.0000	8.0000	8.0000	8.0000	8.0000	8.0000	8.0000	8.0000	8.0000	8.0000	8.0000
37	O	11.9621	11.9770	11.9686	11.9760	11.9644	12.0002	11.9786	11.9852	11.9829	11.9867	11.9857	11.9701	11.9700	11.9689	11.9627	11.9901
38																	
39	Fe2+/(Mg+Fe2+)	0.9424	0.9510	0.9470	0.9396	0.9555	0.9416	0.9564	0.9413	0.9493	0.9451	0.9439	0.9512	0.9454	0.9534	0.9455	0.9526
40	AFM																
41	Al2O3+Fe2O3	0.2623	0.2693	0.2672	0.2634	0.2607	0.2603	0.2611	0.2784	0.2790	0.2760	0.2765	0.2820	0.2664	0.2786	0.2695	0.2622
42	FeO	0.6764	0.6759	0.6750	0.6733	0.6873	0.6777	0.6876	0.6793	0.6845	0.6842	0.6828	0.6829	0.6935	0.6896	0.6907	0.6838
43	MgO	0.0413	0.0348	0.0378	0.0433	0.0320	0.0420	0.0313	0.0424	0.0365	0.0398	0.0408	0.0380	0.0400	0.0337	0.0398	0.0340
44	CFM																
45	CaO	0.1203	0.1621	0.1470	0.1384	0.1226	0.1231	0.1196	0.1231	0.1195	0.1157	0.1155	0.1058	0.0546	0.0826	0.0627	0.1420
46	FeO	0.8291	0.7968	0.8078	0.8096	0.8361	0.8257	0.8418	0.8254	0.8359	0.8358	0.8349	0.8506	0.8938	0.8744	0.8662	0.8173
47	MgO	0.0507	0.0411	0.0452	0.0521	0.0390	0.0512	0.0384	0.0515	0.0446	0.0486	0.0497	0.0436	0.0518	0.0428	0.0511	0.0406
48	ACF																
49	Al2O3+Fe2O3	0.2570	0.2543	0.2556	0.2541	0.2550	0.2546	0.2560	0.2628	0.2642	0.2521	0.2527	0.2599	0.2556	0.2597	0.2549	0.2522
50	CaO	0.0884	0.1209	0.1094	0.1032	0.0915	0.0918	0.0891	0.0920	0.0892	0.0865	0.0863	0.0783	0.0407	0.0613	0.0466	0.1062
51	FeO+MgO	0.6536	0.6248	0.6348	0.6427	0.6536	0.6537	0.6548	0.6552	0.6567	0.6614	0.6610	0.6618	0.7037	0.6790	0.6865	0.6416
52																	
53	CaO	0.1267	0.1691	0.1540	0.1460	0.1283	0.1297	0.1232	0.1298	0.1245	0.1216	0.1215	0.1080	0.0576	0.0847	0.0661	0.1478
54	FeO	0.8733	0.8309	0.8460	0.8540	0.8622	0.8703	0.8658	0.8702	0.8702	0.8784	0.8765	0.8684	0.9424	0.9044	0.9338	0.8503
55	MnO	0.0000	0.0000	0.0000	0.0000	0.0116	0.0000	0.0110	0.0000	0.0053	0.0000	0.0000	0.0236	0.0000	0.0209	0.0000	0.0019
56	n.a. denotes not analyzed																

	AZ	BA	BB	BC
1	date	27-Jan-86	20-Nov-85	12-Dec-85
2	method	eda	eda	wda-eda
3	rock type	3	4	4
4	mineral	ger	ger	ger
5	study area	c	f	f
6				
7	sample	6PLC015	4PLF011	4PLF011
8	PTS area	circ 1	circ 1	circ 1
9	analysis	ger 2	ger 1	ger 1
10				rerun
11	SiO2	37.711	37.211	36.617
12	Al2O3	21.667	21.331	20.103
13	TiO2	0.000	0.000	0.000
14	Cr2O3	0.000	0.000	0.000
15	V2O5	n.a.	n.a.	n.a.
16	Fe2O3	0.000	0.776	1.301
17	FeO	36.276	35.429	34.601
18	MgO	0.943	1.218	0.859
19	MnO	0.087	0.295	0.349
20	CaO	4.051	5.662	5.844
21	K2O	0.000	0.000	0.000
22	Na2O	n.a.	n.a.	n.a.
23	TOTAL	102.766	101.9210	99.6740
24				
25	cations normalized to 8			
26	Si	2.9841	2.9564	2.9873
27	Al	2.0225	1.9974	1.9329
28	Ti	0.0000	0.0000	0.0000
29	Cr	0.0000	0.0000	0.0000
30	V	0.0000	0.0000	0.0000
31	Fe3+	0.0000	0.0462	0.0798
32	Fe2+	2.5330	2.3541	2.3609
33	Mg	0.1112	0.1443	0.1044
34	Mn	0.0058	0.0198	0.0241
35	Ca	0.3435	0.4820	0.5109
36	SUM	8.0900	8.000	8.000
37	O	11.9954	11.976	11.994
38				
39	Fe2+/(Mg+Fe2+)	0.9580	0.9422	0.9577
40	AFM			
41	Al2O3+Fe2O3	0.2767	0.2903	0.2699
42	FeO	0.6929	0.6467	0.6801
43	MgO	0.0304	0.0410	0.0351
44	CFM			
45	CaO	0.1150	0.1617	0.1716
46	FeO	0.8478	0.7899	0.7933
47	MgO	0.0372	0.0484	0.0351
48	ACF			
49	Al2O3+Fe2O3	0.2629	0.2663	0.2627
50	CaO	0.0859	0.1204	0.1263
51	FeO+MgO	0.6612	0.6243	0.6190
52				
53	CaO	0.1192	0.1698	0.1764
54	FeO	0.8798	0.8245	0.8153
55	MnO	0.0029	0.0069	0.0083
56	n.a. denotes not analyzed			

	A	B	C	D	E	F	G	H	I	J	K	L	M	N
1	date	3-Apr-86	3-Apr-86	12-Dec-85	14-Mar-86	14-Mar-86	9-Apr-86	9-Apr-86	9-Apr-86	9-Apr-86	13-May-86	13-May-86	13-May-86	13-May-86
2	method	eda	eda	wda/eda	eda	eda	eda	eda	eda	eda	eda	eda	eda	eda
3	rock type													
4	mineral	hed	hed	hed	hed	hed	hed	hed	hed	hed	hed	hed	hed	hed
5	study area	a	a	a	a	a	a	a	a	a	a	a	a	a
6														
7	sample	5PLA062	5PLA062	4PLA031	5PLA056	5PLA056	5PLA041	5PLA041	5PLA041	5PLA041	5PLA060	5PLA060	5PLA060	5PLA060
8	PTS area	circ 2	circ 2	circ 2	circ 1	circ 2	circ 1	circ 1	circ 2	circ 2	circ 1	circ 1	circ 2	circ 2
9	analysis	hed 1	hed 2	hed 1	hed 1	hed 1	hed 1	hed 2	hed 1	hed 2	hed 1	hed 2	hed 1	hed 2
10														
11	SiO2	47.934	47.921	47.899	49.040	48.842	49.147	49.035	48.825	48.726	49.352	49.457	49.697	49.428
12	Al2O3	0.534	0.519	0.101	0.341	0.380	0.207	0.000	0.297	0.383	0.326	0.000	0.000	0.000
13	Cr2O3	0.000	0.000	0.000	0.000	0.091	0.083	0.112	0.092	0.000	0.000	0.000	0.000	0.000
14	TiO2	0.000	0.000	0.000	0.000	0.000	0.000	0.000	0.000	0.000	0.000	0.000	0.000	0.000
15	MgO	0.652	0.620	1.466	2.139	2.253	1.129	1.056	0.953	0.950	3.257	2.878	2.724	2.350
16	FeO	28.602	28.594	28.905	26.160	26.126	27.096	27.234	27.691	27.621	24.296	25.363	24.991	25.894
17	MnO	0.075	0.000	0.000	0.070	0.065	0.055	0.087	0.000	0.000	0.093	0.079	0.000	0.088
18	CaO	22.147	22.106	22.509	22.810	22.715	22.799	22.650	22.341	22.341	22.985	22.942	22.998	22.872
19	Na2O	0.000	0.000	0.000	n.a.	n.a.	n.a.	n.a.	n.a.	n.a.	n.a.	n.a.	n.a.	n.a.
20	K2O	0.000	0.000	0.000	0.000	0.000	0.056	0.063	0.000	0.000	0.000	0.000	0.000	0.000
21	TOTAL	99.94	99.76	99.88	100.56	100.47	100.46	100.25	100.2	100.03	100.31	100.52	100.41	100.63
22														
23	cations based on 6 oxygens													
24	Si	1.9767	1.9790	1.9850	1.9848	1.9792	1.9967	2.0022	1.9955	1.9942	1.9852	1.9947	2.0013	1.9958
25	Al	0.0259	0.0253	0.0049	0.0162	0.0181	0.0099	0.0000	0.0143	0.0180	0.0155	0.0000	0.0000	0.0000
26	Cr	0.0000	0.0000	0.0000	0.0000	0.0029	0.0027	0.0036	0.0030	0.0000	0.0000	0.0000	0.0000	0.0000
27	Ti	0.0000	0.0000	0.0000	0.0000	0.0000	0.0000	0.0000	0.0000	0.0000	0.0000	0.0000	0.0000	0.0000
28	Mg	0.0401	0.0382	0.0907	0.1290	0.1361	0.0684	0.0643	0.0581	0.0579	0.1953	0.1698	0.1635	0.1414
29	Fe	0.9864	0.9876	0.9324	0.8854	0.8854	0.9218	0.9300	0.9465	0.9454	0.8173	0.8555	0.8416	0.8744
30	Mn	0.0026	0.0000	0.0000	0.0024	0.0022	0.0000	0.0033	0.0000	0.0000	0.0032	0.0027	0.0000	0.0030
31	Ca	0.9765	0.9781	0.9994	0.9891	0.9862	0.9934	0.9909	0.9783	0.9787	0.9906	0.9914	0.9922	0.9885
32	Na	0.0000	0.0000	0.0000	n.a.	n.a.	n.a.	n.a.	n.a.	n.a.	n.a.	n.a.	n.a.	n.a.
33	K	0.0000	0.0000	0.0000	0.0000	0.0000	0.0000	0.0033	0.0000	0.0000	0.0000	0.0000	0.0000	0.0000
34	SUM	4.0102	4.0082	4.0124	4.0069	4.0101	3.9947	3.9978	3.9957	3.9962	4.0071	4.0052	3.9986	4.0041
35														
36	Fe/(Fe+Mg)	0.9609	0.9628	0.9113	0.8728	0.8668	0.9309	0.9353	0.9422	0.9423	0.8071	0.8417	0.8373	0.8608
37	AFM													
38	Al2O3	0.0125	0.0122	0.0024	0.0079	0.0088	0.0050	0.0000	0.0071	0.0094	0.0076	0.0000	0.0000	0.0000
39	FeO	0.9490	0.9510	0.9092	0.8659	0.8592	0.9263	0.9353	0.9355	0.9335	0.8010	0.8417	0.8373	0.8608
40	MgO	0.0386	0.0368	0.0884	0.1262	0.1321	0.0687	0.0647	0.0574	0.0572	0.1914	0.1583	0.1627	0.1392
41	CFM													
42	CaO	0.4880	0.4881	0.4941	0.4937	0.4912	0.5009	0.4991	0.4934	0.4940	0.4945	0.4938	0.4968	0.4934
43	FeO	0.4920	0.4928	0.4610	0.4419	0.4410	0.4647	0.4685	0.4773	0.4766	0.4080	0.4261	0.4214	0.4360
44	MgO	0.0200	0.0191	0.0448	0.0644	0.0678	0.0345	0.0324	0.0293	0.0292	0.0975	0.0801	0.0819	0.0705
45	ACF													
46	Al2O3	0.0084	0.0083	0.0012	0.0040	0.0045	0.0025	0.0000	0.0036	0.0048	0.0039	0.0000	0.0000	0.0000
47	CaO	0.4849	0.4850	0.4935	0.4917	0.4890	0.4996	0.4991	0.4916	0.4917	0.4926	0.4938	0.4968	0.4934
48	FeO+MgO	0.5087	0.5087	0.5052	0.5043	0.5065	0.4979	0.5009	0.5048	0.5035	0.5035	0.5062	0.5032	0.5068

APPENDIX 4

SAMPLE	method	SiO2	Al2O3			TiO2			Fe2O3T			MgO	CaO			Na2O		
		%		%			%			%		%		%			%	
Fe-R-1	INAA		0.58	±	0.01				76.09	±	1.47		3.92	±	0.21	0.02	±	0.00
Fe-R-1dp	INAA		0.57	±	0.01	0.18	±	0.04					3.03	±	0.19			
Fe-R-1(Abbey)	recom	18.96	0.52	±	0.04	0.03	±	0.06	75.86			0.30	3.29	±	0.10	0.03	±	0.02
Fe-R-2	pp	53.45	4.41			0.24			33.82			2.01	2.40			0.40		
Fe-R-2	fb: pp	48.31	5.33			0.19			39.39			2.00	2.23			0.68		
Fe-R-2	INAA		5.35	±	0.03	0.18	±	0.04	39.36	±	0.78		2.13	±	0.18	0.31	±	0.01
Fe-R-2(Abbey)	recom	49.2	5.61	±	0.13	0.18	±	0.03	39.21			2.1	2.17	±	0.09	0.51		0
Fe-R-3	pp	63.45	0.06			<0.00			32.17			1.26	1.18			<0.01		
Fe-R-3	fb: pp	52.87	0.01			0.01			44.76			0.99	0.84			0.18		
Fe-R-3(4E034)	INAA								45.84	±	1.08					0.02	±	0.00
Fe-R-3(Abbey)	recom	53.61	0.09	±	0.02	0.01	±	0.01	44.50			1.02	0.84	±	0.06	0.03	±	0.03
Fe-R-4	pp	57.32	1.80			0.07			33.67			1.34	0.01			<0.01		
Fe-R-4	fb: pp	50.08	1.69			0.07			40.07			1.29	2.30			0.03		
Fe-R-4(4E016)	INAA		1.86	±	0.01				39.64	±	0.96		2.09	±	0.17	-		
Fe-R-4(Abbey)	recom	50.07	1.70	±	0.07	0.07			39.92			1.41	2.23	±	0.05	0.05	±	0.03
SY-3	pp	61.71	10.48			0.11			5.70			1.90	7.82			4.06		
SY-3	fb: pp	59.67	11.89			0.14			6.45			2.70	8.11			4.37		
SY-3(Abbey)	recom	59.68	11.80			0.15			6.42			2.67	8.26			4.15		
W1	INAA		15.01	±	0.07	1.02	±	0.09					10.77	±	0.54	2.12	±	0.07
W1	recom		14.98	±	0.26	1.07	±	0.06					10.94	±	0.17	2.13	±	0.11
BCR-1	INAA		13.56	±	0.06	2.36	±	0.11					7.11	±	0.43	3.36	±	0.08
BCR-1	recom		13.62	±	0.25	2.22	±	0.10					6.95	±	0.15	3.28	±	0.11
AGV-1	INAA		17.20	±	0.08	1.04	±	0.09					5.00	±	0.35	4.16	±	0.09
AGV-1	recom		17.14	±	0.34	1.06	±	0.05					4.94	±	0.14	4.25	±	0.12
5PLA074	pp	54.48	20.26			0.57			9.87			3.3	0.21			0.23		
5PLA074dp	pp	55.56	20.47			0.56			9.66			3.26	0.21			0.24		
5PLA074	fb: pp	56.31	18.96			0.71			9.49			3.67	0.20			0.23		
5PLA074dp	fb: pp	54.47	19.17			0.67			9.54			3.57	0.19			0.34		
4PLE029	pp	59.32	1.80			0.19			31.99			1.22	3.35			0.06		
4PLE029dp	pp	58.34	1.84			0.19			33.64			1.26	3.38			0.07		
4PLE029	fb: pp	59.99	2.88			0.17			30.86			1.82	2.86			0.37		
4PLE029dp	fb: pp	60.05	2.95			0.16			30.76			1.78	2.84			0.37		
4PLE029	INAA		3.13	±	0.01	0.20	±	0.03	33.47	±	0.83		2.93	±	0.18	0.15	±	0.01
4PLC007	pp	33.58	0.90			0.03			39.05			0.48	2.41			0.04		
4PLC007	fb: pp	36.02	1.40			0.04			47.13			0.69	2.52			0.18		
4PLC007	INAA		1.59	±	0.01				45.39	±	1.19		2.16	±	0.17	0.21	±	0.01
5PLB046	pp	51.25	1.89			0.05			32.66			0.68	2.52			0.06		
5PLB046	fb: pp	49.89	2.58			0.05			38.71			0.88	2.33			0.36		
5PLB046	INAA		2.75	±	0.02				38.94	±	0.94		2.39	±	0.17	0.23	±	0.01
5PLA017	pp	54.99	2.61			0.11			25.86			0.67	3.27			0.02		
5PLA017	fb: pp	53.63	4.19			0.10			31.98			0.84	3.56			0.17		
5PLA017	INAA		4.16	±	0.02	0.12	±	0.03	31.70	±	0.83		3.40	±	0.22	0.17	±	0.01
5PLA010	pp	44.56	1.36			0.06			25.78			0.22	3.91			0.09		
5PLA010	INAA		2.06	±	0.01	0.10	±	0.04	29.96	±	0.81		3.10	±	0.18	0.10	±	0.01
5PLA020	pp	26.17	2.38			0.09			32.92			0.41	4.27			0.09		
5PLA020	INAA		3.03	±	0.02	0.09	±	0.05	38.06	±	1.05		3.47	±	0.19	0.06	±	0.01
5PLA064	pp	47.29	2.47			0.09			31.37			0.13	3.00			0.06		
5PLA064	INAA		3.66	±	0.02	0.08	±	0.04	38.62	±	0.93		2.93	±	0.19	0.09	±	0.01
5PLB031b	pp	35.76	1.32			0.07			54.75			0.59	3.48			0.11		
5PLB031b	INAA		2.44	±	0.01	0.07	±	0.03	49.94	±	1.18		3.09	±	0.20	0.21	±	0.00
5PLB073	pp	30.65	2.11			0.09			47.67			0.86	2.22			0.07		
5PLB073	INAA		3.33	±	0.02	0.07	±	0.03	43.88	±	1.09		1.93	±	0.15	0.14	±	0.01
4PLC008	pp	11.67	1.37			0.02			44.02			0.17	2.05			0.08		
4PLC008	INAA		2.04	±	0.01				49.64	±	1.07		1.90	±	0.16	0.12	±	0.02
4PLE015	pp	34.65	1.75			0.16			52.26			1.30	3.17			0.04		
4PLE015	INAA		3.78	±	0.02	0.10	±	0.04	47.65	±	0.95		2.98	±	0.21	0.11	±	0.00
4PLE033	pp	47.83	1.45			0.11			34.52			0.48	1.76			<0.01		
4PLE033dp	pp	47.13	1.39			0.10			36.12			0.45	1.75			<0.01		
4PLE033	INAA		3.81	±	0.02	0.08	±	0.03	39.78	±	0.96		1.88	±	0.15	0.03	±	0.00
4PLC005.1 Alumina	fb: pp	92.12	0.18			0.01			2.90			0.08	0.05			0.07		
4PLC005.2 Steel	fb: pp	91.83	0.02			0.01			3.87			0.13	0.04			0.05		

fb: pp= XRF fusion bead on majors and XRF pressed powder on trace

pp=XRF pressed powder on all elements

INAA=neutron activation

dp=duplicate

- not analysed or not given

INAA Na long count except where not quantified by long count, then used short count

recommended values for FeR-1, 2, 3, 4 from Abbey et al. (1983)

recommended values for SY-3 from Abbey (1980)

recommended values for W1, BCR-1 and AGV-1 from Gladney and Burns (1983)

SAMPLE	method	K2O	MnO			P2O5	LOI	TOTAL	Au	Ag	As			Ba
		%	%			%	%	%	ppm	ppm	ppm			ppm
Fe-R-1	INAA		0.225	±	0.004						7.784	±	0.33	
Fe-R-1dp	INAA		0.228	±	0.005									
Fe-R-1(Abbey)	recom	0.02	0.220	±	0.040	2.39					8			1000
Fe-R-2	pp	1.70	0.130			0.37	1.12	100.05		-	-			-
Fe-R-2	fb: pp	1.29	0.130			0.28	0.00	99.83		5	8			308
Fe-R-2	INAA		0.122	±	0.003						1.677	±	0.47	
Fe-R-2(Abbey)	recom	1.33	0.12			0.27	0.98 H2O	0.07 CO2		-	2			240
Fe-R-3	pp	0.02	0.090			0.08	1.98	100.27		-	-			-
Fe-R-3	fb: pp	0.01	0.100			0.05	0.00	99.77		9	8			14
Fe-R-3(4E034)	INAA										-			
Fe-R-3(Abbey)	recom	0.03	0.080	±	0.000	0.07	0.20 H2O	1.20 CO2		-	1			11
Fe-R-4	pp	0.30	0.230			0.18	4.90	99.82		-	-			-
Fe-R-4	fb: pp	0.28	0.180			0.12	3.72	99.83		6	10			47
Fe-R-4(4E015)	INAA		0.197	±	0.004						3.33	±	1	
Fe-R-4(Abbey)	recom	0.29	0.190	±	0.000	0.13	0.72 H2O	4.88 CO2		-	3.8			43
SY-3	pp	4.32	0.290			0.58	2.64	99.41		-	-			-
SY-3	fb: pp	4.26	0.320			0.54	1.15	99.61		<1	22			398
SY-3(Abbey)	recom	4.20	0.320			0.54	0.42 H2O	0.38 CO2	0.66 F%	-	20			430
W1	INAA		0.160	±	0.005									
W1	recom		0.168	±	0.016									
BCR-1	INAA		0.185	±	0.005									
BCR-1	recom		0.182	±	0.012									
AGV-1	INAA		0.093	±	0.004									
AGV-1	recom		0.098	±	0.008									
5PLA074	pp	4.87	0.050			0.11	5.97	99.70	0.03	<1	9			2609
5PLA074dp	pp	4.88	0.040			0.10	4.84	99.88	0.03	<1	7			2629
5PLA074	fb: pp	4.51	0.050			0.11	5.97	100.21	0.03	<1	9			2609
5PLA074dp	fb: pp	4.55	0.050			0.10	5.73	100.38	0.03	<1	7			2629
4PLE029	pp	0.14	0.050			0.57	0.62	99.31	<0.03	4	<1			143
4PLE029dp	pp	0.14	0.050			0.59	1.35	98.85	0.03	6	7			125
4PLE029	fb: pp	0.15	0.040			0.44	0.62	100.20	<0.03	4	<1			143
4PLE029dp	fb: pp	0.14	0.050			0.44	0.60	100.17	0.03	6	7			125
4PLE029	INAA		0.040	±	0.002						1.538	±	0.7	
4PLC007	pp	0.03	0.020			0.16	9.39	86.09						
4PLC007	fb: pp	0.02	0.010			0.12	9.39	97.53	87.40	20	600			12
4PLC007	INAA		0.024	±	0.001						1037.53	±	15	
5PLB048	pp	0.07	0.050			0.29	4.70	94.22						
5PLB048	fb: pp	0.08	0.070			0.23	4.70	99.91	0.45	8	20			22
5PLB048	INAA		0.044	±	0.002						19.565	±	1.51	
5PLA017	pp	0.04	0.020			0.28	3.79	91.87						
5PLA017	fb: pp	0.05	0.030			0.21	3.79	98.55	48.17	9	3792			26
5PLA017	INAA		0.023	±	0.001						7590	±	97	
5PLA010	pp	0.05	0.020			0.19	0.18	76.42	47.49	17	150890			50
5PLA010	INAA		0.015	±	0.001						165717	±	2097	
5PLA020	pp	0.06	0.020			1.45	0.31	68.17	37.58	19	183438			33
5PLA020	INAA		0.018	±	0.001						188048	±	2380	
5PLA064	pp	0.05	0.005			0.19	0.00	84.66	7.75	8	57965			51
5PLA064	INAA		0.009	±	0.001						96560	±	1222	
5PLB031b	pp	0.07	0.050			0.15	1.44	97.80	4.53	9	2889			25
5PLB031b	INAA		0.049	±	0.002						4783	±	60	
5PLB073	pp	0.06	0.080			0.14	9.47	93.43	9.29	9	8896			14
5PLB073	INAA		0.069	±	0.002						13000	±	163	
4PLC006	pp	0.05	0.020			0.34	0.30	60.09	34.29	27	215385			4
4PLC006	INAA		0.015	±	0.001						209791	±	2631	
4PLE015	pp	0.07	0.090			0.40	2.36	96.26	0.82	9	1891			63
4PLE015	INAA		0.086	±	0.003						3627	±	45	
4PLE033	pp	0.01	0.070			0.72	5.17	92.14	1.58	8	1002			44
4PLE033dp	pp	0.01	0.070			0.67	5.46	93.15	1.27	7	1070			44
4PLE033	INAA		0.081	±	0.002						2285	±	29	
4PLC005.1 Alumina	fb: pp	0.01	<0.01			<0.01	4.50	99.92	0.17	<1	57			<8
4PLC005.2 Steel	fb: pp	0.01	0.020			<0.01	4.42	100.41	0.99	<1	33			<8

SAMPLE	method	B	Ba	Co	Cr	Cu	La			Ni	Pb	Rb	S	Sc		
		ppm	ppm	ppm	ppm	ppm	ppm			ppm	ppm	ppm	ppm	ppm		
Fe-R-1	INAA						8.4	±	0.8					0.7	±	0.1
Fe-R-1dp	INAA															
Fe-R-1(Abbey)	recom	6		12	7	100	12			8	5200		2600	0.8		
Fe-R-2	pp	-	-													
Fe-R-2	fb: pp	<1	31	16	61	53	12			29	5	63	1547	4		
Fe-R-2	INAA						11.8	±	1.1					5.1	±	0.1
Fe-R-2(Abbey)	recom	-	-	7	47	45	14			21	11	66	1700	6		
Fe-R-3	pp	-	-													
Fe-R-3	fb: pp	4	16	<2	18	20	5			18	9	5	298	2		
Fe-R-3(4E034)	INAA						1.81	±	0.5					-		
Fe-R-3(Abbey)	recom	-	-	2	8	8	2			10	9	-	300	-		
Fe-R-4	pp	-	-													
Fe-R-4	fb: pp	<1	32	10	15	20	10			7	12	20	1089	<1		
Fe-R-4(4E016)	INAA						8.49	±	1.1					1	±	0.2
Fe-R-4(Abbey)	recom	-	-	2	9	13	8			8	8	16	1100	1.5		
SY-3	pp	-	-													
SY-3	fb: pp	2	2184	7	11	6	1288			23	109	207	701	1		
SY-3(Abbey)	recom	-	2200	12	10	16	1350			11	130	206	500	12		
W1	INAA															
W1	recom															
BCR-1	INAA															
BCR-1	recom															
AGV-1	INAA															
AGV-1	recom															
5PLA074	pp	3	41	20	190	1	18			76	13	116	139	23		
5PLA074dp	pp	1	31	27	184	4	17			76	14	115	99	23		
5PLA074	fb: pp	3	41	20	190	1	18			76	13	116	139	23		
5PLA074dp	fb: pp	1	31	27	184	4	17			76	14	115	99	23		
4PLE029	pp	<1	26	25	46	7	9			17	5	7	190	5		
4PLE029dp	pp	<1	23	16	47	10	9			19	10	9	226	6		
4PLE029	fb: pp	<1	26	25	46	7	9			17	5	7	190	5		
4PLE029dp	fb: pp	<1	23	16	47	10	9			19	10	9	226	6		
4PLE029	INAA						10.7	±	1.1					4.9	±	0.3
4PLC007	pp															
4PLC007	fb: pp	0.5	3.5	13	105	355	2			9	1	8	219377	7		
4PLC007	INAA													1.4	±	0.3
5PLB046	pp															
5PLB046	fb: pp	1	31	16	28	113	2			12	27	6	60198	3		
5PLB046	INAA						3.74	±	0.7					1	±	0.3
5PLA017	pp															
5PLA017	fb: pp	8	32	6	43	149	2			6	8	3	118894	5		
5PLA017	INAA						4.97	±	1.5					2.9	±	0.3
5PLA010	pp	18	26	48	78	174	2			113	6	7	74934	2		
5PLA010	INAA													2.1	±	0.3
5PLA020	pp	0.5	3.5	60	52	349	2			112	12	9	131401	5		
5PLA020	INAA															
5PLA064	pp	0.5	13	31	51	171	2			37	11	6	97910	3		
5PLA064	INAA													1.6	±	0.3
5PLB031b	pp	3	7	18	29	42	2			3	7	5	7578	1		
5PLB031b	INAA													1.7	±	0.3
5PLB073	pp	2	11	20	60	127	2			25	29	3	90943	2		
5PLB073	INAA													2.5	±	0.4
4PLC006	pp	25	3.5	117	103	2121	2			486	10	8	207327	5		
4PLC006	INAA													1.6	±	0.2
4PLE015	pp	0.5	41	18	61	55	2			13	2	5	47464	6		
4PLE015	INAA						7.0	±	0.8					5.0	±	0.2
4PLE033	pp	3	49	20	37	133	22			16	3	4	120129	2		
4PLE033dp	pp	2	32	11	72	130	13			17	7	4	114415	3		
4PLE033	INAA						11.4	±	1.2					2.4	±	0.3
4PLC006.1 Alumina	fb: pp	<1	<7	<2	3	6	<4			4	4	<1	8531	2		
4PLC006.2 Steel	fb: pp	<1	<7	4	47	24	<4			8	4	3	3194	1		

SAMPLE	method	Sm			Sr	U	V			W	Y	Zr	Zn
		ppm			ppm	ppm	ppm			ppm	ppm	ppm	ppm
Fe-R-1	INAA	1.77	±	0			96.7	±	3.0				
Fe-R-1dp	INAA						97.8	±	3.1				
Fe-R-1(Abbey)	recom				90		100	?				3500	13
Fe-R-2	pp							±					
Fe-R-2	fb: pp				65	<1	42.0	±		<	17	33	42
Fe-R-2	INAA	2.6	±	0.1			40.9	±	2.3				
Fe-R-2(Abbey)	recom				58	-	37	?		-	15	43	30
Fe-R-3	pp							±					
Fe-R-3	fb: pp				35	<1	6.0	±		2	8	30	10
Fe-R-3(4E034)	INAA	0.64	±	0			10.5	±	1.2				
Fe-R-3(Abbey)	recom				31	-	8	?		-	8	38	2
Fe-R-4	pp							±					
Fe-R-4	fb: pp				62	<1	14.0	±		<	12	19	31
Fe-R-4(4E016)	INAA	2.37	±	0.1			18.1	±	1.5				
Fe-R-4(Abbey)	recom				62	-	11	?		-	8	27	18
SY-3	pp							±					
SY-3	fb: pp				303	425	29.0	±		41	737	241	307
SY-3(Abbey)	recom				306	650	51.0	±		-	740	240	320
W1	INAA						263.9	±	9.1				
W1	recom						260.0	±	25.0				
BCR-1	INAA						419.9	±	13.0				
BCR-1	recom						404.0	±	40.0				
AGV-1	INAA						116.2	±	5.6				
AGV-1	recom						123.0	±	12.0				
5PLA074	pp				181	3	140.0	±		8	16	80	112
5PLA074dp	pp				185	<1	147.0	±		6	16	58	111
5PLA074	fb: pp				181	3	140.0	±		8	16	60	112
5PLA074dp	fb: pp				185	<1	147.0	±		8	16	58	111
4PLE029	pp				170	3	16.0	±		<	16	20	41
4PLE029dp	pp				170	<1	21.0	±		2	16	15	37
4PLE029	fb: pp				170	3	16.0	±		<	16	20	41
4PLE029dp	fb: pp				170	<1	21.0	±		2	16	15	37
4PLE029	INAA	2.38	±	0.1			13.2	±	1.1				
4PLC007	pp							±					
4PLC007	fb: pp				23	0.5	15.0	±		1	10	10	23
4PLC007	INAA	0.66	±	0.1			14.2	±	1.2				
5PLB046	pp							±					
5PLB046	fb: pp				90	2	8.0	±		1	10	17	21
5PLB046	INAA	0.78	±	0.1			26.1	±	1.7				
5PLA017	pp							±					
5PLA017	fb: pp				380	2	33.0	±		1	13	24	29
5PLA017	INAA	0.9	±	0.1			28.1	±	1.7				
5PLA010	pp				203	5	31.0	±		5	14	74	21
5PLA010	INAA						11.3	±	0.8				
5PLA020	pp				315	0.5	47.0	±		2	20	72	21
5PLA020	INAA						19.8	±	1.1				
5PLA064	pp				119	0.5	40.0	±		7	10	46	26
5PLA064	INAA						22.0	±	1.5				
5PLB031b	pp				91	0.5	13.0	±		1	12	7	25
5PLB031b	INAA	0.74	±	0.1			13.4	±	1.3				
5PLB073	pp				53	6	24.0	±		8	17	12	34
5PLB073	INAA	1.11	±	0.1			19.0	±	1.4				
4PLC006	pp				25	0.5	40.0	±		1	8	36	19
4PLC006	INAA						13.6	±	0.9				
4PLE015	pp				189	2	26.0	±		1	17	33	38
4PLE015	INAA	1.39	±	1.4			26.0	±	1.8				
4PLE033	pp				222	<1	22.0	±		<	13	27	34
4PLE033dp	pp				233	<1	22.0	±		<	13	5	31
4PLE033	INAA	1.18	±	0.1			23.6	±	1.6				
4PLC005.1 Alumina	fb: pp				1	<1	<	±		<	3	<	10
4PLC005.2 Steel	fb: pp				2	2	4.0	±		<	6	<	6